A Thesis entitled

AN INVESTIGATION INTO AN IMAGE INTENSIFIER COMPRISING ELECTRON IMAGE DELAY AND SELECTION

by

JOHN BEESLEY, B.Sc.

Submitted for the degree of Ph.D.
in the University of London

Applied Physics Section,
Physics Department,
Imperial College,
London, S.W.7.

July, 1964.

ABSTRACT

The suitability of various types of photon detector for the purpose of high speed photography is discussed. The advantages of the photoemissive surface over other detectors are indicated. The performances of complete photon recording systems, each using a photoemissive surface as the primary photon detector, are shown to depend almost wholly upon the type of image intensifier employed.

The development of electron optical devices as high speed shutters is described, together with those physical experiments which make use of these devices. In particular, the need for a device containing an electron image delay section and an electron optical shutter is discussed.

The theoretical performance of an electron image tube is described. The techniques used in the manufacture of such tubes are indicated, together with their practical development. Experimental evidence is presented which fully describes the working range of such a device.

A preliminary investigation into the use of the electron image delay tube as a high speed framing camera is presented. It is demonstrated practically that the device can be operated in this mode. Further possible developments of such a device are indicated.

The electronic circuitry, which was developed to enable the high speed operation of the electron image delay tube, is fully described.

CONTENTS

Chapter 1 The recording of photon information p.7

1.1 The photon distribution
1.2 The ideal photon detector
1.3 The equivalent quantum efficiency
1.4 Photon detectors
1.4.1 The human eye
1.4.2 The photographic emulsion
1.4.3 The photoemissive surface
1.5 Photon recorders employing a photoemissive surface
1.5.1 The photocell
1.5.2 The photomultiplier
1.5.3 The television camera
1.5.4 The image intensifier

Chapter 2 The performance of existing image intensifiers.. p.19

2.1 Practical requirements of an image intensifier
2.2 The simple image intensifier
2.3 The cascade image intensifier
2.4 The transmission secondary emission intensifier
2.5 The channelled secondary emission intensifier
2.6 Electronographic image intensifiers
2.6.1 Lallemand's electronographic image intensifier
2.6.2 Barrier membrane image intensifiers
2.6.3 The Lenard window image intensifier
2.7 The equivalent quantum efficiencies of image intensifiers
2.8 The recording efficiency of image intensifier systems
2.9 Spurious noise in image intensifiers
2.10 The choice of image intensifier

Chapter 3 The development and use of electron optical devices for high speed photography p.51

3.1 The use of infra-red image converters as light shutters

3.2 The use of television cameras as light shutters

3.3 Simple image intensifiers developed as light shutters

3.4 Multistage image intensifiers incorporating electron optical shutters

3.5 Physical experiments requiring the use of an image intensifier containing an electron optical shutter

3.5.1 Experiments with spark gaps and vacuum discharges

3.5.2 Time resolved spectroscopy

3.5.3 The photography of nuclear particles in luminescent chambers

3.5.4 The recording of Cerenkov rings using image intensifiers

3.5.5 The determination of nuclear particle beam profiles

3.6 Electron image delay using transit time storage

Chapter 4 The theoretical performance of an electron image delay tube p.77

4.1 The variation of image delay with applied voltage

4.2 The electron time dispersion in the image delay time

4.3 The light gain required to record single photoelectrons

4.4 The geometrical resolution

4.5 Image persistence due to phosphor decay time

4.6 The seal-off pressure requirement for the image delay tube

Chapter 5 The general techniques used in the manufacture of electron optical image delay tubes p.98

5.1 The preparation of the vacuum envelope

5.2 The preparation of the metal electrodes

5.3 The preparation of the cathode plate, the phosphor plate and the mica membranes

5.4 The preparation of the phosphor screens

5.5 The preparation of the Caesium ampoule and the Antimony evaporator

5.6 The tube assembly, seal-up and processing

5.7 The preparation of the tube for testing

Chapter 6 Electronic circuitry used in testing the electron image delay tubes p.114

6.1 The avalanche transistor

6.2 The Hirsch circuit

6.3 Pulse circuitry using plug-in modules

6.4 The generation of square gating pulses of mμsec duration

6.4.1 The generation of a pulse of 22 mμsec duration

6.4.2 The generation of a pulse of 11 mμsec duration

6.4.3 The generation of a pulse of 4·5 mμsec duration

6.5 The measurement of various parameters of the Tektronix 545A oscilloscope

6.5.1 The rise time of the light output from P.16 phosphor under cathode ray excitation

6.5.2 The measurement of the triggering delay of the Tektronix 545A oscilloscope

6.6 A high-gain, large-bandwidth amplifier

Chapter 7 The construction and performance of simple image delay tubes p.147

7.1 The construction of early image delay tubes

7.2 The performance of the early image delay tubes

7.3 The conclusions drawn from the performances of the early image delay tubes

7.4 The performance of a delay tube containing a tungsten filament

Chapter 8 The construction and performance of a tube containing an electron image delay section, an intensifier and a high speed electron optical shutter p.164

8.1 The construction of the tube

8.2 Experimental results gained from the first ten tubes

8.2.1 The collection of photocurrent by the electrodes

8.2.2 The estimation of pressure inside the sealed-off tube

8.2.3 The investigation of the current collected by the equipotential delay section

8.2.4 The blue light gain of the cascade image intensifier

8.2.5 Image persistence due to phosphor decay time

8.2.6 The geometrical resolution

8.2.7 The measurement of the speed of the electronic shutter

8.2.8 The investigation of spurious electron storage in the delay section of the tube

8.3 Experimental results gained from tubes numbered XI - XIII

8.3.1 The collection of photocurrent by the electrodes

8.3.2 The further investigation of spurious electron storage in the delay section of the tube

8.4 General conclusions from the performance of the tube

Chapter 9 The preliminary investigation of a new type of framing camera p.230

9.1 Introduction

9.2 The investigation of the change in temporal distribution of the electron image with the number of transits made in the delay section

9.3 The deterioration of the geometrical resolution of the electron image with prolonged temporal storage

9.4 The operation of the tube at high framing rates

9.5 The conclusions from the performance of the delay-tube as a framing camera

Acknowledgements p.263

References p.264

Chapter 1 The recording of photon information

1.1 The photon distribution

The facility of recording a phenomenon made manifest by the emission of photons has long been a requirement in experimental technique.

Special means of photon recording have to be employed where the total integrated number of photons over the period of observation is small. The photon flux may be expressed by the equation:-

$$\int_{t=0}^{t=T} \frac{dn}{dt}\, dt = N$$

Where $\frac{dn}{dt}$ is the rate of arrival of photons at the detector, T is the period of observation and N is the total number of photons.

Three cases of this equation may be considered:-

(1) When $\frac{dn}{dt}$ is very small and T is very large. This condition applies in certain astronomical observations, where the problem is to distinguish the faint star images from the fluctuations in the background illumination. Upon integration the signal increases proportionately to T and the r.m.s. fluctuations proportionately to $\sqrt{T}$. If the integration proceeds linearly, the discrimination will improve proportionately to $\sqrt{T}$. The requirement therefore, is to make the effective exposure time as large as possible.

(2) When both $\frac{dn}{dt}$ and T are intermediate in value. This condition applies in the medical examination of patients using X-radiation. A fluoroscopic screen is used to convert the X-radiation to photons of visible light for observation. Since high doses of X-radiation must be avoided the value of N, which is directly dependent on the dose, must be kept as small as possible.

(3) When $\frac{dn}{dt}$ is of moderate to large value and T is extremely small. This condition applies in the observation of phenomena of short duration most commonly found in the fields of nuclear physics, plasma and gas discharge physics. The requirement here is to detect the small number of photons and to provide a high speed shutter, in order that extraneous information may be excluded.

1.2 The ideal photon detector

The ideal photon detector would have the following properties:-

(a) Every incident photon would be detected as an individual separate event of equal weight, i.e. the quantum efficiency would be unity.

(b) The information storage capacity would be infinite.

(c) The detector would accommodate any distribution of photons in space and time.

(d) The detector response would be uniform at all wave-lengths of the incident photons.

The conditions (a) and (b) stated above assume an ideal incident signal which is noise free. However, the incident photon distribution obeys Poissonian statistics[1] and therefore the r.m.s. fluctuations in $\bar{N}$ is $\sqrt{\bar{N}}$. There is also statistical fluctuations in the rate of absorption of photons at the detector. This means that both the signal and the detector have characteristics describable by electrical signal to noise ratios. Zweig[2] has shown that this precludes the possibility of achieving unity in quantum efficiency. Jones[3] has shown that this also limits the information capacity of a radiation detector.

Practical photon detectors have a limited working range of incident illumination, i.e. they may be under or overloaded. The light collecting optics available and the physical size of the detector limit the spatial photon distribution which may be observed.

Practical photon detectors have spectral response variations, and must be chosen according to the wave-length of the incident photon signal.

The performance of a photon detector considering the properties (a), (b), (c) and (d) has led to the introduction of the concept of the equivalent quantum efficiency of the detector.

1.3 The equivalent quantum efficiency

The output signal of a detector caused by a given input signal is commonly termed its "sensitivity". It is not evident

how the sensitivities of detectors of widely different types can be compared.

Rose[4] [5] [6] has compared the performance of different types of detector by considering their signal to noise ratios to that of an ideal detector under the same conditions. The ideal detector has a mean squared signal to noise ratio, R_1, equal to that of the incident radiation. If under the same conditions, an actual detector gives a measurement of mean squared signal to noise ratio R, its performance as a detector may be expressed by ε_e, where

$$\varepsilon_e = \frac{R}{R_1}$$

This means that if N photons are necessary for a perfect detector to obtain a given measurement, and if an actual detector requires Q incident photons, then

$$\varepsilon_e = \frac{N}{Q}$$

Fellgett[7] [8] has called ε_e the "Equivalent quantum efficiency" of the detector. (R.C. Jones[9] terms the sensitivity of a detector "the responsive quantum efficiency" and ε_e "the detective quantum efficiency").

In general ε_e is a function of the conditions of use. The performance of the device is represented by a family of curves showing the variation of ε_e with the significant operational parameters.

This thesis is concerned with the detection of an extremely small number of photons over an extremely short period of time, i.e. case 1.1.(3). Detectors available for this purpose are now considered.

1.4 Photon detectors

1.4.1 The human eye

The output of the detection process of the human eye is not a signal-to-noise ratio; rather the output is the probability of detecting a given radiation signal. Thus the output is the result of a decision making process. In order to define $\mathcal{E}_e$ the decision making abilities of the human eye must be compared with the decision making abilities of an ideal device. Suppose that to make a given kind of discrimination, an ideal device would require the signal to noise ratio K, then

$$\mathcal{E}_e = \frac{K^2}{R_1}$$

Where R_1 is the mean squared signal to noise ratio of the incident radiation, which the eye requires to make the same discrimination.

In the determination of $\mathcal{E}_e$, various values of K have been assumed or calculated depending upon the degree of discrimination required in a particular experiment. Rose[4] [5] [6] [10] has assumed a value of K equal to 5. R.C. Jones has used values of K equal to 1·14[11] and 1·22. At a wavelength of 5500Å the peak

value of $\mathcal{E}_e$ from the last measurement is $\simeq$ 1%.

The eye maintains a fairly high level of measured performance over an exceedingly large range of scene illumination; 10^{-6} to 10^{2} ergs/cm.^{2} $\mathcal{E}_e$ falls with increasingly shorter observation times, and as the illumination decreases. At the illumination of 5.10^{-10} ergs/cm.^{2} and of duration $\simeq$ 10 mμs (typical case 1.1(3)), $\mathcal{E}_e$ would be virtually zero. The eye can only distinguish as separate entities those events occuring at less than 12-13 c/s.

1.4.2 The photographic emulsion

The photographic emulsion is most commonly used as a primary or secondary detector where permanent recording of the incident radiation is required.

Fellgett[13] has expressed the equivalent quantum efficiency, $\mathcal{E}_e$, of an emulsion by the formula

$$\mathcal{E}_e = \frac{\gamma^2 \log_{10} e}{a\, D_{10} Q}$$

Where Q is the number of photons required to give a density D, $\gamma = dD/d \log_e Q$ (photons cm.$^{-2}$) and a is the mean grain area.

Fellgett[14] and Jones[15] using sensitometric data supplied by Eastman Kodak have calculated the value of $\mathcal{E}_e$ for Royal-X, Tri-X, Plus-X and Pan-X. The maximum value $\mathcal{E}_e$ is 1% using Royal-X emulsion at an exposure of $\simeq 10^{-3}$ ergs/cm.^{2} where the wavelength of the incident radiation is 4300Å. $\mathcal{E}_e$ is strongly dependent on

exposure, its maximum value occuring at a rather low photographic density, 0·1 to 0·2 $\log_{10}$ units above the fog level. At an exposure of less than about 3.10^{-4} ergs/cm.^{2} (4300Å radiation) Royal-X emulsion gives no image at all i.e. $\mathcal{E}_e = 0$. The range of the photographic emulsion may be extended towards lower incident exposures by suitably pre-exposing or post-exposing. Using this technique an integrated incident radiation of down to 10^{-5} ergs/cm.^{2} may be detected with Royal-X emulsion, i.e. when $\mathcal{E}_e$ is ·1%.

1.4.3 The photoemissive surface

The photoemissive surface has the immediate advantage of linearity over the human eye and photographic emulsion. Quantum efficiencies, $\mathcal{E}_o$, of up to 35% (measured with 2870°C tungsten light) have been reported[16] for photoemissive surfaces. Because of the low dark current produced by the photoemissive surface, $\simeq 10^3$ photoelectrons/cm.^{2}/sec for the multialkali cathode at 20°C,[17] $\mathcal{E}_e = \mathcal{E}_o$ over an extremely large range of input signal intensities, i.e. while the signal photocurrent » noise photocurrent. In case 1.1.(3) the noise introduced at the photoemissive surface by the dark current during a time of 10 mμs may be neglected in comparision with the signal.

Provided every signal induced photoelectron could be recorded without the introduction of spurious noise; a recording system, employing a photoemissive surface as primary radiation detector,

would have $\mathcal{E}_e = \mathcal{E}_o$ in the range considered.

The photoemissive surface is therefore, not only the most efficient detector in the wavelength range 1,000-14,000 Å, but also the only one to be operative down to incident intensities of 5.10^{-10} ergs/cm.^{2}.

Various types of photoemissive recorder may now be considered, again noting the requirements of case 1.1.(3).

1.5 Photon recorders employing a photoemissive surface

1.5.1 The photocell

The photocell is the simplest type of photoemissive device. The magnitude of an incident radiation may be recorded electrically from the output current of the photocell. The value of $\mathcal{E}_e$ diverges from $\mathcal{E}_o$ as the inaccuracy of measuring the output current, assuming that the anode collects the photocurrent with 100% efficiency.

1.5.2 The photomultiplier

The photomultiplier extends the range of the photocell down to incident intensities of 5.10^{-10} ergs/cm.^{2}. The statistical fluctuation in the internal electron multiplication causes $\mathcal{E}_e$ to diverge from $\mathcal{E}_o$. This problem is considered in the next chapter applied to image intensifiers.

1.5.3 The television camera

The television camera differs essentially from the photomultiplier and the photocell by virtue of its ability to

record two-dimensional photon information. In all types of television camera tube, noise is introduced into the signal current by the processes of internal signal generation and by external amplifying circuits. The noise limiting performance of various tubes has been considered by Rose[6], Fellgett[13], McGee[18] and Jones[19].

The image orthicon[20], of all the commercial television camera tubes, has the best response at low levels of incident radiation. It has a peak equivalent quantum efficiency of $\triangleq 4\%$ at an incident intensity of 10^{-2} ergs/cm.^{2} (4,000 Å radiation) and an $\mathcal{E}_e$ of $\cdot 1\%$ at $\triangleq 10^{-5}$ ergs/cm.^{2}. Its equivalent quantum efficiency has been expressed by Fellgett[13] to be

$$\mathcal{E}_e = \frac{\mathcal{E}_o \alpha_m}{\beta - m}$$

Where, $\mathcal{E}_o$ is the quantum efficiency of the photocathode

α is the fraction of emitted photoelectrons crossing the target mesh.

m is the number of electrons generated at the target by an incident photoelectron.

β is the reciprocal of the fraction of the incident scanning beam accepted by the target.

The performance of television systems may be extended to lower levels of incident illumination using an image intensifier section ahead of a conventional image orthicon camera in the same vacuum envelope. The resulting tube, the intensifier orthicon,

was first constructed by Morton[21]. The performance of a tube having two stages of cascade amplification has been described by Morton and Ruedy[22].

The internal current gain of ≏100 was not sufficient to enable the observation of single photoelectrons emitted from the photocathode. This has been achieved by Reynolds[23] using a two stage cascade image intensifier ahead of the intensifier orthicon, having a gain of 5-10.

The performance of the hybrid intensifier orthicon at these extremely low light levels may properly be regarded as owing more to its image intensifier section than its image orthicon section. Thus it may be considered as an image intensifier for the purposes of this discussion.

1.5.4 The image intensifier

In its simplest form the image intensifier consists of a semi-transparent photocathode and a parallel phosphor screen in the same vacuum. The ideal simple image intensifier comprises a perfectly uniform photocathode, a perfectly uniform output phosphor screen and a perfect electron optical focusing system, i.e. no geometrical resolution would be lost in image transmission. Fellgett[13] has expressed the equivalent quantum efficiency of an ideal simple image tube thus

$$\mathcal{E}_e = \frac{\mathcal{E}_0}{1 + 1/m} ,$$

Where $\mathcal{E}_o$ is the quantum efficiency of the photocathode and m is the number of photons produced by a single photoelectron at the phosphor screen. Mandel[24] has shown that m can be as large as 1,300. Therefore

$$\mathcal{E}_e = \mathcal{E}_o$$

However, for permanent recording a secondary detector is required.

This is usally a photographic emulsion which has an equivalent quantum efficiency of $\mathcal{E}_{e'}$. The overall performance of the combined system is then

$$\mathcal{E}_e = \frac{\mathcal{E}_o}{1 + 1/m\alpha\mathcal{E}_{e'}}$$

Where α is the fraction of the emitted photons from the phosphor screen arriving at the secondary detector. If the full quantum efficiency of the photoemissive surface is to be realised then $m\,\mathcal{E}_{e'}\alpha \gg 1$. The quantity $m\,\mathcal{E}_{e'}\alpha$ is the number of grains made developable by a single photoelectron.

Practical realisation of the condition $m\,\mathcal{E}_{e'}\alpha \simeq 10$ requires the further development of the simple image intensifier. Such developments are considered in detail in the next chapter.

The theoretical values of $\mathcal{E}_e$ indicated above are for the case of an ideal image intensifying system. However, the inhomogeneities in the elements of the image tube limit the resolution of the image intensifier. These inhomogeneities

produce statistical fluctuations in the photon-electron conversion processes in the tube. These fluctuations cause the measured value of $\mathcal{E}_e$ to depart from the value of $\mathcal{E}_e$ for a perfect image intensifier. The measured value may be denoted by $\mathcal{E}_{e(w)}$ where w is the geometrical resolution of the image tube. As the geometrical resolution of the tube is increased, by reducing the degree of the inhomogeneities in the elements of the image tube, the measured value of $\mathcal{E}_{e(w)}$ more nearly approaches the theoretically perfect value of $\mathcal{E}_e$, i.e. $\mathcal{E}_{e(w=\infty)}$.

Statistics of multiplication affects resolution but also signal/noise. This latter not considered

Chapter 2 The performance of existing image intensifiers

2.1 Practical requirements of an image intensifier

The number of photons produced by an event of the type described in 1.1.(3) is extremely small. It is important therefore, to choose an image intensifier recording system capable of separately recording the highest possible number of available photoelectrons.

The value of the equivalent quantum efficiency $\mathcal{E}_e$, for each type of intensifier exactly describes this requirement. In all cases $\mathcal{E}_e$ may approach $\mathcal{E}_o$, the quantum efficiency of the primary photocathode, but never exceed it. Therefore a photocathode of the highest possible quantum efficiency is required.

In this application high storage capacity is not an important parameter, or contrast detectivity, because of the small number of photons. As few spurious events as possible must be introduced by the intensifiers.

The most important image intensifiers will now be described. Then their performance, with regard to their equivalent quantum efficiencies and their efficiencies in detecting photoelectrons, will be discussed.

2.2 The simple image intensifier

The physical components of this device responsible for intensification are the single primary photocathode and the output phosphor. The electron image, formed at the photoemissive surface,

is accelerated and focused onto the phosphor. Mandel[24] has calculated the photon gain of such a tube from the values of cathode efficiency, phosphor efficiency and accelerating voltage. He discussed the case of an Sb-Cs photocathode (90 μA/lm. sensitivity) illuminated by a source having the same spectral distribution as sunlight. The output phosphor considered is an aluminium backed ZnS:Ag phosphor having a conversion efficiency of 20%. The maximum light gain using an accelerating voltage of 20 KV is 32. If however the illuminating source has the same spectral distribution as the output phosphor, the gain is increased to 200. The measured gain in experimental tubes of this type has been as high as 100[25] using an accelerating voltage of 25 KV.

This gain is reduced when permanent recording, using a lens and a photographic emulsion, is required. In the case where two F/1 lens are used in combination at unity magnification, the proportion of light transmitted from the output phosphor to emulsion is only 13%. Therefore the original gain of 100 is reduced to 13.

This reduction in gain may be almost entirely eliminated by placing the photographic emulsion in direct contact with a thin vacuum tight membrane onto which the output phosphor has been deposited[26] [27]. In an experimental tube[25] using an end window of mica, 12-15 μ thick and ~ 25 mms in diameter, a

photographic gain of 100 with a resolution of 30 lp/mm was achieved.

If an electron impinges upon the output phosphor creating 10^3 photons, it produces a photon density of 2.10^8 photons/cm. on the photographic emulsion. It is assumed that all the photons created arrive at the photographic emulsion and that the halo of light produced on the emulsion is $\simeq 15$ μ in diameter (corresponding to the 30 lp/mm output resolution). Since Eastman Kodak Royal X emulsion requires 10^9 photon/cm. to reach a photographic density of 1 ($\log_{10}$ units), the tube just fails to record single photoelectrons.

2.3 The cascade image intensifier

In order to achieve a higher gain several of the simple intensifiers may be cascaded in series. The combining of such sections in a single envelope was first suggested by scientists at Philips Gloeilampenfabrieken[28] in 1928. The phosphor of one stage being deposited on one side of a thin membrane, usually glass or mica, and the photocathode of the next stage being deposited on the other side. To ensure the highest possible efficiency in each stage the spectral distribution of phosphor and photocathode must be matched as closely as possible. The most efficient combination available appears to be that of the tri-alkali photocathode matched with the ZnS:Ag phosphor.

Multistage tubes of this type have been produced by several

workers[29,30,31,32,33,34,35]. Of these, the device made by Zavoiskii et.al. was the first to have sufficient gain to enable the photographic recording of single photoelectrons. The resolution of the cascade tube is limited by the combined thickness of the phosphor screen and membrane, the diameter of the phosphor particles, the electron-optics and the number of stages. Since the number of stages limits the resolution, as few stages as possible must be used, provided adequate gain can be achieved. The high voltages needed on each stage to achieve adequate gain, produces problems of background noise.

McGee and others at Imperial College have developed a three-stage cascade tube having a blue light (Wratten 47B fitter) gain of 10^5 at an applied overall voltage of 47 KV. The average spurious noise in a cascade tube of this type is $\simeq$1000 output scintillations/cm^2/sec, the lowest $\simeq$300/cm^2/sec. The maximum currently obtainable resolution is $\simeq$23 lp/mm across of useful diameter of 38 mms[36].

2.4 The transmission secondary emission intensifier

The use as a multiplying element, of a material transmitting secondary electrons, was first suggested by Orvin[37] in 1934. Electrons emitted by the photocathode are accelerated and focused onto the thin multiplying film. The secondary electrons transmitted are further accelerated and focused onto another film, and so on, until adequate multiplication has been achieved. The final output

is taken from a phosphor screen.

Several tubes of this type have been reported[38,39,40,41,42] Wachtel[39] has achieved an electron gain of 1,500 using six multiplying KC1 films. The multiplying dynode consists of a 500Å thick KC1 film, deposited on a 150Å thick Al layer to provide a conductive backing. These layers are given mechanical support by a nickel mesh of 50% open area. It was found that the secondary emission of KC1 decreased under electron bombardment, but BaF_2 proved to be much better in this respect. A four stage tube having BaF_2 as secondary emitter was made having an electron gain of 2,450. The photon gain was 10,000 with a 15 μA/Lm photocathode and 15 K.V. on the phosphor stage.

The first really satisfactory T.S.E. tube was produced by Wilcock et.al.[40]. It has sufficient gain to enable single photoelectrons to be recorded. The use of a transparent supporting membrane removed the Moire fringe type of pattern produced by the series of supporting meshes. The multiplying dynodes consisted of a 500Å thick layer of KC1 and a 200Å thick layer of Al on a supporting film of Al_2O_3 of 450Å thickness. Tubes having five such dynodes had an electron gain of $\simeq$ 3,500 and a blue light gain of $\simeq 10^5$ with a photocathode sensitivity of 20 uA/lm. The resolution was initially 15 lp/mm. Later tubes[41] made by 20th Century Electronics in which the dynode spacing was halved and the magnetic field doubled, have a resolution of 30 lp/mm. The usual spurious noise

produced in a tube of this type is 100-500 output scintillations/ cm^2/sec; the lowest $\simeq 10/cm^2/sec$[43]. Recently a tube constructed by the English Electric Co. has been operated partially enclosed, together with its potential divider chain, in transformer insulating oil. Geometrical resolutions of up to 50 lp/mm have been achieved[44] using this technique.

One important parameter of this type of tube is the mean number of transmitted secondaries produced by the secondary emitter per incident primary electron. The value of this parameter for BaF_2 and KCl films is in the range 5-8. For many reasons it is desirable to increase the value of this parameter. If it is larger the total number of dynodes required to produce a given gain may be reduced. This results in an improvement in resolution, and reduces the voltage required for the same gain. The most important improvement is that the probability of an incident electron producing not one transmitted secondary electron is lessened. Also the spread in scintillation intensities at the output phosphor is reduced. Goetze[45] has reported a new type of transmission secondary electron process, in which this parameter has a value of 50-100, using large internal electric fields on thin insulating films. It is hoped that a series of such films having all these desirable characteristics will produce a more satisfactory T.S.E. tube.

2.5 The channelled secondary emission intensifier

The channelled image intensifier was proposed by McGee[46] in

1953. In this device photoelectrons liberated from the photocathode are accelerated and focused onto a set of independent channels, in which secondary emission occurs. The secondary electrons produced are then accelerated and focused onto a further set of channels, carefully aligned to minimize the number of electrons straying from one channel to another. Using several stages sufficient gain can be achieved to enable the recording of single photoelectrons. The light output is taken from a phosphor screen. The resolution is dependent on the dynode structure, since brightness variations smaller than a single channel diameter will not be distinguishable. It is independent, however, of the number of dynodes and therefore the gains used.

Satisfactory secondary emission yields occur at primary electron energies of only a few hundred volts, so that a potential of a few kilovolts is sufficient to produce the required electron gain. This is in contrast with the tens of kilovolts required for the intensifiers described in sections 2.3 and 2.4. Also since the electron optical focusing of the tube is entirely electrostatic, no focusing solenoids are required.

Burns and Neumann[47] have used a channel system of trapezoidal cross section, in which magnesium oxide was used as secondary emitter.

Work at Imperial College[48,49] has used a dynode structure consisting of a set of short cylinders, their ends sliced at 55°

to their axes. MgO, $SbCs_3$ and KCl were used as secondary emitters. A ten stage tube was made having an electron gain of $\simeq 2\ 10^4$ at 530V/stage, using KCl. The limiting resolution was 0.5 lp/mm. It was found that about 65% of secondaries produced reached the following stage.

2.6 Electronographic image intensifiers

In this type of intensifier photoelectrons liberated from the photoemissive detector are accelerated and focused onto an electron sensitive emulsion. Photoelectrons are recorded as individual events, since each one may produce a large number of developable grains. This system therefore provides a valuable gain over direct photography. In certain applications, such as astronomy, the storage capacity of information is an important consideration. Since electron sensitive emulsions contain much finer grains than ordinary photographic emulsions, their capacity is much greater. Their fog level is an order of magnitude less ($\log_{10} D_{fog} = \cdot 02$) and their response considerably more linear.

Several image intensifiers using this principle have been developed.

2.6.1 Lallemand's electronographic image intensifier

Lallemand and his collaborators[50,51,52,53,54] have developed a continuously pumped tube in which both the photocathode and electronographic emulsion are in the same vacuum compartment. The electron optical focusing system is entirely electrostatic.

The overiding problem which had to be overcome was the poisoning of the photocathode, which resulted in it losing sensitivity, due to organic vapours evolved from the emulsion. An exposure of many hours can now be obtained by refrigerating the emulsion, which greatly reduces the liberation of vapours, and by refrigerating the photocathode, which makes it less reactive with the vapours. A titanium ion pump is employed to remove residual gas. A mechanical plate changer is incorporated to enable several exposures to be taken with the same photocathode. A demountable vacuum system is used, in order that the plates may be removed. A prefabricated cathode is supplied for each fresh sequence of exposures.

Gains of up to 100 in exposure time over unaided photography have been claimed, with a resolution of 70 lp/mm.

2.6.2 Barrier membrane image intensifiers

The greatest drawback of the Lallemand device is that because of its demountable nature it has to be prepared for each new operation. Several workers[55,56,57,58] have used a thin membrane to separate the compartment containing the photocathode from that containing the emulsion. The membrane is made as thin as possible in order that it can be highly transparent to electrons while isolating the emulsion vapours from the photocathode. The emulsion is placed as close to the membrane as possible, in order that resolution is not degraded because of electron scatter after transmission. The emulsion is removed from the compartment after

exposures, a moveable shutter being employed to protect the thin membrane from the atmospheric pressure.

In general this type of tube has not proved satisfactory, although development is in progress.

2.6.3 The Lenard window image intensifier

This device, although electronographic in operation, is essentially different from the two previously described types in that it is a completely sealed-off tube. The tube may be used, throughout its life, without having to be prepared for each exposure, which is a great saving in time. The thin membrane used is made of mica, and is constructed to withstand atmospheric pressure[59, 60]. Early tubes had a mica thickness of 6-8μ and an area of 0·5 cm by 3·0 cm. Photoelectrons are accelerated to 50 KV and focused on this membrane, against which the emulsion is tightly pressed. About 75% of the original photoelectrons pass through the mica window and strike the emulsion. Nuclear stripping emulsions are used, held on a curved surface which matches the curvature of the mica window. Using windows of 4-5μ thickness, resolutions of up to 90 lp/mm have been achieved[61].

2.7 The equivalent quantum efficiencies of image intensifiers

2.7.1 The simple image intensifier

It has been noted in section 1.5(c) that the quantum efficiency of the ideal simple image intensifier $\mathcal{E}_e$ was given by

$$\mathcal{E}_e = \frac{\mathcal{E}_0}{1+1/m.}$$

Since m is large $\mathcal{E}_e = \mathcal{E}_o$ down to the smallest light levels. However, for the recording of an electron image, an image intensifier needs an optical coupling system and a photographic emulsion. The $\mathcal{E}_e$ for the recording system is then

$$\mathcal{E}_e = \frac{\mathcal{E}_o}{1+1/m\alpha\mathcal{E}_{e'}}$$

Although it has been seen that the photoemissive effect is linear with decreasing intensity of illumination, the photographic effect is highly non linear. At the intensities under immediate consideration i.e. 5.10^{-10} ergs/cm^2, $\mathcal{E}_{e'}$ is zero, and therefore $\mathcal{E}_e$ tends to zero. If electronic gain is introduced into the simple image intensifier, e.g. those intensifiers described in sections 2.3, 2.4 and 2.5, the value of m is increased by this factor. Since the intensity of illumination at the emulsion is also increased by this factor, the value of $\mathcal{E}_{e'}$ is now finite. Usually the value of this increase is arranged to be sufficiently large so that the factor $1/m\alpha\mathcal{E}_{e'}$ may be neglected and $\mathcal{E}_e$ tends to $\mathcal{E}_o$.

In practice however, the electron gain is subject to a statistical fluctuation, which decreases the value of the signal to noise ratio at the output of the multistage image intensifier. This results in a decrease in the value of $\mathcal{E}_e$ of the image intensifier.

2.7.2 The cascade image intensifier

Mandel[62] has calculated the mean squared deviation in the number of photons produced at the output of a cascade image

intensifier. In order to calculate this he used general formulae for the fluctuation in the number of particles in an interaction. If a primary particle gives rise to λ secondaries, where λ is a stochastic variate, n incident particles making independent interactions will give rise to μ secondaries, such that

$$\bar{\mu} = \bar{n}\,\bar{\lambda}$$

$$\text{and} \quad \overline{\Delta^2\mu} = \overline{\lambda^2}\,\overline{\Delta^2 n} + \bar{n}\,\overline{\Delta^2\lambda}$$

A bar is used to denote the average, and the sign Δ denotes the deviation from the mean. These relations hold for any probability distribution.

Let there be $\bar{n}$ photons incident upon the primary photocathode of a cascade image intensifier having r stages, each of gain $\bar{G}$. The total number, N_r, photons produced at the output phosphor, is given by

$$\bar{N}_r = \bar{n}\,\overline{G^r}$$

Mandel[62] showed that

$$\overline{\Delta^2 N_r} = \bar{n}\,\overline{G^{2r}}\,\frac{1}{\bar{\xi}_o}\left(\frac{\bar{G}}{\bar{G}-1}\right)$$

where $\bar{\xi}_o$ is the quantum efficiency of the primary photocathode.

However, these values must be corrected to take into account those primary photoelectrons lost in collision with a gas molecule, captured by a mesh while passing through it and those whose probability of appearing as an output scintillation is zero. Let the fraction of primary photoelectrons which do appear as an output

scintillations be denoted by $\bar{\mathcal{E}}_1$. $\bar{N}$ and $\overline{\Delta^2 N}$ thus become,

$$\bar{N}_r = \bar{\mathcal{E}}_1 \bar{n} \bar{G}^r \quad .. \quad .. \quad .. \quad (1)$$

and $$\overline{\Delta^2 N_r} = \bar{n}\, \overline{G^{2r}}\, \frac{\bar{\mathcal{E}}_1}{\bar{\mathcal{E}}_o} \left(\frac{\bar{G}}{\bar{G}-1} \right) \quad .. \quad .. \quad (2)$$

$\mathcal{E}_o$

It was noted in section 1.3 that the equivalent quantum efficiency was defined as

$$\bar{\mathcal{E}}_e = \frac{R}{R_1}$$

If only the image tube is considered, $\mathcal{E}_e$ is the equivalent quantum efficiency of the intensifier and may be denoted by $\mathcal{E}_{e(\text{intensifier})}$.

$$R = \frac{\bar{N}_r^2}{\overline{\Delta^2 N_r}} = \frac{\bar{\mathcal{E}}_1^2\, \bar{n}^2 \bar{G}^{2r}\, \overline{\mathcal{E}_o}}{\bar{\mathcal{E}}_1\, \bar{n}\, \bar{G}^{2r} \left(\frac{\bar{G}}{\bar{G}-1} \right)} = \bar{\mathcal{E}}_1\, \bar{n}\, \bar{\mathcal{E}}_o \left(\frac{\bar{G}-1}{\bar{G}} \right)$$

$$R_1 = \frac{\bar{n}^2}{\overline{\Delta^2 n}} = \frac{\bar{n}^2}{\bar{n}} = \bar{n}$$

since the input photons obey Poissonian distribution[1].

Therefore $$\bar{\mathcal{E}}_{e(\text{intensifier})} = \bar{\mathcal{E}}_1\, \bar{\mathcal{E}}_o \left(\frac{\bar{G}-1}{\bar{G}} \right) \quad .. \quad (3)$$

In pure cascade tubes $\bar{\mathcal{E}}_1 \triangleq 1$, since there are no meshes and molecule-electron collision is negligible. The probability that an electron gives no output scintillation, due to statistical fluctuations in the electron multiplication (G) at the first stage,

is very small since $\bar{G} \doteq 100$. Electrons may also be lost because they impinge upon "pinholes" in the first phosphor screen. In the best case, obtained when using settled phosphor ($< 10\mu$) of 2 mg/cm^2, $\bar{\varepsilon}_1$ can be 98%(63). However, using fine grained phosphor ($\leq 3\mu$) deposited by cataphoresis the electron loss is entirely negligible i.e. 3.10^{-4}%. Under these conditions

$$\bar{\varepsilon}_{e(\text{intensifier})} \doteq \bar{\varepsilon}_o$$

The value of ε_e derived here, describes an ideal cascade image intensifier, in that it is assumed that perfectly uniform phosphor screens are present. In practical devices, the graininess of the phosphor screen produces the overwhelming component of the output noise fluctuations. If the phosphor screens can be improved, for example by using evaporated phosphors, the value of ε_e derived may be approached.

The cascade image intensifier by itself does not record information. A complete recording system consists of an intensifier, an optical coupling system and a photographic emulsion (fig.1 (a)). Let δ be the collecting efficiency of the lens, and ε_e the quantum efficiency of the emulsion.

The number ($\bar{\tau}$) of photons arriving at the emulsion is

$$\bar{\tau} = \bar{N}_r \bar{\delta} \quad .. \quad .. \quad .. \quad .. \quad (4)$$

$$\text{and } \overline{\Delta^2 \tau} = \bar{\delta}^2 \overline{\Delta^2 N_r} + \bar{N}_r \bar{\delta} (1-\bar{\delta}) \quad .. \quad .. \quad .. \quad (5)$$

The number of developable grain produced in the emulsion by τ is P,

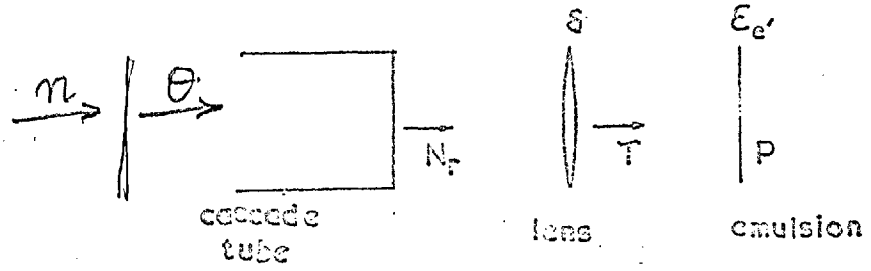


FIG.1(a) The recording system for a cascade tube

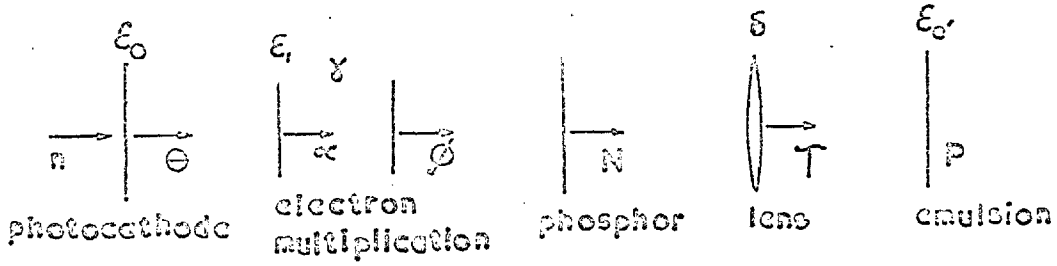


FIG.1(b) The recording system using a T.S.E. tube

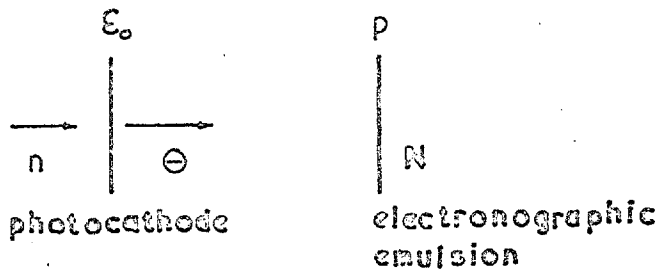


FIG.1(c) The recording system using a Lallemand device

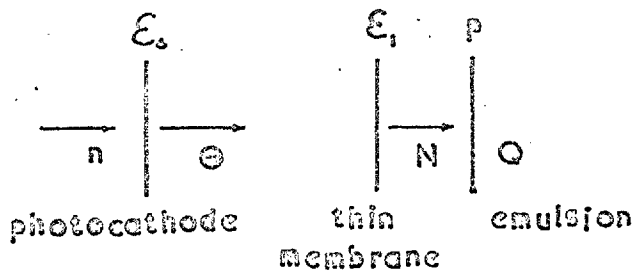


FIG.1(d) The recording system using a barrier-membrane device

where $\bar{P} = \bar{T}\bar{\varepsilon}_{e'}$ .. .. (6)

and $\overline{\Delta^2 P} = \bar{\varepsilon}_{e'}^2\,\overline{\Delta^2 T} + \bar{T}\,\bar{\varepsilon}_{e'}(1-\bar{\varepsilon}_{e'})$ .. .. (7)

Using eqns. (1), (4) and (6)

$$\bar{P} = \bar{\delta}\,\bar{\varepsilon}_{e'}\,\bar{\varepsilon}_1\bar{n}\overline{G^r}$$

Using eqns. (2), (5) and (7)

$$\overline{\Delta^2 P} = \bar{\delta}\,\bar{\varepsilon}_{e'}\,\bar{\varepsilon}_1\bar{n}\overline{G^r}\left[\frac{\bar{\varepsilon}_{e'}\overline{G^r}}{\bar{\varepsilon}_o}\left(\frac{\bar{G}}{\bar{G}-1}\right) + \bar{\delta} + 1\right]$$

The equivalent quantum efficiency of the recording system may be denoted by $\varepsilon_{e(system)}$ where

$$\varepsilon_{e(system)} = \frac{\overline{P^2}/\overline{\Delta^2 P}}{\overline{n^2}/\overline{\Delta^2 n}} = \frac{\bar{\varepsilon}_1\,\bar{\varepsilon}_o}{\dfrac{\bar{G}}{\bar{G}-1} + \dfrac{\bar{\varepsilon}_o(\bar{\delta}+1)}{\overline{G^r}}}$$

Since $\bar{\varepsilon}_o \simeq 1$, $\bar{\delta} \simeq 0{\cdot}1$ and $\overline{G^r} \simeq 10^6$ the term $\bar{\varepsilon}_o(\bar{\delta}+1)/\overline{G^r}$ may be neglected.

Therefore $\bar{\varepsilon}_{e(system)} = \bar{\varepsilon}_1\,\bar{\varepsilon}_o\left(\dfrac{\bar{G}-1}{\bar{G}}\right)$ .. .. (8)

Comparing eqns. (3) and (8)

$$\bar{\varepsilon}_{e(intensifier)} = \bar{\varepsilon}_{e(system)}$$

The performance of the recording system is therefore almost wholly dependent on the performance of the image intensifier.

2.7.3 The transmission secondary emission image intensifier

Let there be $\bar{n}$ photons incident on the photocathode, whose quantum efficiency is $\mathcal{E}_o$, producing $\bar{\theta}$ photoelectrons (fig.1 (b)).

Therefore $$\bar{\theta} = \bar{n}\,\bar{\mathcal{E}}_o$$

and $$\overline{\Delta^2\theta} = \overline{\mathcal{E}_o^2}\,\overline{\Delta^2\bar{n}} + \bar{n}\,\overline{\Delta^2\mathcal{E}_o}$$

Since the probability distributions $p(\mathcal{E}_o)$ of $\mathcal{E}_o$ is of the form

$$p(1) = \bar{\mathcal{E}}_o,$$

$$p(0) = 1 - \bar{\mathcal{E}}_o,$$

$$p(\bar{\mathcal{E}}_o > 1) = 0,$$

so that $$\overline{\Delta^2\mathcal{E}_o} = \bar{\mathcal{E}}_o\,(1 - \bar{\mathcal{E}}_o)$$

thus $$\overline{\Delta^2\theta} = \bar{\mathcal{E}}_o^2\bar{n} + \bar{n}\,\bar{\mathcal{E}}_o(1 - \bar{\mathcal{E}}_o)$$

$$= \bar{n}\,\bar{\mathcal{E}}_o$$

This is indicative of the fact that the statistics of the photo effect may be described by Poissonian distribution. This has been shown by Sauter[64].

Introducing the factor $\mathcal{E}_1$, having the same probability distribution as $\mathcal{E}_o$, the number of photoelectrons to be multiplied is α where

$$\bar{\alpha} = \bar{\mathcal{E}}_1\bar{\theta} = \bar{n}_1\,\bar{\mathcal{E}}_1\,\bar{\mathcal{E}}_o$$

and $$\overline{\Delta^2\alpha} = \bar{\mathcal{E}}_1\bar{\theta}$$

It has been shown experimentally that electron multiplication

follows exponential distribution[43]. Let the electron gain be γ, so that the number of electrons arriving at the output phosphor screen is given by ϕ where,

$$\bar{\phi} = \bar{\alpha}\,\bar{\gamma} = \bar{n}\,\bar{\varepsilon}_1\bar{\varepsilon}_o\,\bar{\gamma}$$

and
$$\overline{\Delta^2\phi} = \overline{\gamma^2}\,\overline{\Delta^2\alpha} + \bar{\alpha}\,\overline{\Delta^2\gamma}$$

$$= \overline{\gamma^2}\,\bar{\alpha} + \bar{\alpha}\,\overline{\gamma^2}, \text{ since } \overline{\Delta^2\gamma} = \overline{\gamma^2}$$

$$= 2\,\overline{\gamma^2}\,\bar{\alpha}$$

$$= 2\,\overline{\gamma^2}\,\bar{n}\,\bar{\varepsilon}_1\bar{\varepsilon}_o$$

ϕ electrons incident upon the phosphor screen of quantum yield β give rise to N photons, where

$$\bar{N} = \bar{\phi}\,\bar{\beta} = \bar{n}\,\bar{\varepsilon}_1\bar{\varepsilon}_o\,\bar{\gamma}\,\bar{\beta} \qquad \ldots\ \ldots \qquad (9)$$

and
$$\overline{\Delta^2 N} = \bar{\beta}^2\,\overline{\Delta^2\phi} + \bar{\phi}\,\overline{\Delta^2\beta}$$

Mandel[62] has suggested that it is unlikely that the distribution of β departs very greatly from the Poissonian form, so that $\overline{\Delta^2\beta} = K\bar{\beta}$, where K is a constant of order unity to allow for the departure from Poisson form.

Then
$$\overline{\Delta^2 N} = 2\bar{\beta}^2\overline{\gamma^2}\,\bar{n}\,\bar{\varepsilon}_1\bar{\varepsilon}_o + \bar{n}\,\bar{\varepsilon}_1\bar{\varepsilon}_o\,\bar{\gamma}\,\bar{K}\,\bar{\beta}$$

$$= \bar{\beta}\,\bar{\gamma}\,\bar{n}\,\bar{\varepsilon}_1\bar{\varepsilon}_o\,(2\bar{\beta}\,\bar{\gamma} + K) \qquad \ldots\ \ldots \qquad (10)$$

Since $\bar{\delta} \simeq 10^3$ for a T.S.E. tube[40] and $\bar{\beta} \simeq 10^3$ for a typical phosphor screen[24], $\bar{\beta}\bar{\delta} \gg K$.

Therefore $\overline{\Delta^2_N} = 2\bar{\beta}^2\bar{\delta}^2\bar{n}\,\bar{\varepsilon}_1\bar{\varepsilon}_o$

Now $$R = \frac{\bar{N}^2}{\overline{\Delta^2_N}} = \frac{\bar{n}^2\,\bar{\varepsilon}_1^2\bar{\varepsilon}_o^2\bar{\delta}^2\bar{\beta}^2}{2\bar{\beta}^2\bar{\delta}^2\bar{n}\,\bar{\varepsilon}_1\bar{\varepsilon}_o}$$

and $$R_1 = \bar{n}$$

Thus $$\varepsilon_{e(\text{intensifier})} = \frac{R}{R_1} = \frac{\bar{\varepsilon}_1\bar{\varepsilon}_o}{2} \qquad \text{(11)}$$

It has been established experimentally by Davison and Sephton at Imperial College that the value of $\bar{\varepsilon}_1 \simeq .4$ for a T.S.E. tube.

Therefore $$\varepsilon_{e(\text{intensifier})} \simeq \frac{\bar{\varepsilon}_o}{5}$$

It is readily seen from the above considerations that if the transmission secondary electron yields could be increased the multiplying statistics of the tube would be improved and values of ε_e approaching ε_o would be achieved. A complete recording system (fig.1 (b)) has a lens and an emulsion in addition to the T.S.E. tube.

It may be shown, by following the same proceedure described in section 2.7.2, that the number of developable grains produced by an incident signal n is $\bar{P}$. From eqns. (9), (4) and (6)

$$\bar{P} = \bar{n}\ \bar{\mathcal{E}}_1 \bar{\xi}_o \bar{\gamma} \bar{\beta} \bar{\delta}\ \bar{\mathcal{E}}_{e'}$$

From eqns. (10), (5) and (7), if it is assumed that K = 1

$$\overline{\Delta^2 P} = \bar{n}\ \bar{\mathcal{E}}_1 \bar{\xi}_o \bar{\gamma} \bar{\beta} \bar{\delta}\ \bar{\mathcal{E}}_{e'} (2 \bar{\beta} \bar{\gamma} \bar{\delta}\ \bar{\mathcal{E}}_{e'} + 1)$$

Now $$\mathcal{E}_{e(system)} = \frac{\bar{P}^2 / \overline{\Delta^2 P}}{\bar{n}^2 / \overline{\Delta^2 n}}$$

$$= \frac{\bar{\mathcal{E}}_1 \bar{\xi}_o}{2 + 1/\bar{\beta} \bar{\gamma} \bar{\delta} \bar{\mathcal{E}}_{e'}}$$

Since $\bar{\beta} \doteq 10^3$, $\bar{\gamma} \doteq 10^3$, $\bar{\delta} \doteq 10^{-1}$, & $\bar{\mathcal{E}}_{e'} \doteq 10^{-2}$ to 10^{-3},

$$1/\bar{\beta} \bar{\gamma} \bar{\delta}\ \bar{\mathcal{E}}_{e'} \doteq 10^{-3} \text{ to } 10^{-2}$$

$$\mathcal{E}_{e(system)} \doteq \frac{\bar{\mathcal{E}}_1 \bar{\xi}_o}{2} \qquad .. \quad .. \quad .. \quad (12)$$

Again, considering eqns. (11) and (12), it is seen that the performance of the recording system is most dependent on the intensifier.

2.7.4 The channelled secondary emission intensifier

There is a certain amount of controversy over the exact nature of the multiplying distribution found in this type of tube. Several workers[65,66] have reported an exponential pulse height distribution at the output, for single input electrons. The equivalent quantum efficiency would then exactly follow that calculated in 2.7.3 i.e.

$$\mathcal{E}_{e(intensifier)} = \frac{\bar{\mathcal{E}}_1 \bar{\xi}_o}{2}$$

It has also been reported[67,68] that the distribution is not of Poissonian form and not quite as degraded as in an exponential distribution. If a factor β is introduced to allow for departure from Poissonian form then,

$$\bar{\mathcal{E}}_{e(\text{intensifier})} = \frac{\bar{\mathcal{E}}_1 \bar{\mathcal{E}}_o}{(1-\beta)} \text{ where } o < \beta < 1$$

No exact evaluation of $\bar{\mathcal{E}}_e$ may be ascertained, since the values of $\bar{\mathcal{E}}_1$ and β are not known. Since however, the secondary emission yield is rather low (a maximum value of 10 for KCl[69]) $\bar{\mathcal{E}}_e$ might be expected to depart strongly from $\bar{\mathcal{E}}_o$.

Again, it may be shown that

$$\bar{\mathcal{E}}_{e(\text{intensifier})} = \bar{\mathcal{E}}_{e(\text{system})}$$

2.7.5 Electronographic image intensifiers

(a) The Lallemand device

Let n photons incident upon the photocathode produce θ photoelectrons (fig.1 (c)).

$$\theta = \bar{n}\ \bar{\mathcal{E}}_o$$

and $$\overline{\Delta^2\theta} = \bar{n}\ \bar{\mathcal{E}}_o$$

Let each photoelectron produce $\bar{p}$ developable grains in the electron sensitive emulsion. The total number of recorded events, $\bar{N}$, is given by

$$\bar{N} = \bar{n}\ \bar{\mathcal{E}}_o\ \bar{p}$$

and $\overline{\Delta^2 N} = \overline{p^2 n}\ \bar{\varepsilon}_o + \bar{n}\,\bar{\varepsilon}_o \overline{\Delta^2 p}$

If the distribution in the number of developable grains produced by single electrons follows Poissonian distribution, $\overline{\Delta^2 p} = \bar{p}$

Therefore $\overline{\Delta^2 N} = \overline{pn}\ \bar{\varepsilon}_o (\bar{p} + 1)$

$$\bar{\varepsilon}_{e(system)} = \frac{\overline{N^2}/\overline{\Delta^2 N}}{\bar{n}^2/\overline{\Delta^2 n}} = \frac{\bar{n}^2 \bar{\varepsilon}_o^2\ \overline{p^2}/\overline{pn}\ \bar{\varepsilon}_o(\bar{p} + 1)}{\bar{n}}$$

$$= \frac{\bar{\varepsilon}_o}{(1 + 1/\bar{p})}$$

If the Lallemand tube is operated with an overall potential of 20KV, $p \triangleq 7$.

Therefore $\bar{\varepsilon}_e = \frac{7}{8}\ \bar{\varepsilon}_o$

(b) <u>The barrier-membrane device</u>

Let n photons be incident upon the photocathode, quantum efficiency ε_o, providing θ photoelectrons (fig.1 (d)).

$$\bar{\theta} = \bar{n}\ \bar{\varepsilon}_o$$

and $$\overline{\Delta^2 \theta} = \bar{n}\ \bar{\varepsilon}_o$$

If the fraction of electrons transmitted through the membrane is $\bar{\varepsilon}_1$, the total number is N, where

$$\bar{N} = \bar{\theta}\ \bar{\varepsilon}_1$$

$$\overline{\Delta^2 N} = \bar{\varepsilon}_1^2\, \overline{\Delta^2 \theta} + \theta\ \overline{\Delta^2 \varepsilon_1}$$

Let the output distribution in the number of transmitted electrons deviate from Poissonian by a factor K i.e.

$$\overline{\Delta^2 \epsilon_1} = K \bar{\epsilon}_1 \text{ where } K > 1$$

Thus $$\overline{\Delta^2 N} = \bar{n}\ \bar{\epsilon}_o \bar{\epsilon}_1 (\bar{\epsilon}_1 + K)$$

Let each photoelectron produce $\bar{p}$ developable grains in the electron sensitive emulsion. The total number, Q, of recorded events is given by

$$\bar{Q} = \bar{p}\ \bar{N}$$

and $$\overline{\Delta^2 Q} = \overline{p^2}\ \overline{\Delta^2 N} + \bar{N}\ \overline{\Delta^2 p}$$

If $\overline{\Delta^2 p} = \bar{p}$, i.e. the distribution of developable grains follows a Possonian distribution, then

$$\overline{\Delta^2 Q} = \overline{p^2}\ \bar{n}\ \bar{\epsilon}_o \bar{\epsilon}_1 (\bar{\epsilon}_1 + K) + \bar{n}\ \bar{\epsilon}_o \bar{\epsilon}_1 \bar{p}$$

$$= \bar{p}\ \bar{n}\ \bar{\epsilon}_o \bar{\epsilon}_1 \left\{ \bar{p} (\bar{\epsilon}_1 + K) + 1 \right\}$$

$$\text{Now } \epsilon_{e(\text{system})} = \frac{\overline{Q^2}/\overline{\Delta^2 Q}}{\overline{n^2}/\overline{\Delta^2 n}} = \frac{\overline{p^2 n^2}\ \overline{\epsilon_1^2}\ \overline{\epsilon_o^2}/\bar{n}\ \bar{\epsilon}_o \bar{\epsilon}_1 \bar{p} \left\{ \bar{p} (\bar{\epsilon}_1 + K) + 1 \right\}}{\bar{n}}$$

$$= \frac{\bar{\epsilon}_1 \bar{\epsilon}_o}{\bar{\epsilon}_1 + K + 1/\bar{p}}$$

(c) The Lenard window device

This is an exactly analogous case, mathematically, to (b)

Therefore $$\epsilon_{e(\text{system})} = \frac{\bar{\epsilon}_1 \bar{\epsilon}_o}{\bar{\epsilon}_1 + K + 1/\bar{p}}$$

In the best possible case, using an infinitesimally thin mica window, all the photoelectrons are transmitted with uniform energies i.e. $\bar{\mathcal{E}}_1 = 1$ and K = 0. Under these conditions

$$\mathcal{E}_{e(system)} = \frac{\mathcal{E}_o}{1+1/\bar{p}}$$

It has also been assumed that no photoelectron reaches the electronographic emulsion with so little energy that its record is indistinguishable from the fog level. The latter assumption is valid because the fog level of an electronographic emulsion is so low i.e. $\cdot 02$ Log_{10} units.

Wheeler[70] found that $\bar{\mathcal{E}}_1 \simeq \cdot 7$ for a mica of 8 μ thickness. If it is assumed that the output distribution in the number of transmitted electrons is Poissonian i.e. K = 1, and that the mean number, $\bar{p}$, of grains produced by a photoelectron is 7; then

$$\bar{\mathcal{E}}_e = \frac{49}{129}\ \bar{\mathcal{E}}_o$$

2.8 The recording efficiency of image intensifier systems

The equivalent quantum efficiency of an image intensifier is a quantity which could be determined by experiment; being the ratio of the output to input signal to noise ratios. One of the parameters of the image intensifier which may be extracted from $\bar{\mathcal{E}}_e$ is the efficiency of recording a single photoelectron, $\bar{\mathcal{E}}_r$.

It is $\bar{\mathcal{E}}_r$ and not $\bar{\mathcal{E}}_e$ which is most generally experimentally measured, and is of direct concern in this thesis.

$\bar{\mathcal{E}}_r$ is the product of two factors i.e. $\bar{\mathcal{E}}_r = \bar{\mathcal{E}}_1 \bar{\mathcal{E}}_2$ where $\bar{\mathcal{E}}_1$ has been described in section 2.7.2.

$\bar{\mathcal{E}}_2$ is dependent on the amplitude distribution of the output pulses. A photoelectron is not recorded in each case where the amplitude of the output pulse is less than the discrimination level chosen for the cutting off of noise in the recorder. In the case of a photographic emulsion the discrimination is determined by the fog level. $\bar{\mathcal{E}}_2$ is the fraction of photoelectrons recorded above the fog level.

$\bar{\mathcal{E}}_r$ is usually determined by counting the number of events recorded due to a given primary photoelectric current. $\bar{\mathcal{E}}_1$ may be determined by making use of a recording device such as a high-gain, low-noise photomultiplier in which the discrimination level can be reduced to achieve $\bar{\mathcal{E}}_2 = 1$.

Fleisher[71] has described a method of determining experimentally $\bar{\mathcal{E}}_1$ and $\bar{\mathcal{E}}_2$ without measuring small fluxes of particles. He showed that

$$\bar{\mathcal{E}}_1 = \bar{K}\,\bar{\sigma}/\bar{v}$$

where $\bar{\sigma}$ is the coefficient of secondary emission at the first dynode, $\bar{K}$ is the average amplitude at the output when only one electron is emitted from the first dynode and $\bar{v}$ is the average amplitude at the output.

Also $\bar{\mathcal{E}}_2 \sim e^{-v_d/v}$ where v_d is the discrimination level.

Thus $$\bar{\varepsilon}_r = \frac{\bar{K}\,\bar{\sigma}}{\bar{v}}\, e^{-v_d/v}$$

2.8.1 The single-stage image intensifier

This may be considered as the first stage of a cascade image intensifier. In this case, as was shown in section 2.7.2, $\bar{\varepsilon}_1 \triangleq 1$

Let a single-stage tube be illuminated by light of wavelength 4800 Å i.e. each photon has an energy $\triangleq 4.10^{-12}$ ergs. The output energy at the phosphor screen due to a single photoelectron is 4.10^{-4} ergs/cm^2, if the tube has a gain of 100 and a resolution of 50 lp/mm. An optical system of 10% efficiency, used at 1:1 magnification, would then deliver an energy of 4.10^{-5} ergs/cm^2 onto a photographic emulsion. Since this is well below the fog level of a photographic emulsion, $\bar{\varepsilon}_2 = 0$.

Therefore $$\bar{\varepsilon}_r = 0.$$

2.8.2 The cascade image intensifier

The value of $\bar{\varepsilon}_r$ has been experimentally measured by Reynolds [72,73] for an R.C.A. three stage cascade tube type C73491C. A weak light was shone onto the photocathode and the photocurrent was measured. The intensity of the illumination was then reduced by a large known factor and photographs were taken. The number of spots recorded were counted. From these measurements $\bar{\varepsilon}_r$ was found to vary linearly with the voltage applied to the tube. $\bar{\varepsilon}_r \triangleq 5\%$ and 85% at 10KV and 55KV respectively. At high overall voltage, the gain in each stage is high and $\bar{\varepsilon}_1 \triangleq 1$. Therefore $\bar{\varepsilon}_2 \triangleq .85$, the loss of

information being largely due to the fact that 15% of the output pulses are recorded below the emulsion fog level. At the lowest applied voltage while $\bar{\varepsilon}_2$ falls, $\bar{\varepsilon}_1$ must also depart appreciably from unity.

2.8.3 The transmitted secondary emission intensifier

The value of $\bar{\varepsilon}_r$ has been measured by several groups at Imperial College. Binnie et.al.[74] have estimated the value of $\bar{\varepsilon}_r$ in two different experiments. In the first, tracks of minimum ionizing particles were recorded in Na I(Th), Cs I_2, plastic and glass scintillators using a 20th Century Electronics tube with a 20 μA/Lm cathode and an English Electric tube with a trialkali cathode of 100 μA/Lm. By comparing the number of spots/cm of track calculated to that actually obtained an estimate of $\bar{\varepsilon}_r$ was obtained. It was found that $\cdot 25 < \bar{\varepsilon}_r < \cdot 5$. In a second experiment, counting the spots photographed forming a Cerenkov ring to that calculated, a more accurate value of $\bar{\varepsilon}_r \simeq 30\%$ was obtained. This latter value of $\bar{\varepsilon}_r$ is for the English Electric tube only.

Sephton and Davison[75] have counted the number of output scintillations due to a given photocurrent, using a photomultiplier and a photographic emulsion. It may be assumed that when a photomultiplier is used $\bar{\varepsilon}_2 \simeq 1$, therefore $\bar{\varepsilon}_r \simeq \bar{\varepsilon}_1$. In this case it was found that $\bar{\varepsilon}_1 = \cdot 4$. This means that 60% of the signal information is lost inside the image intensifier. Using a photographic emulsion $\bar{\varepsilon}_r \simeq \cdot 3$. From these two measurements it is seen that $\bar{\varepsilon}_2 \simeq \cdot 75$.

Todkill[76] has found, using a single stage tube, that 50% of the primary photoelectrons gave no secondary electrons at all at the dynode i.e. in a single stage tube $\bar{\varepsilon}_1 = \cdot 5$.

2.8.4 The channelled secondary emission intensifier

No measurement has been made of $\bar{\varepsilon}_r$ for this type of image intensifier. The mean deviation in the distribution of output scintillation intensities is intermediate between that described by assuming a Poissonian distribution and an exponential distribution. The coefficient of secondary emission at a dynode is approximately half that for a T.S.E. dynode. It may be assumed therefore that $\bar{\varepsilon}_r$ for a channelled secondary emission intensifier is less than that of a T.S.E. tube.

2.8.5 Electronographic image intensifiers

(a) The Lallemand device

Since almost every photoelectron is recorded $\bar{\varepsilon}_r \simeq 1$.

(b) The barrier membrane device and the Lenard window tube

In both types the value of $\bar{\varepsilon}_1$ departs from unity because of the fraction of electrons lost in the membrane.

In the Lenard window tube $\bar{\varepsilon}_1 \simeq \cdot 7$. Although there is an appreciable spread in the energies of the electrons transmitted through the mica window, only a few percent are not recorded because of this distribution. This is due to the fact that the fog level i.e. the discrimination level in an electron sensitive emulsion is extremely low.

Therefore $\bar{\varepsilon}_2 \doteq 1.$

Hence $\bar{\varepsilon}_r \doteq \bar{\varepsilon}_1 \doteq .7$

2.9 Spurious noise in image intensifiers

When a limited number of photoelectrons are available for recording, the most troublesome noise is from spurious output events equalling in intensity, or effect, many photoelectron output events. This noise seems to originate at the photocathode and is probably due to positive ions, formed by photoelectrons colliding with free molecules, being accelerated towards the photocathode and ejecting 10-20 electrons.

In a multistage image intensifier this noise figure could be several hundred scintillations/cm^2/sec. In a photographic exposure of several milliseconds, in order that the total light output from a 10 cm^2 P11 phosphor may be integrated, the noise may be of the order 10 scintillations. In extreme cases this noise could equal the total number of signal scintillations. When an image intensifier is used for high speed photography, and an electrostatic shutter is incorporated in the primary photocathode stage to provide gating pulses of nano-second duration, this noise is in effect eliminated. Using a T.S.E. tube with full applied voltage, Sephton[43] found that if the photocathode were "turned off" by applying a negative bias to the first accelerating annular ring, exposures of up to 10 seconds could be taken without bright scintillation noise appearing.

Catchpole[36] has had similar experience using a cascade image intensifier. If noise originates at the second photocathode of a three stage cascade intensifier, its output intensity is proportional to the gain in the last two stages only, which is a factor of ≐ 100 less than the overall gain. This noise may be greatly reduced when a tube is used for high-speed photography by incorporating an electronic shutter of millisecond duration in the last stage to operate in conjunction with the shutter at the primary photocathode.

Some of the spurious noise, produced at the output of a T.S.E. tube is due to the amplification of penetrating primary electrons. A penetrating primary electron is arbitrarily defined as an electron emitted from a dynode with an energy of 50 e-V. These "fast" electrons are not focused at the next dynode. Todkill[76] has found that ≐ 10% of the total number of signal scintillations at the output lie outside the image area. This signal induced background is due to penetrating primaries. In a cascade tube the multiplying sandwich membranes are sufficiently thick, 5 μ, to prevent the penetration of primary electrons accelerated to the normal stage voltage of 15KV.

Electronographic devices have been constructed with very low internal noise. An electron sensitive emulsion has been exposed for 5 hours in conjunction with a Lenard window tube, operated at full applied potential without the background noise produced by the device becoming distinguishable from the fog level of the emulsion, which is

$\log_{10}D = \cdot 02$. The photocathode dark current is negligible at the very short exposure times required.

2.10 The choice of image intensifier

The most important parameter in the choice of an image intensifier, which has to record a very small number of photoelectrons is $\bar{\varepsilon}_r$.

The Lallemand electronographic device has the highest value of all the image intensifiers reviewed here. It has, however, many disadvantages in use arising from its demountable nature. Many hours of preparation are needed before it may be operated.

The barrier membrane device suffers from the same disadvantages of semi-demountable operation.

The Lenard window tube has the advantage of being completely sealed off. The value of $\bar{\varepsilon}_r$ for the Lenard window in the best tube case measured, is $\cdot 7$, which is lower than the best measured value of $\bar{\varepsilon}_r \simeq \cdot 85$ for a multistage cascade tube. In both cases the value of $\bar{\varepsilon}_r$ given is a mean value. The resolution of the Lenard window device is 80-90 lp/mm, whereas the best multistage tube has a resolution of 20-25 lp/mm. In both cases the number of picture points available is $\simeq 5.10^6$ since the diameter of information channel of a multistage tube is 40 mms and the generally useful area of the Lenard window is 1 cm^2.

Of the multistage image intensifiers, the cascade tube has the highest measured value of $\bar{\varepsilon}_r$, namely $\cdot 85$. Its performance indicated by the value of $\bar{\varepsilon}_e$ is generally better than either the T.S.E. tube

or the channelled image intensifier. The smaller mean deviation in the distribution of the output scintillation intensities results in a more uniform distribution of the diameters of photographically recorded scintillations. Greater accuracy of measurement is therefore achieved.

The cascade image intensifier has been shown to be the most suitable image intensifier for general application in case 1.1.(3). It has adequate gain and resolution and also a high value of recording efficiency. In this application its quite high background noise does not limit its performance. The phosphor screen output is more versatile than an electron output and permits the use of known optical recording techniques.

Chapter 3 The development and use of electron optical devices for high speed photography

3.1 The use of infra-red image converters as light shutters

Infra-red image converters were developed just before and during the Second World War for military use in night observation. A photocathode which is sensitive to infra-red radiation was used as detector, the output being observed as visible light from a phosphor screen.

In England the E.M.I. type CV144 image converter[77] consisted of a photocathode and phosphor screen 5mms. apart in a vacuum envelope. No special electrostatic focusing system was employed, resolutions of 350 lines/inch being obtained by applying an accelerating voltage of 3 to 10KV. The German A.E.G. Bildwander tube[78] and the American R.C.A. IP25[79] gave similar performance, their more elaborate electrostatically focusing systems taking longer to develop. The latter two tubes were more useful as high speed shutters. Their higher accelerating voltage (15 to 20KV) producing a brighter output image and their internal electrodes enabled switching at lower voltages.

Courtney-Pratt[80,81] in 1949 was the first worker to suggest the use of image converters for high speed photography. In his early experiments he used the A.E.G. Bildwander tube to study the detonation of lead azide. He demonstrated the three types of operation of which an electron optical device is capable.

(1) Streak or smear photography, in which a point or line electron image is deflected across the output phosphor to observe its variation with time. A set of external magnetic coils were used to obtain a deflection of the electron beam of ≏ 2,000 m/sec on the output phosphor.

(2) Single frame photography, in which an internal electrode is electrically pulsed to permit the electron beam to reach the output phosphor. Another frame may not be taken until the first image has decayed to negligible intensity on the output phosphor.

(3) Multiple frame photography, in which a series of sequential images are displayed on separate areas of the phosphor screen. Courtney-Pratt obtained a sequence of nine images, having a frame time and interval of ≏ 1 msec, using phased magnetic deflection fields.

The R.C.A. IP25 was used by Markstein[82] stroboscopically to observe periodic flow disturbances in the infra-red radiation from flame gases. Hogan[83] has also used this tube stroboscopically up to several thousand cycles/sec., and has obtained single frames of duration 2 usec.

3.2 The use of television cameras as light shutters

About the same time that Courtney-Pratt suggested using the infra-red converters for high speed photography, Saxe and Prime[84] suggested using a television camera for the same purpose. Prime and Turnock[85] experimentally investigated these suggestions using

the Emitron television camera. It was proposed that charge images be prevented from forming on the photoemissive mosaic surface by applying a retarding electric field large enough to prevent electron emission. In order to do this the final anode (collecting ring) was biased to 100 volts negative from its normal earth potential. An electrical pulse of 150 volts positive was applied to the anode to obtain saturated photoemission. It was found that the mosaic still retained approximately 1/25th of its sensitivity when "biased off". There was some image spreading due to charge leakage. It was felt that the Orthicon and Image Orthicon would be more satisfactory in these respects. Devaux[86] found that it was impossible to make use of a Vidicon tube as a high speed shutter owing to the excessive inertia of the sensitive layer.

3.3 Simple image intensifiers developed as light shutters

The first image intensifier to be specially designed for high speed photography was the ME1200-ME1201 type of tube made by Mullards Ltd.[87,88] It consisted of a photocathode, a cylindrical accelerating electrode and an output phosphor. The photocathode used was either Sb-Cs or Ag-O-Cs of 25mm diameter. Since most light sources are in the 4,200 Å region of the spectrum, the Sb-Cs photocathode is generally more useful than the Ag-O-Cs. The cylindrical electrode enabled entirely electrostatic focusing and was employed as the gating electrode. The output phosphor was either Willemite having a decay time of a few msec, or ZnS(Ni killed)

having a 5 μsec decay time. The former allows stroboscopic operation of ≙200 frames/sec, the latter ≙200,000 frames/sec. The overall applied voltage was 6KV, the focusing electrode voltage 3KV. The resolution at the output phosphor was ≙25 lp/mm.

Courtney-Pratt[81] achieved streak photography speeds of up to 60,000 m/sec using the ME1200. Richards[89] developed electrical circuits in order to operate the ME1201 in the three modes of operation described above. Gibson et.al.[90] have applied gating pulses of up to 14KV using coaxial pulse shaping lines, of duration ≙100 mus.

Saxe and Chippendale[91,92] extended this technique of applying high voltage pulses by coaxial lines in the photography of spark discharges. The spark chamber and the ME1201 AA were enclosed in a matched coaxial line system of 13Ω impedance. A large voltage drop appears across the chamber when the spark occurs. This is shaped into a square transient by the cable and is applied to the image tube as a gating pulse. Total exposure times of down to 7 μsec were obtained using this technique. Grover[93] and Curzon[94] have prefered to operate the ME1201 in diode operation with the grid and the anode coupled together. It was found that in triode operation, image rotation and blurring occured, due to the turn off pulse on the grid. Exposures of down to 10 μsec were achieved using a line pulse circuit having two coaxially constructed thyratrons as a switch. King and Hett[95] have used the ME1201 tube as a framing

camera at rates of 2.10^4 - 2.10^6 frames/sec having 4-8 images in each output display.

In 1957 Linden and Snell[96] theoretically derived focusing conditions for both electrostatically and electromagnetically focusing image intensifiers of triode construction.

Stoudenheimer and Moor at R.C.A.[97] applied these conditions in the design of an image converter having highly efficient gating and deflecting grids. The converter has two focusing grids and two deflecting electrodes. A resolution of 22 lp/mm was achieved applying an overall voltage of 15KV. The tube may be gated on with 17V/KV and off with 4V/KV at speeds down to 10 mμs. The deflecting voltage required is 75V/inch/KV.

Zavoiskii et.al.[98, 99] started to develope in Russia, from 1949 onwards, a series of high speed shutter tubes. The first was the PIO-I, having an electrostatically focused triode structure. Gating pulses of 20KV were applied to obtain exposure times of down to 100 mμs. A geometrical resolution of 60-70 lns/mm (the translation from Russian states "strokes/mm", but lp/mm are probably meant) was achieved. The tubes of type PIM-3 and PIM-4 incorporated a new type of shutter. The initial tubes were single-stage devices and entirely electrostatically focused consisting of a photocathode, the shuttering electrodes and an output phosphor. The electron beam from the photocathode is deflected across a small retangular aperture in a flat plate to obtain a short time resolution. A second pair of

deflecting plates placed just after the aperture having a deflection sensitivity equal and opposite to the first pair, ensures image immobility during exposure. Two pairs of oscilloscope deflecting plates, orientated at right angles to each other, are incorporated to deflect the image of any part of the output phosphor screen. Screening plates are placed between the deflecting plates to avoid field interaction between them. The deflector plates of PIM-4 have approximately twice the sensitivity of PIM-3. The PIM-3 has an output screen diameter of 70 mms, the PIM-4 a diameter of 140 mms.

The geometrical resolution of 60-70 lns/mm in the centre of the output phosphor falls off to 2/3 this value at the edge. The exposure time was limited to $\simeq 10^{-8}$ sec. in the early work by the speed of electronic circuitry. The primary purpose of the oscilloscope deflecting plates was to produce a series of consecutive frames spaced round the output phosphor. Komelkov et.al.[100] have developed electronic circuitry which applies multistep deflecting pulses to the horizontal and vertical plates of the oscilloscope type and rectangular pulses to the shutter plates. The number of frames in a row and the number of rows were determined by the number of steps of the deflecting pulses. The repetition rate of the camera was determined by the time interval between steps. Exposure was made at the moment the image stopped. Speeds of up to 5.10^{6} frames/sec have been achieved, with exposures as brief as 50 μsec. The total number of frames in a series was 16. The frames size was 5 mm by

5 mm with geometrical resolution of 30 lns/mm. Nesterikhin and Komelkov[101] have achieved better time resolution and larger frames by taking consecutive single pictures on separate tubes. Several single-stage PIM-3 tubes were used with no deflector plates. The control circuits needed were simpler and more reliable. Speeds of 3.10^7 frames/sec were achieved with exposures of down to 15 mμsec.

Zavoiskii and Fanchenko[102 103] have extended the temporal resolution by operating a PIM-3 or PIM-4 tube in the "electron optical chronographic mode" described below. This technique may only be applied to substantially point images, whose luminous intensity varies with time. The shutter plates were used to select an event of $\simeq 10^{-9}$ sec duration. The oscilloscope deflecting plates were pulsed to sweep the electron beam round an arc of a circle approximately equal to the size of the output phosphor. They have shown theoretically that the minimum time resolvable is $\simeq 10^{-14}$ sec.

In England, Mandel[104] has developed a photoelectronic shutter which requires extremely low voltage for its operation. In its final form it consists of two metal meshes mounted a few centimeters from the photocathode in a magnetically focused simple image intensifier. The first mesh acts as a control grid, whilst the second acts as an auxiliary electrode. Its introduction increases the control sensitivity and makes the electron focus less dependent on the control mesh potential. Shutter tubes, having an off-on control voltage range of about 3.V and a resolution of 15-18 lp/mm

were made.

3.4 Multistage image intensifiers incorporating electron optical shutters

The first image intensifier of high light gain, incorporating an electron optical shutter was developed in Russia, using the cascade image intensifier made by Butslov in 1952[105]. The first half of the tube incorporating the PIM-3 or PIM-4 type of shutter tube was entirely electrostatically focused, the second half incorporating the intensifier was magnetically focused. The final output resolution was ≃10 lp/mm. Simonov and Kutukov[106] have used mismatched coaxial cables to generate the deflection and shutter pulses. The framing rates achieved ranged from 10^6/sec to 10^8/sec. The exposure times could be made as large as the interframe times, or as short as 5.10^{-9} secs. The step impulses required were of several kilovolts amplitude, their shapes being within •1% of the theoretical shape to obtain a resolution of 10 lp/mm. The number of frames in a sequence were 6 to 15. The light gain of the three-stage intensifier was 8,000.

Huston and Walters[107] have produced an exactly similar shutter to that in the PIM-3 and PIM-4 tubes. The shutter section is to be incorporated in a image intensifier of the type described by Chippendale and Folkes[108]. The shutter has all the characteristics described for the PIM-3 and PIM-4 tubes. The intensifier consisted of a self-supporting selenium layer upon which was deposited an

aluminium signal plate, and an electron gun which scanned the selenium target in the vidicon principle. The electron image was focused upon the target, arriving with sufficient energy to penetrate the signal plate and to produce bombardment induced conductivity in the selenium. The charge stored at the target, which was many times greater than the primary photoelectron charge, was scanned by the "reading" section of the tube. The tube output was developed across a load resistance and could be recorded by normal television means. The threshold detectivity of 50 photoelectrons per image point, limited the range of tube operation.

The photoelectric shutter developed by Mandel[104] has been incorporated in a T.S.E. image intensifier of the type developed by Wilcock et. al.[40]. The resulting tube had a blue light gain of $\simeq 10^5$, a geometrical resolution of $\simeq$8 lp/mm and a shutter speed of nanosecond duration.

When an exposure of 1 μsec or longer was required using multistage image intensifiers many workers have found it convenient to apply gating pulses to focusing electrodes or whole stages of the image intensifier. In this case no special photoelectric shutter was required. Emberson[109] has described the operation of a T.S.E. image intensifier gated by (a) diode switching and (b) ring switching. In diode switching the focusing annular rings were held at the normal potential and the photocathode was pulsed on by applying a 2KV negative pulse. In ring switching, the first annular ring was biased

to turn the tube off, and was pulsed to 450V to switch the tube on. The tube was then operating in a non-uniform focusing field which produces slight distortion. However, the lower voltage required in combination with the lower resistance and capacity across which the gating pulse was applied, resulted in faster switching. Speeds of down to 0.1 μsec were achieved. In both modes of switching, geometrical resolutions of ≃ 10 lp/mm were obtained.

3.5 Physical experiments requiring the use of an image intensifier containing an electron optical shutter

During the last ten years, the development of image intensifiers capable of recording single photoelectrons along with the possibility of extremely fast electron optical shutters has led to the investigation of phenomena not previously observable. The type of photon distribution in these cases was indicated in section 1.1.(3).

3.5.1 Experiments with spark gaps and vacuum discharges

The first experiments to observe D.C. breakdown across a spark gap were those of Saxe and Chippendale[91, 110] in 1955 using the ME1201 image converter. The luminous intensity, produced by the breakdown in air at atmospheric pressure across a gap .77 cm wide, was sufficient not to require intensification to be photographically recorded. The image tube provided an electron optical shutter of a few nanoseconds. It was found that the breakdown occurs in two phases. In the first phase, a diffuse glow completely bridges the electrode gap. In the second phase, a filamentary channel moves from

the cathode to the anode in $\simeq 3.10^{-9}$secs.

The study of the formation of sparks of 10^{-10}secs total duration in air, N_2 and H_2 at pressures of up to 20 atmospheres requires the use of an intensifier having a light gain of 10^3 to 10^4 and a temporal resolution of 10^{-11}secs. Zavoiskii and Fanchenko[102,103] have used a PIM-3 image tube, operated in the "electron optical chronographic mode", for this work. Later work[111] has extended this study of the initial stages of the channel expansion of a spark to oxygen and deuterium. The maximum rate of current rise was $\simeq 3.10^{12}$ amps/sec. It was found that the initial expansion is due to a shock wave which travels, in the case of deuterium, at 7.10^6 cms/sec.

Zavoiskii and Smolkin [112] have again used electron optical chronography to investigate the time resolution of a pair of parallel plate spark counters. Babkin et. al.[113] have used the same technique to measure the time interval between the passage of a cosmic ray particle through two spark counters. It was found from the microphotometered photographs of the circular sweeps, that the spread in the transit times between the two counters for the cosmic rays was $<4.10^{-10}$secs.

Simonov and Kutukov[106] have studied the low density plasma produced when a large current is passed through a wire, placed initially in a vacuum, causing it to give off gas. A PIM-3 converter having a light gain of 8,000 was used taking a series of frames of

5.10^{-8} secs duration at intervals of 10^{-7} secs.

3.5.2 Time resolved spectroscopy

It is of interest to investigate the variation with time of a spectral line produced by Fabry-Pérot etalon and a monochromator. The usual mechanical methods of obtaing spectral line profiles limit the temporal resolution to $\simeq 5.10^{-5}$ secs. Malyshev et.al.[114] have used the PIM-3 image converter to obtain resolving times of a few μsec.

Akhamtov et.al.[115] have used the image sweeping characteristic of the PIM-3 device to study magnetoacoustic resonances in a cold plasma. The resonance absorbtion of the energy of the electromagnetic field at frequences of 12.5 Mc/s and 50 Mc/s were studied by sweeping the image of the glow discharge at sweep speeds of μsec/cm.

Butslov et.al.[116] have used an image shaping tube to deliver a shaped spectrum to the photocathode of the normal PIM-3 shutter tube. The shaping produced a 70 times compression of the spectral line height and a 3 times extension in line width by the use of a quadrupole magnet. The electron density of the spectral lines was increased 20 times. A resolving time in the μsec region was produced by this method.

3.5.3 The photography of nuclear particles in Luminescent chambers

The passage of a nuclear particle through a homogeneous scintillating crystal produces radiation in the visible spectrum. The particle track can be recorded photographically, if an image

intensifier, having a blue light gain of 10^4 to 10^6, is interposed between the chamber and the camera. The geometry of the single crystal scintillator is shown in fig. 2(a). The parameters of some scintillators are given in fig. 2(b). These values were compiled by Perl and Jones[117]. The crystal efficiency shown by N is always given for a particle producing a minimum ionizing track. The slower particles will produce greater numbers of photons, so it is the worst case that is being considered. The chief advantage of scintillation chambers is that their time resolution is 10^{-6} sec or less. An image tube can be gated at this speed to record a particle track. The image is usually stored on an intermediate phosphor screen until electronic selection can be completed. It can be seen from fig. 2(b) that the most attractive scintillator available is unactivated Cs I cooled to 77°K. (It appears that the high efficiency of Cs I, claimed by Perl and Jones, has not been repeated). It does however, limit the maximum rate of particle flux to $\simeq 10^6$ particles/sec if only single interesting particle tracks are to be recorded.

It has been shown by Perl and Jones[118] that the number of photoelectrons, n per cm of image track for unity optical magnificatio is given by

$$n = \mathcal{E}_o N E \frac{a^2}{d^2}$$

Where $\mathcal{E}_o$ is the quantum efficiency of the photocathode, N the number of light quanta per cm of track, E the lens coupling efficiency

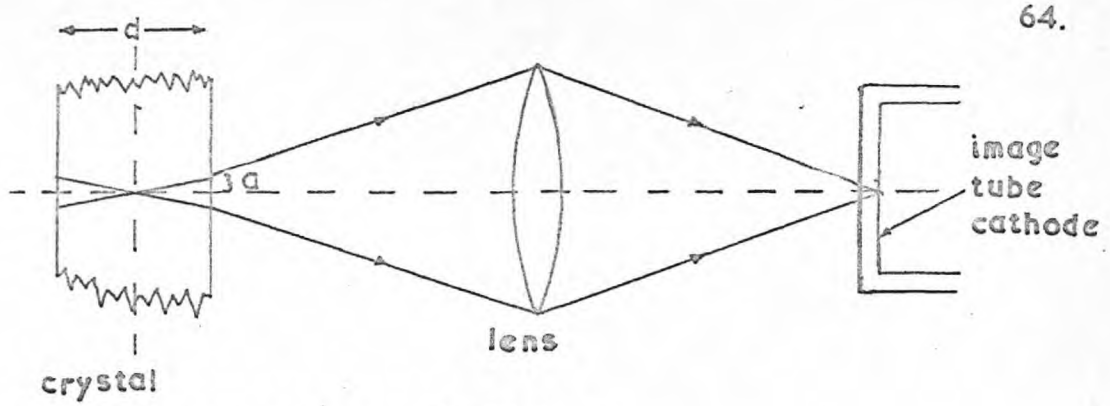


FIG. 2(a) Single crystal scintillator

Material	Decay time sec	Scintillator Efficiency	No. of quanta per cm. of track length, N
Plastic	$<10^{-8}$	6%	42,000
Anthracene	10^{-8}	10%	70,000
NaI(Th)	$\cdot 5.10^{-6}$	8%	115,000
CsI(Th)	$1\cdot 5.10^{-6}$	8%	140,000
CsI(77°K)	$<10^{-6}$	59%	1,000,000

FIG. 2(b) Some scintillator parameters

Material	n	Crystal resn.(cm.)	Max. depth focus(cm.) (R=10,000)	Max. cross sect.(cm.)	F/Number
NaI	50	·01	·2	1	1·4 onto 2 cm. cathode
	5	·1	7	10	1·6 .. 2 .. .. / 4·8 .. 10 .. ..
	2·5	·2	19	20	4·4 .. 10 .. ..
	1	·5	73	50	3·4 .. 10 .. ..
Plastic	5	·1	3	10	·8 .. 2 .. .. / 2·5 .. 10 .. ..
	1	·5	31	50	1·7 .. 10 .. ..
	5	2	160	200	7 .. 10 .. ..

FIG. 2(c) Some geometrical parameters of the crystal chamber

a the maximum radius of the circle of confusion and d is the crystal thickness.

The value of a sets the limit on the spatial resolution of the scintillation chamber. The depth of focus, and thus the useable crystal thickness, depends on the F/number of lens used. If there are R resolution elements in the image intensifier system, it is important that the cross section dimensions of the crystal be less than $a\sqrt{R}$. If this were not the case, there would be more image elements than the intensifier could transmit. Some parameters of the scintillation chamber recording system are given in fig. 2(c) for a Na I and a Plastic scintillator. It can be seen that in the case of a plastic scintillator, of dimensions 10 x 10 x 3 cms a minimum ionizing particle would produce 5 photoelectrons/cm of track length using an F/.8 lens. The track resolution in this case is .5 lp/mm. If under the same conditions Cs I at $77^{\circ}K$ were used 125 photoelectrons/cm of track length would be produced.

Reynolds and Condon[119] in 1957 manufactured a new type of lumincescent chamber consisting of a parallel array of plastic filaments. These filaments of .5 to 1 mm in diameter were placed in close contact to each other. The chief advantage of this chamber is in the use of the plastic material. Its fast decay time, i.e. $<10^{-8}$ sec. enables high particle flux rates to be used. High flux rates coupled with high selectivity enable the investigation of rare events which are important to substantiate theoretical work.

The construction of the plastic chamber in filamentary form rather than as an homogeneous one enables a greater fraction of available photons produced to reach the photocathode. The various methods of coupling a chamber to an image tube are shown in figs. 3(a), 3(b) and 3(c). The lens coupling method shown in fig. 3(a) preserves the resolution, but 80% of the light is lost in transmission. The chamber may be directly butted to the face of the image tube, fig. 3(b), preserving most of the intensity, but degrading the optical resolution. If a glass fibre face plate is incorporated into the image tube, fig. 3(c), luminous intensity and resolution can be preserved. Potter and Hopkins[120] have compared various coupling methods when the tube is required to be some distance away from the chamber. One of the most efficient methods, shown in fig. 4 is to couple the plastic chamber to the lens by glass fibres. This method is 2.5 times more efficient than normal lens coupling.

Reynolds[121] and Condon[122] have calculated that the mean number of photons produced at the end of a single fibre, due to a minimum ionizing particle, is 190. In this case the fibre was 10 cms long and 1 mm in diameter. If the lens coupling efficiency for this radiation were 10% and the quantum efficiency of the photocathode were .1, then $\simeq$ 2 photoelectrons would be produced per excited fibre. Waters et.al.[123] have found that when μ mesons crossed 35 filaments, the mean number of filaments recorded was 13 i.e. a 37% recording probability.

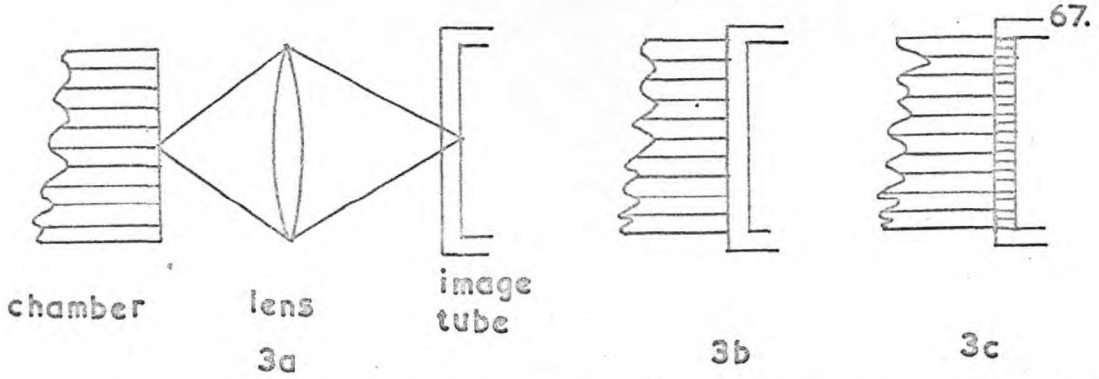


FIG. 3 Three types of optical coupling for a filamentary chamber

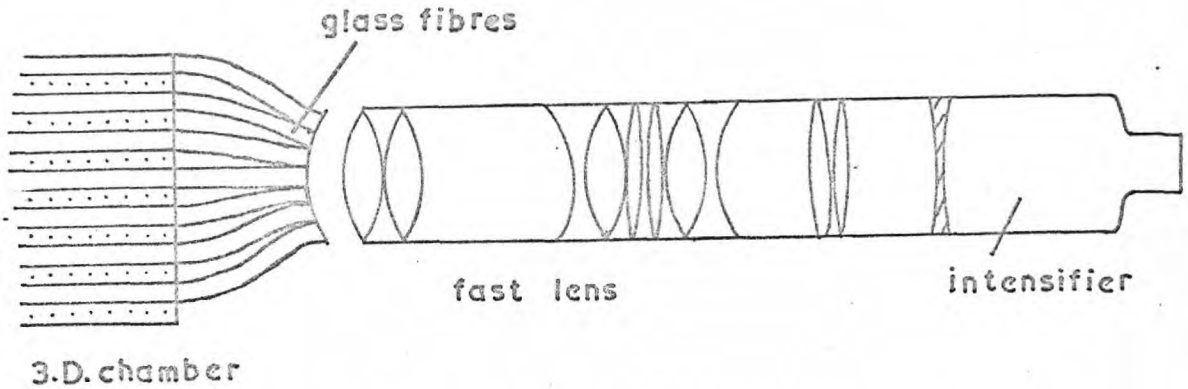


FIG. 4 An efficient optical coupling system for large chamber–intensifier separations

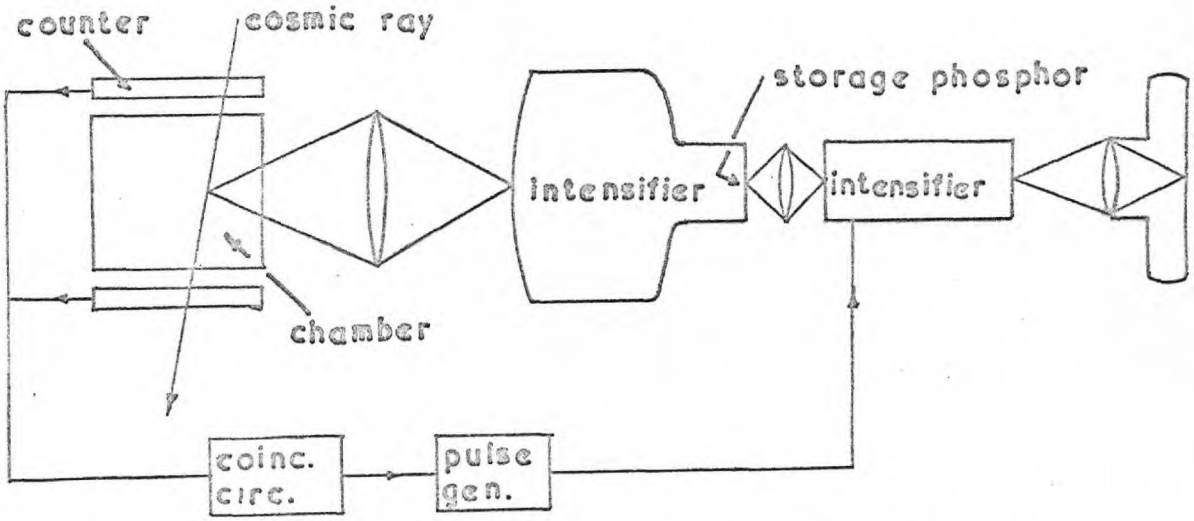


FIG. 5 A general image intensifier system for recording scintillation tracks

In general, under the same conditions, the performances of the homogeneous and the filamentary chamber is the same, i.e. image resolution of ≃1 lp/mm and ≃5 photoelectrons per cm of image track. The time resolution of the plastic filamentary chamber is ≃100 times lower than that of a comparable homogeneous chamber. The experimental arrangement of the chamber and image intensifier used to record nuclear tracks is shown in fig. 5. The image of the nuclear track is focused onto an image tube and is stored on an intermediate phosphor which has a fast decay time. P15, P16 and P24 phosphors having decay times of 3 μsec, ·1 μsec and 1·5 μsec respectively, have been used. This time allows a coincidence counter system to trigger a pulse generator, which can switch on a high gain image intensifier. The selected event is thus intensified, excluding extraneous events, and may be photographically recorded.

The first successful application of image intensifiers for the photography of elementary particle tracks in a luminescent chamber was made by Zavoiskii et.al. in 1952[30,105]. They photographed "stopping" and minimum ionizing protons and also cosmic ray tracks in a Cs I(Tl) homogeneous chamber. Also in Russia, Demidov and Fanchenko[124] have used the intensifying PIM-3 tube to photograph cosmic rays.

Butslov et.al.[125] have used four blocks of filamentary scintillator and three image intensifiers to measure the elastic scattering at small angles of charged particles.

In the U.S.A. Reynolds et.al.[119,121] developed the plastic filamentary chamber. Various arrangements of image intensifier systems have been used by Reynolds and his group at Princeton University[126,127] to investigate the interactions of both the π and μ meson component of cosmic rays. Perl and Jones[128] of Michigan University photographed in 1959 cosmic ray μ meson tracks in a Na I(Tl) chamber. They describe the use of such a chamber to record nuclear tracks of particles produced by a Bevatron accelerator in several papers[129, 130, 131]. An image intensifying system essentially similar to the Michigan arrangement has been used by Hill et.al[132] at M.I.T. In this case the final output was taken from from a R.C.A. intensifier orthicon system in conjunction with a Kinescope and camera. Lande et.al.[133] have also successfully used a similar scintillation chamber assembly.

All the experiments described above have used image intensifiers employing the cascade principle. Goetze et.al.[134,135] at the Westinghouse Research Laboratories are the only group in the U.S.A. to have used T.S.E. image intensifiers. In 1961, they reported the photography of minimum ionizing tracks in Na I(Tl) using two 4-stage tubes in cascade.

At Bonn University, Geise and Gildermeister[136] have built a three-stage cascade intensifier and photographed minimum ionizing cosmic ray particles in a Cs I crystal.

At Imperial College, London, Binnie et.al.[7] using two

T.S.E. image intensifiers in tandem have recorded photon tracks in Na I(Tl), Cs I(Tl), plastic and glass chambers.

3.5.4 The recording of Cerenkov rings using image intensifiers

When a particle traverses a radiating medium Cerenkov light is emitted only at an angle Θ to the direction of the particle, where Θ is given by $\tan \Theta = 1/\beta n$; βc being the particle velocity and n the refractive index of the radiating medium. An optical system of focal length f will, therefore, produce a ring of radius f tan Θ in the focal plane. Consequently, a measurement of the size and position of a ring should give a sensitive measure of the particle velocity and direction.

The use of an image intensifier system for the purpose of recording Cerenkov rings was first proposed by Roberts[137] in 1960. The number of "spots" expected on the photograph, due to the Cerenkov ring, is given by the expression,[138,139]

$$N = \frac{\pi \alpha r \eta}{A} \int \frac{1}{\lambda^2} T(\lambda) S(\lambda) d\lambda$$

where α is the fine structure constant, r is the radius of the ring image, η is the probability that a single photoelectron be recorded, A is the ratio of the image distance to lens aperture, λ is the wavelength of the radiation, $T(\lambda)$ is the transmission of the lens and $S(\lambda)$ is the spectral response of the photocathode. In practice N is < 10 spots per ring.

The general experimental arrangement of the Cerenkov camera is shown in fig. 6. The passage of a particle through the radiator

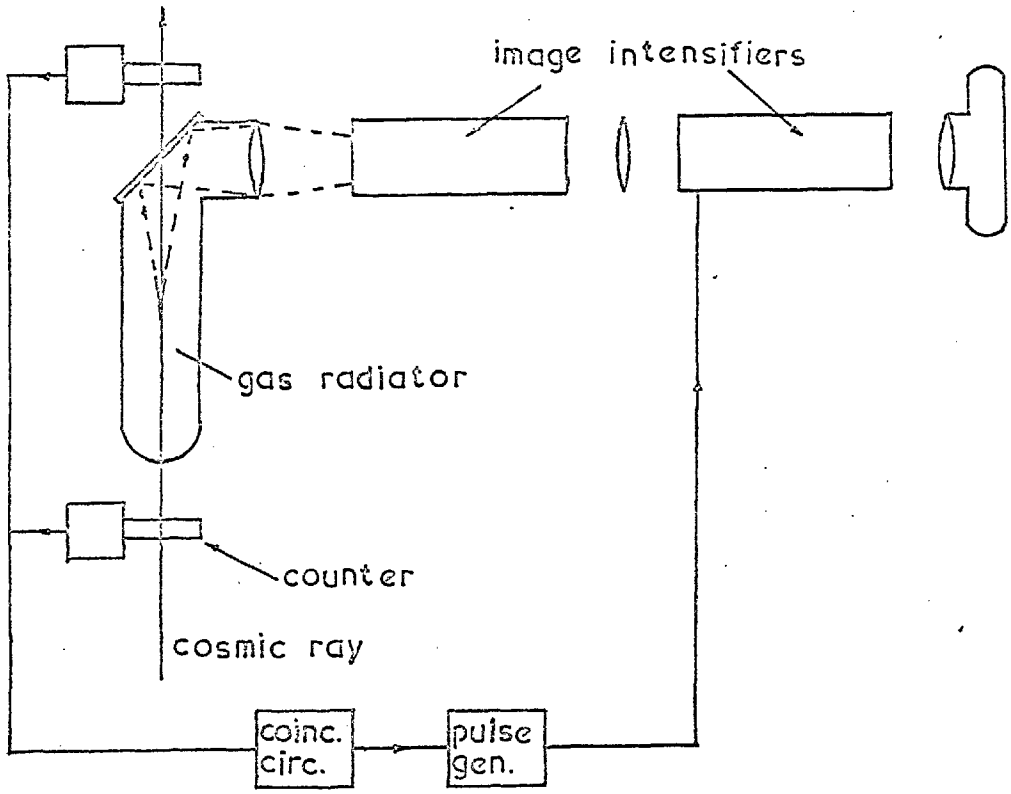


FIG. 6 The Cerenkov-ring camera

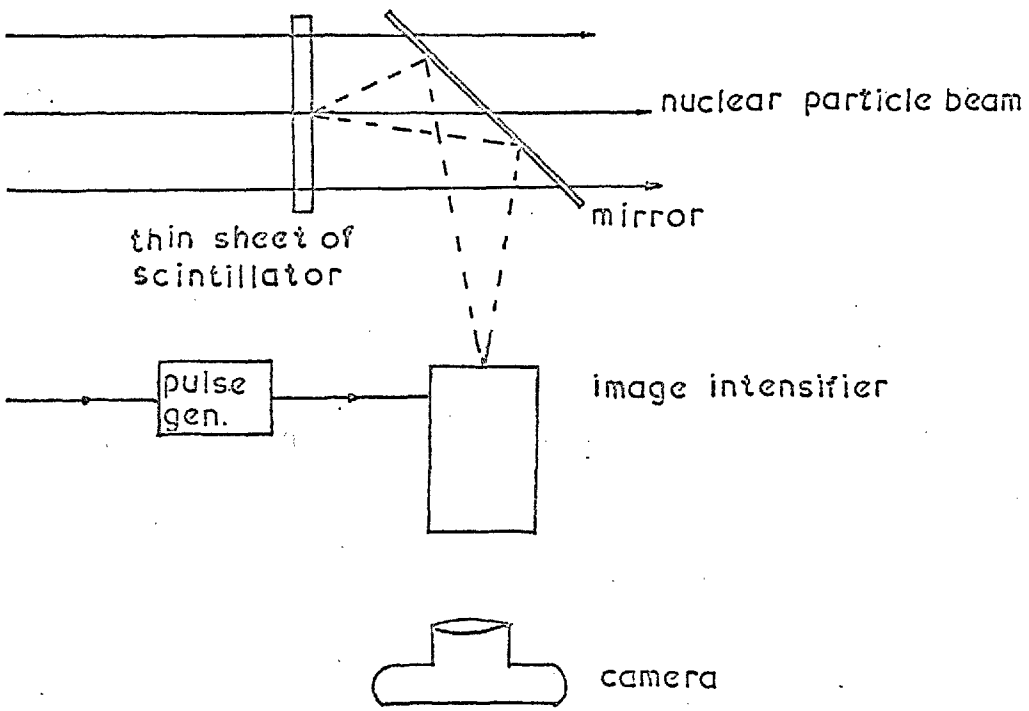


FIG. 7 A particle beam profile camera

produces a cone of Cerenkov light, which is focused by an optical system to form a ring image on the photocathode of the image intensifier. This information is "stored" on the output phosphor of the first tube until a gating pulse from the coincidence counters turns on the second image intensifier. The Cerenkov ring is thus selectively recorded photographically.

Poultney et.al.[139,140] were the first group to successfully photograph a focused ring of Cerenkov light from a single particle. They photographed rings produced by 820 meV/C negative mesons passing through a lucite cone radiator. 4 to 6 spots per ring were observed depending on the gain in the intensifier system.

Butslov et.al.[141] have photographed rings of Cerenkov radiation produced by the passage of single cosmic rays through plexiglass.

Binnie et.al.[142] using the low intensity 700 meV/C proton beam from the Saclay accelerator have photographed the Cerenkov rings of single pions. The gain required in the image intensifier system was 3.10^4.

3.5.5 The determination of nuclear particle beam profiles

It is often quite important to accurately locate a beam of nuclear particles. A photographic film or small scintillation counter can easily detect a beam having greater than 10^5 particles/pulse Jones and Perl[143] suggested the use of a small scintillation chamber used in conjunction with an image intensifier to locate weak beams ($< 10^3$ particles/pulse). Both Jones and Perl[143] and Waters et.al.[144

have used a small filamentary chamber directly butted onto the face plate of an image intensifier for this purpose. Binnie et.al. [74] have used a variety of scintillator arrangements, a typical one being shown in fig. 7.

3.6 Electron image delay using transit time storage

One requirement of most of the experiments indicated in section 3.5 is the ability of the electron optical system to store an image while decision circuits switch on a following section, acting as a fast gate. A typical system is shown in fig. 5. The image in these experiments, was stored using the decay time of a fast phosphor. If sufficient image intensification was provided before and after the phosphor store, a negligible fraction of information was lost due to only the decay tail intensity being gated through the output section. This loss of light always occured since the fast phosphor received the image and started to decay in less than 10^{-8} sec after the image formation while the command signal reached the electron gate in $\simeq 10^{-7}$ sec. The electron gate was opened for a time of $\simeq 10^{-6}$ sec since the decay time of the fast phosphors was of this order.

The initial fast decay of P15 is followed by a long slow decay component. Thus if the particle flux rate is high many unwanted pictures would build up a persistence pattern on the output phosphor which would constitute an unwanted noise output. Hill et.al. [132] have estimated for a P15 phosphor that if events occur at rates of

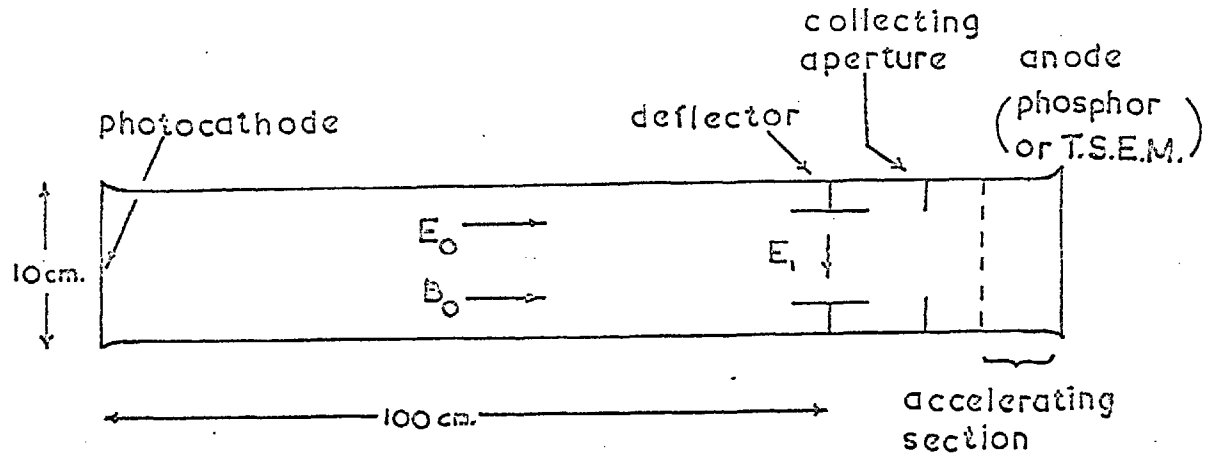


FIG. 8 A transit-time image storage tube

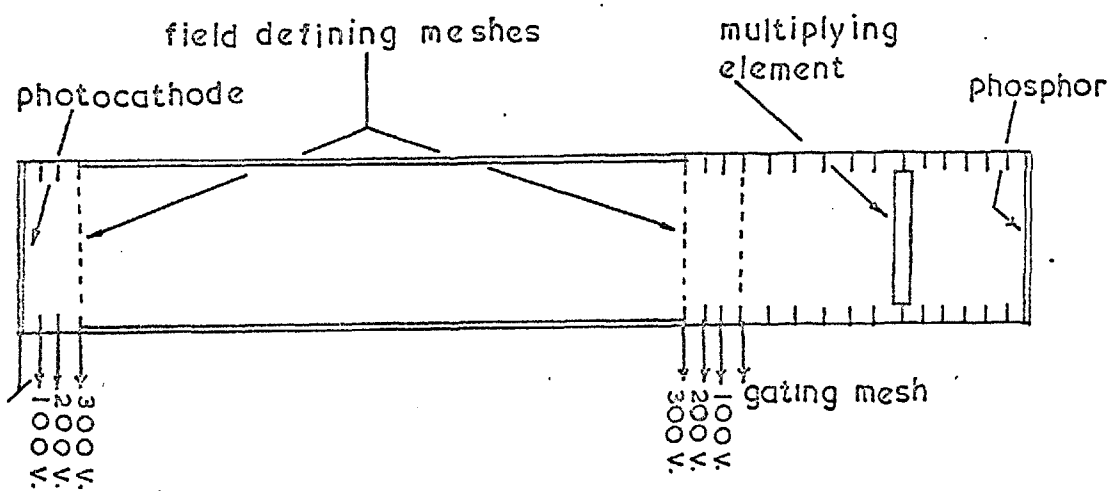


FIG. 9 An electron image delay tube

greater than 10^5 per second the wanted signal to unwanted noise is unity.

If events taking place at higher rates are to be analysed, a faster store than that provided by a phosphor must be used. This is also the case when part of an event, which varies continuously with time, is to be recorded in $< 10^{-6}$ secs. The storage time required is 10^{-7} secs with a time dispersion of $\pm 10^{-9}$ secs. The time dispersion and not the storage period limits the time resolution. An optical delay line can fulfill this requirement, however the need for large-aperture, low-loss storage creates practical difficulties. The use of electron transit time storage was first suggested by L.W. Jones and has been considered by Hill et.al.(132). He proposed using an image intensifier designed for low velocity electrons, shown in fig. 8. Photoelectrons are accelerated in a uniform electric field and confined to helices of .25 mm diameter by the axial magnetic field. The transit time is 2.10^{-7} sec with a dispersion of 2.10^{-8} sec due to the spectrum of initial velocities of the photoelectrons. Shuttering action is accomplished after the transit time delay by a large transverse electric field E which sweeps out electrons in about 2.10^{-8} sec.

Electrons are normally collected on an aperture ahead of the output phosphor. When the deflecting field is removed, the electrons pass undeflected to the output stage. McGee(145) proposed an electron image delay tube shown in fig. 9. The electron image is accelerated

to 300v and is allowed to drift down a field free region held at 300v. The electrons are constrained to move in cycloidal paths by a strong axial magnetic field. The electrons are then decelerated so that they reach the gating mesh with only their emission energy. This gating mesh is of the type described by Mandel[104] which can switch the electron beam on or off with only $\simeq$ 5V. If the tube length is $\simeq$ 100 cm and the equipotential drift section is maintained at 300v, the transit time of electrons is $\simeq 10^{-7}$ secs. The time dispersion of the electrons is $\simeq 10^{-9}$ secs. The practical development of such a device is described in the following chapters of this thesis.

Chapter 4 The theoretical performance of an electron image delay tube

4.1 The variation of image delay with applied voltage

A diagram of the electron image delay tube is shown in fig.10, illustrating the delay section. The same battery potential which is applied to the equipotential electrode, length d_2, is used to accelerate the photoelectrons over a distance d_1, and finally decelerate them over the distance d_3. The accelerating and decelerating fields are held uniform by the annular electrodes.

The electrons are emitted from the photocathode with a small energy of $\simeq$ lev in a polar distribution. The axial electric field imparts axial acceleration to the photoelectrons. The component of the emission velocity perpendicular to the axis causes the electrons to move in a cycloidal path constrained by the magnetic field. The time taken for an electron to travel from the photocathode to the gating mesh is dependent only opon its axial velocity. For the purposes of the following analysis the axial emission velocity will be neglected.

The time taken, t_1, for an electron to be accelerated by a uniform electric field from zero to an energy eV over a distance d_1, is given by

$$t_1 = \sqrt{\frac{2d_1^2 m}{eV}} \qquad \ldots \qquad \ldots \qquad \ldots \qquad (1)$$

Similarly, the time taken, t_3, for an electron to be decelerated by

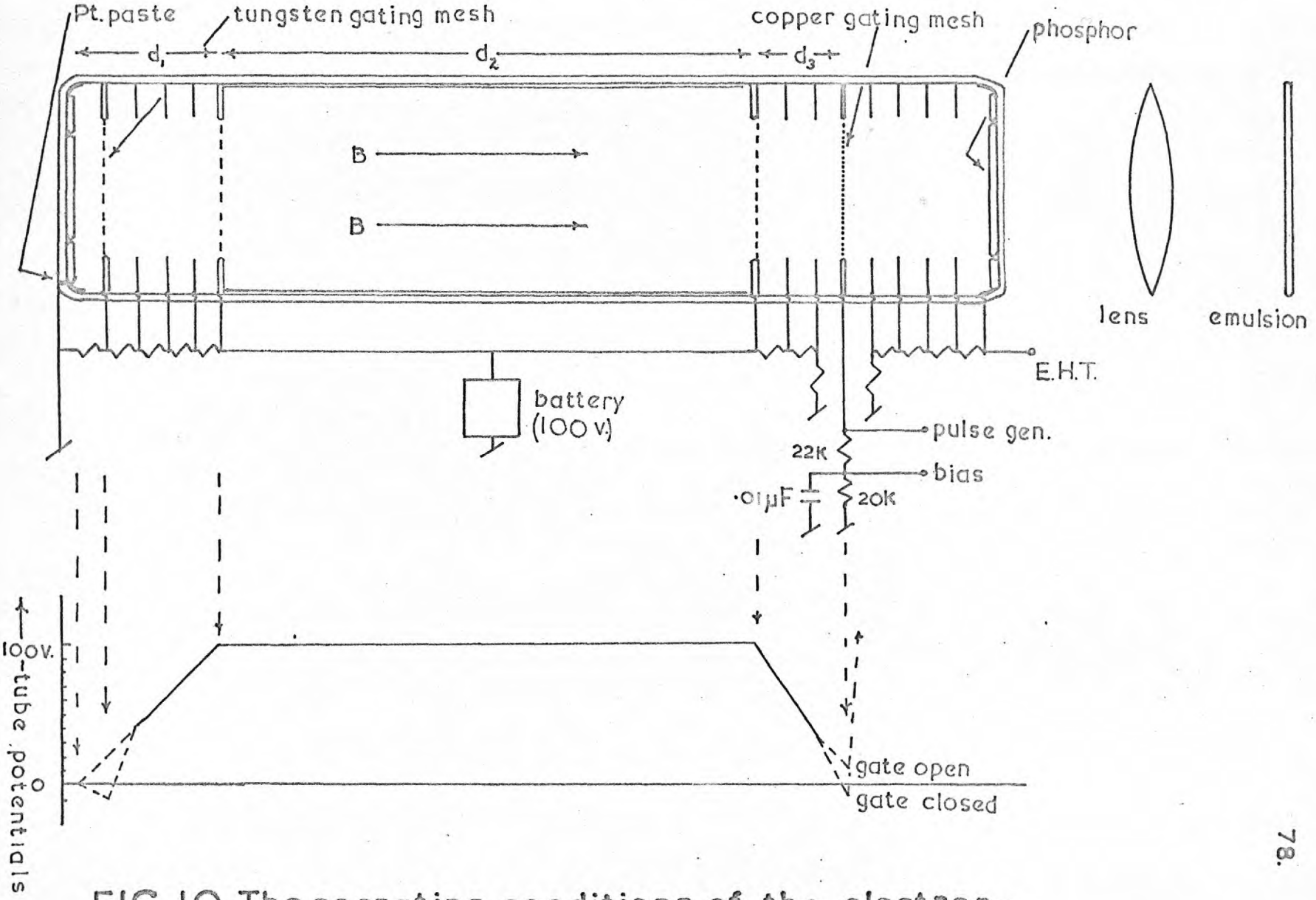


FIG. 10 The operating conditions of the electron-image delay tube

a uniform electric field from eV to zero energy over a distance d_3, is given by

$$t_3 = \sqrt{\frac{2d_3^2 m}{eV}} \qquad .. \qquad .. \qquad (2)$$

The time taken, t_2, for an electron to travel over a distance d_2 in the equipotential region, maintained at a potential V, is given by

$$t_2 = \sqrt{\frac{d_2^2 m}{2eV}} \qquad .. \qquad .. \qquad (3)$$

The total transit time, T, of the electron is given by

$$T = t_1 + t_2 + t_3$$

and from eqns 1, 2 and 3

$$T = \sqrt{\frac{m}{2eV}} \, (2d_1 + 2d_3 + d_2) \qquad .. \qquad (4)$$

Therefore $$T = \frac{K}{\sqrt{V}}$$

where $$K = \sqrt{\frac{m}{2e}} \, (2d_1 + 2d_3 + d_2)$$

which is a constant for a given tube geometry.

The delay section geometry was standardized at the following values:

$$d_1 = 5\text{cms}, \; d_2 = 50 \text{ cms and } d_3 = 3\text{cms}.$$

Therefore $$K = 1{\cdot}11.10^{-6} \text{Kgm.}^{\frac{1}{2}}\text{coul}^{-\frac{1}{2}}\text{meter}.$$

The variation in the electron image delay time with applied

voltage for a single transit of the delay section is given by

$$T = 1{\cdot}11.10^{-6}V^{-\frac{1}{2}} \qquad .. \qquad .. \qquad (5)$$

This variation is illustrated in fig. 11.

The primary purpose of this type of delay tube incorporating a fast shutter was to provide a fast image "store" and "gate" for a luminescent camera, described in section 3.5.3, and a Cerenkov camera, described in section 3.5.4. The coincidence circuits used in these experiments are able to produce a gating pulse on the fast shutter in $\triangleq 10^{-7}$ sec. Fischer and Zorn[146] have shown that in an analogous system this delay may be reduced to $\triangleq$ 33 musec. It can be seen from fig. 11 that for a delay of $\triangleq$ 100 musec $\triangleq$ 100V need be applied to the drift section.

4.2 The electron time dispersion in the image delay time

The total transit time in the delay section of an electron emitted from the photocathode with zero energy, is given by eqn 4.

$$T_o = \sqrt{\frac{m}{2eV}}\,(2d_1+2d_3+d_2)$$

An electron emitted from the photocathode with an energy of edV will possess this same energy upon reaching the end of the delay section (total distance $d_1+d_2+d_3$). The transit time, T_{dV}, for the electron in the latter case is given by

$$T_{dV} = \sqrt{\frac{m}{2e}}\left\{\frac{2d_1+2d_3}{\sqrt{dV}+\sqrt{V+dV}} + \frac{d_2}{\sqrt{V+dV}}\right\}$$

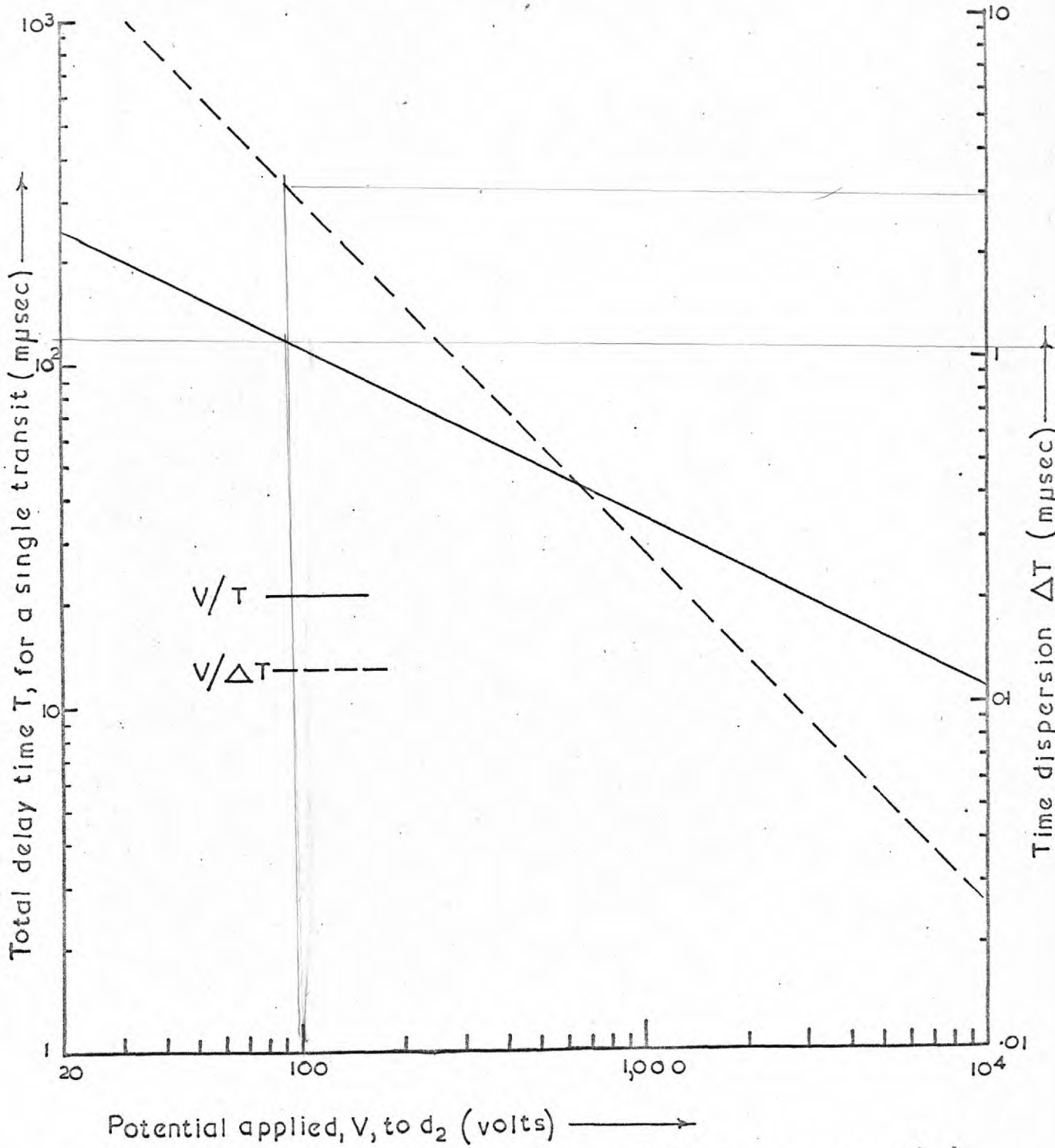


FIG. 11. The variation of T and ΔT with potential

The time dispersion, ΔT, in the image delay time is given by

$$\Delta T = T_o - T_{dV}$$

Therefore $$T = \sqrt{\frac{m}{2e}} \left\{ (2d_1+2d_3) \left(\frac{1}{\sqrt{V}} - \frac{1}{\sqrt{dV}+\sqrt{V+dV}}\right) + d_2 \left(\frac{1}{\sqrt{V}} - \frac{1}{\sqrt{V+dV}}\right) \right\} \quad .. \quad (6)$$

The variation of the time dispersion with applied voltage is illustrated in fig. 11, where the range of the energy of emission, dV, is taken to be 1eV. It can be seen that if the applied voltage is 100V, the time dispersion $\Delta T \triangleq 3$ μsec.

In practice the electron image is gated through the copper mesh, which is pulsed to $\triangleq 10$ volts positive. Thus the decelerating potential gradient, over the distance d_3, is less steep than that indicated in the theoretical treatment given above. It can be shown that this reduction in potential gradient reduces ΔT by $\triangleq 15\%$.

It can be seen by a numerical inspection of eqn 6, that the first term on the right hand side contributes $\triangleq 90\%$ to the total time dispersion, when the applied potential is 100 volts; i.e. $\triangleq 90\%$ of the total time dispersion occurs in accelerating and decelerating regions. Thus, the time dispersion can be considerably decreased by reducing the distances d_1 and d_3. If, for example, the distances d_1 and d_3 were reduced so that $d_1+d_2 = 1{\cdot}5$ cms, T would then be approximately ·8 μsec, when the applied potential was 100 volts.

4.3 The light gain required to record single photoelectrons

The electron image delay tube requires sufficient internal

electron multiplication to operate down to the low light levels required. In extreme cases the scintillations produced by individual photoelectrons will have to be recorded on a photographic emulsion. Consider fig. 10. Let there be an internal electron gain of $\bar{n}$ after the electronic gate and let the conversion efficiency of the output phosphor be $\bar{\emptyset}$.

Therefore the number of output photons per primary photoelectron $= \bar{n}\bar{\emptyset}$. If the overall resolution of the image tube is R lp/mm, the collection efficiency of the lens is $\bar{\alpha}$ and magnification of the lens system is m, the number of photons arriving at the emulsion/cm^2/ photoelectron $= 400.\bar{n}\bar{\emptyset}R^2\bar{\alpha}/m^2$. Let this number equal that required to produce an adequate recording density $\bar{D}$ on the photographic emulsion.

$$\text{Thus } D = 400\bar{n}\bar{\emptyset}R^2\bar{\alpha}/m^2 \qquad .. \qquad (7)$$

If the quantum efficiency of the photocathode is $\bar{\mathcal{E}}_o$, the light gain of the image tube, $\bar{G}$, is given by

$$\bar{G} = \bar{\mathcal{E}}_o\,\bar{n}\bar{\emptyset} \qquad .. \qquad (8)$$

From eqns 7 and 8,

$$R^2\bar{G} = \frac{\bar{\mathcal{E}}_o D m^2}{400\bar{\alpha}} \qquad .. \qquad (9)$$

If the quantum efficiency, $\bar{\mathcal{E}}_o$, of the photocathode is 0·1, the transfer efficiency, $\bar{\alpha}$, of the lens system is 0·1 (using 1:1 magnification) and Eastman Kodak Royal X emulsion is used exposed to

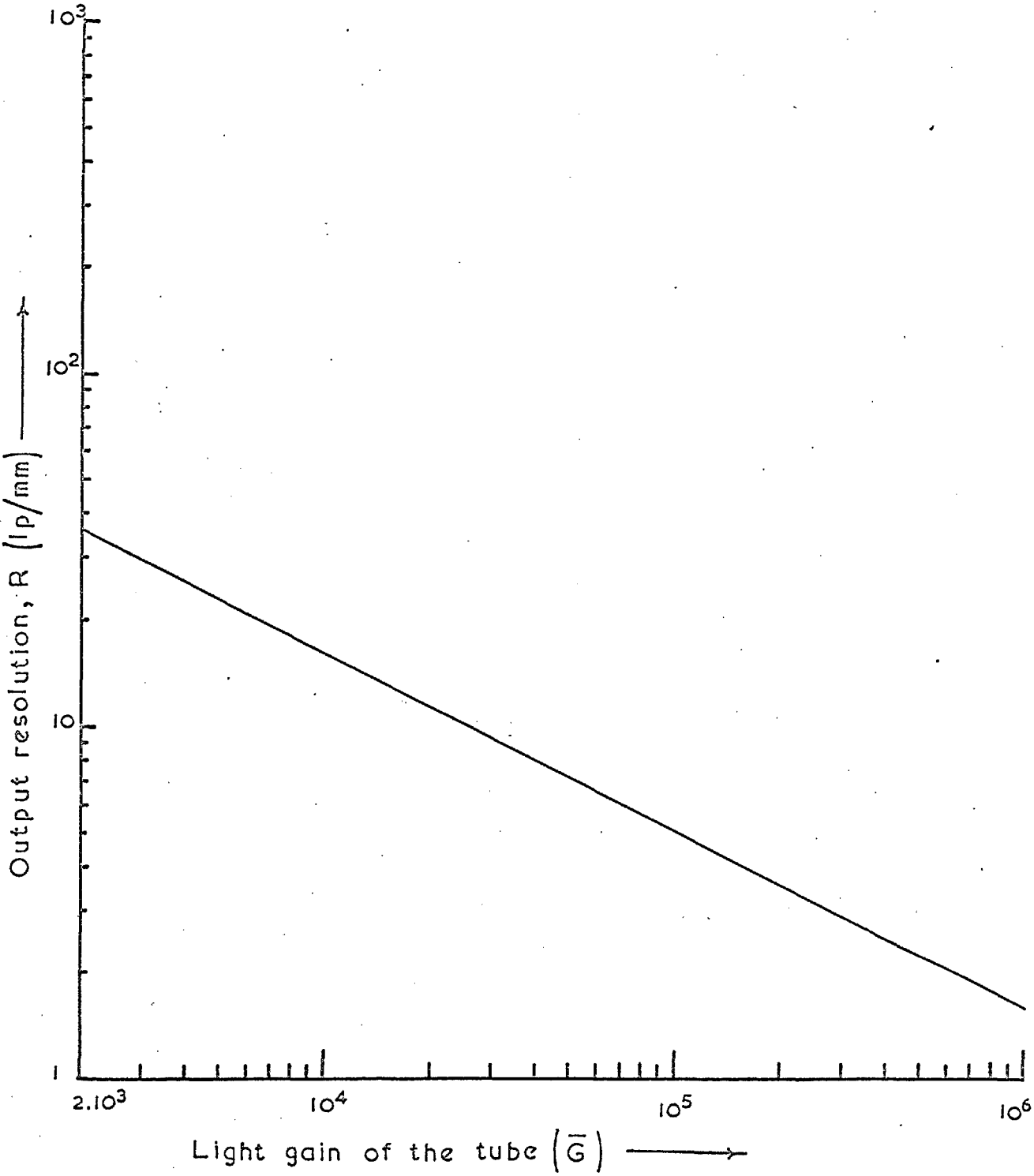


FIG. 12 The conditions required to enable single photoelectrons to be recorded

a density of 1·0 (D = 10^9photons/cms[14]) then,

$$R^2\bar{G} = 2{\cdot}5.10^6 \qquad .. \qquad .. \qquad (10)$$

The variation in blue light gain with resolution required to photographically record single photoelectrons, under the conditions stated in eqn 10, is illustrated in fig. 12. It can be seen from eqn 10, that an image intensifier having a blue light gain of 10^5 requires a resolution of $\geq$5 lp/mm to meet this recording criterion.

4.4 The geometrical resolution

No attempt is made to focus the electron image in the delay section of the tube. The geometrical resolution is maintained by the strong magnetic field, which limits the extent of the cycloidal deviation from the axis.

The worst possible resolution due to the magnetic field may be estimated as follows. Let the maximum emission energy, perpendicular to the axis of the tube, of the photoelectron be eV_T

$$\text{Thus } \tfrac{1}{2}\, mv^2 = eV_T \qquad .. \qquad (11)$$

$$\text{and } \frac{mv^2}{r} = Bev \qquad .. \qquad (12)$$

where B is the magnetic flux density and r the radius of the electron in orbit

From eqns 11 and 12

$$r = \frac{1}{B}\sqrt{\frac{2V_T m}{e}} \qquad .. \qquad .. \qquad (13)$$

If $\bar{E}_o$ is the value of the maximum emission energy along the axis, the maximum value of this energy in a direction θ to the axis is given by

$$E_\theta = E_o \cos^2\theta$$

number or energy

It is assumed that the emission of the photoelectrons follows a Lambertian distribution. The component of the energy distribution perpendicular to the axis E_T is given by

$$E_T = E_\theta \sin\theta = E_o \sin\theta\cos^2\theta$$

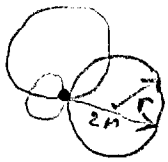
The maximum value of E_T is given when $\frac{dE_T}{d\theta} = 0$ i.e. when $\tan\theta = 1/\sqrt{2}$

Hence $$E_{T(max)} = E_o \frac{2\sqrt{3}}{9}$$

Now $$E_o = eV_o \text{ and } E_T = eV_T$$

Therefore $$V_T = V_o \frac{2\sqrt{3}}{9} \qquad .. \qquad .. \qquad (14)$$

Substituting eqn 14 in eqn 13



$$r_{max} = \frac{1}{B}\sqrt{\frac{m4\sqrt{3}V_o}{e9}}$$

The Resolution is given by

$$R_{min} = \frac{\cdot 001}{2.4\, r_{max}} = \frac{\cdot 001 B}{4}\sqrt{\frac{9e}{4\sqrt{3}mV_o}} \text{ lp/mm}$$

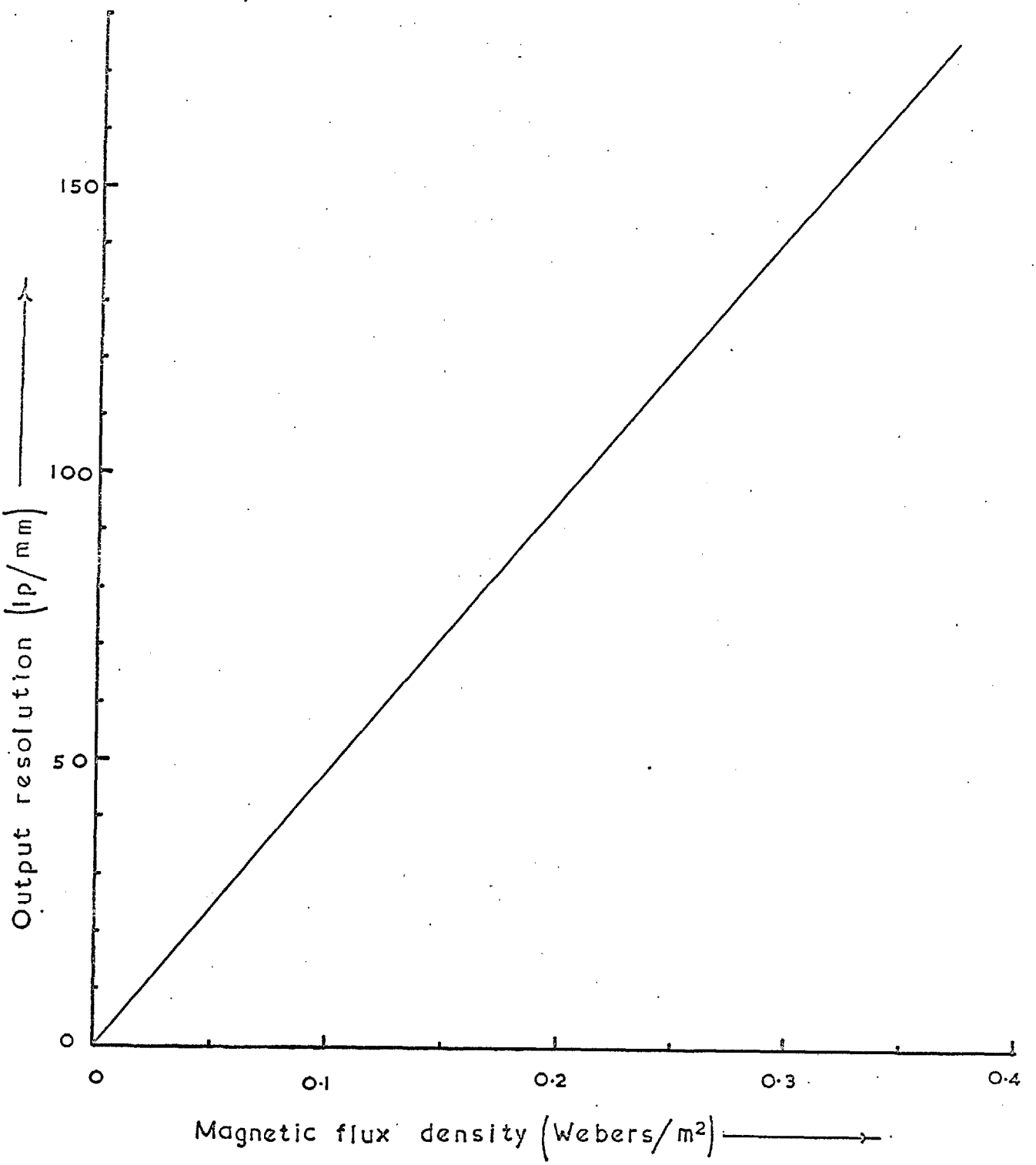


FIG. 13 The variation of resolution with magn. field

if all quantities are in M.K.S. units.

This is a pessimistic estimate of the geometrical resolution, since it assumes a square wave output intensity pattern of 100% modulation. The resolving criterion due to Rayleigh may be used to obtain a better estimation of geometrical resolution. Rayleigh's criterion states that two neighbouring lines will be just resolved when the centre of one maximum falls on the first minimum of the adjacent line, i.e. when the centres of the maxima are separated by half the width of the lines. The line half width is given by r, thus

$$R_B = \frac{\cdot 001}{r} = \cdot 001B\sqrt{\frac{9e}{4\sqrt{3}mV_o}}$$

If the maximum energy of axial emission of the photoelectron is leV, V_o = 1 volt.

Then $$R_B = B4\cdot 75.10^2 \text{ lp/mm} \qquad .. \qquad (15)$$

where B is in M.K.S. units.

Equation 15 indicates that the resolution is directly proportional to the magnetic flux density applied. The value of the resolution limited by the magnetic flux density is illustrated in fig. 13. It can be seen that at $\cdot 05$ webers/m^2 the resolution is limited to $\simeq$ 24 lp/mm. In practice this resolution is further degraded by inhomogenity in the electromagnetic and electrostatic applied fields.

If a cascade intensifying section is incorporated in the delay tube, further degradation will occur at the multiplying sandwiches. In a three-stage cascade tube the two sandwiches limit the resolution to ≙ 25 lp/mm. If this limiting resolution be denoted by r_2, the resulting resolution R is given by

$$\frac{1}{R^2} = \frac{1}{r_1^2} + \frac{1}{r_2^2}$$

For R to be within 5% of r_2, r_1 has to have a value of ≙ 80 lp/mm. It can be seen from fig. 13 that a magnetic flux density of ≙ •2 webers/meters^2 is required to fulfill this condition. The magnetic focus coils made by Electro-Winds Ltd. are normally operated to produce a flux density of ≙ •015 W/m^2, without undue heat being generated. Flux densities of up to ≙ •05 W/m^2 have been obtained operating the coils for short periods only. To obtain higher flux densities without damaging the coils, the coil current must be used in pulsed operation. The gating circuits would have to be arranged to be sensitive only during the relatively flat peak of the current pulse which produces the intense magnetic field.

The geometrical resolution is also degraded by the electrical gating pulse applied to the control mesh deviating from a perfectly square pulse. This effect is lessened in the case of intense magnetic field focusing compared with normal loop focusing.

The resolution required for accurate Cerenkov ring measurement,

in the experiment described in section 3.5.4, is $\simeq$ 5 lp/mm. across an output phosphor screen diameter of $\simeq$ 40 mms. The number of linear resolution elements in a luminescent chamber of 10 cm. width is $\simeq$ 200, if the maximum radius of the circle of confusion of the coupling optics at the chamber is .5 mms. If the number of resolution elements across an image tube diameter of 40 mms. is to be $\gtrsim$ 200, the resolution required is $\gtrsim$ 2.5 lp/mm.

If in the extreme case there is only one photoelectron per image element and the light gain available in the image tube is $\lesssim 10^5$, the geometrical resolution required for recording is, from fig. 12, $\gtrsim$ 5 lp/mm. The initial requirement for geometrical resolution therefore is $\gtrsim$ 5 lp/mm.

4.5 Image persistence due to phosphor decay time

The complete image delay tube consists of a delay section, an electronic gate and an intensifier section. One of the most efficient intensifiers was shown in Chapter 2 to be the cascade intensifier. The cascade image intensifier has an output image persistence time depending on the decay times of the phosphors used. Mandel[147] has shown that for an n-stage cascade intensifier the output intensity, I_n, is given by

$$I_n(t) = \frac{NA}{\lambda} \left(\frac{At}{\lambda} \right)^{n-1} \frac{e^{-t/\lambda}}{(n-1)!}$$

Where N is the total number of photons produced due to an electron pulse of δ function distribution, A is the stage gain, λ is the decay

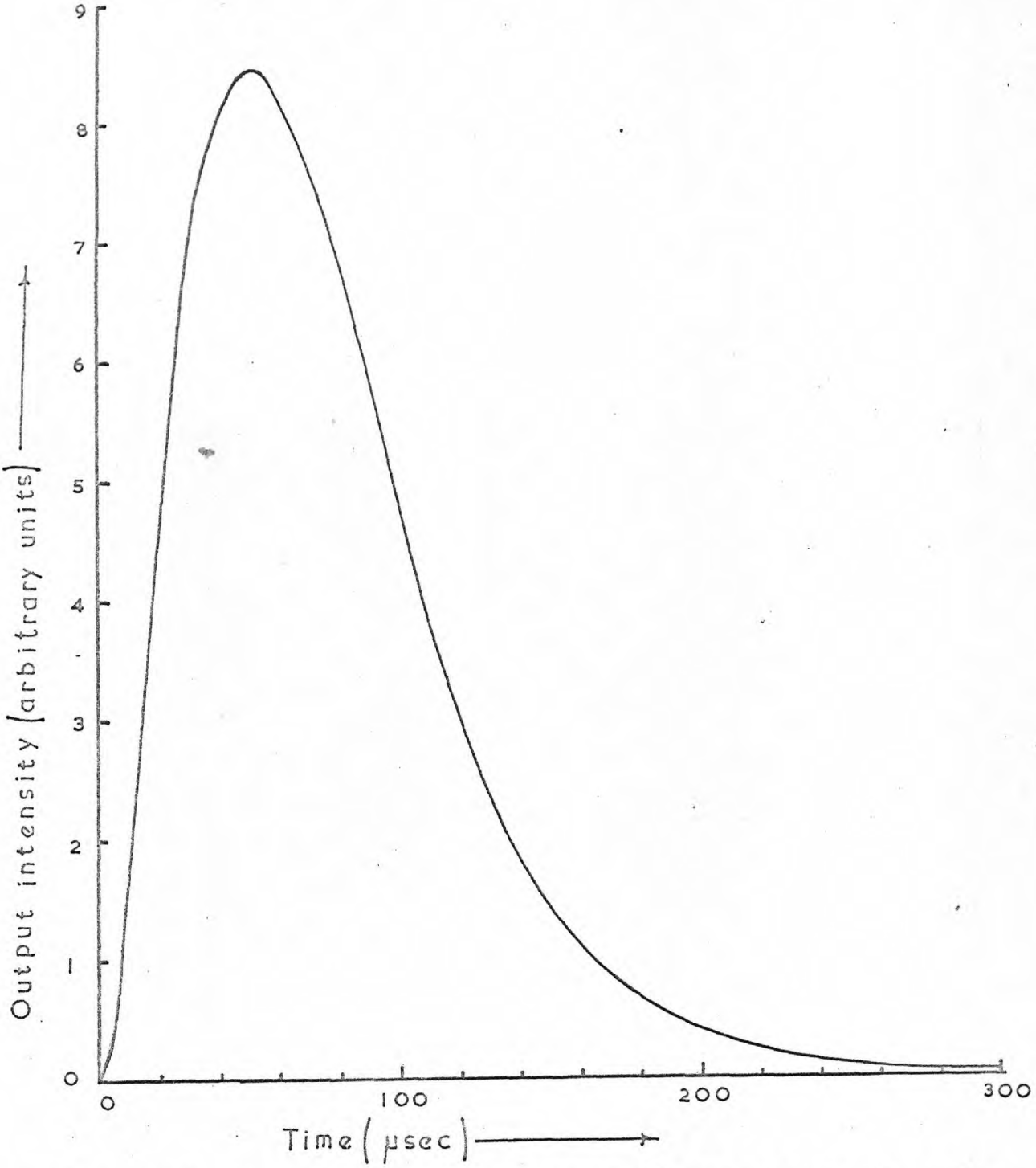


FIG. 14 The image persistence on the output phosphor of a three-stage cascade intensifier

time of the phosphor and t is the time interval from the application of the electron pulse on the first phosphor.

The maximum in the output intensity due to the input δ function occurs at a time given by

$$t = (n-1)\lambda$$

The temporal output intensity of a three-stage cascade intensifier containing P11 phosphors having a decay time of $\lambda = 25\ \mu s$ is given by

$$I_3(t) = C\ t^2\ e^{-t/\lambda}$$

where C is a constant. $I_3(t)$ has a maximum value when $t = 2\lambda = 50\ \mu s$. This relationship is illustrated in fig. 14.

In the practical case considered in sections 3.5.3 and 3.5.4 the input pulse of electrons on the intensifying section of the tube would be $\triangleq$ 10 musec long. This would approximate well to the theoretical δ function, since 10 musec is very small compared to the 25 µsec decay time of the phosphor. It can be seen from fig. 14 that the output intensity is substantially zero after ·5 msec. This would limit the number of frames separately recordable to $\triangleq 10^3$/sec. It has been assumed that the long tail component of P.11 phosphor is negligible. The intensity of this component depends on the manufacture of the phosphor.

4.6 The seal-off pressure requirement for the image delay tube

The quantity $\bar{\varepsilon}_1$ introduced in section 2.7.2 to be the fraction

of photoelectrons appearing at the output phosphor as recordable scintillations, depends on the pressure in delay section. If, in a normal image intensifier having an accelerating field gradient throughout, an electron loses axial energy in a collision with a free molecule, it will still be accelerated by the field and appear at the output. Thus in a normal image intensifier $\bar{\varepsilon}_1$ is not reduced by electron collision. It can be seen from fig. 10 that the delay section of the tube may be regarded as a potential well. If an electron loses more than $\simeq$ 10eV axial energy in collision, it will be trapped in the delay section of the tube. Those electrons losing less than $\simeq$ 10eV, the approximate positive gating voltage applied to the control mesh, will not be trapped and will be accelerated to the output phosphor.

It was noted in section 2.8 that the recording efficiency of the image intensifier system depended on the value of $\bar{\varepsilon}_1$. It is important therefore, when the number of photoelectrons to be recorded is small, to keep $\bar{\varepsilon}_1$ as high as possible, i.e. to reduce the number of possible collisions with free molecules. It is also desirable to reduce the number of ions produced by image electrons colliding with free-molecules, since it has been found by Miyake[148] that the photoemissive surface deteriorates in sensitivity under ion bombardment.

The fraction of electrons f(x) travelling a distance of at least x is given by

$$f(x) = e^{-x/\lambda_e}$$

From the Kinetic theory of gases

$$\lambda_e = \frac{4}{\pi n d^2}$$

Where n is the number of molecules/unit volume, d is the average effective molecular diameter of the residual gas and λ_e is the mean free path of an electron in the gas.

$$\text{Now } \frac{n_1}{P_1} = \frac{n_2}{P_2}$$

Where p is the pressure expressed in mms. of Mercury, the subscripts to 1 and 2 refering to atmospheric and seal-off values respectively.

$$\text{Thus} \qquad \lambda_e = \frac{4P_1}{\pi n_1 p_2 d^2}$$

If p_2 = 760 mms. Hg., $n_1 = 2{\cdot}69.10^{19} cm^{-3}$ and $d = 3{\cdot}69.10^{-8}$ cms.

$$\lambda_e = \frac{2{\cdot}64.10^{-2} \text{cms.}}{P_2} \qquad .. \qquad (17)$$

Substituting 17 in 16

$$f(x) = e^{-xP_2 37{\cdot}88}$$

$$\log_e f(x) = -37{\cdot}88xP_2 \qquad .. \qquad (18)$$

x is the total distance that the electron travels in the delay section along its cycloidal path.

Refering to fig. 10, the time taken for an electron to travel the distance d_1 is given by eqn. 1 to be

$$t_1 = \sqrt{\frac{2d_1^2 m}{eV}} \qquad .. \qquad .. \qquad (19)$$

Let the electron be emitted from the photocathode perpendicularl to the axis of the tube, with an energy eV_T. The mean speed of the electron over the distance d_1 is:

$$\frac{\sqrt{\frac{2e}{m}}\left(\sqrt{V_T} + \sqrt{V_T+V}\right)}{2} \qquad .. \qquad .. \qquad (20)$$

Therefore, the total distance traversed in the accelerating section, is:

$$d_{1t} = \sqrt{\frac{2e}{4m}}\left(\sqrt{V_T} + \sqrt{V_T+V}\right)\sqrt{\frac{2d_1^2 m}{eV}}$$

$$= d_1\left(\sqrt{\frac{V_T}{V}} + \sqrt{1+\frac{V_T}{T}}\right) \qquad .. \qquad (21)$$

Similarly the total distance traversed in the decelerating region is:

$$d_{3t} = d_3\left(\sqrt{\frac{V_T}{V}} + \sqrt{1+\frac{V_T}{V}}\right) \qquad .. \qquad (22)$$

The mean speed of the electron in the equipotential delay section is:

$$\sqrt{\frac{2e}{m}}\left(\sqrt{V_T+V}\right)$$

Since the transit time of an electron in the equipotential delay section is $t_2 = \sqrt{\frac{d_2^2 m}{2e}}$, the total distance traversed is:

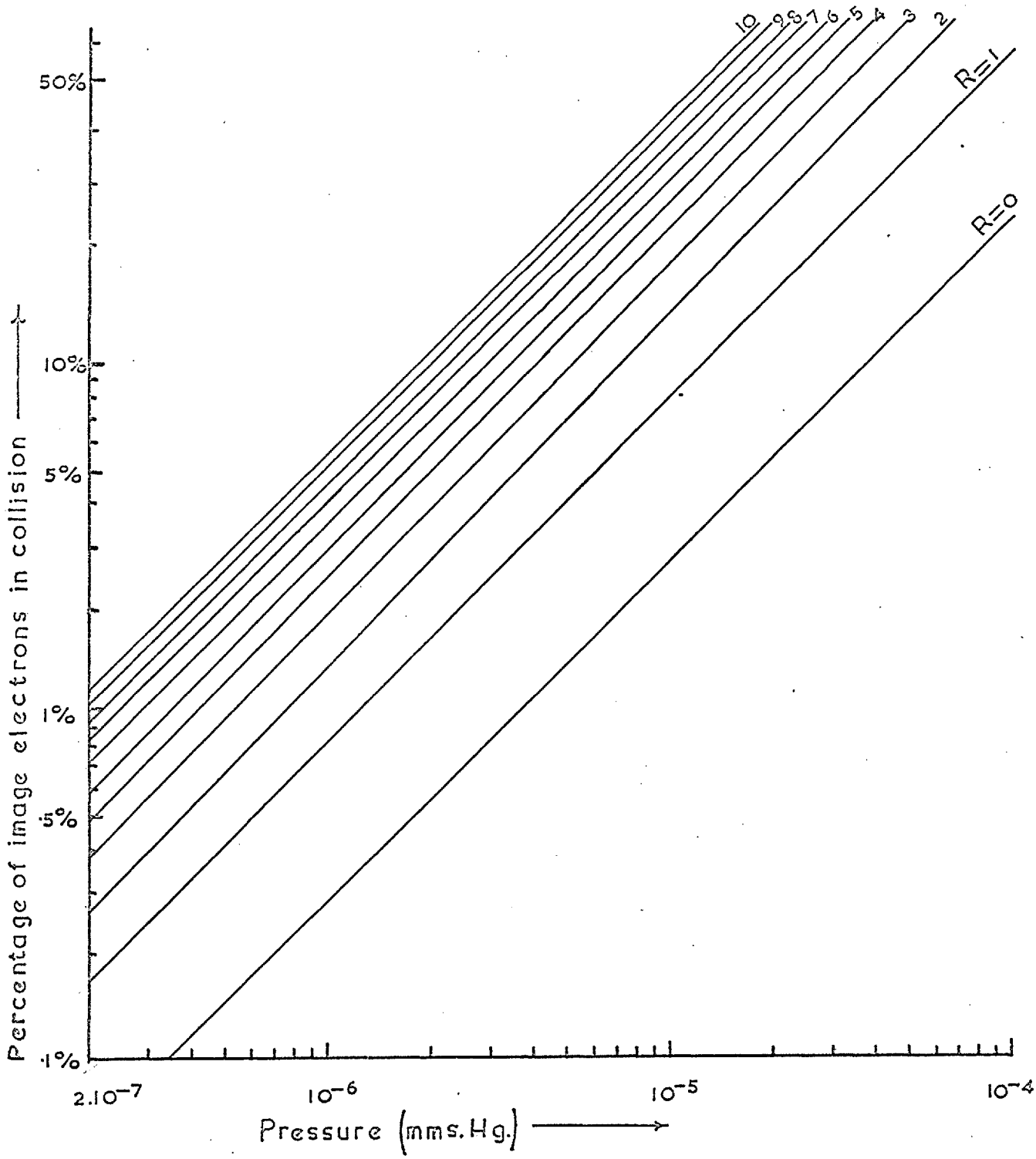


FIG. 15 The variation of electron loss with pressure

$$d_{2t} = \sqrt{\frac{2e}{m}}\left(\sqrt{V_T+V}\right)\sqrt{\frac{d_2^2 m}{2e}}$$

$$= d_2\sqrt{1+\frac{V_T}{V}} \qquad .. \qquad .. \qquad (23)$$

The total distance travelled

$$x = d_{1t}+d_{2t}+d_{3t}$$

$$= (d_1+d_3)\sqrt{\frac{V_T}{V}}+(d_1+d_2+d_3)\sqrt{1+\frac{V_T}{T}}$$

If d_1 = 5 cms., d_2 = 50 cms., d_3 = 3 cms., V_T = 1 volt. and V = 100 volts.

$$x = 59{\cdot}1 \text{ cms.}$$

Substituting this value of x in eqn. 18

$$\log_e f = -\ 2{\cdot}79.10^3 P_2 \qquad .. \qquad .. \qquad (24)$$

The graph of 1-f, expressed in %, against P_2 is illustrated in fig. 15. 1-f is the fraction of electrons involved in collision in the delay section of the tube. It can be seen from fig. 15 that if less than 1% of the electrons are to be involved in a collision, then the pressure must be $< 3{\cdot}5.10^{-6}$ mms. Hg. (for an image completing only one transit in the equipotential delay section; denoted by R = 0).

N.B. R = 1,2,3... etc. denote an electron stream completing three, five, seven...etc. transits in the delay section.

Chapter 5 The general techniques used in the manufacture of electron optical image delay tubes

The same general manufacturing techniques were common to all the image delay tubes constructed by the author, and will be described in this chapter. The individual peculiarities of each tube will be considered in later chapters.

5.1 The preparation of the vacuum envelope

The vacuum envelope was made by the glass blowers from cylindrical Pyrex glass tubing, of $\simeq$ 60 mms internal diameter, by sealing two optically flat circular Pyrex windows in each end. The tube was provided with a constriction in the main pumping stem, in order that it could be given a pre-pumping test for leaks by pumping and baking and sealing off under vacuum. The tube was then left for as long as was conveniently possible, and if no discharge were produced by a Tesla coil, the envelope was assumed free from leaks. A Helium mass spectrometer leak detector was used on some tubes to locate the exact position of possible leaks.

If the tube were found to be free from leaks it was cut open at the point where the tube was to be sealed up after assembly. In all the early tubes the cut ends were ground and polished flat, in order that a Ag CL seal could be made at that point. In later tubes the final seal was completed using gas-air-oxygen flames, the tube being held in a glass blowing lathe. In the latter case the ends were left unground.

The metal electrodes were held in place inside a tube by three flat metal tags which fitted into slots ground in the wall of the glass envelope. The tube was placed in a small lathe and the positions of the metal electrodes accurately marked on the outside of the tube. Using a thin rotary diamond wheel in conjunction with the lathe, slots were cut to coincide with the positions marked.

The inside of the tube was next cleaned using the following proceedure. The tube was scrubbed with a solution of Teepol detergent in hot water, rinsed for about 30 mins in running tap water, then given several rinses with double distilled water and dried with analar acetone.

The electrostatic field was defined on the inner surface of the glass envelope by a series of metal rings. These were painted on the inside wall of the tube using platinum metallizing paste type number T177, made by Johnson-Matthey & Co. These rings were approximately 2 mms in width. Rings of silver metallizing paste type number X351 were painted in corresponding positions on the outside of the tube. Electrical contact between the outer and inner metal rings was made by platinum tapes previously sealed through the glass[149]. The paste rings were dried using an infra-red lamp and fired into the glass at a temperature of $\simeq 600^{\circ}C$.

When the tube was cool, the platinum paste rings were buffed using a rotating rubber wheel to remove loose surface material. This prevented small particles of metal being dislodged when the metal

electrodes were assembled in the tube. Electrical continuity between the outer and inner metal rings was checked. The tube was then rewashed.

The tube was replaced in the lathe and the input and output windows of the tube defined using liquid bright platinum paint. Also the long equipotential delay electrode was similarly painted. Since in the latter case the thin platinum paint might have been scratched on assembly and electrical contact broken, longitudinal strips of platinum paste had previously been painted on. Those tubes which were later joined by a AgCl seal, had platinum paint on the polished seal up surfaces. Small discs of platinum paint were also painted on the points where the platinum tapes first emerged on the outside of the glass envelope. Finally, a small sector of each of outer rings was painted with a thick silver metallizing paste type number X353, in order that electrical connexions could afterwards be soldered to the rings using silver-loaded solder. The tube was again baked to $\simeq 600^{\circ}C$ to fire in the rest of the painted surfaces. The tube was allowed to cool to a temperature of $\simeq 500^{\circ}C$ and then AgCl was applied to the small platinum discs on the tapes to form round blobs. This was a precaution against leaks through the tape seals, which could have formed during the baking of the tube. When the tube was cool aqua-dag was painted on the AgCl blobs to protect them from deterioration due to the action of light. The envelope was then enclosed in a plastic bag to keep it clean prior to assembly.

5.2 The preparation of the metal electrodes

All the metal electrodes were made from stainless steel. Those used in the construction of a complete delay-intensifier tube are shown in fig. 39. The plain metal annuli received from the workshop were first vacuum-stoved up to a temperature of 1000°C. Further handling of the parts was performed wearing nylon gloves to prevent contaminating the parts with finger grease. Various spring clips, stops and guides were spot-welded to the annuli using inconel strips. Magnetically operated catches were also appropriately added using small soft iron slugs attached to sprung inconel strips. The metal parts were fitted into place in the tube to make sure that they were securely held and that all the magnetically operated catches functione correctly using dummy parts. The inconel metal parts were always mounted on the side of the metal annulus which faced the photocathode. Any sharp points on these parts were then shielded from the positive potential gradient by the annulus, and field emission prevented.

Some marks were produced on the side facing the phosphor by the spot welding process. These marks were initially removed by physical polishing. In later tubes all sharp edges were removed by electro-polishing. Electro-polishing was accomplished by making each annulus in turn the anode in a bath containing a mixture of 45% glycerol, 45% orthophosphoric acid and 10% distilled water, by volume[150]. After electro-polishing the parts were rinsed in running hot water for 30 mins. then placed in a 20% solution of HCl for 5 mins. to

remove any traces of the polishing bath. The parts were then washed in cold running water for 10 mins; rinsed with distilled water and dried with analar acetone. The parts were finally vacuum-stoved up to a temperature of 400°C. to remove any surface chemical contaminatio It was not advisable to go much above 400°C. in this operation, since this would have reduced the tension in the inconel springs.

5.3 The preparation of the cathode plate, the phosphor plate and the mica membranes

The cathode and output phosphor glass discs were cut from microscope cover slide plate, which was soda glass ≏ 1 mm in thickness using a circular glass cutter. The discs were cut slightly larger than the intended final diameter, the excess being ground away using a lathe and several grades of carborundum powder. The rounded edge produced was finally polished using emery cloth. The smooth finished edge prevented field emission and also did not offer a sharp edge across which it would have been difficult to establish and maintain electrical contact using bright platinum paint. The discs were cleaned using Teepol, distilled water and analar acetone in the usual manner. The discs were then painted on both sides with platinum paint leaving a clear central area of the required diameter, and fired in at 530°C. The cathode plate is shown in fig. 16d.

In the later tubes a cascade image intensifier was incorporated into the output section of the electron image delay tube. Two mica membranes were required to provide support for the multiplying

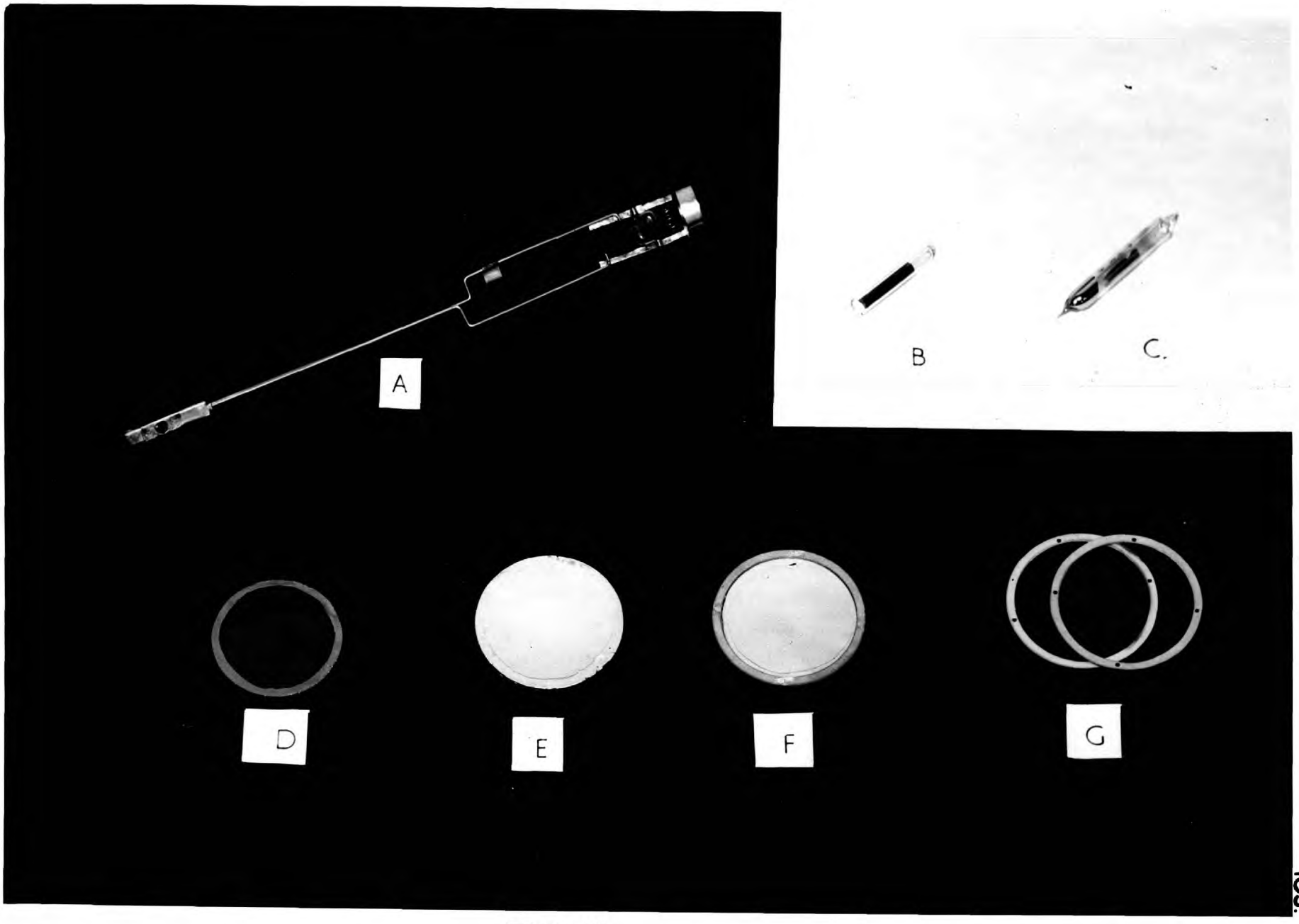


FIG. 16

sandwiches. The mica sheets were obtained commercially, cut into discs of 45 mm. in diameter and of 4-5μ in thickness. The discs were painted as above and fired in. The mica discs were then stuck down onto 2" squares of glass using an organic filming solution. The glass plate served to protect the side of the mica-disc, upon which the photoemissive surface was to be formed, from contamination by the solutions used in settling the phosphor screen.

5.4 The preparation of the phosphor screens

ZnS: Ag phosphor was settled on one side of the mica discs and the glass plate using the technique of sedimentation from a suspension of the phosphor in barium nitrate and potasium silicate solutions. The method was developed by Levy & West Ltd. and was as follows:-

Two stock solutions were made up using a double distilled water. Solution A-Barium nitrate having a concentration of ·22 gm/litre. Solution B-Potassium silicate of specific gravity 1·020.

The discs were placed in a dish 13 cm. in diameter, which was scrupulously cleaned, together with 168 cc. of solution A. 246 mgm of ZnS: Ag phosphor powder were weighed out, i.e. enough to produce ≏1 mg/cm^2 after sedimentation on the bottom of the dish. The powder was mixed with a few drops of solution A in a conical flask, and gently ball milled using small pyrex glass balls to break up the crystal aggregates. 48·5 cc. of solution A and 23 cc. of solution B were then added to the conical flask, and the mixture poured into the dish.

The settling process took place in ≏ 2 hours, after which the

settling solutions were siphoned off and the phosphor screens dried under an infra-red lamp. Aluminium backings were then placed on the back of the phosphor screens by the technique of "floating" them on. A layer of sodium chloride 1000Å thick was evaporated through holes 5 cm in diameter onto clean glass plates in a demountable vacuum system. Magnetically operated shields slightly reduced the size of the holes and an aluminium layer also of 1000Å was then evaporated onto the plates. The plates were removed from the system and immersed in distilled water, which dissolved the salt leaving the aluminium films floating freely on the surface. The end plates and micas, having the phosphor settled upon them; were immersed in a weak potassium silicate solution (8% of stock solution) and brought up under the floating aluminium layers. The plates were removed from the water and dried slowly in a dust free atmosphere.

The mica discs were separated from their glass plates by baking them for half an hour at 350°C. in air, to completely remove the organic binder which stuck the discs to the plates. The completed mica discs were each mounted between two molybdenum rings, using four aluminium rivets to hold the assembly together. The completed end phosphor, a mounted mica discs, and the molybdenum rings used in their assembly are shown in fig. 16 under e, f and g respectively.

"Floated" aluminium backings had several advantages over the former technique of evaporating the aluminium layer onto an organic film which had been previously deposited on the phosphor. They did

not require the use of the organic film, which might have left a small residue when baked away which could have decreased the efficienc of the phosphor. The "floated" backings were opaque, except for a few pinholes, whereas the evaporated backings were partially transparent. The improved opacity of the "floated" backings enhanced the phosphor output efficiency, and reduced the caesium penetration during the activation of the photocathode.

5.5 The preparation of the Caesium ampoule and the Antimony evaporato

The Sb-Cs photoemissive surface was the type of photocathode used in experimental tubes. The tri-alkali photocathode would have been more efficient, but its greater difficulty of manufacture precluded its use in purely experimental tubes.

The liquid metal caesium was produced in glass ampoules in the following manner. Caesium chromate, aluminium powder and tungsten powder were mixed in the proportions of 1:1:8 by weight and placed inside a nickel capsule. This capsule was placed inside a wide bore glass tube, having narrow bore glass ampoules sealed to its bottom, and the tubing sealed onto a pumping system. The ampoules had thin glass tails which were to be broken under vacuum using a magnetic hammer. The whole arrangement was pumped and baked at 400°C. for several hours to achieve a reasonable vacuum. The nickel capsule was heated by R.F. action until the caesium chromate reacted with the aluminium to produce free caesium. The tungsten powder controlled the rate of chemical reaction. The caesium was distilled into the

ampoules, which were then sealed off under vacuum.

Antimony, unlike caesium, does not react with air, and could therefore be evaporated from a prepared evaporating source. The evaporator consisted of a flat coil of nickel wire, which completed an electrical circuit with tantalum metal strip 1 mm wide, 0·003" thick and 20 mmϕ long. Upon the tantalum strip was spot welded a 1 mm diameter disc of nickel sheet, which the antimony wetted in preference to tantalum. The tantalum strip was enclosed by a nickel shied to restrict the direction of evaporation of the antimony. Evaporation was accomplished by allowing the nickel coil to inductively pick up radio frequency energy, which brought the tantalum strip up to the temperature required for antimony to evaporate.

The tantalum strip was placed 2·5 mmϕ below the 4 mm diameter aperture in the nickel shield. In most cases the source was required by geometry to be only 3 cmϕ from the surface to be covered, which was 4 cmϕ in diameter. An unobstructed simple source, in these conditions, would have produced an evaporated layer much thicker at the centre than at the edges. To reduce the amount of antimony evaporated in the centre, a 2·5 mm disc of nickel mesh, having a 50% shadow ratio, was fixed to the centre of the source aperture, sandwiched between two coarse tungsten meshes of low shadow ratio. The meshes were mounted on a movable flap, which enabled the evaporator to be loaded through the aperture. The evaporator was thoroughly degassed under vacuum, and then placed in a stream of argon gas where

the tantalum strip was heated and the antimony wetted on.

A tungsten wire filament was incorporated across the nickel pick-up coil of the evaporator. The filament was arranged to glow just before the temperature of the tantalum reached that required to evaporate antimony. This advanced warning of evaporation assisted in preventing too much energy being applied to the coil and producing uncontrollable evaporation.

Fig. 16a shows the complete antimony evaporator, b the soft iron slug enclosed in an evacuated glass capsule, used as a magnetic hammer and c the glass ampoule containing caesium.

5.6 The tube assembly, seal-up and processing

The parts were assembled in the two sections of the tube using the long assembly tools shown in fig. 33c. Electrical continuity was checked between each part and its external connexion, and the magnetically operated catches were checked to ensure their correct functioning.

In the early tubes a silver chloride seal was used. The two parts of the tube to be sealed, having polished platinized flat surfaces, were brought together. The region of the join was heated to about 450°C, using an electrical heating coil, and silver chloride melted in to completely run round and fill up to join. During the heating argon was passed through the tube to prevent oxidation of the metal parts. When cool, the tube was sealed onto the vacuum system.

In the later tubes, which were longer and heavier, it was

difficult to safely produce a satisfactory silver chloride seal. This type of seal often gave rise to leaks and in general was a source of tube failure. It was found more satisfactory to seal up the tube at a cut in an unpainted region in the equipotential delay section, placing the two parts of the tube in a glass blowing lathe and using normal high temperature flame sealing. The metal parts were too far away from the join to be oxidized by the flame. The two side arm stubs were sealed up prior to joining and infra-red lamps heated both ends of the tube, which contained phosphor screens. This heating was continued throughout the flame seal-up and afterwards until the region of the join was cool. The moisture produced by the flames was thus condensed in the centre of the tube away from the aluminium backed phosphors. It was found that if an appreciable amount of moisture condensed on the aluminium backing, they tended to peel off when the tube was first pumped down. The join was blown using forming gas, which was continuously passing through the tube during seal-up. After seal-up the tube was sealed onto the vacuum system as quickly as possible and pumped using a gas-ballasted rotary pump to remove the water from the tube. When all the moisture inside the tube had been removed, the tube was let down to atmospheric pressure, the side arm stubs blown open and the side arms for the caesium ampoule and the antimony evaporator added. The tube was then evacuated and tested for leaks. It no leaks were detected the tube was prepared for baking.

The tube was baked at as high a temperature as was possible, since the outgassing rate increased with temperature. It was not advisable to bake above 400°C, since the phosphors would have deteriorated in efficiency. The side arms were kept to a temperature of about 250°C, since above this temperature antimony starts to evaporate and caesium begins to react with the glass of the ampoule. The main body of the tube was therefore wrapped in electrical heating tape, thermally insulated by two layers of asbestos paper. The side arms were maintained by the large oven, which enclosed the whole tube at 250°C. The tube was maintained at 370°C. by the extra heat from the tape. The temperatures were held at those stated by the use of a preset thermostat which regulated the heating elements. The tubes were baked for at least fifteen hours, until the pressure was better than $\simeq 7.5\ 10^{-7}$ mm of Mercury, falling to $\simeq 1.10^{-7}$ mm of Mercury as the tube was cooled to room temperature. When the temperature of the main body of the tube had fallen to $\simeq 150°C$, it was quickly unwrapped and a coat of black vacuum wax applied to all the points of possible leaks, i.e. the platinum tapes and the tube seal-up.

The caesium ampoule was broken using the magnetic hammer and the liberated caesium driven by gentle heating into the side arm, which was cooled by wadding soaked in water. The latter precaution prevented the caesium from prematurely entering the processing compartment of the tube. The excess length of the caesium side arm, containing the broken ampoule and the hammer, was then sealed off.

The antimony evaporator was magnetically positioned in the tube and a layer of antimony evaporated onto the transparent primary photocathode plate. The thickness of the antimony layer was monitored as a 20% decrease in the intensity of the light transmitted through the photocathode plate. In the tubes where a cascade intensifying section was incorporated, the antimony layer could not be monitored using transmitted light since the sandwiches were opaque. Antimony was therefore evaporated until there was a 20% increase in the intensity of the light reflected from the mica surface at an angle of 45°. It had been previously experimentally determined that a 20% decrease in the intensity of transmitted light produced by a layer of antimony, corresponded to a 20% increase in the component of light which was reflected, provided that the light was incident at 45°. In all cases the sensitivity of the primary photocathode upon activation was monitored to produce an optimum value, since it is its quantum efficiency $\bar{\varepsilon}_o$ which determines the equivalent quantum efficiency of the intensifier. The sensitivity of the photocathode was monitored by measuring the photocurrent produced by a standard intensity light source, throughout the activation. The photocurrent was collected by the antimony evaporator which was maintained at 120 volts positive to act as an anode. Electrical connexion from the evaporator was made, using a platinum tape in the side arm, to a galvonmeter and back through a battery to the external connexion of the cathode plate. The processing compartment was then wrapped in

electrical heater tape which was lagged with asbestos sheet and wadding, in order to maintain the chamber at 180° C. The caesium side arm was enclosed by a nichrome wire heating coil and heated gently while monitoring the photocathode sensitivity. When the sensitivity had passed through its maximum value and had fallen to about a half of this value, the caesium side arm heater was switched off together with that of the processing compartment. As the temperature of processing compartment fell, the excess caesium was baked away and became deficient. The sensitivity therefore rose to a maximum and fell. When it had reached about half its maximum value, usually at a compartment temperature of 140-150°C, caesium was reintroduced to the processing chamber to produce an excess of caesium. The chamber was then allowed to cool further and the maximum sensitivity gradually reapproached. Below about 80°C. there was no change in sensitivity. When the tube was cool, the tube was unwrapped and the evaporator withdrawn into the side arm. Both side arms were sealed off, and the tube was left for about 15 mins. while the pump removed any gas liberated from the seal-offs. The final seal-off from the pump was made, black wax being applied to all the seal-offs as a precaution against leaks produced by hair-line cracks.

5.7 The preparation of the tube for Testing

The cathode plate and other moving elements of the tube were moved into position and held down using the magnetic catches. The sensitivity of the photocathode was measured and the tube placed in

a perspex mounting cradle. The cradle enabled the tube to sit axially in the field of the magnetic focusing solenoid. The resistor chain used to hold the internal electrodes at their various potentials was soldered onto the tube. The high potential leads were attached using thick polythene cable, together with the low loss coaxial cables used to apply various gating pulses to the tube. The sharp points of the high potential section were coated with a thick layer of beeswax which prevented corona discharge from any sharp points. Beeswax was found to be more effective than the cold setting silicone rubber solution, which tended to lift from the tube after several months to produce spark channels. The high voltage section was painted with black paint to reduce to a minimum any optical feedback through the walls of the tube.

Chapter 6 Electronic circuitry used in testing the electron image delay tubes

To ascertain the exact behaviour of the delay section of the image tube transistor circuitry had to be developed. The temporal resolution required the production of gating pulses, for the electronic shutter, of duration $\simeq$ 10 μsec. No commercially obtainable equipment was available which would have provided voltage pulses of this duration at the repetition frequency required. Details of the transistor circuits developed will be given in this chapter, and their application in various experiments with image delay tubes will be described in later chapters.

6.1 The avalanche transistor

The operation of a transistor in the avalanche mode provided the basic element in all the circuitry used for generating fast pulses. Initially, transistors required to operate in the avalanche mode had to be selected from transistors designed as high speed switching devices and only an average number of a large number of transistors of a given type would avalanche. Avalanche breakdown in junction transistors was first reported by Schenkel and Statz[151] in 1954. The mechanism of the avalanche switching mode of transistor operation has been described by Ebers and Miller[152]. When, in the case of a p-n-p transistor, the collector-base junction was reversed biased, by applying a collector voltage in excess of the normal operating voltages, the region on either side of the junction became

depleted of mobile carriers. As this reverse bias voltage was increased this depletion layer was extended further into the base and a large field gradient built up across it. Holes diffusing across the base were accelerated to high velocities on entering the depletion layer and generated hole-electron pairs by collision within the crystal structure. Thus for a steady emitter current an increasingly large collector current was produced, as the bias was increased, which tended to infinity at a bias V_A i.e. avalanche breakdown. If the conductivity of the base material was too low or the base region too narrow, the collector depletion layer extended completely across the base without the occurance of avalanche breakdown. This condition was termed "punch-through", requiring a voltage V_p. Avalanche transistors were selected so that V_A was less than V_p but close to it, so that the depletion layer extended across most of the base region.

The circuit used to test transistors, which was essentially similar to that developed by Fullwood,[153] is shown in fig. 17a. To obtain the maximum current gain and the minimum transit time the collector had to be biased to the breakdown voltage V_A. Since V_A differs widely between transistors, it was not practical to apply the bias directly as a voltage. The transistor was therefore automaticall biased to V_A by applying 120 volts negative, the current being limited by the 560 KΩ. The transistor was triggered by a 2V negative pulse of 20 μsec. duration which was applied across 330Ω of the

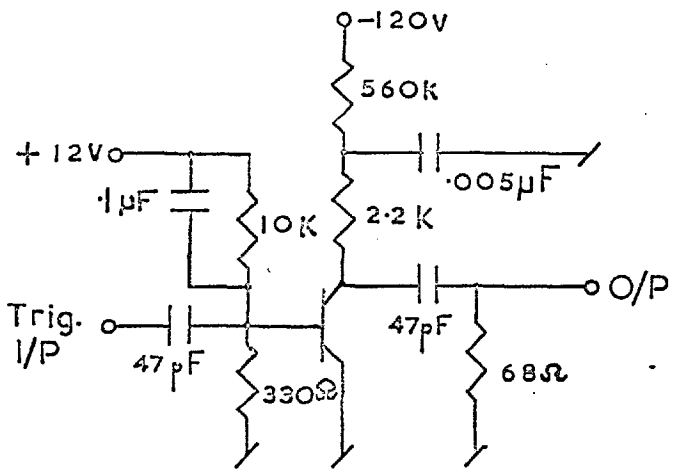


FIG. 17A Avalanche transistor test circuit

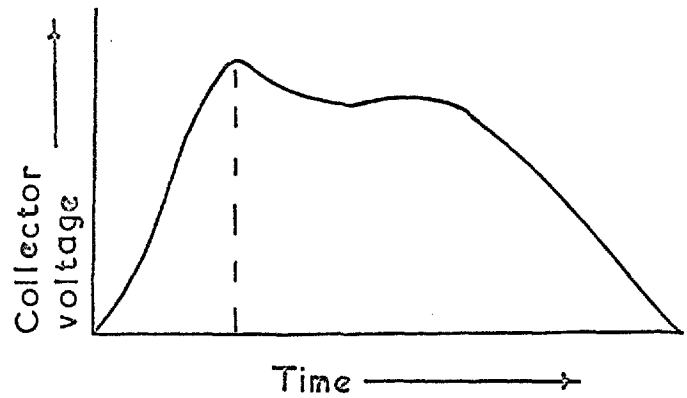


FIG. 17B Collector voltage excursion

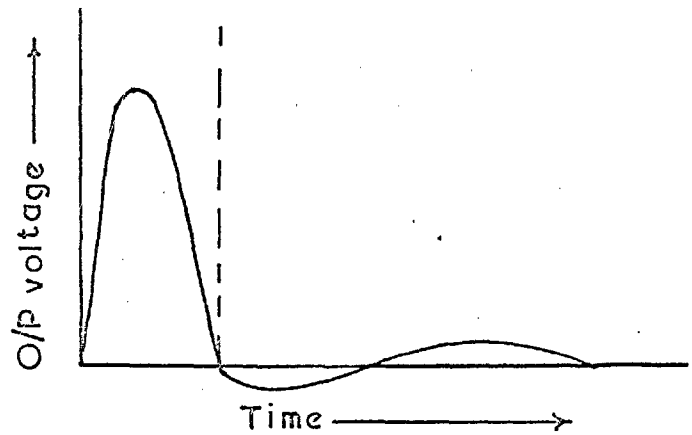


FIG. 17C Output pulse of an avalanche transistor

bias chain. This caused holes to be injected into the base from the emitter, which on entering the collector depletion layer were multiplied by a large factor. Thus a large pulse of current arrived at the collector causing the collector potential to rise sharply towards earth potential. This drop of potential across the base progressively reduced the avalanche effect until it ceased; the collector potential returning with the time constant of the load resistance 2·2KΩ and condenser 47,000pF. The collector voltage excursion during avalanche is shown in fig. 17b. The fast rise of the collector excursion was differentiated by the 47pF condenser and 68Ω resistor to produce a short output pulse shown in fig. 17c.

The test circuit was used to assess the performance of commercially available transistors in the avalanche mode of operation. The table of results, shown in fig. 18, represents the accumulation of evidence of the performance of various types of transistors during the period of circuitry development, which was about two years. The numerical results shown were obtained by measuring the output characteristics of various transistors in the circuit, shown in fig. 17a, using a P6025 cathode follower probe coupled with an N type sampling unit of 545 Tektronix oscilloscope. The intrinsic rise time of the measuring system was ·8 musec. There were three main considerations, shown in fig. 18, in the use of any type of transistor in the avalanche mode; its reliability, performance and its cost. The reliability and retention of initial performance of a transistor

Type	Maker	Cost per unit	No. tested	No. that avalanched	Average r.t. 10-90%	Average max o/p voltage	Average o/p rate (V/ns.)	Remarks
		£-S-d			mμsec			
1. ASZ21	Mullard	—·13·0	4	3	2·5	5·1	1·6	No prolonged testing
2. ASZ23	"	2·11·0	1	1	1·5	5·0	2·7	Reliable
3. 2N501	Philco	2·5·0	20	18	1·3	8·7	4·5	V. Reliable
4. 2N711	Texas	—·11·0	4	4	1·3	6·1	3·7	"
5. 2N960	Motorola	1·11·0	2	2	1·1	6·0	4·4	No prolonged testing
6. 2N976	Philco	2·3·0	13	12	1·3	14·5	8·9	Deteriorated sharply
7. 2G403	Texas	—·5·2	8	5	2·0	2·9	1·2	No prolonged testing
8. 2N1204	Motorola	3·10·0	1	1	1·5	12·0	6·4	Slowly deteriorated
9. 2N413	Texas	—·5·3	4	2	2·0	3·0	1·2	V. Reliable
10. 2N706A	"	—·17·6	5	4	2·2	23·0	8·8	No prolonged testing
11. 2N962	"	1·3·6	5	4	1·2	8·0	5·3	V. Reliable
12. 2G103	"	—·11·8	33	32	2·2	15·6	5·7	"
13. 2G104	"	—·17·6	11	11	2·0	16·5	7·4	"
14. 2N964	"	1·14·0	1	0	0·8	14·0	14·0	"
15. 2S103	"	3·5·0	1	0	—	—	—	———
16. 2N797	"	2·3·0	1	0	—	—	—	———

FIG. 18 Some transistor characteristics

was ascertained over periods of many months operation in avalanche circuits.

Initially, the only transistor obtainable in England, which was manufactured as an avalanche transistor, was the Mullard ASZ23. It was known from the work of Henebry[154] that the 2N711 and the 2N501 transistors avalanched. In early circuits only those transistors numbered 1 to 7 in fig. 18 were investigated. Of these the Philco 2N976 was found to be the best, having a rise time of 8·9 volts per musec. The 2N976 was used successfully in early tube experiments. However, over a period of many months in use its performance deteriorated, sometimes catastrophically. It was found to be unsuitable for the experimental development of circuitry, where transistors may be slightly overloaded. The 2N501 was found to be much better in this respect. It is worth noting that the transistor always exceeds its power rating during avalanche.

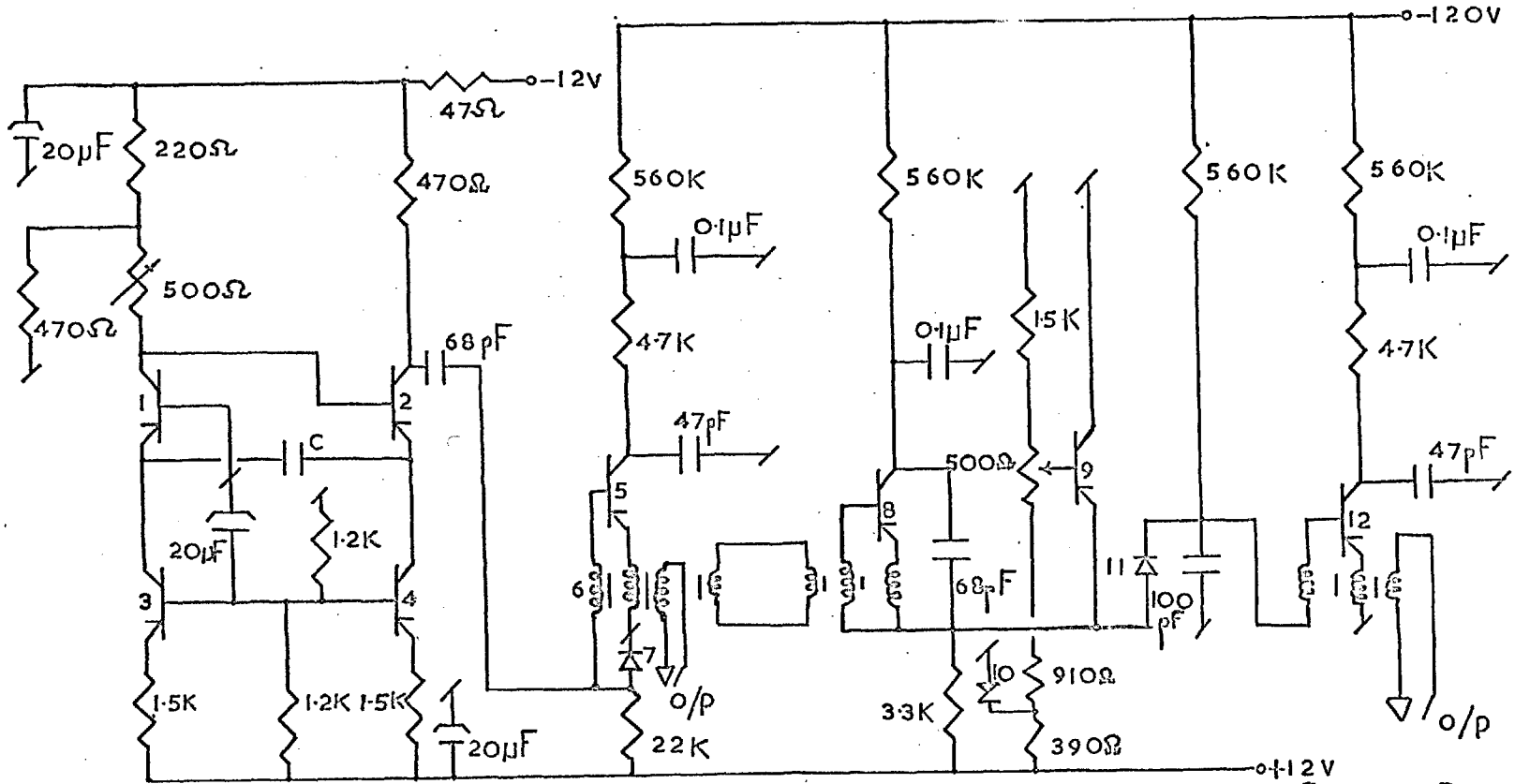
In later work more advanced circuitry was required, and a study was made of various types of transistor for two different requirements. The first requirement was for a cheap reliable avalanche transistor which could be used to develop circuitry and to provide a moderately large output pulse as a trigger in coupling circuit elements together. The second requirement was for an avalanche transistor to provide a voltage pulse of large amplitude with the smallest possible rise time. The first requirement was fulfilled by the Texas 2G103 and the second by the Texas 2N964. In the case of the latter transistor the

rise time of the measuring equipment was not sufficiently fast to indicate the true rise time of the transistor.

6.2 The Hirsch Circuit

The circuit shown in fig. 19 was developed by G. Hirsch while at Imperial College. It produced two output avalanche pulses each of ≏10 mμsec. duration and of 10v amplitude, with a variable delay of from 40-130 musec. between the pulses at a variable repetition rate of 5-50KC/S. Section A of the circuit contained a free running emitter-coupled multivibrator. The two Mullard OC45 transistors were operated as constant current tails to supply the fast switching ASZ21's. The output square wave was taken from the collector of transistor No. 2 (whose frequency was given by Bowes[155] to be $= \frac{1}{4}RC$). C had the value ·1μF and R was the resistance of the collector load of transistor No. 1, which was varied by the use of the 500Ω potentiometer to enable the square wave frequency to be continuously variable. This design of multivibrator has been used in all experiments over a period of 18 months with complete reliability.

The square wave output was differentiated by the LC combination of the 68pF and the inductive load of the base transformer which was wound on a Mullard FX2431 ferrox-cube. The square wave, the leading edge of which rose to 8 volts in 20 mμsec., was differentiated to give positive and negative pulses of 20 mμsec duration and ≏ 1·5 volts amplitude. The positive pulses were clipped by the OA90 diode, the negative pulses being used to trigger the 2N976 transistor in the



Section A
1. ASZ 21
2. "
3. OC45
4. "

Section B
5. 2N976
6. FX2431 Ferroxcube
7. OA90

Section C
8. 2N976
9. OC45
10. OAZ 206
11. AAZ 13

Section D
12. 2N976

FIG. 19 The Hirsch circuit

avalanche mode. This transistor is shown in section B of fig. 19. The emitter 2 contained a transformer which fed back degeneratively, when the transistor avalanched, to reverse bias the emitter-base junction. Therefore, the transistor saw an input pulse whose maximum width was determined by the total propagation delay from the input, through the feedback circuit, back to the input. This delay was of the order 1-2 μsec. The differentiated output pulse was taken from another winding of the feedback transformer.

Section C in fig. 19 shows the delay element of the circuit. Part of the avalanche voltage of the 2N976 was tapped off by a single winding on the feedback transformer to provide a negative trigger for the delay element. This negative trigger was transformer coupled to transistor number 8, whose collector was held by the ·1μF condenser so that the avalanche voltage pulse appeared on the emitter as a negative pulse of about 1 μsec. duration and 15 volts in peak amplitude. The emitter line was d.c. coupled to the base of the avalanche transistor number 12, via a Mullard AAZ13 high speed switching diode. This line was held at a fixed positive potential by the current flowing through the 3.3 KΩ resistor. This current had two components; one flowing through the diode and up through the 560KΩ , the other flowing through the OC45. The current through the OC45 was controlled by the base voltage, which was held by the bias chain. The bias chain was held at a fixed voltage drop against fluctuations in the +12 volts supply by the Mullard OAZ206 Zener

diode. The 500Ω potentiometer controlled the base voltage of the OC45 transistor, which varied the total current through the 3·3 KΩ resistor and thus the positive voltage on the line. The large negative pulse produced by the avalanche of transistor number 8 switched off the diode and the 100pF condenser charged up from the positive voltage of the line towards - 120 volts through the 560KΩ resistor. When however it became more negative than the negative pulse on the line, the AAZ13 diode switched on, returning the line to the steady positive bias.

Section D in fig. 19 shows the second output avalanche transistor circuit. The transistor number 12 was triggered when the negative-going ramp appearing on the 100pF condenser became slightly negative with respect to earth. The delay in the firing of the transistor 12 after transistor 5 was equal to the time taken for the negative-going ramp to travel from the positive bias voltage of the line until it became slightly negative. The delay was altered by varying the positive voltage of the line. The second output pulse was obtained by differentiating the avalanche excursion voltage on the collector of transistor 12 in a similar manner to that of the first output pulse from transistor number 5.

Fig. 20a shows a photograph of the Hirsch circuit, which was constructed on Veroboard. The two gating outputs were taken from two Amphenol type 83-1R sockets, which were screwed into a right-angled metal mounting strip attached to the Veroboard. The gating pulses

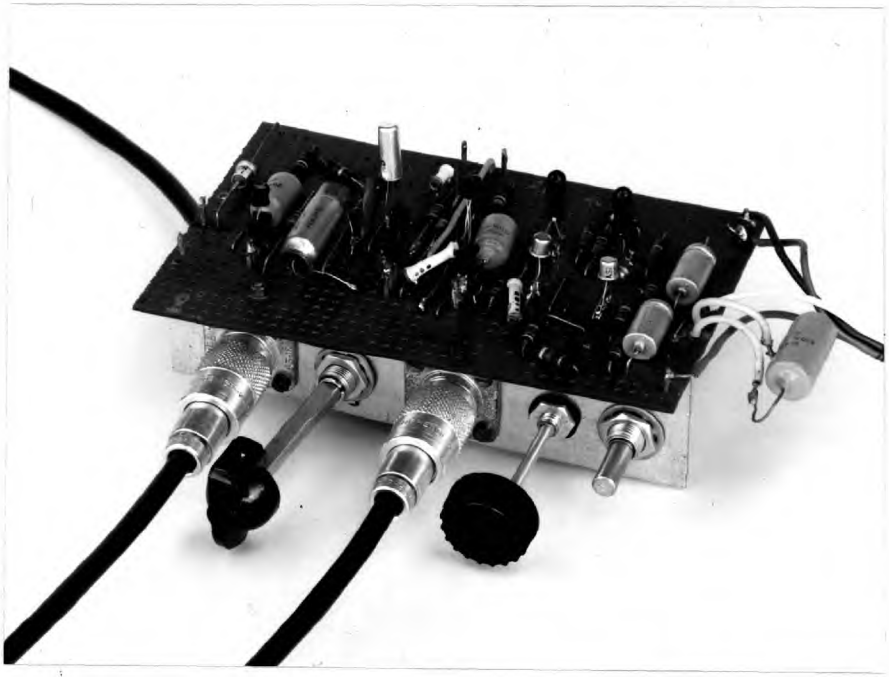


FIG. 20A The Hirsch circuit

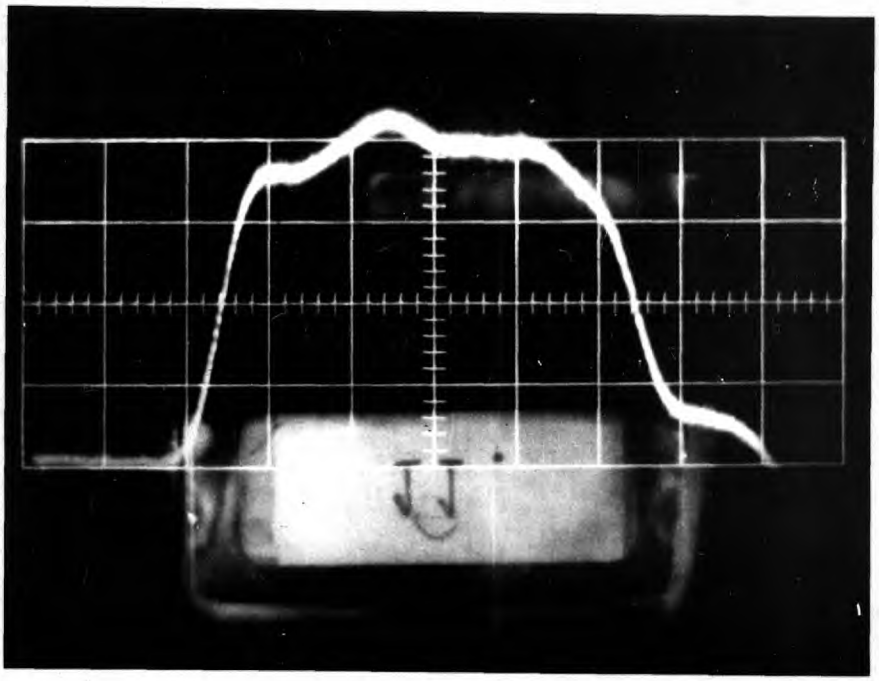


FIG. 20B The output pulse from the Hirsch circuit

were applied to the delay-tube using UR70 70Ω impedance coaxial cable.

Fig. 20b shows a photograph of an oscilloscope trace of a gating pulse, using the Tektronix type N plug-in unit, taken directly from a 50Ω output impedance of the circuit. The vertical scale is 2 volts per division, the horizontal 2 mμsec. per division. The pulse is seen to be approximately square having a rise time of ≏ 1 mμsec. to an amplitude of ≏ 8 volts for a duration of ≏ 10 mμsec. The gating pulse produced by the avalanche circuit shown in fig. 20 produced an approximately triangular pulse of ≏ 2-3 musec. half width duration. The emitter-earth 47pF condenser of that avalanche circuit was replaced by 2' length of UR70 coaxial cable which was used to lengthen and shape the pulse. The inner of one end of the cable was attached to the collector, the output being taken from the outer across 75Ω . The other end was "trimmed" using a small variable condenser of ≏ 2-8pF, to obtain the optimum pulse shape. It must be noted that each transistor required different trimming capacities to produce its optimum shape.

6.3 Pulse circuitry using plug-in modules

In later experimental work a series of pulses were required at various extremely long or short delays. The circuit arrangement described in section 6.2 was not sufficiently flexible to meet these requirements. It was therefore decided to build up the basic circuit elements on completely separate plug-in modules, which could be easily re-arranged in the circuit. These circuit modules were built

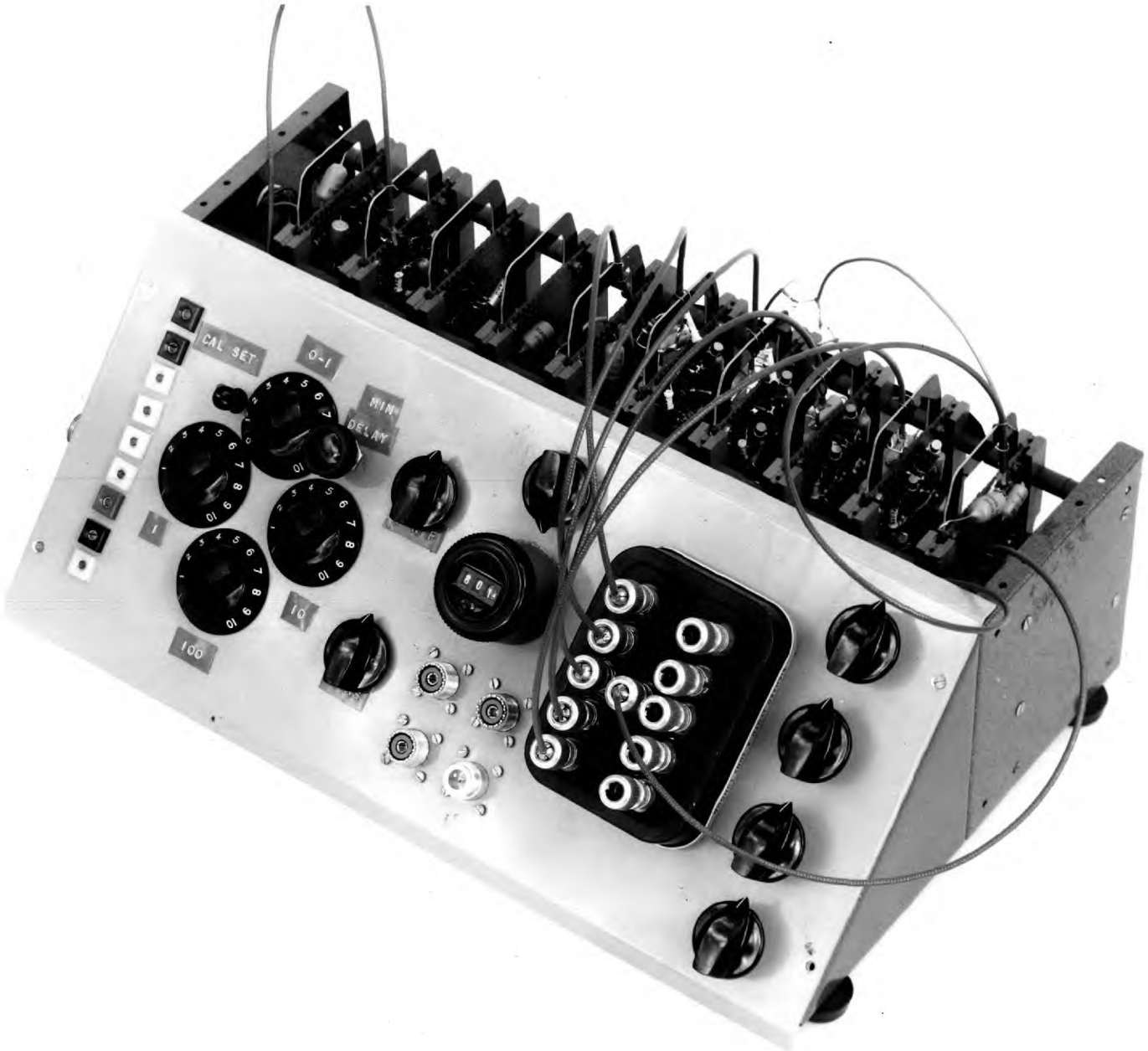


FIG. 21

up upon plug-in Veroboards type VB2503, which fitted into edge connectors (VB3086). A 17" length of Veroboard type VB1501 was used to interconnect the contacts of the edge connectors. Each circuit module was built up upon 16 copper strips; the 12 volts positive and negative lines, the 120 volts positive and negative lines, the earth lines and the pulse trigger lines being common to all plug-in modules. The whole assembly was housed in Lektrokit chassis panelling. A photograph of a complete gating circuit for the framing camera, described in chapter 9, is shown in fig. 21.

Five separate types of circuit modules were designed:

Module one (M.1) Master oscillator and the positive and negative pre-trigger generator.

Module one is illustrated in fig. 22a. It comprised the free running multivibrator, described in section 6.2, adjusted to operate at frequencies of 1-5Kc/s. The voltage square wave generated on the collector of the ASZ21 was differentiated to produce negative spikes which triggered the 2G103 transistor in the avalanche mode. A 1KΩ load was placed in both the emitter and collector circuits of the 2G103 transistor. Hence a positive collector excursion and a negative emitter excursion were produced upon avalanche. Both these voltage excursions were differentiated by the 82pF and 100Ω networks, to supply positive and negative pre-triggers.

Module two (M.2) The output pulse generator

Module two is illustrated in fig. 22b. It comprised the standard

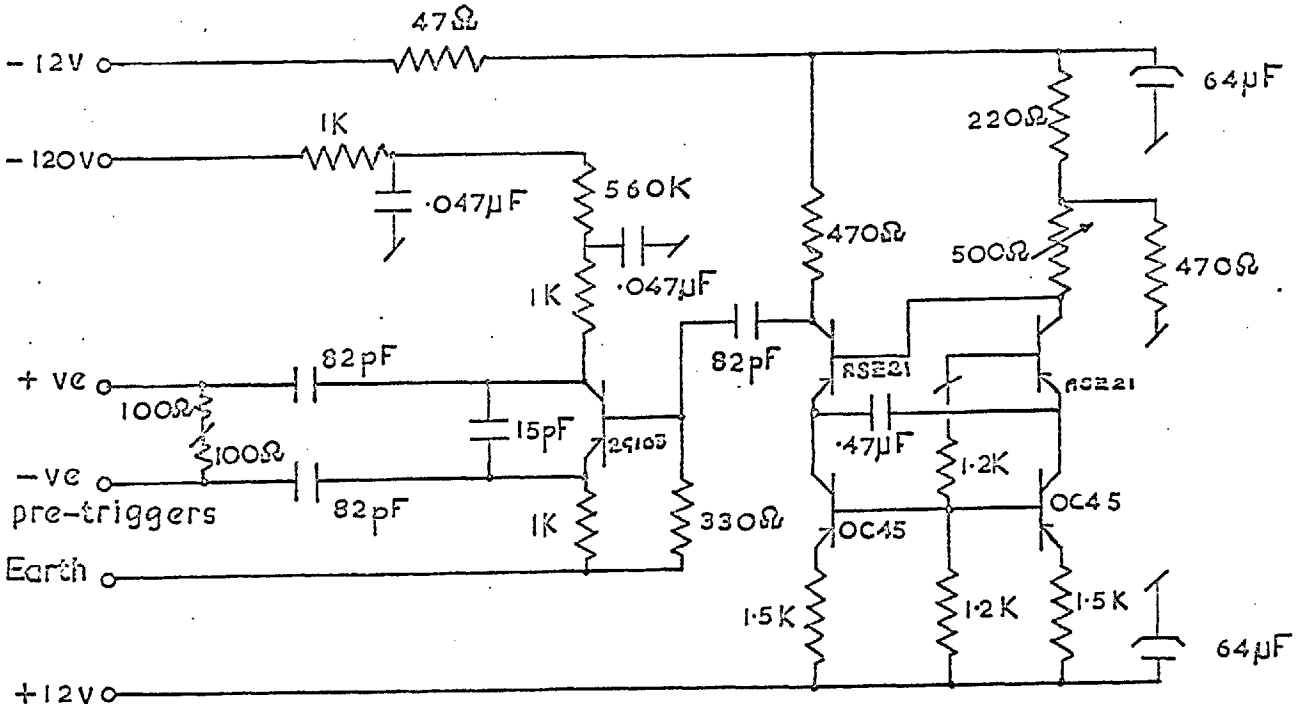


FIG. 22A Module one (M1)

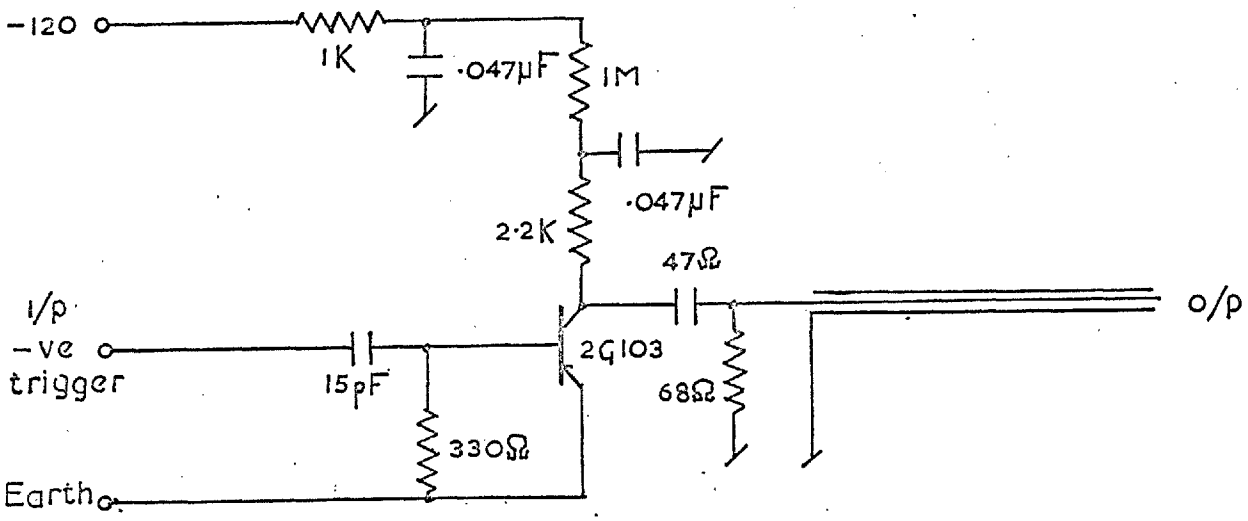


FIG. 22B Module two (M2)

avalanche transistor circuit, described in section 6.2, which required a negative pulse of $\simeq$ 2 volts amplitude and $\simeq$ 10 μsec. duration for triggering. The collector voltage excursion was differentiated using an RC combination to produce the output pulse. The shaping of this output pulse using coaxial cables will be described in the next section. This pulse was taken to the circuit output socket (Transradio Ltd. type GE071/75) using 75Ω impendance sub-miniture cable type N03/75.

Module three (M.3) The delay voltage bias generator

Module three is illustrated in fig. 23a. It supplied an extremely accurately controlled positive voltage bias which determined the length of temporal delay between the input and output triggers of module four. The OAZ226 Mullard Zener diode dropped a constant voltage of $\simeq$ 6•5 volts across the 2•2 KΩ resistor in series with the control potentiometer. The control potentiometer was one of two different types which could be switched in as desired. The first type was a 5KΩ potentiometer manufactured by Colvern Ltd. (type CLR26/00 having 10 turns with a Linear accuracy of $\pm$0•1%). This potentiometer was set using a Colvern digitised dial with an accuracy of $\pm$•01% over a three decade range. The second type was a step potentiometer illustrated in fig. 25. This comprised three decades of resistors arranged in ganged pairs in order that the potentiometer maintained a constant load across the reference voltage supplied. The first decade consisted of ten pairs of 200Ω resistors, each

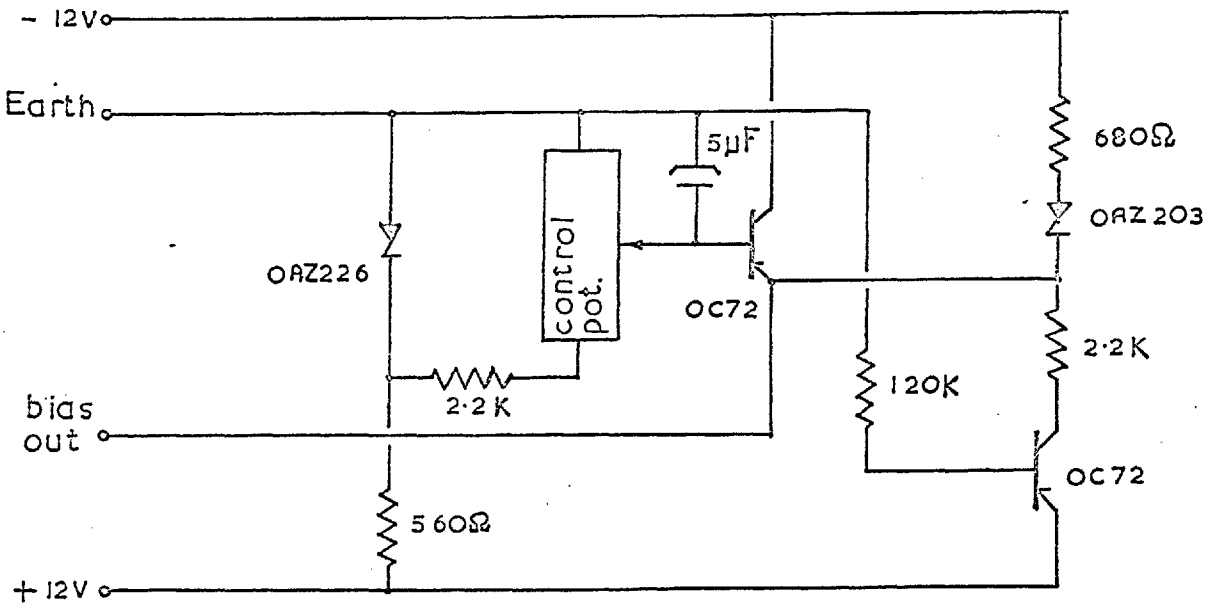


FIG. 23A Module three (M3)

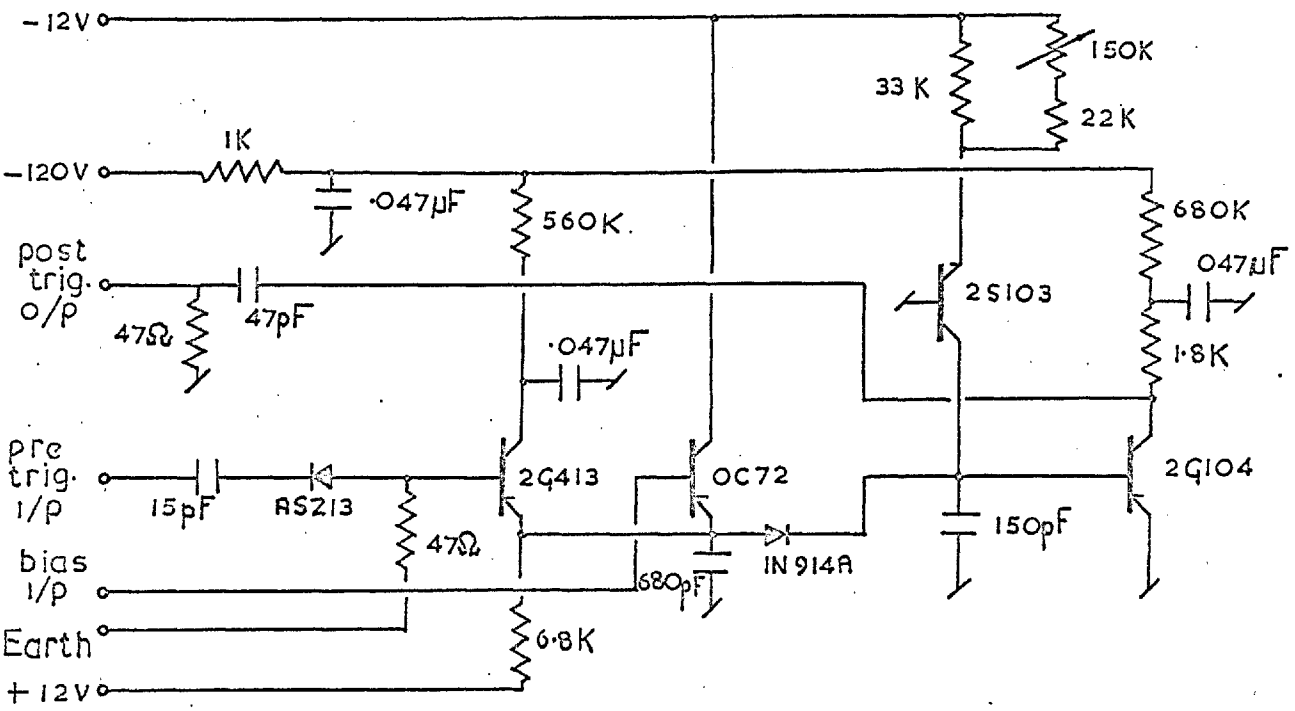


FIG. 23B Module four (M4)

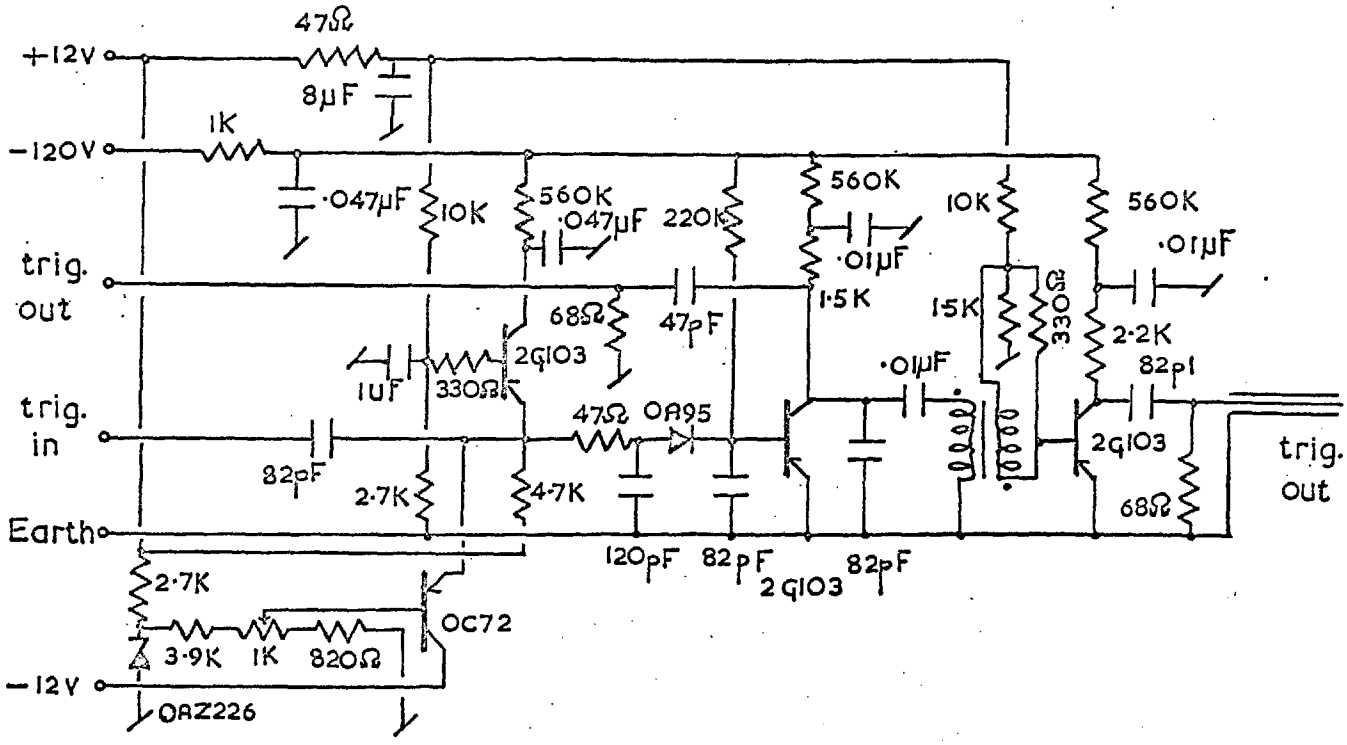


FIG. 24A Module five (M5)

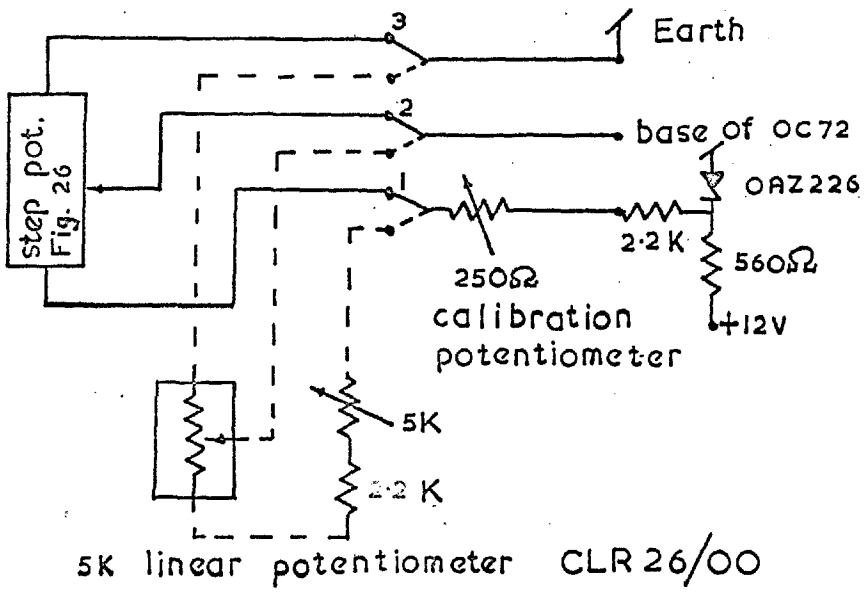


FIG. 24B The voltage holding network for the calibrated delay

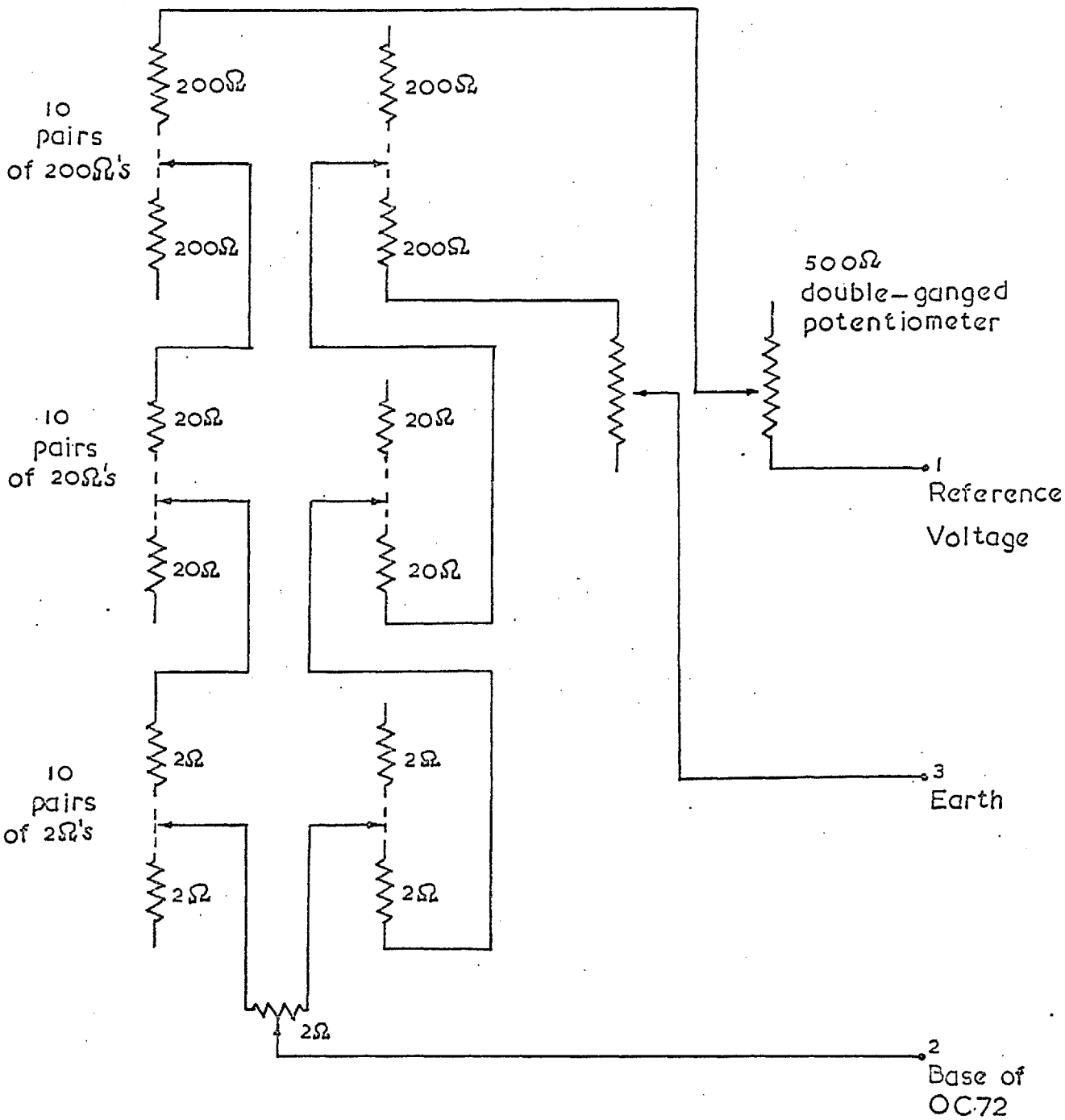


FIG. 25 The step-potentiometer used for the calibrated delay

having a resistance value within ±0·1%. The second decade consisted of ten pairs of 20Ω resistors each having a resistance value within ±0·1%. The third decade consisted of ten pairs of 2Ω resistors each having a resistance value within 1%. A 2Ω potentiometer was included to provide a fourth decade resistance range. Thus a resistance could be set on this control potentiometer to within 0·1% of the total resistance. A 500Ω double ganged potentiometer was employed as shown in order that a minimum resistance of up to 500Ω could be placed in series with the step-potentiometer.

The switching arrangement between the two control potentiometers is illustrated in fig. 24b. The resistance in series with the 5KΩ Colvern potentiometer was adjusted using another 5KΩ potentiometer until the voltage drop across both control potentiometers was exactly the same. Thus both control potentiometers were able to be set at the same voltage output over a three decade range, with a slightly less setting accuracy over a fourth range. The voltage and therefore the temporal delay could be varied in incremental steps or continously as was convenient in a particular experiment.

The voltage from the control potentiometer was applied to the base of OC72 transistor, which by emitter followed action produced the same voltage at the bias output. This bias was applied to the base of the 2G104 transistor in module four and determined the temporal delay. Since the maximum reverse base-emitter voltage which could be applied to the 2G104 transistor was 3·5 volts, the output

bias from module three was arranged never to exceed ± 3 volts. Since, during the break before the make of the step-potentiometer, the output bias could rise to 6·5 volts, an OAZ203 Zener diode was incorporated to hold the bias output voltage to 3·2 volts. An OC72 transistor was biased to supply a current through the OAZ203, which held it below its voltage turnover point.

Module four (M.4) The delayed trigger generator

Module four is illustrated in fig. 23b. It supplied an output trigger pulse accurately delayed with respect to the input trigger pulse; this delay being controlled by the bias from module three. The temporal delay was achieved using very similar circuitry to that described in section 6.2. The negative ramp, which determined the delay, was generated by allowing the 150pF condenser to charge up towards the - 12 volts supply. The 2S103 transistor supplied a constant current in order to produce a linear ramp, i.e. a linear temporal delay. The temporal delay provided by the circuit was adjusted, until the control potentiometer scale was calibrated exactly against the temporal scale of the Tektronix oxilloscope, by varying the 150KΩ potentiometer of module four and the 250Ω potentiometer illustrated in fig. 24b.

Module five (M.5) The double delayed trigger generator

This module is illustrated in fig. 24a. It provided two output trigger pulses delayed variably, but with no calibration facility. The circuitry was arranged as described in section 6.2, the component

values shown providing a delay of 50-300 μsecs.

6.4 The generation of square gating pulses of μsec. duration

The positive voltage gating pulses which were applied to the copper mesh of the delay tube, were required to be as square in shape as possible if geometrical resolution of the electron image was not to be lost. The normal avalanche pulses were squared using the capacitance of sub-miniature coaxial cables in the RC differentiating network. The circuits used to obtain pulses of total duration 22 μsec., 11 μsec. and 4·5 μsec. are described below.

6.4.1 The generation of a pulse of 22 μsec. duration

The circuit developed for the generation of a pulse of 22 μsec. duration is illustrated in fig. 26a. The transistor used in the avalanche mode was the Texas 2G103. The avalanche circuit previously described in section 6.1 was employed, with the addition of a 15pF feedback condenser across the base-collector junction. The differentiating capacitor used was the 20pF condenser in parallel with the coaxial cable. The section of cable denoted 1 was 25 cms. of Transradio type NO3/50 and determined, with the 20pF condenser, the length of the pulse. A loop of the same cable, denoted by 2, determined the fall time of the trailing edge of the pulse. Its length was adjusted to 30 cms. which produced the most nearly square pulse shape. The shaped pulse was carried to the circuit output socket (4) by a length of transradio cable type NO3/75. This pulse was carried to the tube by a length of Transradio AIT cable (5) where its

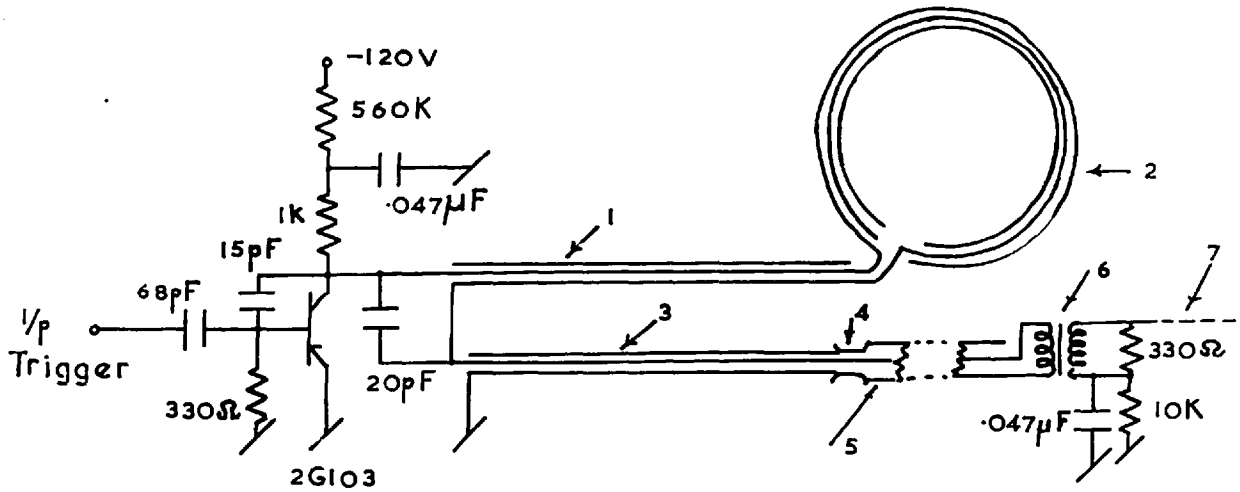


FIG. 26A A 22 μsec. duration pulse generator

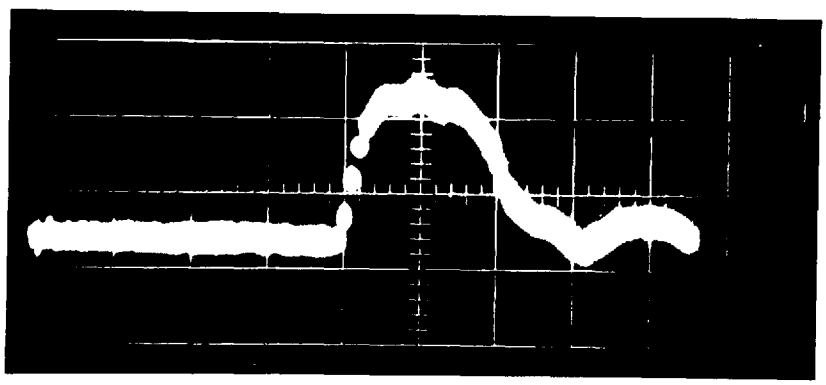


FIG. 26 B 5 V/cm. / 10 μsec/cm

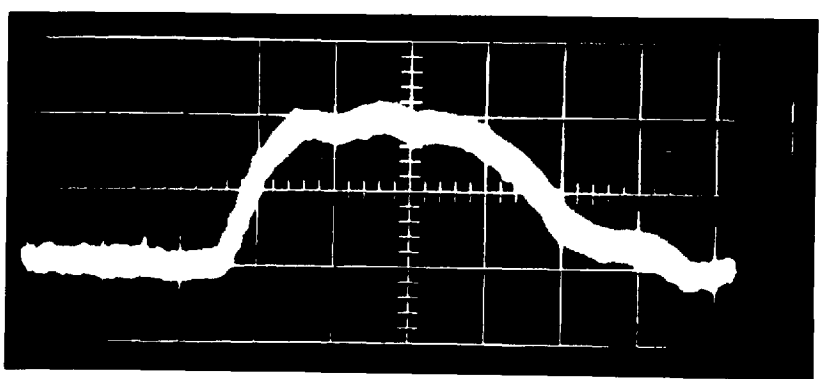


FIG. 26C 5 V/cm / 5 μsec/cm

amplitude was approximately doubled using a ferrite transformer (6). The resulting pulse was applied to the copper mesh (7) of the tube across a matching 330Ω resistance.

The voltage pulse shapes obtained on the copper mesh ring measured using the N type Tektronic sampling unit with the P6025 cathode-follower probe, are shown in fig. 26b and fig. 26c. Fig. 26b shows the applied pulse where the vertical scale of the oscilloscope was 5V/cm division and the horizontal scale was 10 musec./cm division. Fig. 26c shows the same pulse where the sweep speed was 5 musec./cm division.

6.4.2 The generation of a pulse of 11 musec. duration

The generation of a shorter pulse than that developed by the circuit described in the previous sub-section required a few alterations to the circuit shown in fig. 26a. The 20pF condenser was removed, cable 1 was retained and cable 2 shortened to a 9 cm length. In addition, a 15pF condenser was connected between the free inner and outer connections of cable 2. The pulse applied to the tube was measured as above, the resulting oscillograms being shown in fig. 27. Fig. 27a shows the oscillogram of the applied pulse, with a vertical scale of 5V/cm division and a horizontal scale of 5 musec./cm division. Fig. 27b shows the same pulse, with a horizontal scale of 2 musec./cm division. Fig. 27c shows the linearity of the step-control potentiometer of module three, when the circuit step-delay was increased in steps of 10 musec. The horizontal scale of fig. 27c

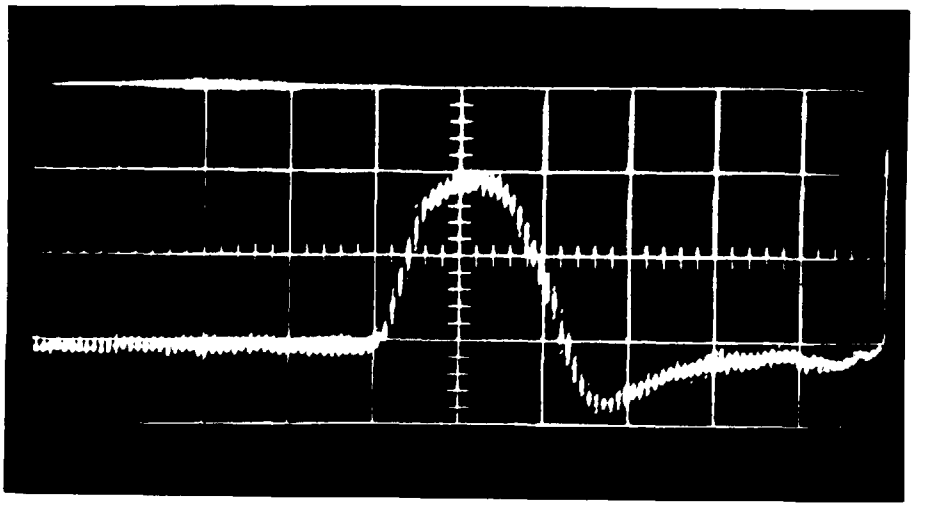


FIG. 27A 5V/cm/ 5 mμsec/cm

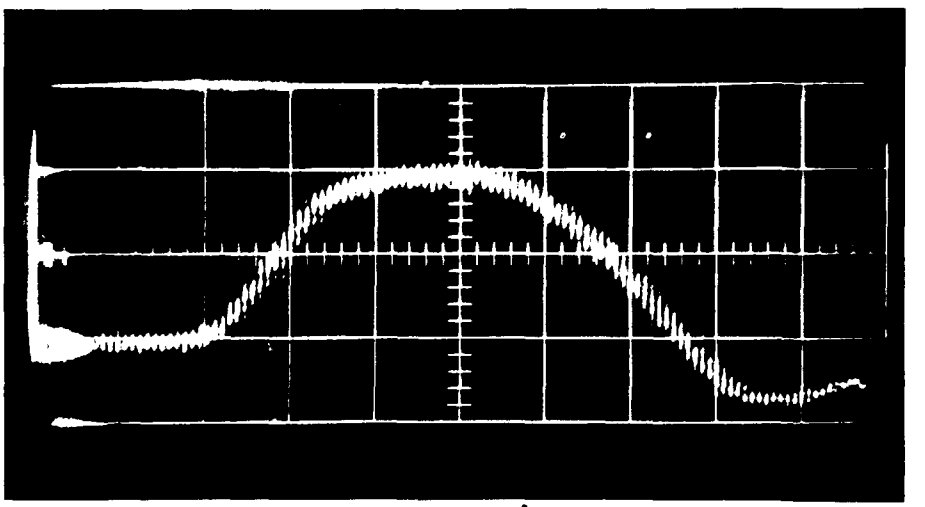


FIG. 27B 5V/cm/ 2 mμsec/cm

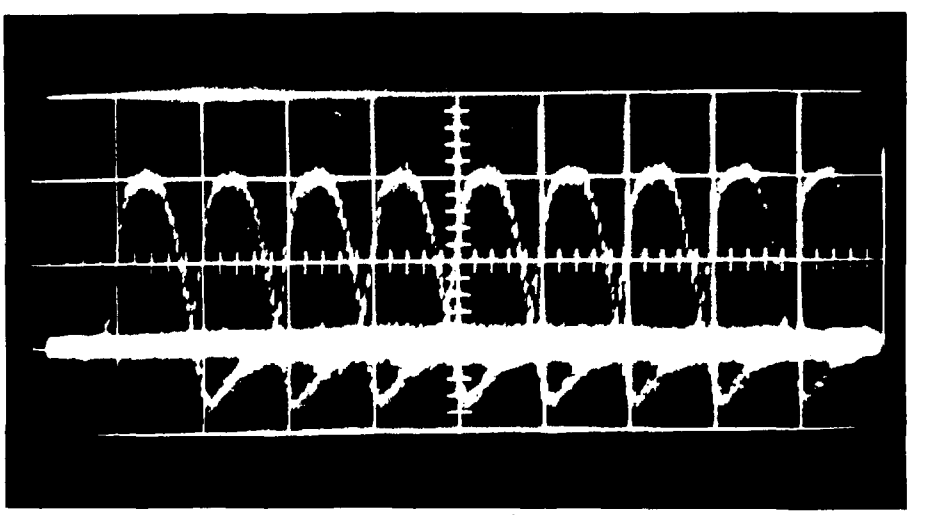


FIG. 27C 5V/cm/ 10 mμsec/cm

was 10 μsec./cm division.

6.4.3 The generation of a pulse of 4·5 μsec. duration

The generation of a pulse of 4·5 μsec. duration required further modification to the circuit shown in fig. 26a. A Texas 2N964 transistor replaced the 2G103 previously used. The length of cable required as cable 1 needed to be 4 cms long to produce a pulse of length 4 μsec. Since a single length did not provide sufficient capacitance to obtain maximum pulse height, three cables (type NO3/50) each of length 4 cms were used in parallel. A loop of NO3/50 cable, 7 cms in length, was used as cable 2 to provide pulse squaring action. Since the pulse shape would have been slightly degraded by using the ferrite transformer, the pulse was applied directly to the copper mesh using 68Ω matching resistance without using a transformer.

The pulse appearing on the copper mesh ring was measuring using the oscilloscope as above, and is shown in figs. 28a and b. The oscilloscope horizontal sweep speeds are 2 μsec./cm and 1 μsec/cm in figs. 28a and b respectively. The vertical scale in both cases is 4 V/cm division. It is seen that the rise time of the pulse is $\lesssim$ 1 μsec. Since the combined rise time of the P.6025 probe and the N type sampling unit is $\triangleq$ .8 μsec., any serious work to produce a pulse of shorter duration must use a faster sampling oscilloscope, e.g. a Tektronix type 661, which has a rise time of ·1 μsec.

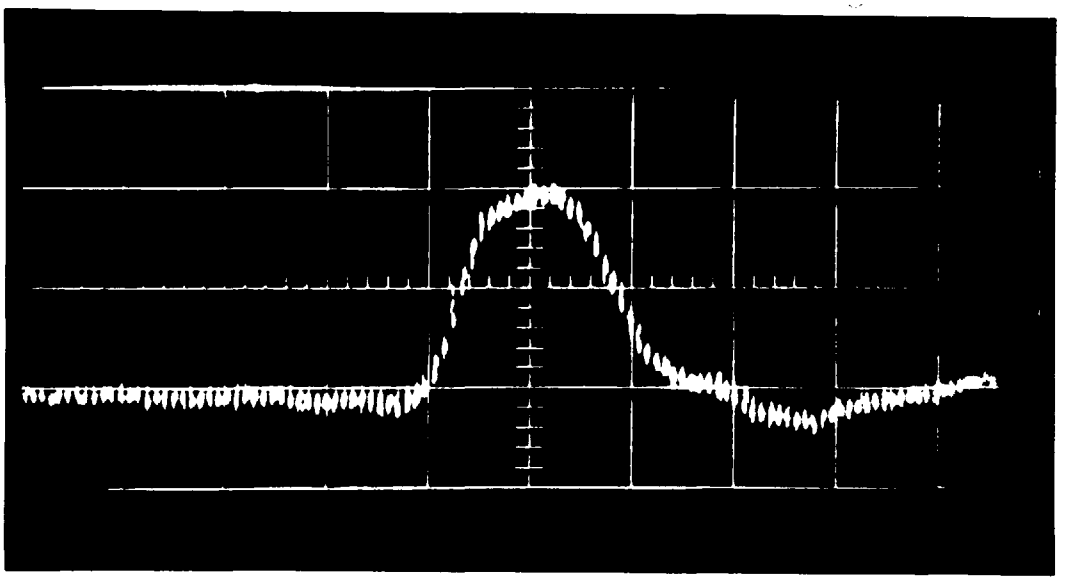


FIG. 28A 4V/cm/ 2 mμsec/cm

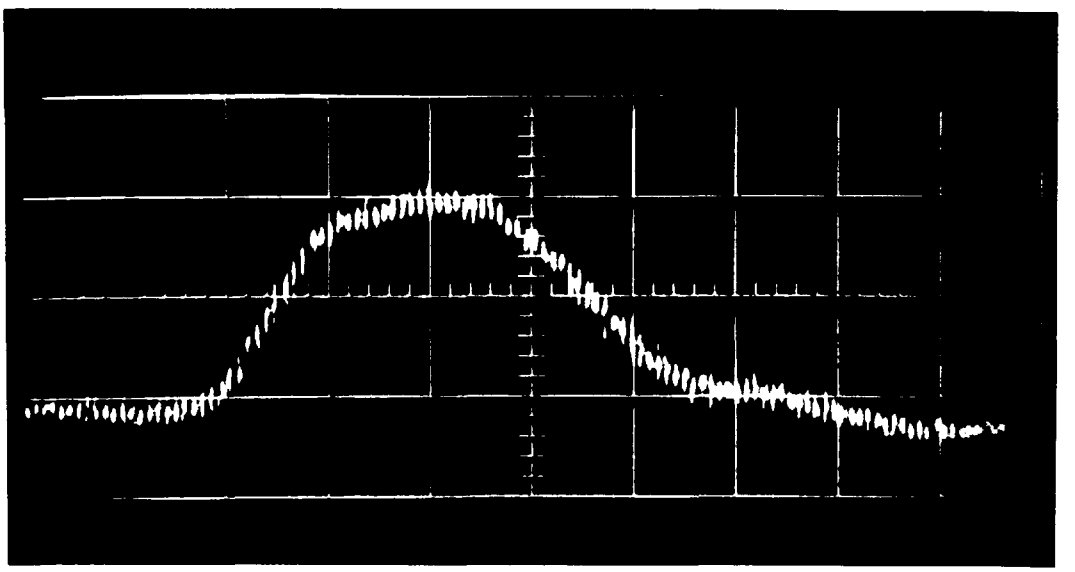


FIG. 28B 4V/cm/ 1 mμsec/cm

6.5 The measurement of various parameters of the Tektronix 545A oscilloscope

6.5.1 The rise time of the light output from P.16 phosphor under cathode ray excitation

The P.16 phosphor screen, deposited in the C.R.T. of a Tektronix 545A oscilloscope was used as a triggered high speed light source. The rise time of its light output was measured using the experimental arrangement illustrated in fig. 29. Two oscilloscopes were used triggered by the circuit containing modules M.1-2-3-4-2, which are described in section 6.3. The pre-trigger pulse triggered the horizontal time base of the Tektronix 545A oscilloscope which contained the P.16 phosphor C.R.T. tube. The horizontal trace produced on the oscilloscope was completely covered except for a vertical slit 1 mm. in width. A light output pulse produced by the trace crossing the slit was collected and converted into an amplified electrical pulse by the Mullard 56AVP photomultiplier. This pulse was displayed on the Tektronix 551 oscilloscope using the N type sampling plug-in unit. The N unit was triggered by a pulse from the trigger circuit accurately delayed with respect to the pre-trigger pulse. Since the delay between the pre-trigger being applied to 545A and the trace first appearing on the CRT screen was $\triangleq$ 150 musec. and since the slit was placed at the centre of the trace, which was swept at 20 musec./cm, the output signal pulse from the photomultiplier appeared $\triangleq$ 250 musec. after the pre-trigger was applied to the 545A

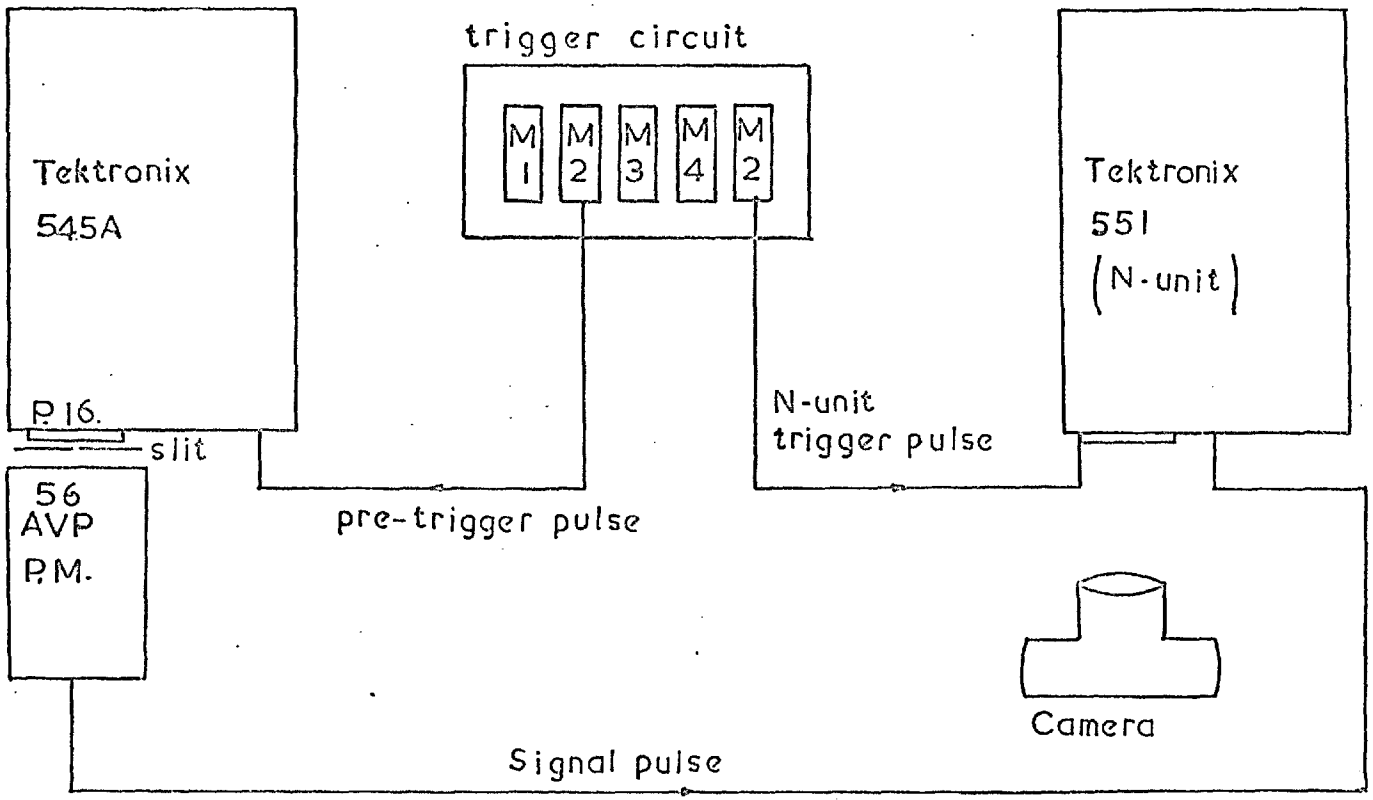


FIG. 29 The experimental arrangement used to determine the rise time of P16 phosphor

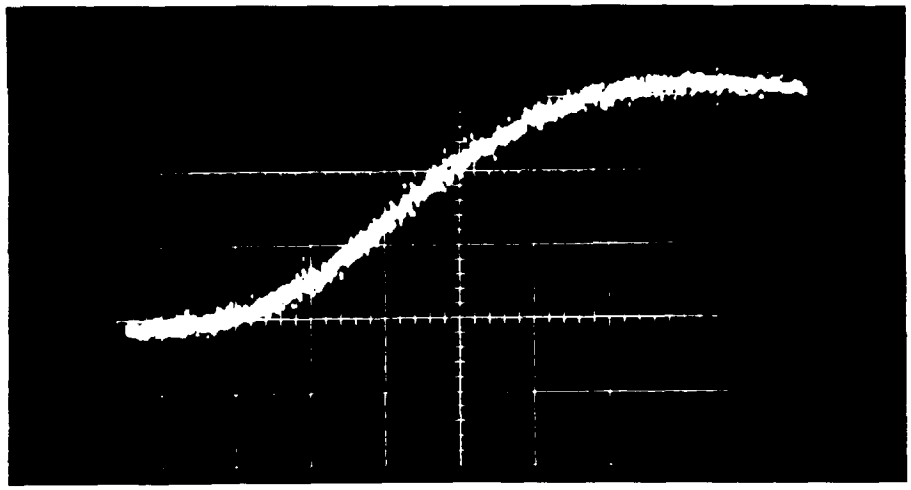


FIG. 30A Arb.units / 1mμsec/cm

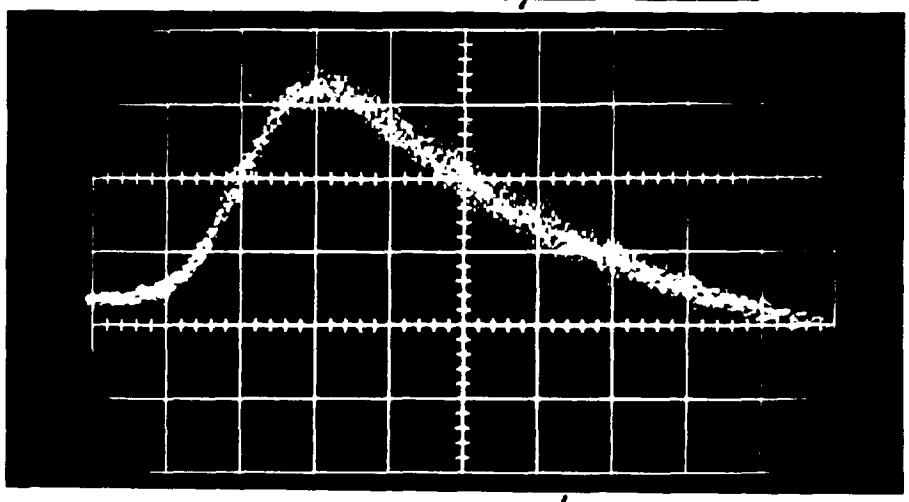


FIG. 30B Arb.units / 10 mμsec/cm

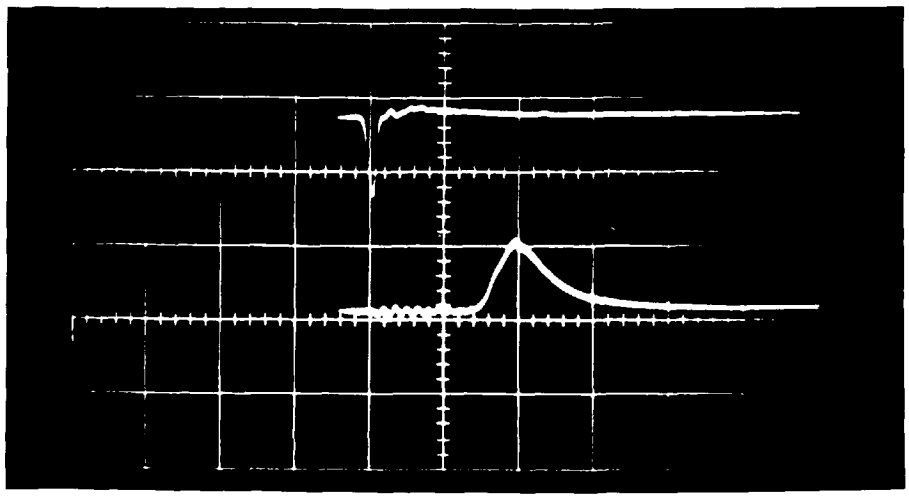


FIG. 30C Arb.units / 100 mμsec/cm

oscilloscope. The N type unit required to be triggered ≙ 45 mμsec. prior to the signal pulse being applied. Therefore the delay between the two triggers provided by the Trigger circuit needed to be ≙ 205 mμsec. The final adjustment between the trigger and signal pulse was completed using the small delay variation available in the N type plug-in unit.

The resulting oscilloscope traces, recorded photographically, are shown in figs. 30a and 30b. Fig. 30a shows the rise time of the light output pulse from the P.16 phosphor, where the horizontal scale is 1 mμsec./cm division. It is seen that the 10-90% rise time of the trace is 3·5 mμsec. Since the rise time of the oscilloscope slit source was 2 mμs, the rise time of the N type plug-in unit was ·6 mμs, and the rise time of the Mullard 56AVP photomultiplier was 2 mμs; the rise time of the P.16 phosphor under electron bombardment was given by t where:

$$3{\cdot}5^2 = 2^2+2^2+{\cdot}6^2+t^2$$

Hence $t \triangleq 2$ mμsec.

Fig. 30b shows the rise time and fall time of light output pulse from P.16 phosphor where the oscilloscope trace crossed the slit in ≙ 15 mμs. The decay time to zero light output is seen to be ≙ 70 mμs; where the horizontal scale is 10 mμs/cm division.

6.5.2 To measure the triggering delay of the Tektronix 545A oscilloscope

It was of interest to measure the delay required by the circuitry

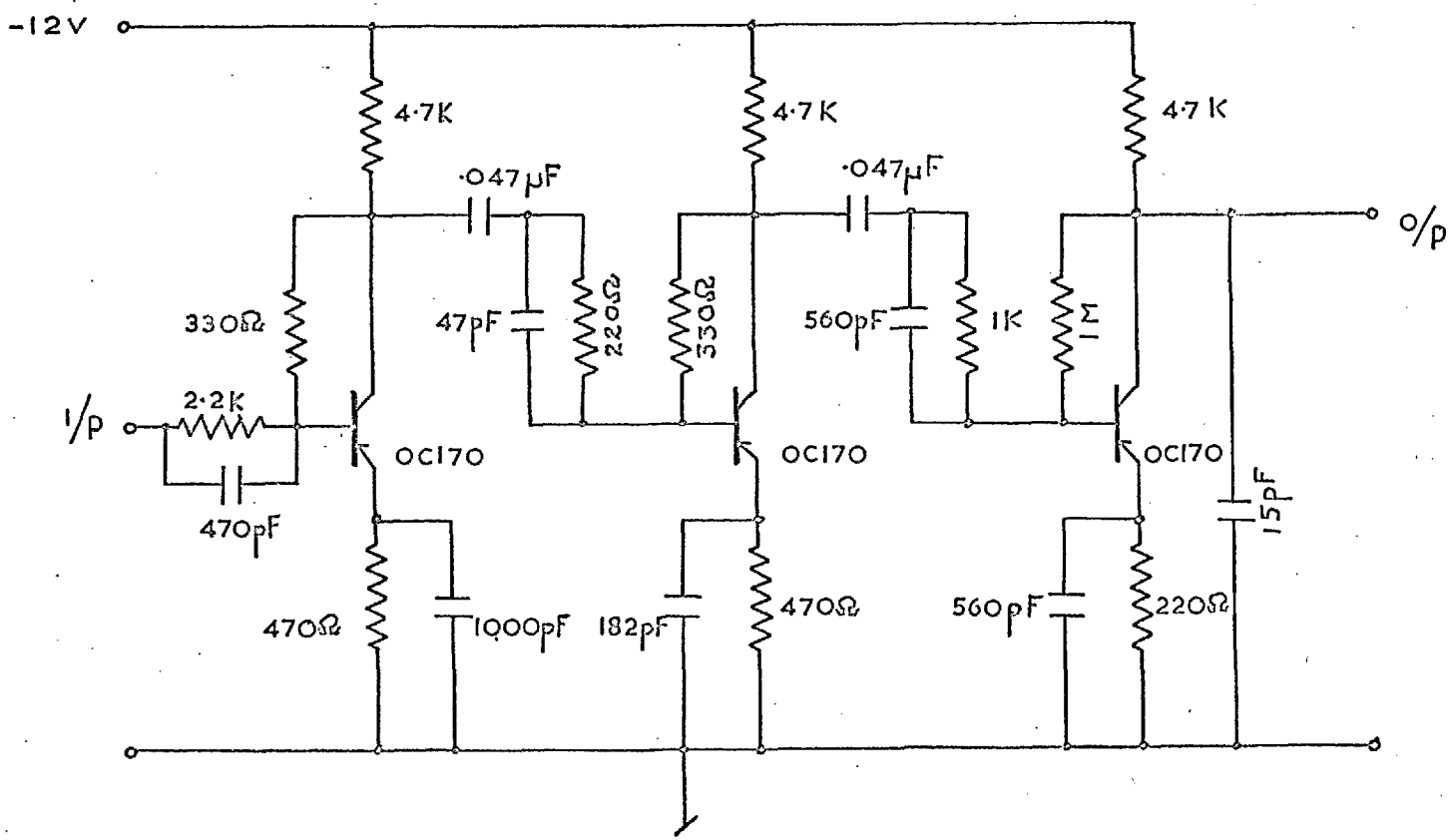


FIG. 31 A high-gain, large-bandwidth amplifier

of the Tektronix 545A oscilloscope to produce the start of the horizontal sweep of the oscilloscope trace after being triggered. The experimental arrangement, illustrated in fig. 29, was modified in the following manner. The N plug-in unit of the Tektronix 551 oscilloscope was removed and replaced by an L plug-in unit, the oscilloscope being then used as a normal double-beam oscilloscope using two L plug-in units. The pre-trigger pulse applied to the Tektronix 545A oscilloscope was displayed on the top beam of the 551 oscilloscope; the signal pulse from the 56AVP photomultiplier was displayed on the lower beam. The two L units used had the same internal delay between a signal being applied at their inputs and appearing on the vertical deflection plates. The oscilloscope traces produced are shown in fig. 30c, where the horizontal scale of the trace is 100 mus/cm. The delay between the two pulses is seen to be $\pm$ 150 musec, which is the Triggering delay of the Tektronix 545A.

6.6 High gain - large band width amplifier

A high-gain, large-bandwidth amplifier, comprising three Mullard OC170 transistors, is illustrated in fig. 31. The amplifier has a flat response over frequencies of 1KC/S - 10MC/S, with a voltage gain of 2,000.

Chapter 7 The construction and performance of simple image delay tubes

This Chapter describes the development of tubes having a delay section, but having no electron multiplying elements.

7.1 The construction of early image delay tubes

Six tubes were constructed by the author having the same general design as that shown in fig. 32. The first two tubes were each manufactured as a single envelope; a cylinder 62 cms. long and ≏ 7 cms. in external diameter, with the photocathode end ground and polished flat. When the tube was painted and the paint fired in, it was assembled from one end using the two long assembly tools shown in fig. 33c. The metal electrodes and other parts were assembled in succession from the phosphor end towards the photocathode end. The gating mesh was fabricated from 600 t.p.i. Cu mesh having ≏ 50% shadow ratio. The potential of both ends of the equipotential delay section were well defined using very coarse tungsten meshes of ≏ 50 t.p.i. The photocathode plate was mounted by clips on the photocathode side of the metal annulus which held the first tungsten mesh. The tube was sealed-up with a circular flat Pyrex end plate, which had been painted with platinum paint on both sides, using the silver chloride sealing technique. This platinum layer served to facilitate the running-in of the silver chloride during the seal-up, and to provide external electrical contact with the photocathode. Argon was continuously passed through the tube during seal-up to

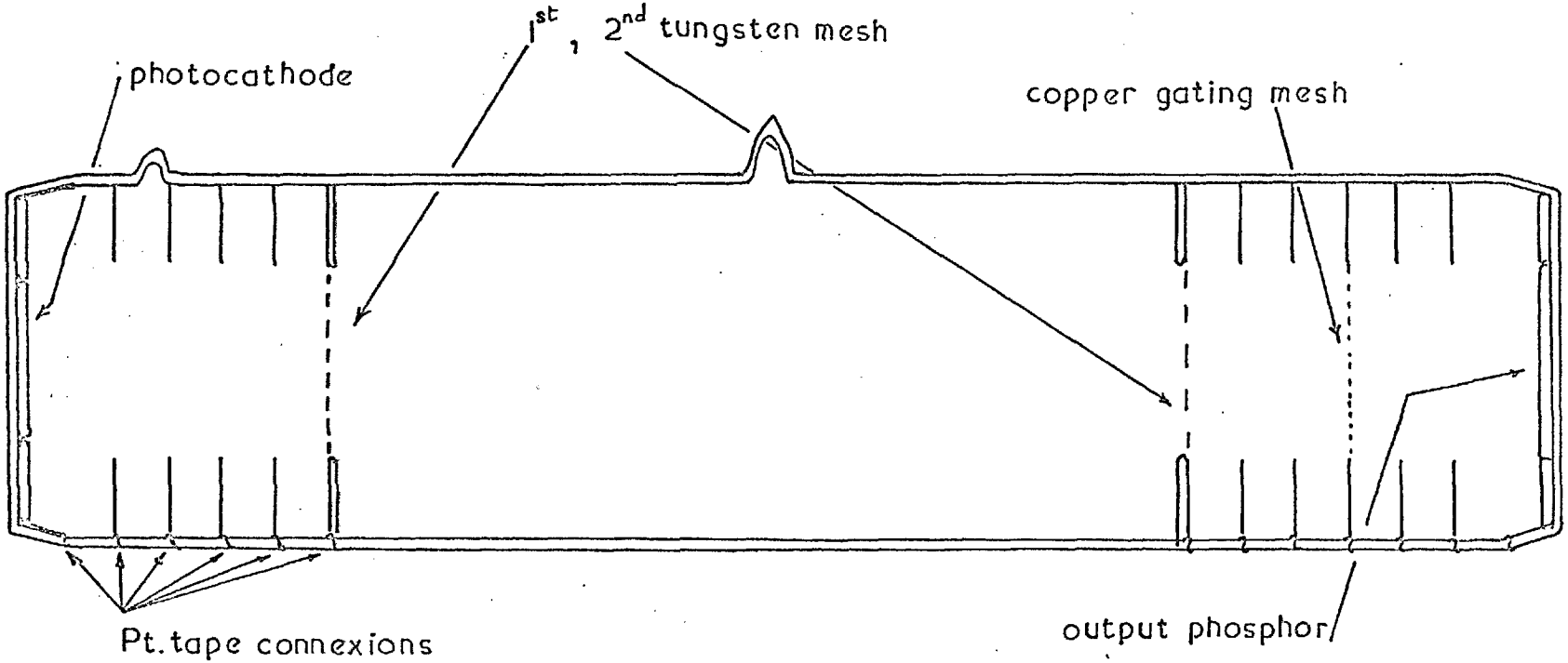


FIG. 32 The simple image-delay tube

prevent oxidation of the metal electrodes.

The tube was sealed onto the pump with the photocathode uppermost. During baking and pumping, the photocathode plate was held slightly open to enable the front section of the tube to be pumped at greater speed. Before activation the magnetic catch holding the photocathode plate open was released to seal-off the front section of the tube as an activation compartment. The antimony layer was evaporated from the position X and the activation completed as described in section 5.6. After the tube was sealed-off from the pump, the photocathode plate was released and moved forward to its final position against the front window, to be held in place by a magnetic catch.

The 3rd and 4th tubes were similar to the first two, in that they contained the same electrode structure. They were however, made in two separate halves to facilitate the envelope preparation and final assembly. Final seal-up was made using the silver chloride sealing technique at a point in the equipotential delay section $\simeq$ 10 cms. from the 2nd tungsten mesh. A photograph of this type of tube looking at the phosphor end is shown in fig. 33a. The design of the 5th and 6th tubes is shown in fig. 10. The tubes were again made in two halves. The high voltage section of the tube was lengthened to enable a higher applied voltage to be used in producing a brighter output image. A second gating mesh, made of tungsten, was incorporated at a distance of 7 mms. from the photocathode so that when the mesh was maintained at 10 volts. positive, a uniform accelerating gradient



FIG. 33

to the 100 volts equipotential section was produced. Since the platinum tape that could be sealed nearest to the end window had to be used to obtain electrical connection with the tungsten mesh, electrical connection to the photocathode was obtained using platinum paste sealed-in at the edge of the front window. In the 5th tube, shown in fig. 33b looking at the photocathode end, the photocathode was activated in its final position. The antimony layer was evaporated onto the photocathode plate through the tungsten mesh, which was R.F. heated afterwards to remove the antimony which had been evaporated onto it. This prevented the formation of a photosensitive surface on the tungsten mesh when the caesium was introduced. It was difficult to obtain a satisfactory monitoring sensitivity whilst activating this tube, probably because there was no effective activating compartment in which to trap a reasonable concentration of caesium vapour. The Sb-Cs photocathode produced had a measured sensitivity of 8uA/Lm after seal-off.

In the 6th tube the cathode plate was placed in the same position as in the first four tubes for activation. The tungsten gating mesh was spot welded to a stainless steel annular ring 0·02" thick and of 34 mms. internal diameter and 38 mms. external diameter. This ring fitted into an annular groove in an annular disc 0·05 thick, which had an external diameter of 57 mms. and an internal diameter of 36 mms. The width of the mesh aperture was limited to 34 mms. by the width of the roll of tungsten mesh available. During processing

the tungsten mesh was held open on a hinge at right angles to its retaining annulus by means of a magnetically operated catch. A photograph of this mechanism is shown in fig. 39b(1). After the photocathode had been activated in the processing compartment and the tube had been sealed off the pump, the photocathode plate was released, moved forward through the aperture of the annulus, which retained the mesh, and clipped into position against the front window. The cathode plate was made 34 mms. in diameter in order that it could be easily moved through the 36 mms. wide circular aperture in the annulus which retained the mesh. After the cathode plate had been clipped into its final position, the catch holding the tungsten mesh open was released and the mesh clipped into its retaining groove by means of another magnetically operated catch.

This method of activating, using an activation compartment separated from the rest of the tube, proved more efficient than one in which no compartment was used. In the five tubes made in the former manner the sensitivities of the Sb-Cs photocathodes produced were in the range 20-30 μA/Lm.

7.2 The performance of the early image delay tubes

The first three tubes each went "soft" after a period of about three weeks. Whether this was due to a leak in the tube envelope or to degassing of the metal parts was not ascertained. The metal parts in the first three tubes were degassed in vacuum using an R.F. generator to heat them. A vacuum stove was available to treat the

metal parts from the fourth tube onwards. In the latter case the lives of the tubes were in general extended beyond three weeks.

In the first four tubes a maximum voltage of 7·5 KV could be applied to the last section of the tube, before internal electrical break down occured. It was found that the copper gating mesh first started to turn the image "on" at a voltage of 1-2 volts positive, the image being fully "on" at ≏ 4·5 volts positive. Loop focusing in the very high voltage section was observed at magnetic fields of from ·005 - ·05Webers/meters^2.

A visual measurement of the output resolution of the delay tube was made using the test pattern described by Baum(156). The variatio of the measured output resolution against the potential applied to the gating mesh is illustrated in fig. 34. At the lower applied magnetic field the resolution exhibits an almost linear increase with the mesh potential. At higher magnetic fields (·05W/m^2 being the highest field that could be applied) the resolution sharply increases with applied mesh potential until a potential of ≏ 25v. After this "knee" potential there was a small increase in resolution with mesh potential. The above measurements were taken on the fourth tube, 240 volts positive being applied to the equipotential section, optimum resolution being found by adjusting the e.h.t. on the output section. The output resolution was observed to increase with the applied magnetic field. This relationship is illustrated in fig. 35a for low applied magnetic fields and a fixed potential of 100 volts

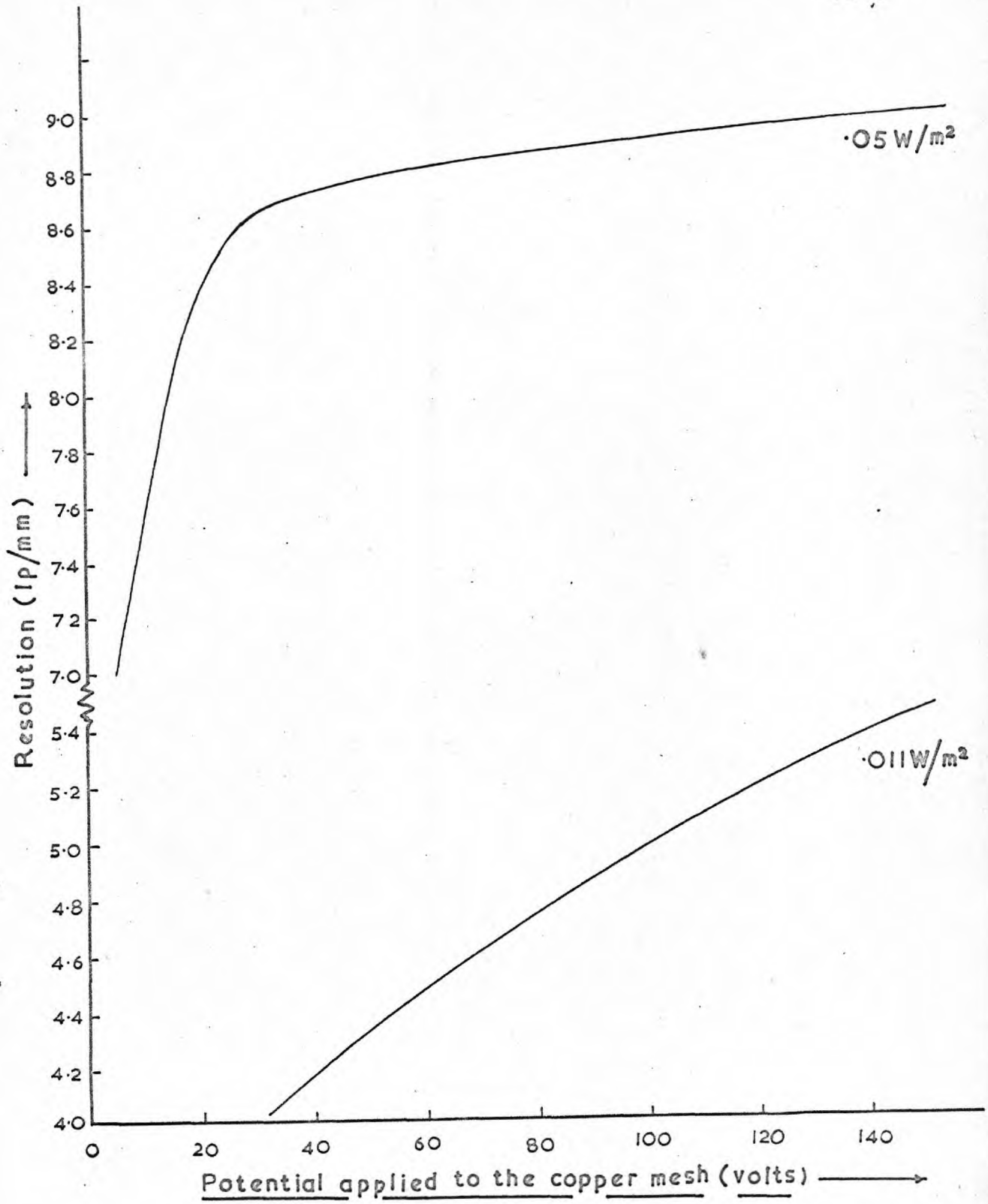


FIG. 34 The variation of resolution with mesh potential

positive applied to the gating mesh.

In tubes numbered five and six, the longer output section allowed potentials of up to 15KV to be applied. This gave a finer control on focusing and a brighter output image which enabled higher values in resolution measurements to be obtained. The resolution was measured using the same method as before, using a voltage of 100 volts positive applied to the equipotential delay section and an applied magnetic field of $\cdot 025 W/m^2$. The variation of the output resolution against the potential applied to the tungsten mesh, with 50 volts positive applied to the copper mesh, is illustrated in fig. 35b. It can be seen that if the potential on the tungsten mesh was increase above 10 volts positive there was very little effect on the output resolution. The variation of resolution against potential applied to the copper mesh is also illustrated. In the latter case, the tungsten mesh was held at a constant potential of 10 volts positive. A "knee" in the curve at $\simeq$ 25 volts was again exhibited. This "knee" is less pronounced than that shown in the upper curve of fig. 34, since the magnetic field strength applied in the latter case was double that applied in the former case.

The maximum output resolution obtainable in tubes numbered five and six was 141p/mm. The resolution was limited to this value by the presence of the 600 t.p.i. copper mesh, which formed a Moiré fringe pattern with the resolution fan pattern.

Tube number six was pulse operated in the fcllowing manner;

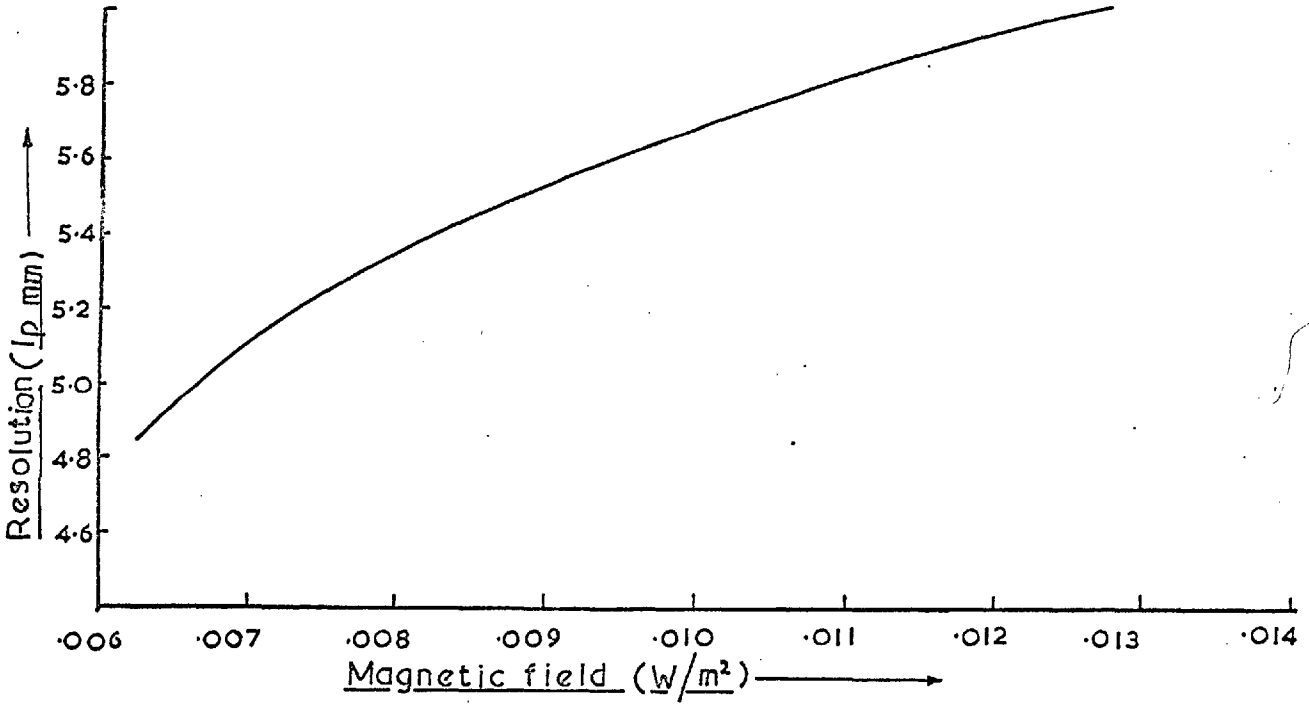


FIG. 35A The variation of resolution with magnetic field

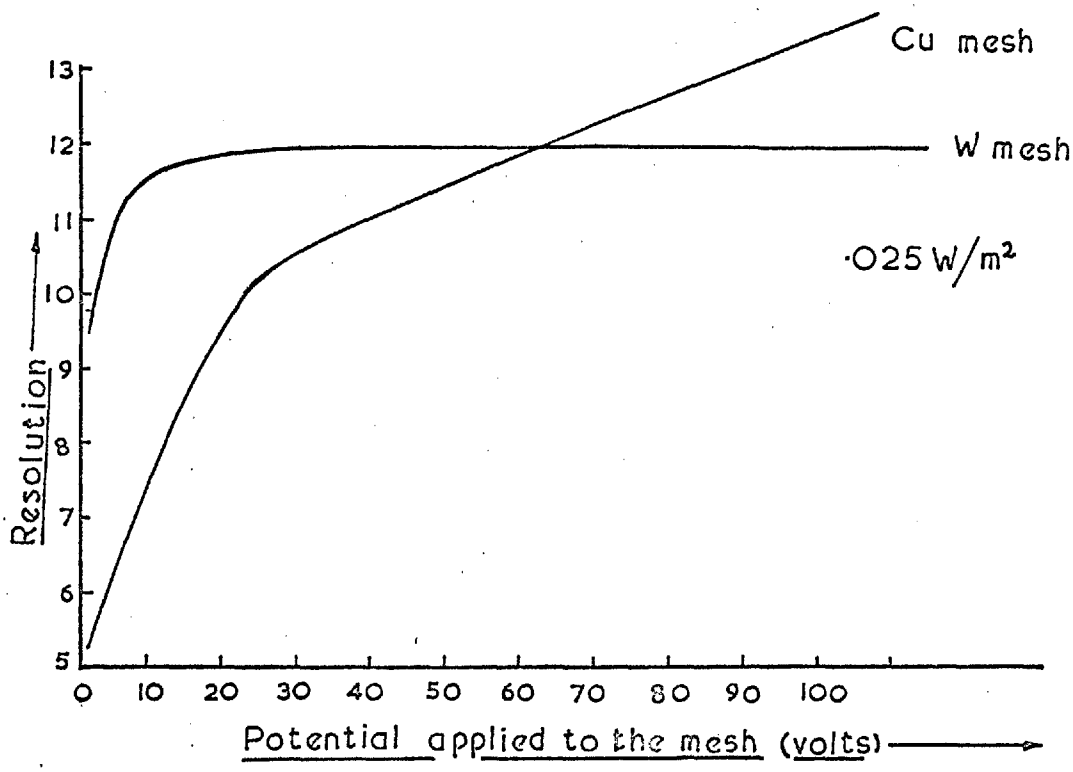


FIG. 35B The variation of resolution with mesh potential

a diagram of the arrangement being shown in fig. 10. The equipotential delay section, the tungsten mesh and the output section were held at 100 volts positive, 10 volts positive and 15KV positive respectively. A bias of 5 volts negative was applied across the 20 KΩ resistor to make sure that the tube was turned off. 15 volts positive gating pulses of 1msec. duration were applied across the 22 KΩ matching resistor, from the high impedance output of a Nagard type 5001 square wave generator. A steady pattern was projected onto the photocathode and the output observed visually. The initial 1:1 mark-space ratio of the gating pulses was reduced by successive factors of ten, until the image was too faint to observe visually. This state occured between mark-space ratios of 1:1,000 and 1:10,000. When the intensity of the input pattern illumination was increased to a value such that the output image was too faint to observe at a mark-space ratio of less than ≏ 1:4,500, the photocathode became overloaded. In this well known effect a potential gradient was built up across the surface of the photocathode by the emission of photoelectrons. The progressively more positive parts of the image were "switched on" by a progressively more positive part of the gating pulse. The onset of this effect was observable when the edge of the pattern failed to be switched on by the positive gating pulse. Since the gating pulse swung to 10 volts positive, starting to switch the image on at 2 volts positive, the edge of the pattern was charged up to 8 volts positive at the

onset of effect. The photocurrent drawn at the onset of the effect was ≏ 5μamps, so that the ohmic resistance across the photocathode was of the order $10^{6}\Omega$. This value of photocathode resistance is in rough agreement with the values obtained by other workers at Imperial College[157,158].

7.3 The conclusions drawn from the performance of the early image-delay tubes

The deterioration of resolution as the potential on either gating mesh was reduced was due to the fact that the axial velocity of the electron beam was reduced, so that perturbations of the electron orbits caused by inhomogeneities in the electric and magnetic fields had a greater effect.

Since the output pulse from an avalanche transistor has a limited amplitude for a given pulse width, the minimum amplitude required to produce a satisfactory resolution had to be found. It can be seen from fig. 35b that when the tungsten mesh was operated with ≏ 10 volts applied, very little resolution was lost. It can be seen from figs. 34 and 35b that when a voltage of ≏ 25 volts amplitude was applied to the copper mesh the "knees" in the curves were reached. If higher potential were applied, especially above magnetic fields of ≏ ·05Webers/m^2, very little extra resolution was achieved. The electronic circuitry was therefore required to produce two pulses, one of ≏ 10 volts amplitude and the other of ≏ 25 volts amplitude.

It can be seen from fig. 35b that the maximum resolution obtainable at a magnetic flux density of ·025Webers/meter^2 is $\simeq$ 13·5 lp/mm. This is in good agreement with the theoretical value of 12·5 lp/mm. indicated in fig. 13.

The Hirsch circuit described in section 6.2, produced pulses 10musec wide, at 50 Kc/s, i.e. a mark-space ratio of 1:2,000. In order that an output image could be comfortably observed when the tube was gated by a series of pulses having a mark-space ratio of 1:2,000, the electron current reaching the output phosphor screen had to be increased by a factor of 10-100. This was achieved in two ways. In the first a heated tungsten filament replaced the photoemissive surface. A description of this tube is given in the next section. In the second method two stages of cascade electron multiplication were incorporated after the delay section and gate. In the latter case the internal electron gain needed to be $\gtrsim 10^3$ in order that the output image could be observed and the photosurface not overloaded. A description of this type of tube will be given in the next chapter.

7.4 The performance of a delay-tube containing a tungsten filament

As was noted in the previous section, the output image could be observed, when the tube was operated under pulsed conditions, only if the electron current arriving at the output phosphor were increased by a factor of 10-100. It was decided to manufacture a tube incorporating a tungsten filament, in order to investigate the

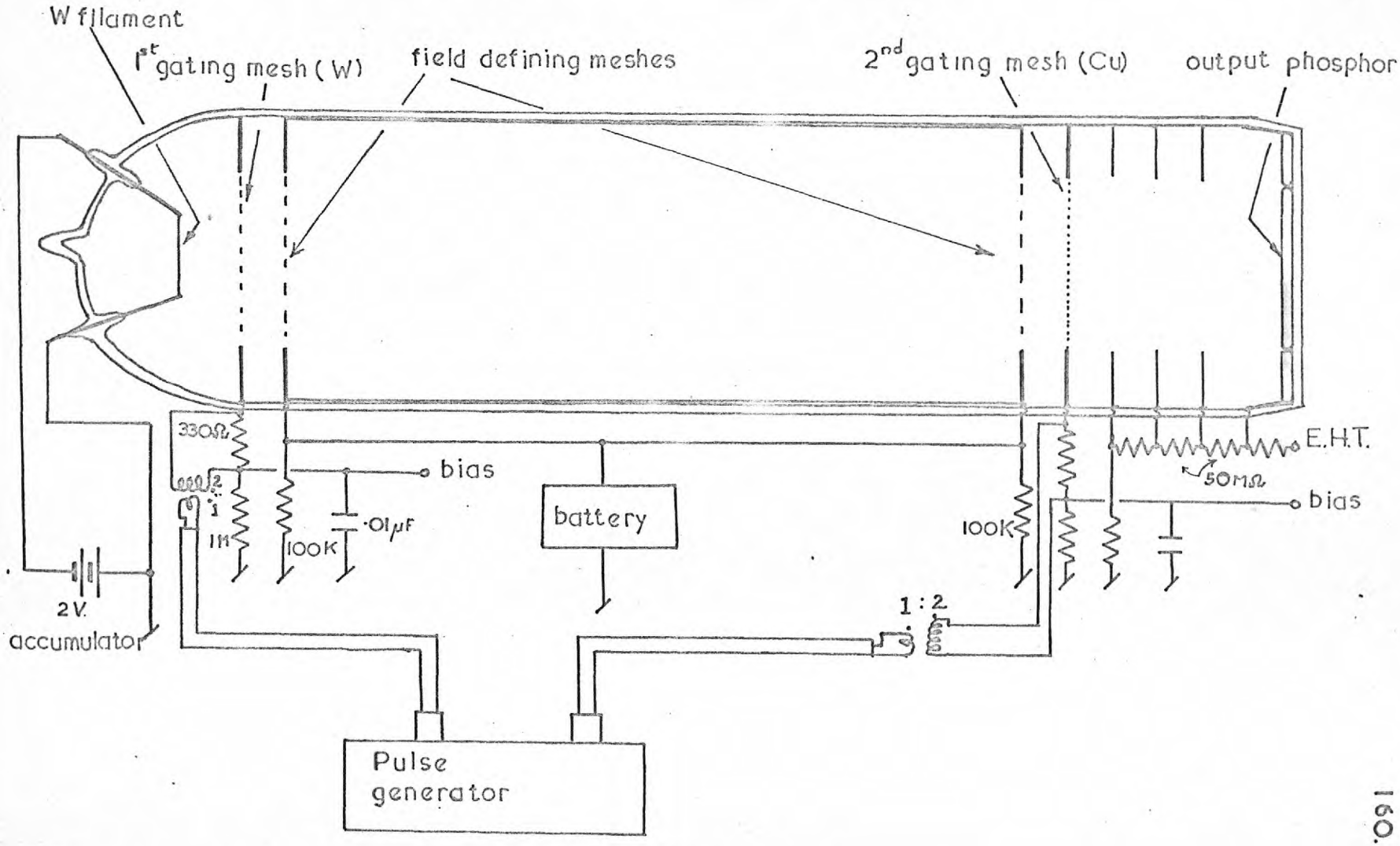


FIG. 36 The tungsten-filament delay tube

gating properties of the meshes and to test the electronic circuitry, without the need of incorporating an image intensifying section in the tube.

The design of the delay-tube containing a tungsten filament is shown in fig. 36. It was essentially similar to tubes numbered five and six, described in section 7.2, except that a tungsten filament replaced the photoemissive surface. Since the mean energy of thermionic emission is ~ lev, the performance of the tube was similar to one with a photoemissive surface.

The components of the tube were prepared in the manner described in chapter five. The tube was pumped, baked and sealed-off, no activation being necessary.

The tube was operated under pulsed conditions in the following manner. A 2 volt accumulator was used to heat the tungsten filament, which supplied ± 100 μamps current. The first tungsten mesh was gated to similate a high speed light source. The mesh was biased to 2 volts negative, by applying a fixed voltage across the ~~20 KΩ~~ 1MΩ resistance, as shown in fig. 36. The current was switched on when the positive gating pulse from the first output of the Hirsch circuit, described in section 6.2, was applied to the tungsten mesh. The pulse appearing at the first output of the Hirsch circuit was ± 8 volts in amplitude and ± 10 μsec in duration. It was doubled in amplitude, using a 2:1 transformer wound on a Mullard FX2249 ferroxcube and applied to the tungsten mesh across a 330 Ω matching impedence.



FIG.37A The tungsten-filament delay tube



FIG 37B



FIG 37C

The bias was decoupled by the 10,000 pF. condensor. The equipotential delay section was held at 100 volts positive, so that the electron pulse arrived at the copper gating mesh ≏ 100 μsec after being gated through the tungsten mesh. The electronic delay of the Hirsch circuit was adjusted until the gating pulse applied to the copper gating mesh from the second output, coincided with electron image pulse arriving there. This coincidence was first ascertained by visual observation at the output phosphor. The second output pulse was exactly similar to the first and applied to the copper mesh in the same manner.

The electronic delay was known from calculation to provide a time delay of from ≏ 40 to ≏ 130 μsec. It was not accurately calibrated since the electronic equipment for this was not available at that time. The delay was altered while the output phosphor was observed. At the minimum delay no output image appeared. The delay was increased to ≏ 100 μsec and the image appeared during an estimate change of delay of 20-30 μsec, after which it was not observed as the delay was increased to its maximum value.

Fig. 37a shows a photograph of the tungsten filament delay tube. Fig. 37b shows a photograph, taken at $^{1}/_{1000}$th of a second on Ilford H.P.3 film, of the output phosphor of the tube with both gating meshes continuously biased to 10 volts positive. Fig. 37c shows a photograph taken $^{1}/_{10}$th of a second on Ilford H.P.3 film of the output phosphor when both meshes were gated as has been described above.

It was thus demonstrated using the tungsten filament tube that an electron image could be delayed by ≏ 100 μsec. and gated at a speed of ≏ 10-15 μsec.

Chapter 8 The construction and performance of a tube containing an electron image delay section, an intensifier and a high speed shutter

8.1 The construction of the tube

This section will deal with the incorporation of two electron multiplying cascade screens in a tube which contains an electron image delay section and two electronic shutters. It was noted in section 7.3 that an internal electron gain of $\geqslant 10^3$ was required to enable an output image to be observed when the tube was operated under the pulsed conditions stated therein. In practical use, as in either a Cerenkov camera or a luminescent chamber camera, the tube must enable single photoelectrons to be recorded. It was shown in section 4.3 that for this condition to be met in a tube having a geometrical resolution of $\simeq 5$ lp/mm, the tube must have a total blue light gain of $\geqslant 10^5$. The two cascade screens together with the primary photocathode and output phosphor constitute a three-stage cascade intensifier, which was shown in chapter 2 to be one of the most efficient types of intensifier for the purpose of recording photoelectrons.

A diagram of the tube is shown in fig. 38. The delay section of the tube is essentially the same as that of the simple tube shown in fig. 10. The delay section comprises the primary photocathode (1), the first "electron gate" (2), the equipotential delay section (7), and the second "electron gate" (8). The first "electron gate"

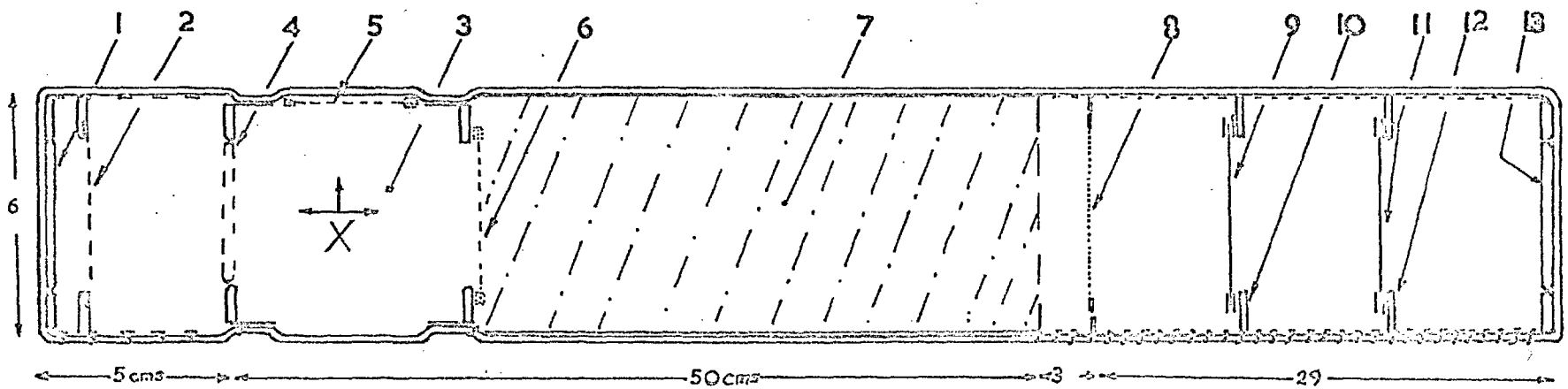


FIG. 38 The image intensifying delay tube

is manufactured from 50 t.p.i.tungsten mesh; the second gate from 600 t.p.i. copper mesh. The front edge of the equipotential delay section is defined by electrode 4. The image intensifying section is the last section of the tube coming after the electron delay and gate. It comprises two cascade screens (9 and 11) and an output phosphor screen.

The three photoemissive surfaces required in this tube, were prepared simultaneously in the activation compartment (3). This compartment is situated between electrodes 4 and 6, which both have thin metal "skirts", tightly fitting into "tooled-down" regions of the glass envelope. The primary photocathode plate was held in the aperture of electrode 4 during activation. A mica disc mounted between two molybdenum rings, described in section 5.4, was clipped against the flat circular window (5) in the glass envelope. An aluminium backed phosphor screen was deposited previously upon that side of the mica disc which faced the window. Electrode 6 has a slit cut across its diameter, which just allowed the mica disc, mounted between its molybdenum rings (45 mms in external diameter), to pass through. Another mica disc, mounted between two molybdenum rings of 46 mms external diameter, was clipped against electrode 6. This mica disc covered the slit in electrode 6 and, with the metal "skirt" of electrode 6, kept the activation compartment reasonably well sealed-off from the rest of the tube.

When the tube was assembled and sealed-up, it was sealed onto

the pumping system with photocathode face-plate resting on the pumping table. The tube was evacuated through two side arms leading to the main pumping stem. The larger of the two side arms evacuated the main body of the tube from its centre, the smaller side arm was constricted and evacuated the activation compartment. The activation compartment was thus separately pumped being kept fairly well sealed and positioned as far away as possible from the high voltage section of the tube. These precautions were designed to prevent the migration of caesium from the compartment to the high voltage section, where it could react with metal electrodes to produce surfaces of low work function, giving rise to field emission. The positioning of the compartment near the pumping table facilitated the activation of the photoemissive surfaces. This activation has been described in section 5.6, the antimony being evaporated in turn on each of the three surfaces from position X.

When the tube was sealed-off from the pumping system, the primary photocathode plate was released from electrode 4 using a magnetic catch. It was passed under the open tungsten mesh, held by electrode 2, as has been described in section 7.1 and clipped into electrode 1 against the front window. The tungsten mesh was then magnetically clipped into electrode 2. The cascade screen which was held on electrode 6, was released and moved through the equipotential delay section to be clipped into its final position (11) on electrode 12. The 600 t.p.i. copper mesh (8) was held open,

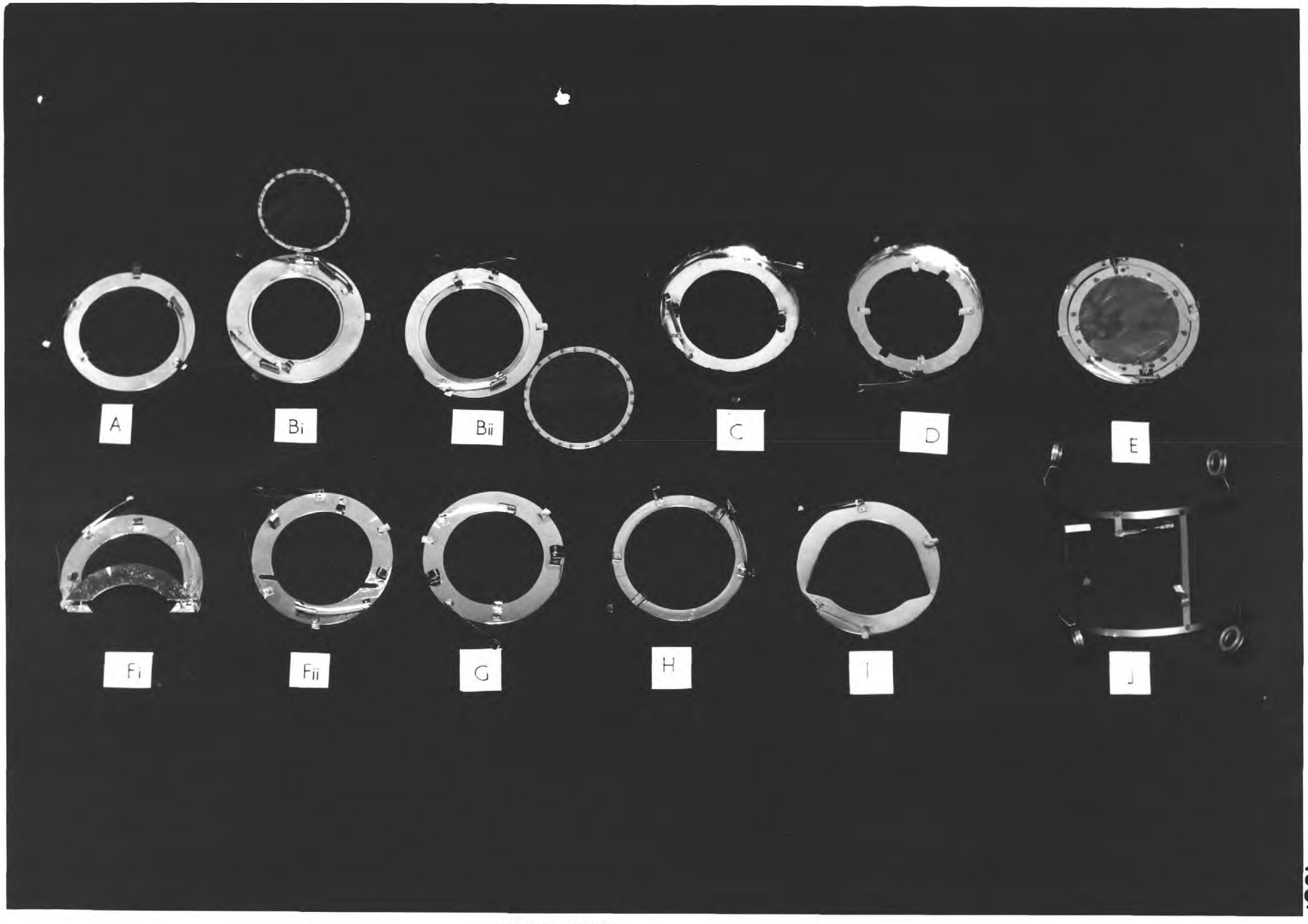


FIG. 39

hinged about its diameter, and a small sector of electrode 10 clipped back to allow the passage of the cascade screen. The small sector of electrode 10 was released using a magnetic catch and rotated through 180° on its hinges, to complete the annular ring of the electrode. The cascade screen, held in position 5 on the flat window, was released, moved through the slits in electrode 6 and along the equipotential delay section to be clipped into its final position (9) on electrode 10. The copper mesh was rotated through 90° about its diameter and clipped into its retaining outer annulus.

Fig. 39 shows the metal electrodes used in the construction of the tube. Electrode 1 is shown in fig. 39a. Electrode 2, with the tungsten mesh held open, is shown in fig. 39b.(i). Electrodes 4 and 6, complete with "skirts" are shown in figs. 39c. and 39d. respectively Electrode 8, with the copper mesh held parallel to its retaining annulus, is shown in fig. 39e. Electrode 10, with a sector clipped back is shown in fig. 39f.(i). Electrode 12 and electrode 13, which holds the output phosphor, are shown in fig. 39g. and 39h. respectively

Fig. 40 shows a completed tube before it was wired up for testing.

Ten tubes of this type were manufactured before a really successfu one was produced. The first tube was sealed up using the silver chloride sealing technique. This seal is usually most satisfactorily made with the two halves placed in a vertical position, the bottom half being clamped and the top half unclamped. Since the top half of the tube was heavy it had to be clamped for safety, the seal being made



FIG. 40

after three attempts. The tube was activated but a leak developed in the seal-up before the tube was sealed off the pump. The tube went soft before it could be tested. Since the silver chloride seal was not satisfactory in this case, it was decided to seal-up all later tubes using the normal gas-air-oxygen flame glass-sealing technique. All the remaining tubes were constructed in two halves the flame seal-up being made in the equipotential delay section at a point 10 cms from the copper mesh.

In the first six tubes, the electrical connection to the primary photocathode was obtained by using platinum paste sealed through the glass at the edge of the front window. This type of connection proved unreliable in this case and was replaced in all further tubes, by a platinum tape situated 7 mms away from the front window. The platinum tape connection to the tungsten mesh was placed 9 mm away from the front window offset by 90° to the first tape.

Very little scientific information was gained from the first nine tubes. The tenth tube, which had a blue light gain of $\simeq 75{,}000$ at an applied potential of 40KV and a primary photocathode with a sensitivity of 55μA/Lm, was investigated exhaustively.

8.2 Experimental results gained from the first ten tubes

8.2.1 The collection of photocurrent by the electrodes

The collection of photocurrent by the various electrodes in the tube was determined using the experimental arrangement shown in fig. 41 The tube was operated in a constant magnetic field of $0{\cdot}05 W/m^2$, and

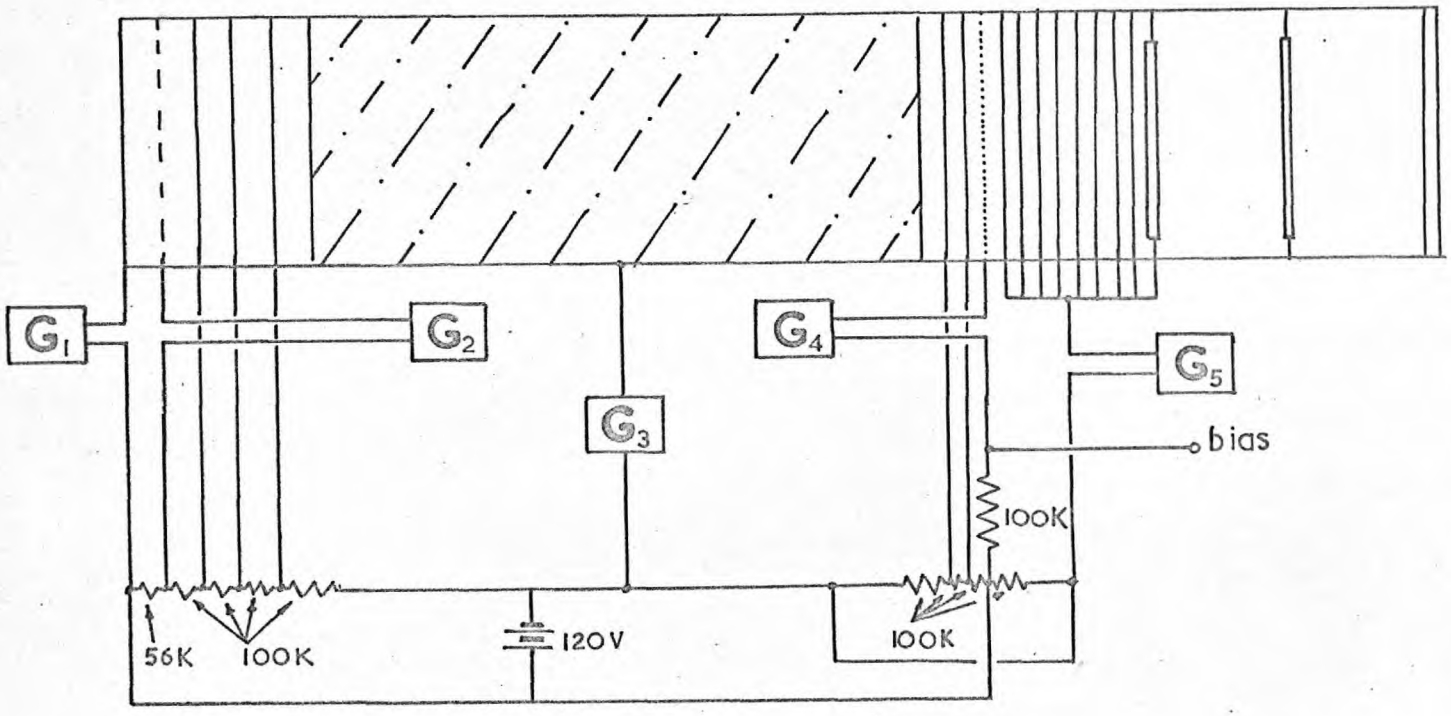


FIG. 41 The experimental arrangement used to determine the currents collected by various electrodes

with constant electrostatic potentials applied to the electrodes. A galvanometer G_1 was placed in the photocathode lead, and measured the electric current emitted by the photoemissive surface. Galvanometers G_2, G_3, G_4 and G_5 measured the electric currents collected by the first "electron gate", the equipotential delay section, the second "electron gate" and the anode respectively. The anode consisted of the first mica sandwich coupled with all the accelerating electrodes in the first cascade section, and was held at the same potential as the equipotential delay section. The five galvanometers were each calibrated against a galvanometer of known accuracy; calibration curves for each being obtained on all ranges.

A light source of constant intensity was focused onto a small central region of the photocathode and all the currents indicated by the five galvanometers were recorded as the potential applied to the second "electron-gate" was varied. The variation of the collected currents with the potential applied to the second "electron-gate" is illustrated in fig. 42. The photocurrent emitted from the photoemissiv surface and the other four currents, which are all collected currents, are all shown as positive currents. The anode current was first collected when the potential applied to the second "electron-gate" was $\simeq 3$ volts positive. At lower voltages than this the photoelectrons were completely reflected by the second "electron-gate". Just over half the returning electron stream was collected by the photoemissive surface with a resulting fall in the apparent electric current leaving

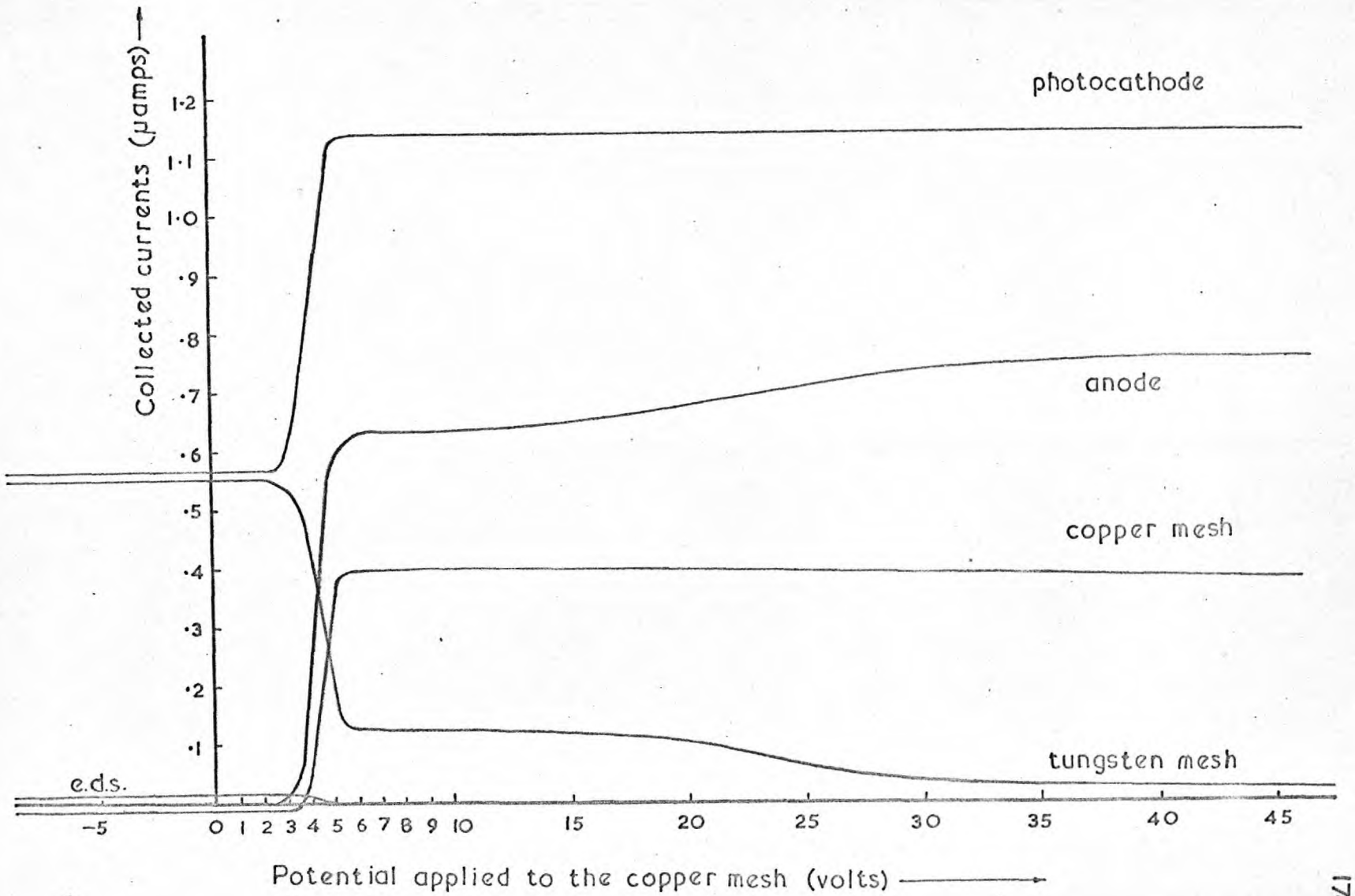


FIG. 42 The variation of the currents collected with the potential applied to the copper mesh

the photocathode. Just under half the returning electron stream was collected by the first "electron-gate". This measurement gave no indication of whether the electron stream made many transits of the delay section or whether the stream made only two, being entirely collected on its first return to the photocathode and tungsten mesh. The equipotential delay section collected about 1% of the photocurrent, when the electron stream was reflected at the second "electron-gate". This collection dropped to about •1% when the second "electron-gate" was > 6 volts. This current was most probably collected on electrodes 4 and 6, shown in figs. 39d and c respectively, since they projected furthest into the electron stream. It could have been collected from the electron stream in the first and second transits in the following case. Scattered light inside the tube could have produced photoelectron emission from the whole photoelectric surface, so that electrons emitted from the edge of the photocathode could have been collected at electrode 4 and 6. Alternatively, if the electron stream had made many transits in the tube, the collection at electrodes 4 and 6 could have been due to electrons which had travelled transversely to the magnetic field. This motion across the magnetic flux lines can be achieved by successive collisions with free molecules causing the electron to perform cycloidal motion round successively adjacent lines of force.

The anode current reached almost its maximum value when the potential applied to the second "electron-gate" was about 5.5 volts positive. At 45 volts positive, about $\frac{2}{3}$ of the photocurrent passed

through the second "electron-gate" and $\frac{1}{3}$ was collected by the gate itself. It can be seen that even when the second "electron-gate" was positive a fraction of the photocurrent was returned to the first "electron-gate". This effect was probably due to the high shadow ratio of the copper mesh (the second "electron-gate"); the electrons colliding with the mesh and being reflected back into the decelerating region after the equipotential delay section. As the potential applied to the second "electron-gate" was increased the fraction of the photocurrent returned to the first "electron-gate" decreased, probably because the electrons reflected from the second gate were less able to escape from the accelerating field at the second gate.

Meshes of lower shadow ratio than the 40% value of the copper mesh were available, but were not considered necessary to use in purely experimental tubes. Clearly, if a mesh of a lower shadow ratio were used for the second "electron-gate" a larger fraction of the photoelectric current would reach the anode.

Very similar curves to that shown in fig. 42 were obtained with the two other tubes tested.

8.2.2 The estimation of pressure inside the sealed-off tube

The estimation of pressure inside the tube after it had been sealed-off the pump was a useful indication of the condition of the tube. Periodic checks on its estimated value indicated the outgassing or leak rate in the tube. An estimate of the fraction of image

electrons lost by collision with free molecules was also made from the knowledge of the pressure inside the tube.

It can be seen from fig. 42 that when the second "electron-gate" was held at a potential of less than 3 volts positive, the current collected changed sign, i.e. an ion current was collected. This current was that due to half the ions produced in the delay section of the tube by the image photocurrent. The other half of the ions produced in the equipotential delay section proceeded to the photoemissive surface, since the ions once formed, retained their thermal energies and had a statistically equal chance of moving towards either ends of the tube constrained by the magnetic field.

The pressure may be estimated from the following analysis. Let the photocurrent be I_o and of this quantity let I_e photoelectrons make a collision during the double transit in the delay section. It is then assumed that all the electrons not involved in collision are returned to the photocathode. Those electrons involved in collision are assumed not to have sufficient energy to return to the photocathode. The latter electrons are trapped in the delay section of the tube, losing their 100 volts energy by inelastic collisions. It is assumed that electrons initially having elastic collision all lose sufficient axial energy to prevent them from returning to the photocathode. Fano[159] has shown that E, the mean energy lost by an electron in the production of an ion pair, is $\doteq$30 eV. E is largely independent of the energy of the ionising radiation, and has very nearly the same value for all gases.

Each photoelectron having 100 volts energy would therefore produce 3 ions by collision. Since only half the ion current is collected by the mesh, $I_p = {}^3/2\ I_e$, where I_p is the value of the ion current collected.

The fraction of electrons involved in collision in the double transit is given by:-

$$(1-f) = I_e/I_o = 2\ I_p/3I_o$$

Whence $$f = 1-2I_p/3I_o$$

The pressure in the sealed-off tube is given from eqn 20 (section 4.6) as:-

$$P = - \frac{\log_e f(x)}{37{\cdot}88x}$$

$$= - \frac{\log_e (1-2I_p/3I_o)}{37{\cdot}88x} \text{ mms. Hg.}$$

where x is the distance traversed by the electron stream in the double transit of the delay section, which was shown in section 4.6 to equal 118·2 cms for the double transit.

Hence $$P = - \frac{\log_e (1-2I_p/3I_o)}{5{\cdot}27.10^3} \text{ mms. Hg.}$$

The curves in fig. 42 were taken two months after the tube was sealed-off the pump. The value of I_o was measured to be 1·135 μamps. when the second "electron-gate" was biased to 50 volts positive. I_p had a value of ·002 μamps. when the gate was biased to 50 volts

negative. Hence the ratio I_p/I_o had a value •00176. If this value of I_p/I_o is substituted in the pressure equation, the estimated pressure in tube No. 10 after two months was $p = 3.10^{-7}$ mms. Hg. It can be seen from fig. 15 that at this pressure •1% of the initial photoelectrons were lost in a single transit of the delay section of the tube. The cathode sensitivity of tube No. 9 fell to 4% of its initial value over a period of six weeks, its pressure during this time rising from 1.10^{-6}mms. Hg. to 2.10^{-5}mms. Hg. This loss in cathode sensitivity may have been due to either an attack by the extra gas itself or by excessive ion bombardment produced by the extra gas.

8.2.3 The investigation of the current collection by the equipotential delay section

When the tube was operated under the conditions stated in section 8.2.1, a small positive current was collected by the equipotential delay section. This indicated a net collection of positive ions under static conditions. This collection was further investigated by operating the tube under pulsed conditions. The circuit arrangement shown in fig. 41 was rearranged in the following manner. Galvanometers G_1, G_4 and G_5 were replaced by d.c. leads, G_2 was replaced by a 22KΩ resistor across which a pulse from a Nagard type 5001 square wave generator could be applied and G_3 replaced by a 1MΩ resistor. The variation of voltage across the 1MΩ resistor was determined using an oscilloscope.

It was calculated that the equipotential delay section had a

capacitance to earth of $\simeq$ 100pF. Excess pick up of external A.C. fields was prevented by the following precautions. The equipotential delay section was held at earth potential through a 1MΩ resistor, the photocathode and anode being held at 120 volts negative for the tube operation. The current to the magnetic solenoid was produced by a stablised current supply. The tube was completely enclosed by an insulated aluminium foil which was earthed. The constant illumination was obtained using a Lucas spot light and a 12V car battery.

The Nagard pulse generator was operated with its earth connection removed, in order to provide positive pulses with respect to the photocathode. Its D.C. level was held at 120V negative using a 150μF condenser from its chassis to the circuit earth. The 22KΩ Nagard matching resistance was connected from the photocathode to the first "electron-gate". A 2μF condenser was placed between the photocathode and the earth to prevent the positive gating pulses appearing on the earth line and producing a spurious signal on the oscilloscope.

The Nagard pulse generator produced pulses of 10 volts amplitude and 10 msec duration on the first "electron-gate". The pulse of electrons produced were accelerated up to the equipotential delay section and then allowed to pass through the "open" second "gate", which was held at 72 volts negative. The anode was held at the photocathode potential; a condition which would reflect almost all the photoelectrons. In these circumstances any positive ions formed

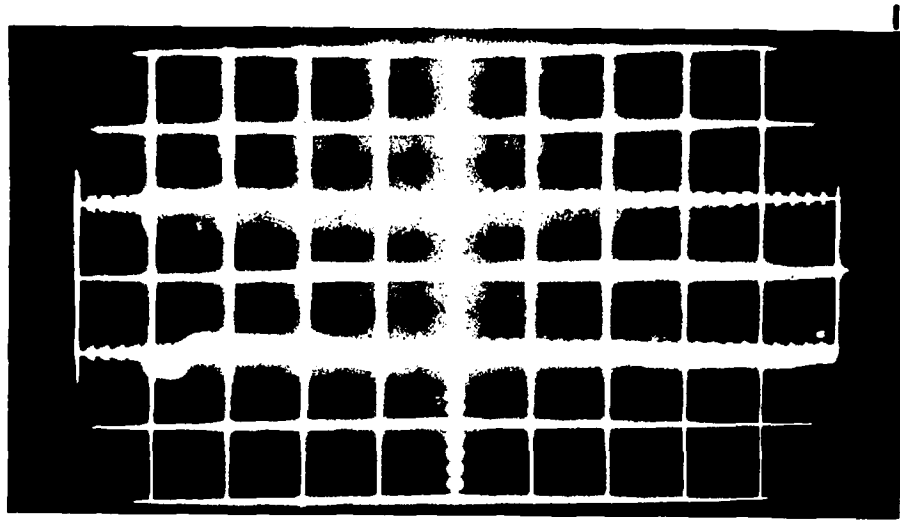


FIG. 43A Arb. units / 5 msec/cm

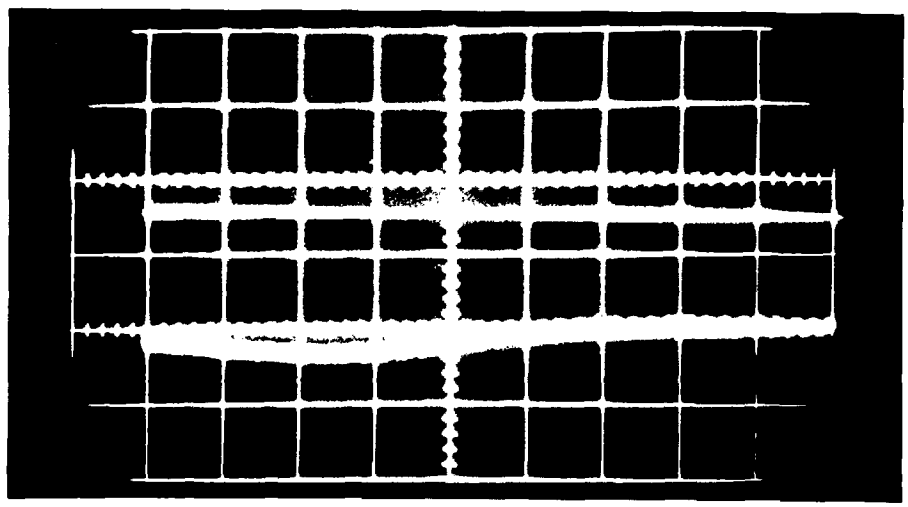


FIG. 43B Arb. units / ·5 msec/cm

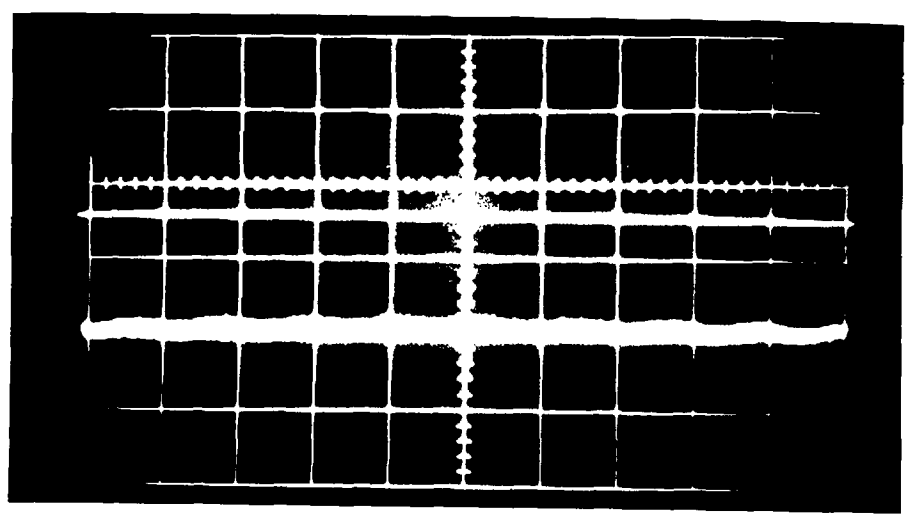


FIG. 43C Arb. units / 40 μsec/cm

in the equipotential delay section of the tube would be expected to arrive, under the action of the field gradients, at either the photocathode or the anode.

The top trace in fig. 43a shows the pulse applied to the first "electron gate", the bottom shows the voltage pulse appearing across the 1MΩ resistor at the delay section. The sweep speed of the traces were both 5 msec/cm division. It can be seen that for ≙ 1 msec a negative voltage appears across the 1MΩ resistor, i.e. a collection of electrons; after which a positive voltage appears. This can be seen in greater detail in fig. 43b where the sweep speeds were both •5 msec/cm division. It can be seen that after ≙ 1•5 msec a ripple frequency appears in the trace. This frequency can be seen from fig. 43c, where the sweep speed was 40 μsec/cm division, to be 25Kc/S.

The collection of electrons by the equipotential delay may be explained as follows. Under the operating conditions outlined a fraction of the image electrons would be trapped in the potential well of the delay section after losing energy in a molecular collision. These trapped electrons would then lose further energy by molecular collision until they reach thermal equilibrium with the free molecules. At each collision the change in direction of the nonaxial velocity component of the electron would cause it to perform its cycloidal motion round a line of magnetic flux adjacent to the original flux line. The sum of the small transverse motions due to each collision would enable the electron to cross the tube transversely to the

magnetic flux lines and be collected by the equipotential delay section. The ripple frequency may be explained by assuming that the electrons travelling at thermal equilibrium energy induce an oscillation in the load. The geometry of the tube was very similar to the Barkhausen-Kurz oscillator[160], which produced in the load a frequency $f = \frac{1}{4} T_o$, where T_o was the transit time of an electron from the anode to the cathode. It was found that like the Barkhausen-Kurz oscillator the frequency of oscillation was independent of the external circuit load. If the velocity of the electron stream under thermal equilibrium is of the order 10^6cms/sec and the length of the delay section is of the order 10^2cms the frequency of oscillation in the tube is of the order 10^4c/s. This is of the same order as the 25KC/S. frequency observed.

The mean time required for an electron to be collected by the equipotential delay section may be estimated as follows.

If the r.m.s. distance the electron has to travel transversely to be collected by the equipotential delay section is noted by $\bar{D}^p$ and $\bar{D}^o$ represents the r.m.s. distance the electron travels between each collision, where p is the total number of collisions then,

$$\bar{D}^p = p\,\bar{D}^o$$

and

$$\bar{D}^p = \frac{dN}{dt}\,\Delta t\,\bar{D}^o$$

where dN/dt is the rate of electron collision and Δt is the mean time required for an electron to be collected.

Now $\frac{dN}{dt} = \frac{v_e}{\lambda_e}$, where v_e is the velocity of the electron and λ_e its mean free path.

Therefore $\bar{D}^p = \frac{v_e}{\lambda_e} \triangle t \; \bar{D}^o$

Since the pressure inside the tube was of the order 10^{-6} mms.Hg. then the value of λ_e is from eqn. 19 (section 4.6) of the order 10^4cms. Since however, the collision cross-section of a gas-molecule depends on the speed of the electrons passing through the gas, the well known Ramsauer effect, the effective value of λ_e is decreased at low electro energies. This decrease is of the order 10 from the values obtained from the Kinetic Theory of gases at an electron energy of $\triangleq$ leV. Therefore a better value of λ_e is taken to be of the order 10^3cms. v_e is taken as 10^8cms/sec i.e. a mean energy of $\triangleq$ leV. $\bar{D}^p$ is taken to be of the order 1 cm. and $\bar{D}^o$ to be the radius of cycloid gyration in a $\cdot 02 W/m^2$ field of an electron of leV energy, i.e. $\bar{D}^o \triangleq 10^{-2}$cms. If these values are substituted in the above equation $t \triangleq 10^{-3}$secs, which is in rough agreement with mean time of the negative slope of the electron collection trace.

The positive part of the trace may indicate either a collection of positive ions or a loss of secondary electrons by the equipotential delay section. The author can offer no satisfactory theoretical explanation of this phenomenon however.

8.2.4 The Blue light gain of the cascade image intensifier

The blue light gain of all the tubes was measured using the

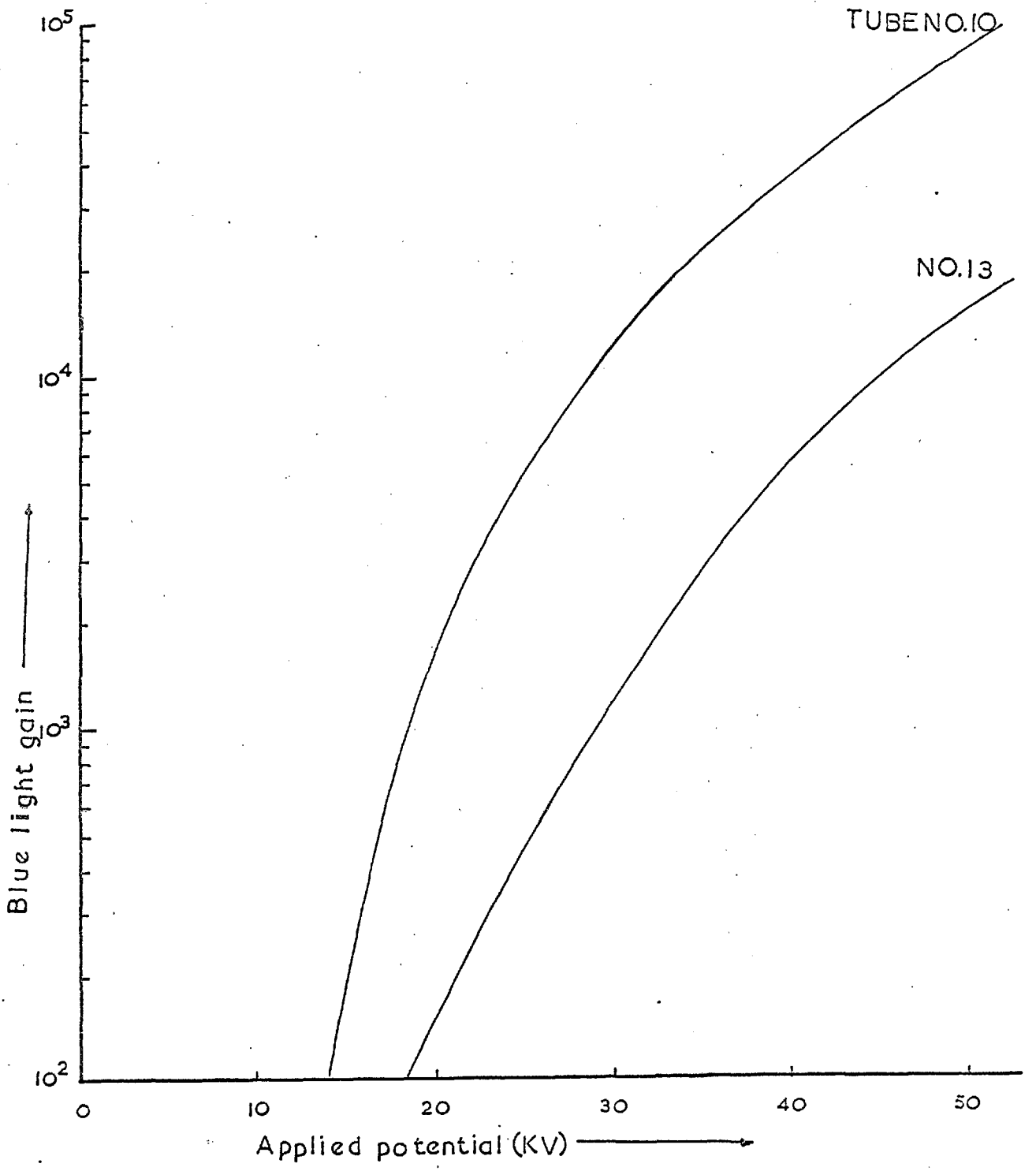


FIG.44 The variation of light gain with potential

following proceedure. A light source of variable intensity was focused onto a small area of the photocathode. The light beam was passed through a Wratten 47B filter, so that the light incident upon the photocathode had a similar spectral distribution to the emission of a P.11 phosphor. A photovoltage cell was placed in front of the photocathode to collect the incident light and the intensity of the incident light was adjusted so that the current output of the photovoltaic cell was •2 μamps. The photovoltaic cell was then placed against the output window of the tube and the accelerating voltage on the intensifier slowly increased until a current of •2 μamps was obtained from the photovoltaic cell. The blue light gain of the tube was then unity. The input light intensity was reduced until the photovoltaic cell current measured at the output of the tube was •04 μamps. The voltage applied to the tube was further increased until the photovoltaic cell current was •2 μamps. This proceedure was repeated until the full operating voltage was applied to the tube. The gain of the tube was thus increased by steps of five, the voltage applied at each step being noted.

For this measurement the tube was operating under normal condition with the positive E.H.T. applied to the output phosphor. The photovoltaic cell was spaced away from the output phosphor by means of a solid perspex light pipe. This prevented the E.H.T. sparking across to the photovoltaic cell and causing a fluctuation in its output curren The reduction in light collection was determined experimentally to be

a factor of 3·7. Fig. 44 shows the blue light gain of two tubes plotted as a function of the applied voltage. The curves were corrected by the factor of 3·7.

8.2.4 Image persistence due to phosphor decay time

The image persistence on the output phosphor due to the combination of the three phosphors of the cascade tube was experimentally determined using the experimental arrangement illustrated in fig. 45a. The first "electron-gate" was biased to five volts negative and was gated open at 100 c/S by a pulse 20 volts positive in amplitude and 1 μsec in width. The second "electron-gate" was biased to 15 volts positive to be continuously open. The pulse of electrons 1 μsec in width was amplified and spread in time by the three-stage cascade image intensifier. The final intensity at the output phosphor was recorded on an oscilloscope using a photomultiplier (P.M.). A double beam oscilloscope was used to record both the gating pulse and the output phosphor intensity, the oscilloscope being triggered from the prepulse output of the Nagard type 5001 square wave generator.

The lower trace of fig. 45b, where the sweep speed was 1msec/cm, shows the output phosphor intensity. It is seen that the intensity decays to zero after ≏5 msecs. This time is longer by a factor of ten than that indicated theoretically in section 4.5. This discrepancy is due to the long tail intensity component in P.11 phosphor.

The lower trace in fig. 45c, where the sweep speed was 10μsec/cm,

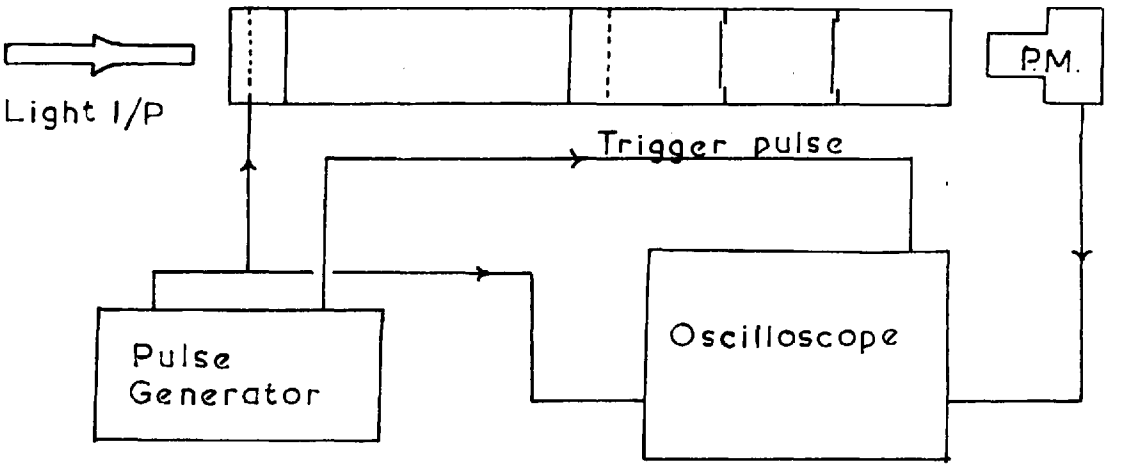


FIG. 45A The dermination of image persistence

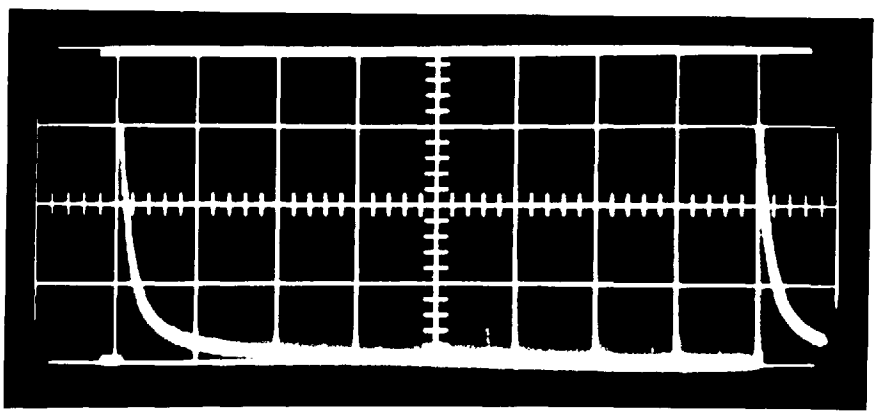


FIG. 45 B Arb. units/ 1msec/cm

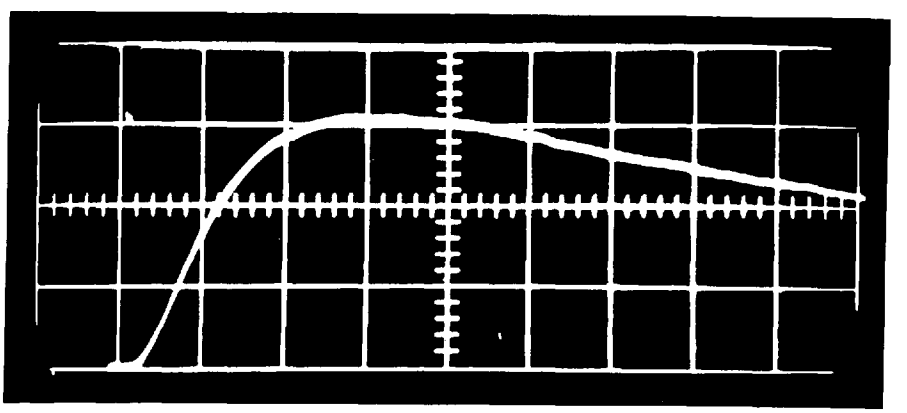


FIG. 45C Arb.units/ 10μsec/cm

shows the rise time of the output phosphor intensity. The upper trace shows the inverted gating pulse 1 μsec in width which was applied to the first "electron-gate". The rise time is seen to be ≃ 30 μsecs.

8.2.5 The geometrical resolution

The geometrical resolution obtained at the output of the tube is limited by several factors. The first factor is the strength of the magnetic field, in which the tube is operated, which determines the image resolution in the delay section (discussed in section 4.4). The second factor is the loss of resolution caused by transmitting the image through the intensifying section, where the resolution is limited by the electron optical focusing and by the thickness of the cascade screens. The third factor arises when the "electron-gates" are pulse operated; resolution is degraded when the gating pulses deviate from a perfectly square shape. The fourth factor is the potential at which the "electron-gates" are operated (discussed in section 7.3).

A visual measurement of the output resolution of the tube was made using the test pattern described by Baum[156]. Fig. 46a shows the value of resolution measured plotted against the flux density of the magnetic field applied to the tube. The equipotential delay section was held at 120 volts positive and the second "electron-gate" at 65 volts positive during these measurements of the output resolution under static conditions. The E.H.T. potentials applied to the three sections of the cascade intensifier were individually adjusted using a potentiometer control box, until the optimum resolution was found.

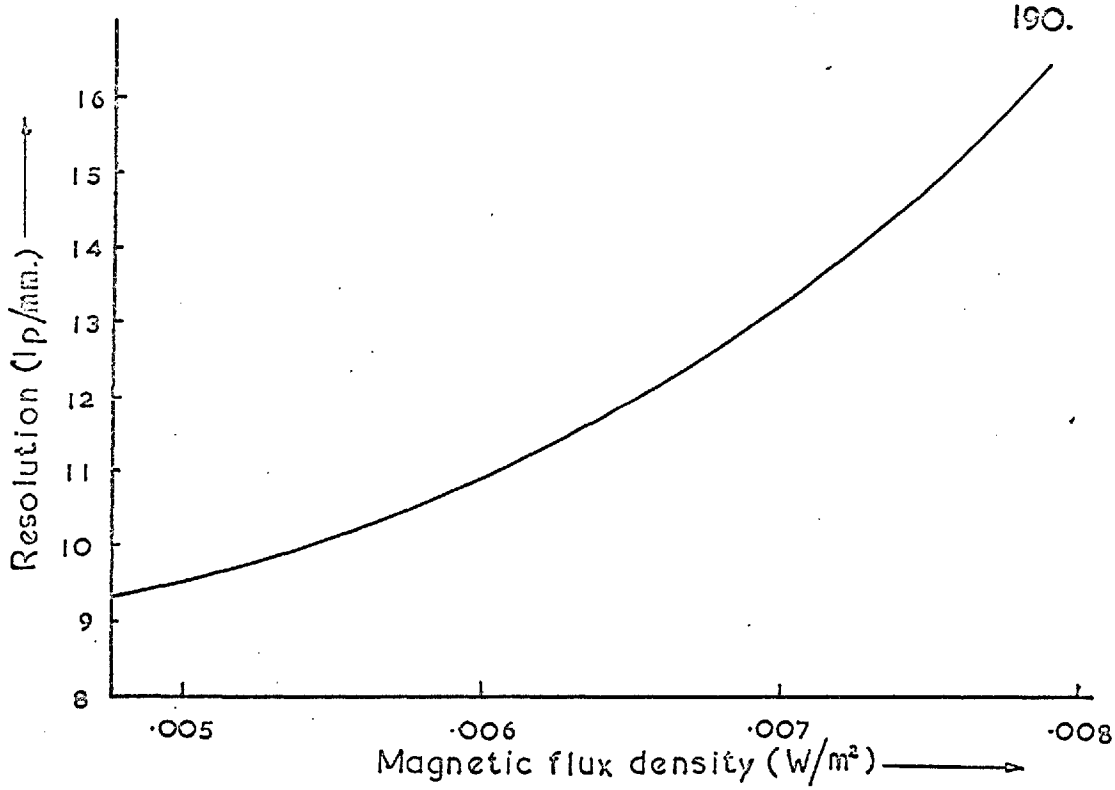


FIG. 46A The variation of resolution with magn. field

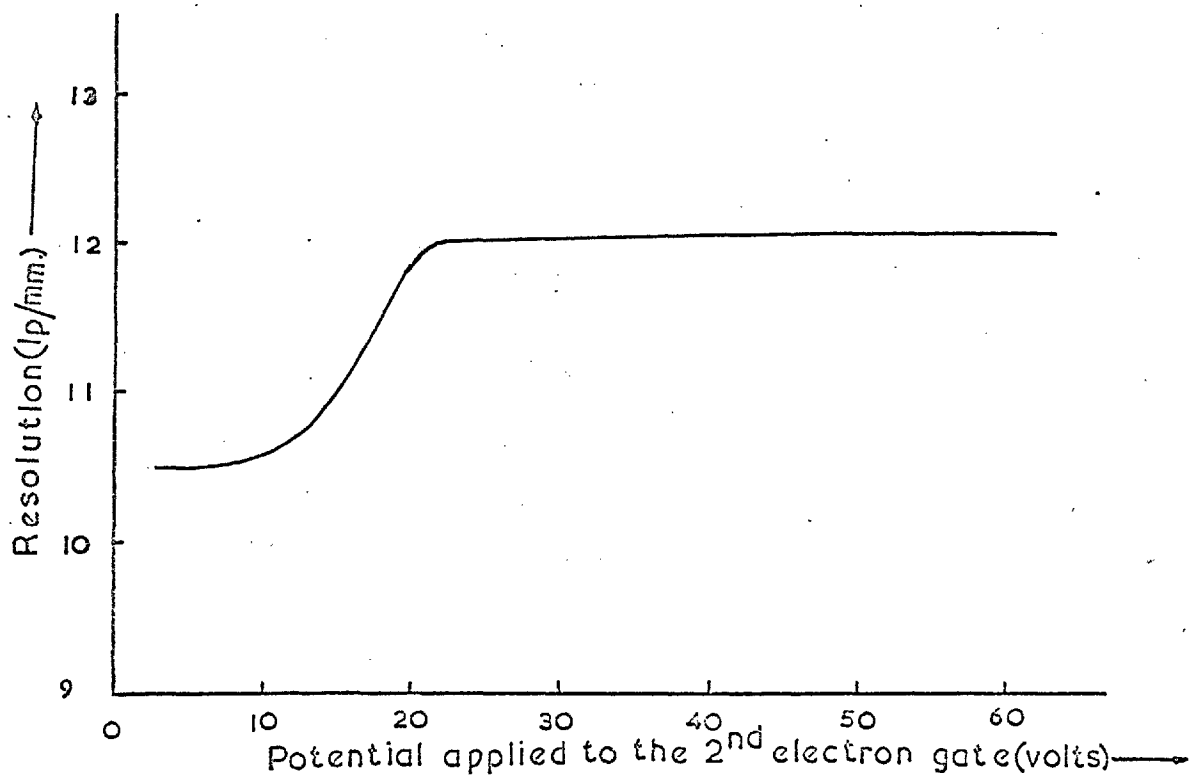


FIG. 46B The variation of resolution with gate potential

Fig. 46b shows the value of resolution measured, plotted against the voltage bias applied to the second "gating-mesh", when the magnetic flux density was $\simeq$·064W/m^2.

It can be seen from fig. 46a that the higher the magnetic field that can be applied the better the output resolution obtained. It can be seen from fig. 46b that under the conditions stated, the output resolution has a value of 10·5 lp/mm from the image "switch on" voltage of 3·5 volts positive until $\simeq$ 10 volts positive, after which the resolution rises to a constant value of 12 lp/mm above $\simeq$ 20 volts positive. Thus, if perfectly square gating pulses of between 3·7 and 10 volts positive are applied to the second "electron-gate" the resolution is 90% of its maximum value.

The output resolution was next recorded photographically when the tube was gated and ungated. The Baum pattern was projected onto the input photocathode, so that the image recorded on the photographic emulsion was linearly magnified by a factor of two. Thus the Baum resolution scale must in this case be divided by two to obtain the true resolution. The applied magnetic field was ·064W/m^2 which produced a visually measured output resolution of $\simeq$ 12 lp/mm. Fig.47 shows some of the result obtained photographically.

Fig. 47a shows the pattern obtained when E.H.T. potential was 23KV and the second "electron-gate" was held at 40 volts positive. Figs. 47b, c and d shows the patterns obtained when the second "electron-gate" was gated with pulses of duration 500 μsecs, 100 μsecs

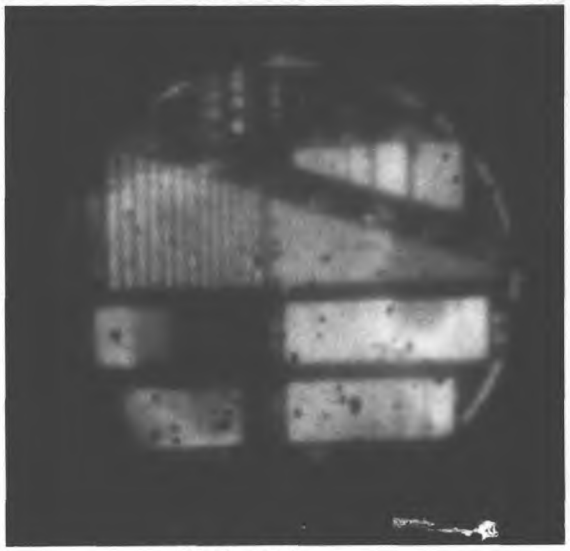


FIG.47A



FIG.47B



FIG.47C

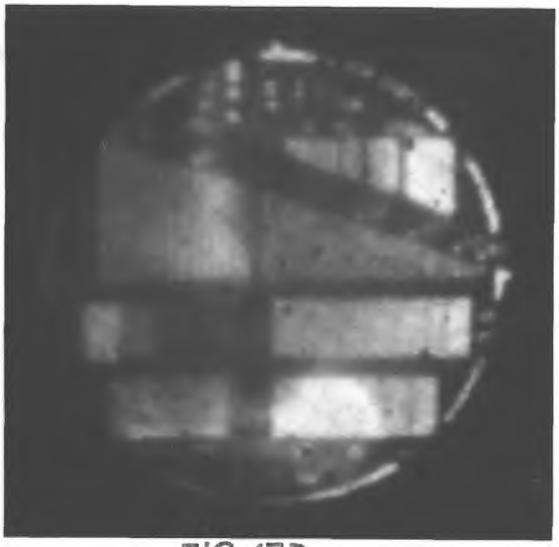


FIG.47D

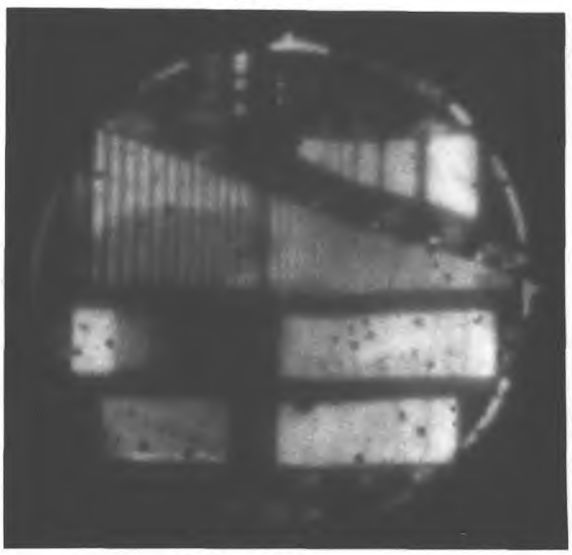


FIG.47E



FIG.47F

and 10 μsecs respectively. The gating pulses were 35 volts in amplitude, obtained from the high impedence output of a Nagard type 5001 square wave generator, and applied across a 22KΩ matching resistor. The second "electron-gate" was reverse biased to 5 volts negative during the experiment. The resolutions indicated in figs.47a, b, c and d are 7 lp/mm, 10 lp/mm, 8•5 lp/mm and 8 lp/mm respectively.

Figs. 47e and f shows patterns obtained when the E.H.T. applied to the tube was 32KV. Fig. 47e shows a resolution of ≏ 10 lp/mm when the second "electron-gate" was held at 40 volts positive. Fig. 47f shows a resolution of ≏ 5 lp/mm when the second "electron-gate" was gated by a triangular shaped pulse of 30 μsec half-width and 15 volts amplitude.

These results indicate that the photographic resolution is less than that obtained visually, i.e. the best photographic resolution was 10 lp/mm compared with 12 lp/mm obtained visually. Also the faster the shutter speed the worse the resolution becomes. The poor shape of the 30 μsec gating pulse produced the rather low value of resolution obtained in that case. Better results, obtained with a 10 μsec gating pulse, will be presented in the next chapter.

8.2.6 The measurement of the speed of the electronic shutter

The speed of the electronic shutter of the Mandel type, which was used in the image delay tube, was inferred by him from the reduction in the photographic density produced by reducing the voltage pulse length applied to the mesh. This method was considered

unsatisfactory by the author for accurately measuring electronic shutter speeds of the order 10 musecs. Several experimental methods were employed before a satisfactory one was found.

The experimental arrangement of the first method is illustrated in fig. 48a. A pre-trigger of the Nagard type 5001 square wave generator was used to trigger the time base of a Tektronix type 545A oscilloscope. The horizontal sweep produced, together with the calibration graticule was focused onto the photocathode of the delay tube. The delayed output pulse of the Nagard generator was used to trigger the delay of the Hirsch circuit (described in section 6.2). The fast avalanche pulse from the Hirsch circuit was used to gate the second "electron-gate" open, during which time-interval part of the electron image of the oscilloscope trace was allowed through. At lower gating speeds, up to $\triangleq$ .5 µsec, the delayed output pulse from the Nagard generator itself could be used as the gating pulse. At the faster gating speeds the output pulse from the Hirsch circuit had to be used. The total delay required between triggering the time base and applying the gating pulse was $\triangleq$ 350 musecs. This time was the sum of three separate delays. The first was the delay between the oscilloscope trace first appearing on the screen and the input trigger being applied, which was found experimentally (section 6.6) to be $\triangleq$ 150 musec. The second was the time needed for the trace to travel to the centre of the screen; $\triangleq$ 100 musec on the 20 musec/cm sweep speed. The third was the time taken for the oscilloscope trace to arrive as an electron image at

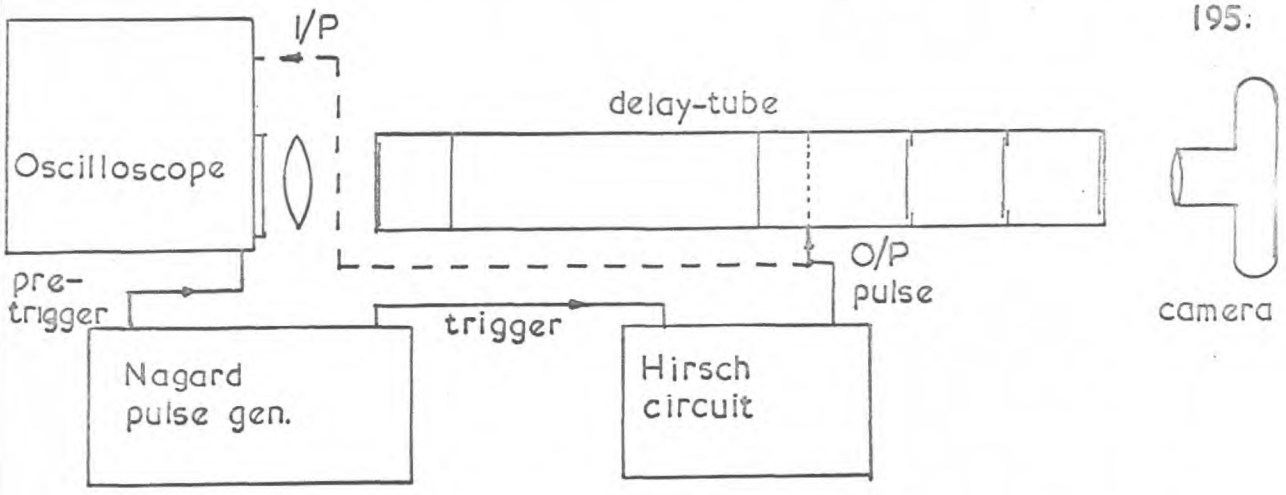
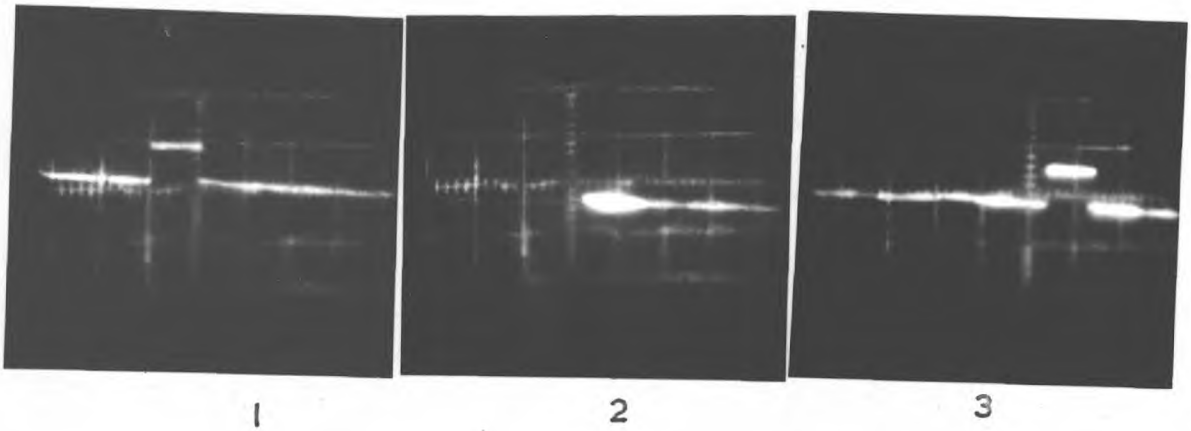


FIG.48A An experimental arrangement used to determine shutter speed



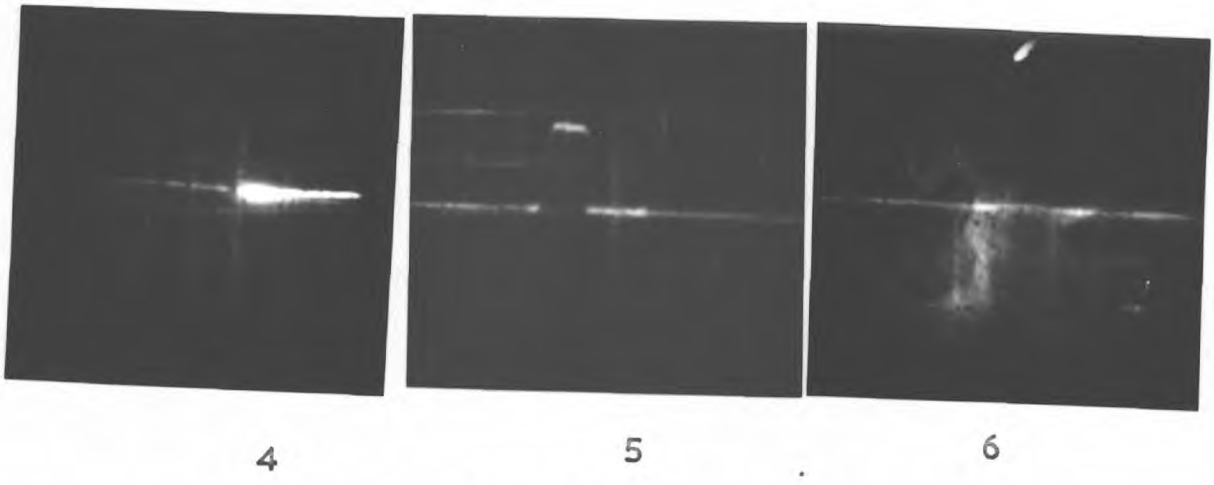


FIG.48B

the second "electron-gate", i.e. ≏ 100 musecs. Since the Hirsch circuit provided a maximum delay of ≏ 140 musecs, the Nagard generator was used to provide the extra delay. The gating pulse was first applied to the horizontal input of the oscilloscope and the resulting trace photographed through the delay tube. The gating pulse was then applied to the tube and a photograph of the oscilloscope trace was taken. The length of the oscilloscope trace on a calibrated time base gave the exact shutter speed of the second "electron-gate".

Some of the results of this experiment are illustrated in fig.48b. Figs. 48b.(1), (3) and (5) show gating pulses of 10 volts amplitude and of 100 μsecs, 5 μsecs and •2 μsecs duration respectively, applied to the oscilloscope. Figs. 48b.(2), (4) and (6) show the output of the delay tube gated by the respective pulses. The thickest part of the trace occured while the gate was open. The after-glow of the P.2 phosphor of the Tektronix c.r.t. was responsible for the extra trace on both sides of that caused by the gating pulse. The faint trace on the left hand side was caused by the previous gating cycle and that on the right hand by the contemporary gating cycle. The phosphor decay limits this method to indicating shutter speeds ≯ 1μsecs.

The second method used in an attempt to ascertain the gating speed of the second "electron-gate" was to microphotometer the photographic negatives obtained in a similar experiment to the previous one. However, in an attempt to reduce the effect of phosphor decay, a Tektronix c.r.t. containing a P.16 phosphor replaced the one containing

the P.2 phosphor. The decay time of the P.16 phosphor was 100 μsecs. It was hoped to separate from the decay that part of the trace due to the gating pulse using the microphotometer technique. However, the phosphor noise prevented any accurate measurement of gating speeds in the millimicrosecond region.

The third method was found to be successful, especially for gating speeds in the 1 - 10 μsec region. The experimental arrangement used for this method is illustrated in fig. 49. The gating circuit used the modules M.1, M.2, M.3, M.4 and M.5, described in section 6.3. The master oscillator in M.1 operated at ≏ 1Kc/S frequency. The first avalanche output from M.2 was used to trigger the horizontal time base of a Tektronix 545A oscilloscope at the same frequency as the master oscillator. The horizontal sweep of the Tektronix c.r.t. containing a P.16 phosphor screen was completely covered except for a vertical slit 1 mm in width. The pulsed spot of light produced, was focused onto the photocathode of the delay tube operated with the first "electron-gate" and the equipotential delay section held at 10 volts positive and 100 volts positive respectively. Since the horizontal sweep speed of the oscilloscope was 20 μsec/cm, the trace crossed the slit in 2 μsec. Thus an electron pulse, having a rise time of ≏ 2 μsec (described in section 6.5), a flat top of 2 μsec and decaying at the P.16 decay rate to zero intensity after ≏ 70 μsec, arrived at the second "electron-gate". It was noted above that the electron pulse arrived at the second "electron-gate" ≏ 350 μsec after

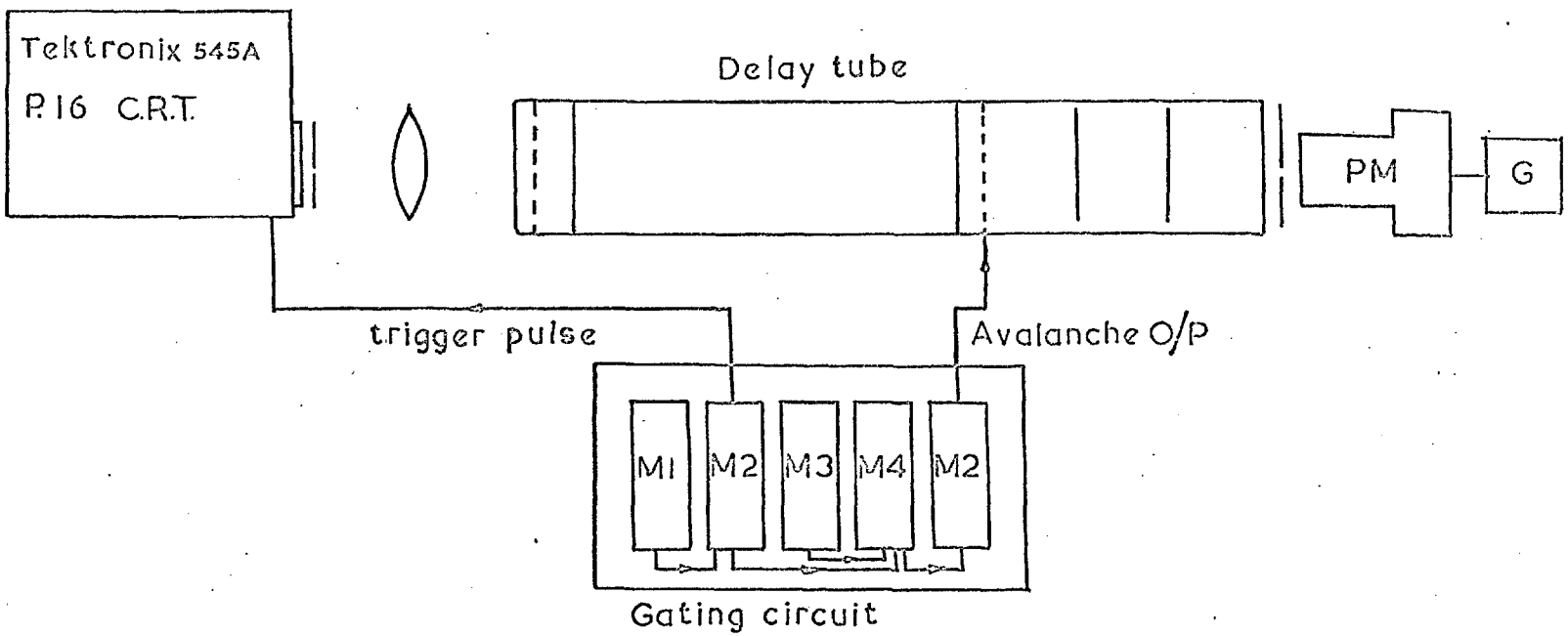


FIG.49 The experimental arrangement used to determine the shutter duration of the electron-gate

the oscilloscope had been triggered by a voltage pulse from M.2. Thus if the calibrated delay of the circuit were set to 350 μsec, the avalanche output gating pulse would have opened the second "electron-gate" just as the electron pulse arrived. In practice the value of the calibrated delay, produced by the gating circuit, was slowly increased, from a value well below 350 μsec, until the trailing edge of the gating pulse just started to allow the leading edge of the electron pulse through the second "electron-gate". As the delay was further increased even more of the leading edge of the electron pulse was allowed through the gate. Eventually, when the delay had been increased sufficiently, a constant fraction of the temporal distribution of the electron pulse was allowed through the gate. This fraction was equal to the ratio of the gating pulse length to the electron pulse length. The part of the electron pulse allowed through the gate by the avalanche pulse was amplified by the cascade section of the delay tube and appeared on the output phosphor. The mean intensity, averaged over many cycles, of the light output from the gated electron pulse was measured using a photomultiplier (P.M.) and a galvanometer (G). The galvanometer current was recorded as the calibrated delay of the gating circuit was increased by steps of 1 μsec. These measurements were plotted as a curve representing the electron pulse "sampled" by the square gating pulse. Assuming that the front edge of the electron pulse was perfectly square, the time taken for the plotted curve to reach a maximum value from its steady

zero value was equal to the duration of the square gating pulse. The plotted curve was normalized to reach the steady value it would have reached if the light output of the P.16 phosphor did not decay, but emitted a constant radiation. The rise time of the latter curve was differentiated to obtain the shape and duration of the gating characteristic of the second "electron-gate", due to the gating pulse. This derived gating characteristic was then compared with the actual voltage gating pulse applied to the second "electron-gate.

The 11 μsec duration gating pulse generator, described in section 6.4.2, was used as the last module (M.2) in the gating circuit in the experiment illustrated in fig. 49. The voltage pulse, measured using a P.6025 probe and an N type Tektronix sampling unit, which was applied to the second "electron-gate" is shown in fig. 27a and 27b. Figs. 27a and 27b show the pulse, where both vertical scales are 5V/cm and the horizontal scales are 5 μsec/cm and 2 μsec/cm respectively. This 11 μsec gating pulse was used to "sample" the electron pulse. The photomultiplier output current due to this sampling action is illustrated in fig. 50 plotted against the calibrated delay time. The time taken for the curve to rise from its initial zero value to its maximum value is 12 μsec. This value of 12 μsec is the duration of the gating pulse, which confirms that a voltage pulse of 11 μsec duration actually gated for this period of time without being appreciabl degraded by stray inductance or stray capacitance.

Fig. 51 shows the curve resulting from the normalization of the

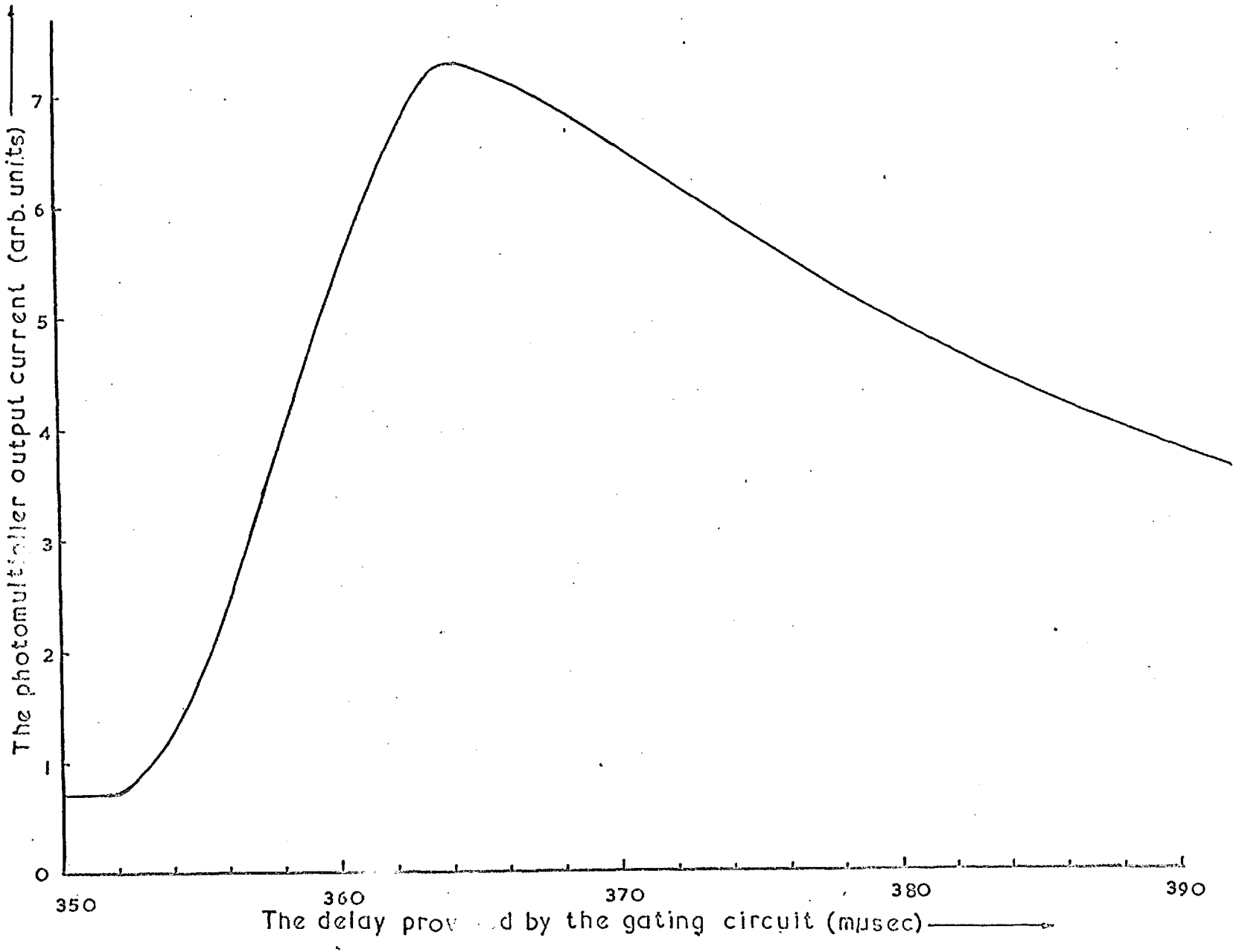


FIG. 50 The measurement of shutter speed

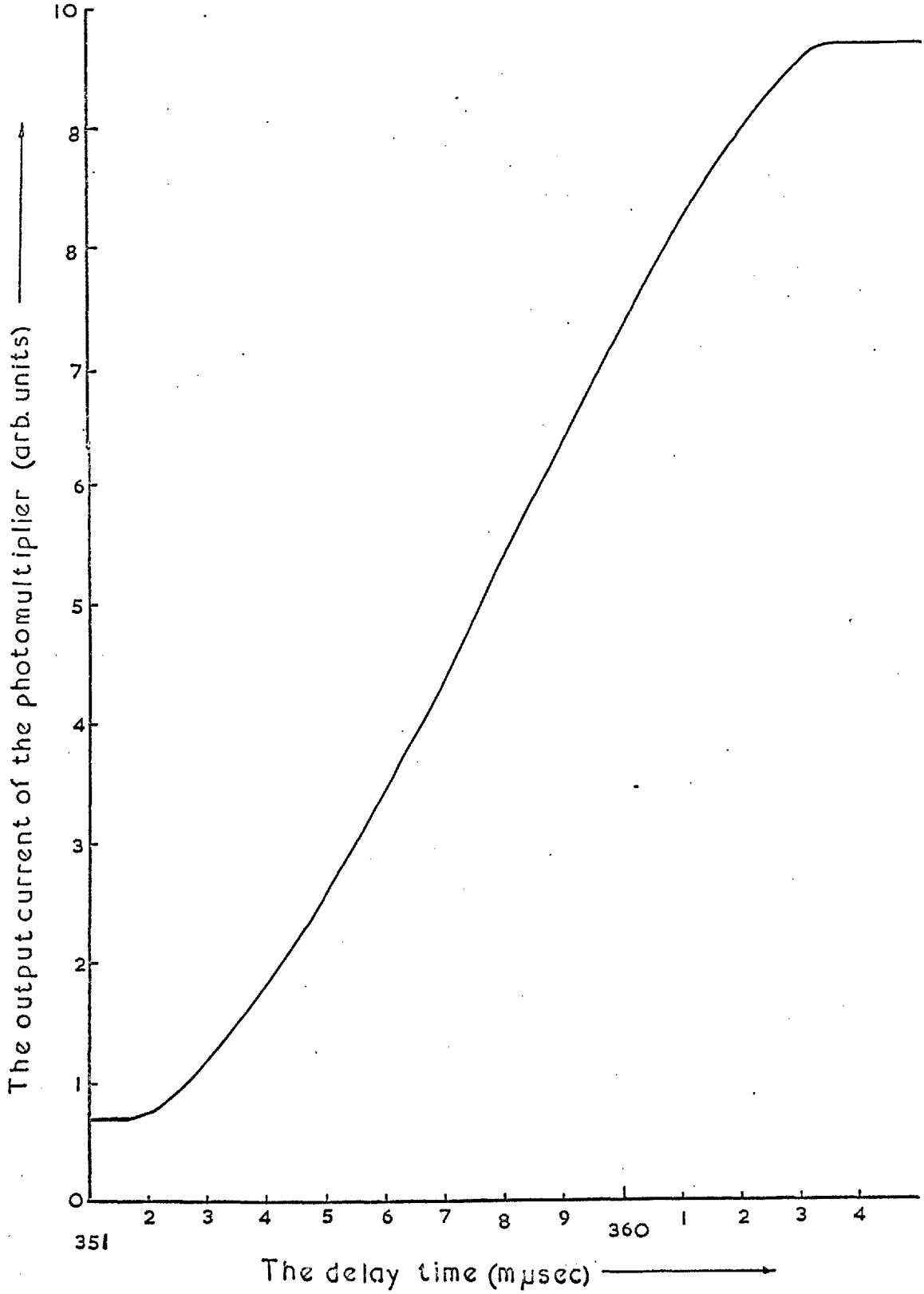


FIG.51 The measurement of shutter speed

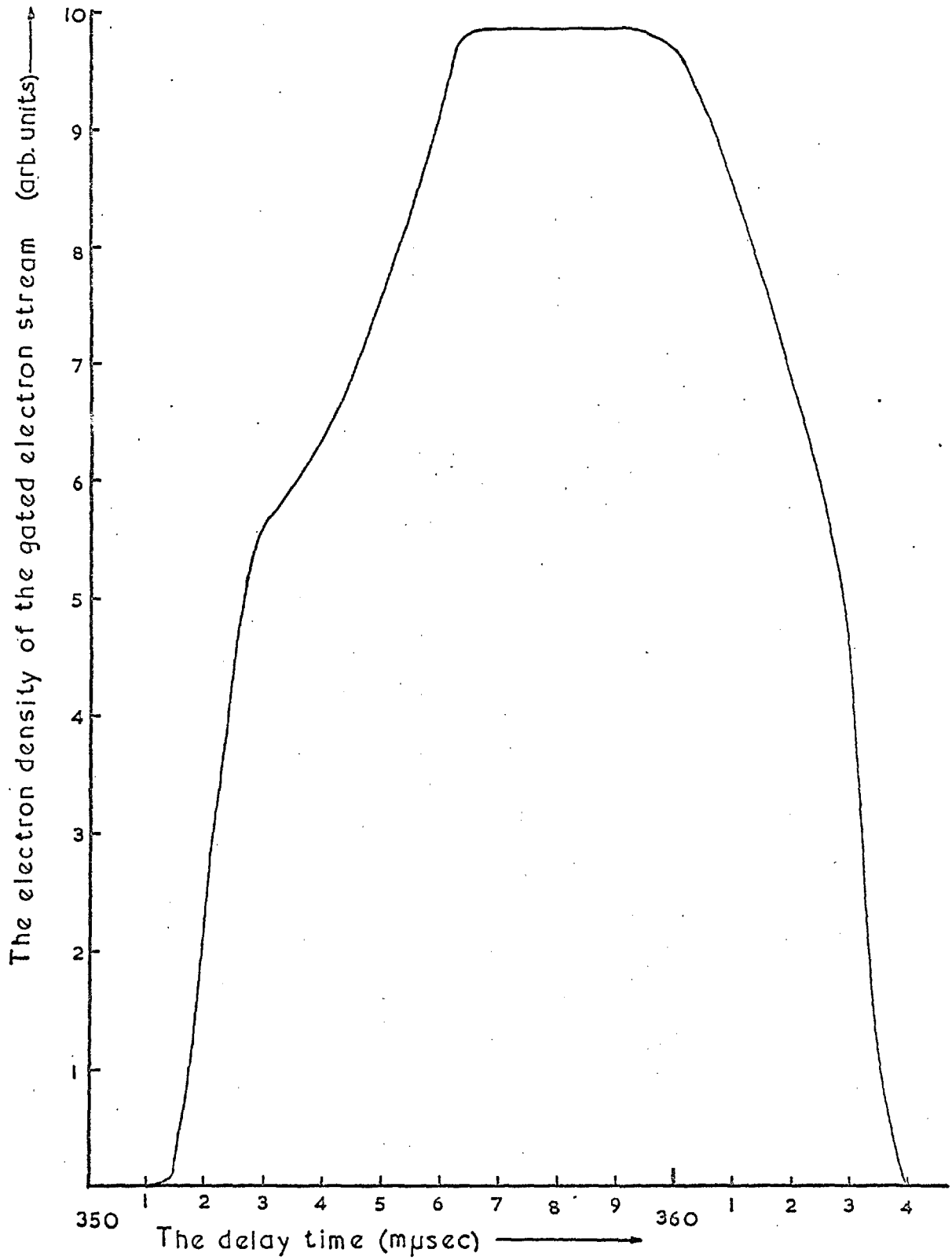


FIG. 52 The gating characteristic of the 2nd gate due to the 11 mμsec. gating pulse

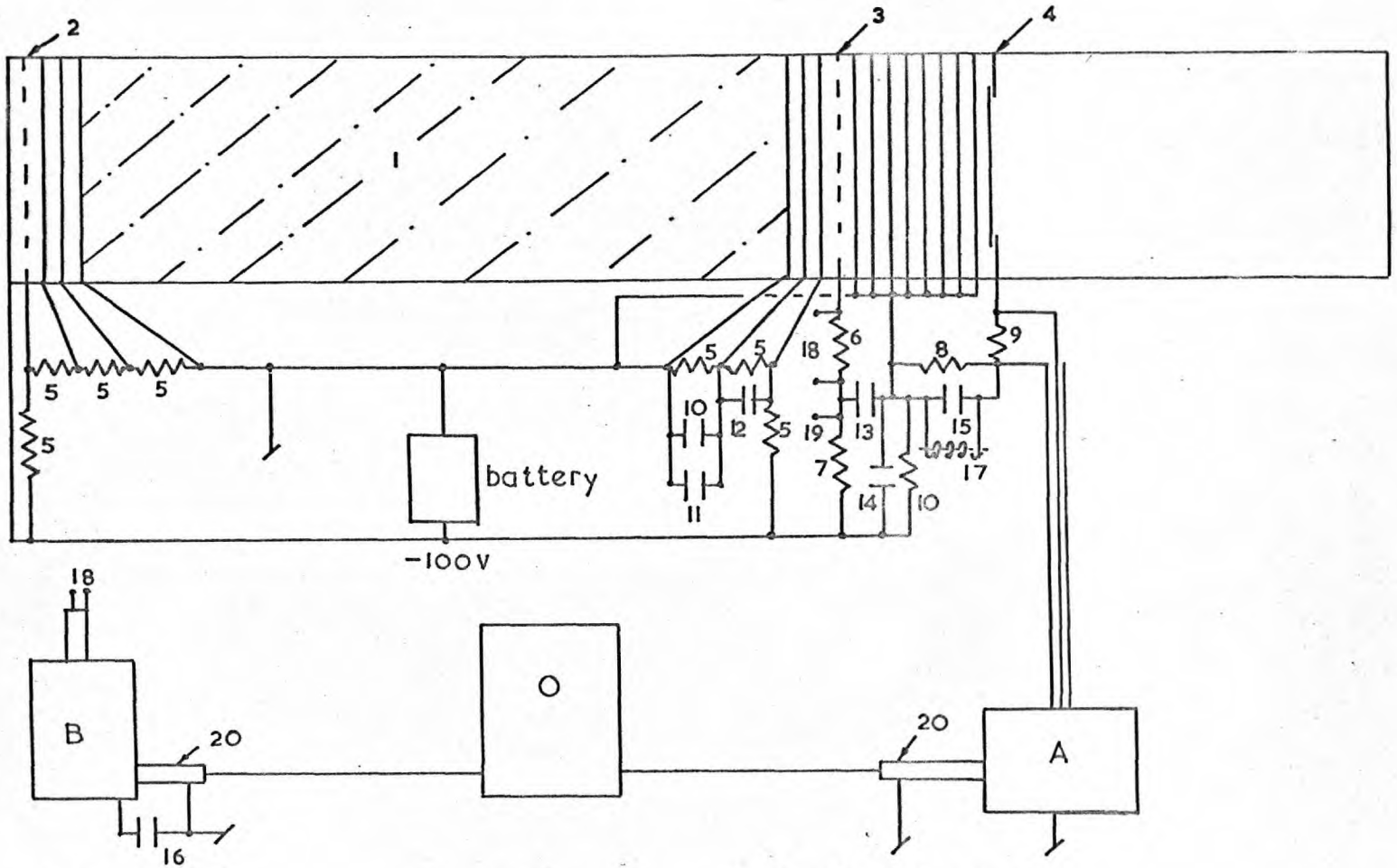
curve shown in fig. 50. Fig. 52 shows the curve resulting from the differentiation of the curve of fig. 51. This latter curve represents the turn-on characteristic of the second "electron-gate" due to the 11 mμsec gating pulse. The leading edge of this curve shows the turn-off characteristic of the gate due to the trailing edge of the voltage gating pulse. The trailing edge of this curve shows the turn-on characteristic of the gate due to the leading edge of the gating pulse. The turn-on rate is seen to be slightly faster than the turn-off rate, which corresponds to voltage rise and fall rates of the gating pulse shown in fig. 27b.

The gating characteristic of the second "electron-gate" using a gating pulse of 22 mμsec duration was also found to correspond to the voltage gating pulse (section 6.4.1).

8.2.7 The investigation of spurious electron storage in the delay-section of the tube

It was necessary, for the completely satisfactory operation of the delay-section of the tube, that the part of the electron stream excluded by the gating action of the second "electron-gate" be returned and completely absorbed in the delay-section of the tube.

Initially, the only method available to investigate the possibility of spurious electron storage was the one which is described below. The circuitry used in conjunction with the delay-tube for this experiment is shown in fig. 53. A Lucas spot light, maintained at a constant intensity by a 12 volt car battery, was focused upon the



5.	100K	9.	68Ω	13.	·47 pF
6.	1 M	10.	100K	14.	·1 μF
7.	1 M	11.	47 pF ceramic	15.	200pF ceramic
8.	100Ω	12.	47pF silver-mica	16.	32 μF

17. ferrite inductance
18. O/P from gating circuit
19. voltage bias
20. Tektronix probe

FIG. 53 The experimental arrangement used to investigate spurious electron storage

photocathode of the delay-tube. The equipotential delay-section (1) and the first multiplying sandwich (4) of the cascade intensifier were held at earth potential. The primary photocathode and the second "electron-gate" (when unbiased) (3) were both held at a fixed potential of 100 volts negative. The first "electron-gate" (2) was maintained at 10 volts positive with respect to the photocathode. A reverse bias (19) of 5 volts negative with respect to the 100 volts negative line, was applied to the second "electron-gate" across a 1MΩ resistance (7). The tube was shielded from stray A.C. fields using the same precautions as those described in section 8.2.3. Under these conditions the continuous electron stream, produced by photoemission at the primary photocathode, was completely reflected at the second "electron-gate" and returned towards the photocathode region. It was assumed that the photocathode region always reflected a fraction r of the returning electron stream so that the electron density built up to a value d_n given by

$$d_n = \frac{a(1-r^n)}{1-r}$$

where n was the number of reflections made by the leading edge of the electron stream at the photocathode region and a was the electron density of the electron stream where n = o.

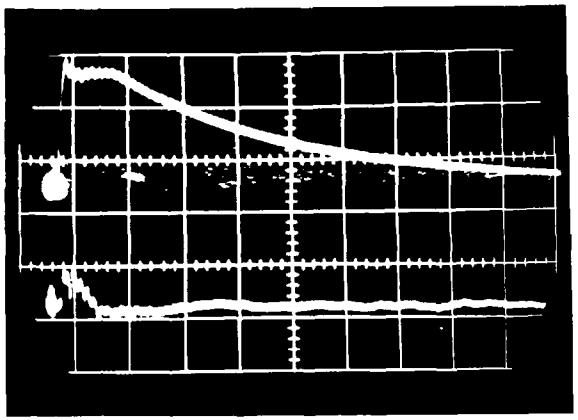
This process was allowed to continue for some seconds. Thus $n > 10^6$ and therefore $r^n \simeq o$, since the time interval between successive reflections of the electron stream at the photocathode region was

$\triangleq$ 200 mμsec. The electron density after some seconds was given by d_{∞} , where

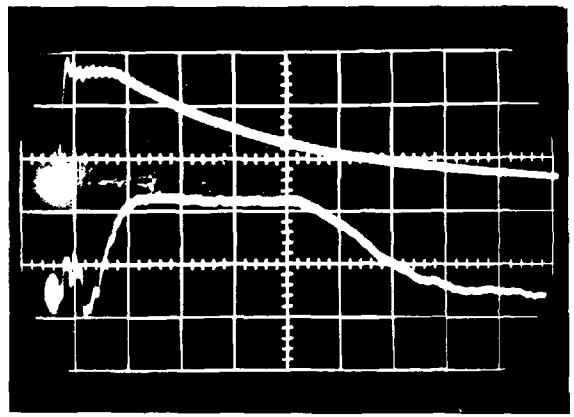
$$d_{\infty} = \frac{a}{1-r}$$

Thus after some seconds an electron stream of uniform electron density was built up; the total storage time of this electron stream in the delay-section being $\triangleq$ 200 mμsec (two transits of the delay-section). Thus when a positive gating pulse of $\triangleq$ 1 μsec duration was applied to the second "electron-gate", the stored electron stream, having an electron density d_{∞} was swept out of the delay-section in $\triangleq$ 200 mμsec. This stored electron stream was followed by an unstored stream, having an electron density a.

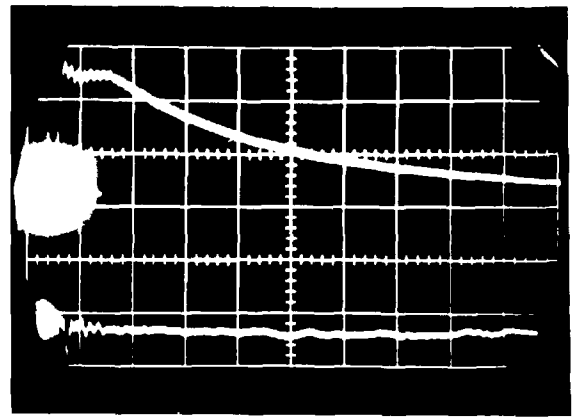
The positive gating pulse was obtained from the Hirsch circuit (8) described in section 6.2. The avalanche voltage excursion of the output transistor was almost wholly applied, through a differentiating network of a 100 pF condenser and the tube resistance of 1MΩ (6), onto the second "electron-gate". This gating voltage pulse is shown in fig. 54a, recorded on the upper beam of the Tektronix 551 oscilloscope (0) where the horizontal scale is 400 mμsec/cm and the vertical scale is 10V/cm. The part of the electron stream allowed through the second "electron-gate" was collected on the aluminium backing of the phosphor of the first sandwich (4). The electron current pulse collected flowed to the circuit earth through 68Ω (9) across which it developed a voltage pulse. This small voltage pulse



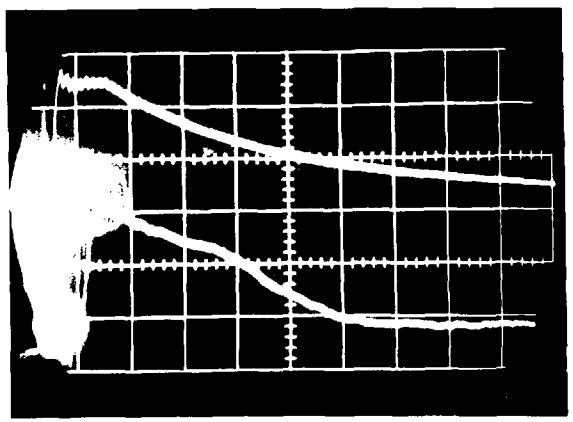
A



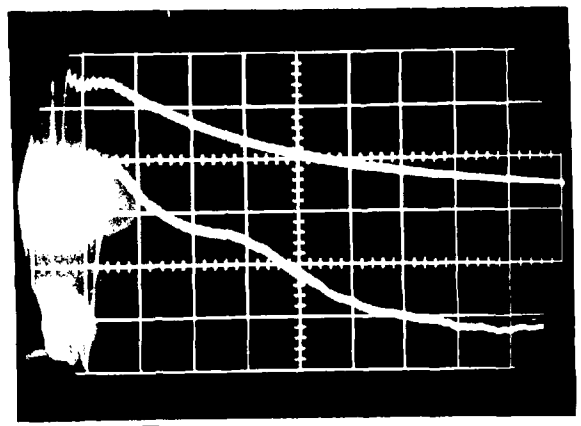
B



C



D



E

FIG. 54 The investigation of spurious storage

(Sweep speed 400 mμsec/cm)

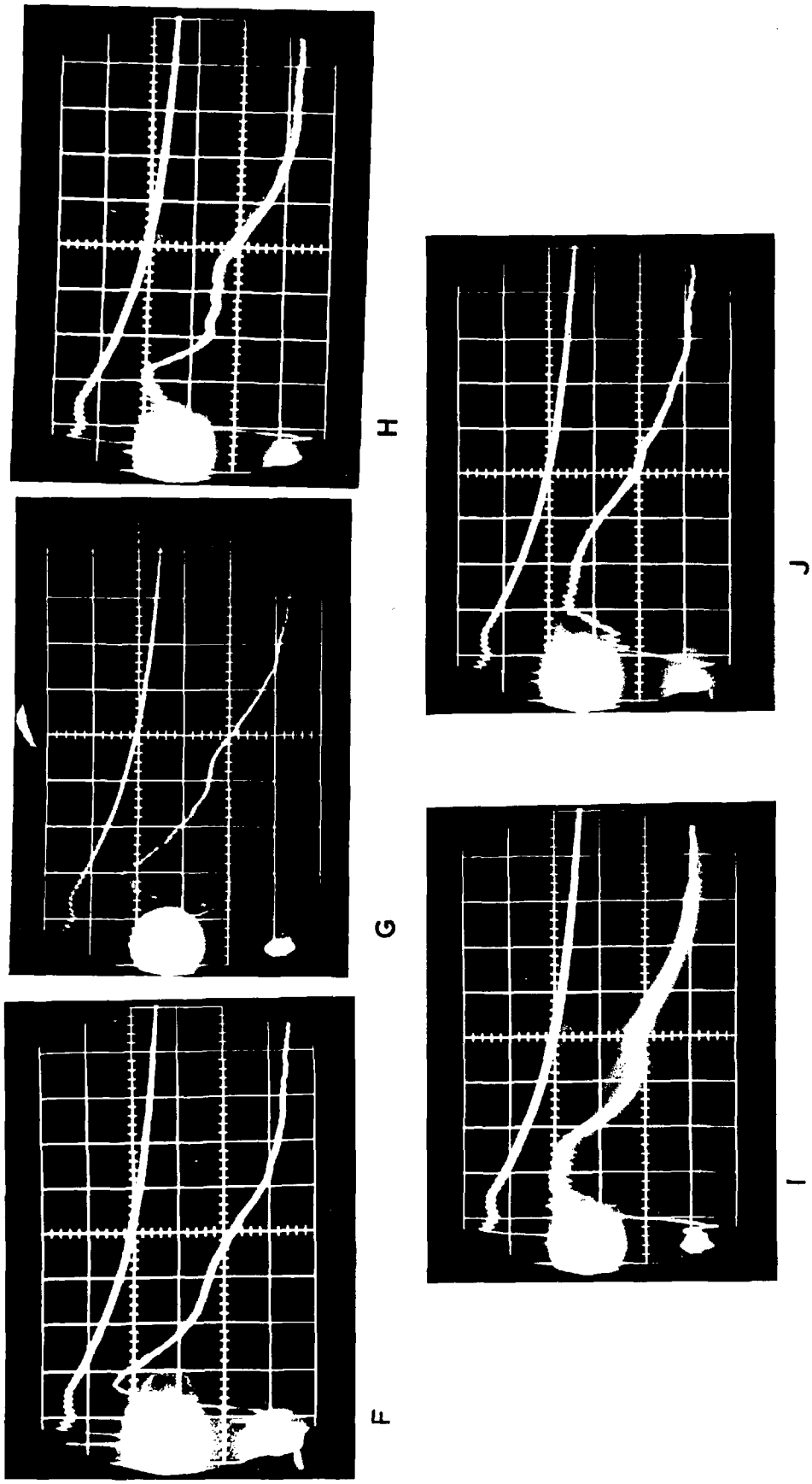


FIG. 54 (Contd.)

was amplified by A, described in section 6.6, and was recorded on the lower beam of the oscilloscope, (O). The voltage pick-up on the earth line of the amplifier (A) due to the voltage gating pulse, was reduced to a minimum using the condensers numbered 10, 11, 12, 13 and 15, the 100Ω resistance (8) and the ferrite cored inductance (17).

The response of the voltage amplifying circuitry to a square electron pulse was checked by applying the voltage gating pulse to the first "electron-gate" (2). The second "electron-gate" was biased to 20 volts positive in order to allow through the whole of the electron pulse without any spurious storage occuring. The amplified voltage pulse resulting from the collection of the electron pulse appeared on the lower beam of oscilloscope, and is shown in fig. 54b. The pick-up by the amplifier (A), due to the gating pulse applied to the first "electron-gate" is shown in the lower trace of fig. 54b. The horizontal sweep speed of the oscilloscope was 400 μsec/cm, the upper vertical scale was 10V/cm and the lower vertical scale was ·2V/cm. The oscilloscope was operated on these ranges throughout the experiment.

The gating pulse was then applied to the second "electron-gate", which was biased to 5 volts negative with respect to the 100 volts negative line. The first "electron-gate" was biased to 10 volts positive with respect to the photocathode. With no illumination applied to the photocathode, the voltage pick-up by the amplifying circuit shown in the lower trace of fig. 54c was due to the gating pulse applied to the second "electron-gate". The photocathode was then

illuminated and the gating pulse applied to the second "electron-gate". The resulting amplified voltage pulses, resulting from the electron pulses arriving at the mica sandwich, are shown in figs. 54d, e, f, g, h, i and j, when the voltages applied to the equipotential delay section were 200V, 100V, 50V, 25V, 16V, 11V and 9V respectively. The total spurious storage times of electrons, equalling the double transit time of the electron stream in the delay-section, can be seen from fig. 11 to have theoretically calculated values of 160, 220, 310, 440, 560, 670 and 740 mμsecs when the voltage applied to the equipotential delay-section is 200, 100, 50, 25, 16, 11 and 9 volts respectively. The figures show that in each case, spurious storage of electrons occured over periods roughly corresponding to the times predicted theoretically. In each case the electron density, which was built up to a value d_∞ during the spurious storage, is seen to be approximately double the electron density of the unstored stream.

Thus $d_\infty \triangleq 2a$.

and $r \triangleq \frac{1}{2}$

It appeared from this experiment that the photocathode region reflected approximately half of the returning electron stream.

Further evidence of spurious electron storage was obtained using the experimental arrangement which is shown in fig. 48a and which is described in section 8.2.6. A c.r.t. containing a P.16 phosphor screen was used in the Tektronix 545A oscilloscope. The Hirsch circuit was adjusted to provide an output avalanche pulse of $\triangleq$ 20 musec duration,

which was applied to the second "electron-gate". A photograph of the part of the graticule of the oscilloscope, which was focused onto the front photocathode of the delay tube, is shown in fig. 55a. It can be seen from fig. 55a that the width of the object area was 2 cms, since each main graticule division was 1 cm. The illumination of the graticule was switched off and the horizontal trace of the oscilloscope c.r.t. brought to the centre of the object area. The oscilloscope sweep speed was set to 40 mμsec/cm division; so that the oscilloscope trace crossed the object area in $\triangleq$ 80 mμsec. The temporal delay provided by the Nagard pulse generator was adjusted until the gating pulse allowed through $\triangleq$ 20 mμsec of the electron stream due to the oscilloscope trace. A photograph of the image appearing on the output screen of the delay tube under these conditions is shown in fig. 55b. The length of the denser part of the image of the trace corresponds to the time during which the gate was open while the electron beam of the Tektronix c.r.t. crossed the P.16 phosphor screen. The decay tail of the image of the trace corresponds to the part of the phosphor, over which the electron beam of the Tektronix c.r.t. had crossed, before the second "electron-gate" was opened. The oscilloscope sweep speed was reset to 200 mμsecs/cm division, so that the trace crossed the object area in 400 mμsec. The temporal delay provided by the Nagard pulse generator was increased, so that the second "electron-gate" was opened to that part of the electron stream which corresponded to the part of the trace which appeared last in the object area. The parts

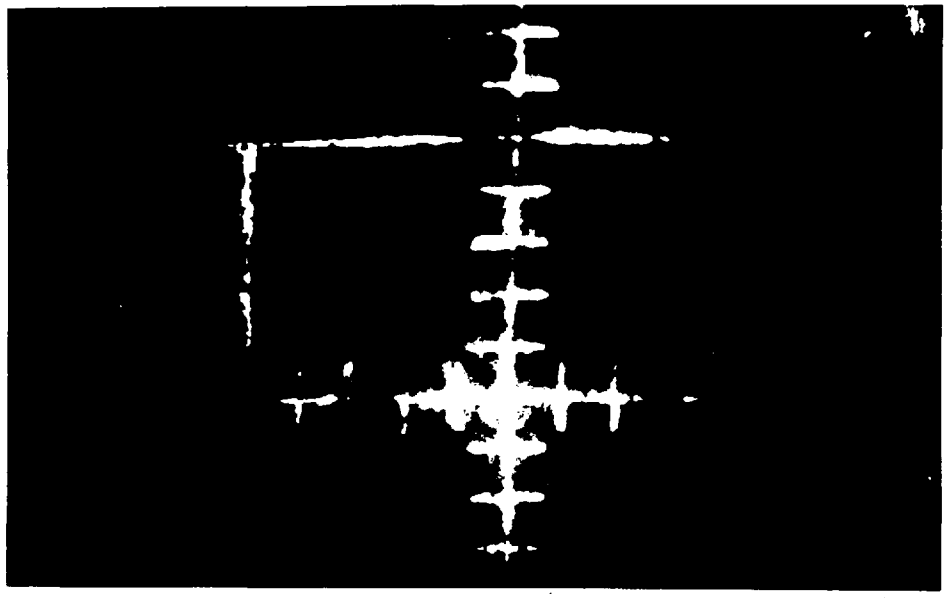


FIG. 55 A The graticule of the oscilloscope (2 cm.)

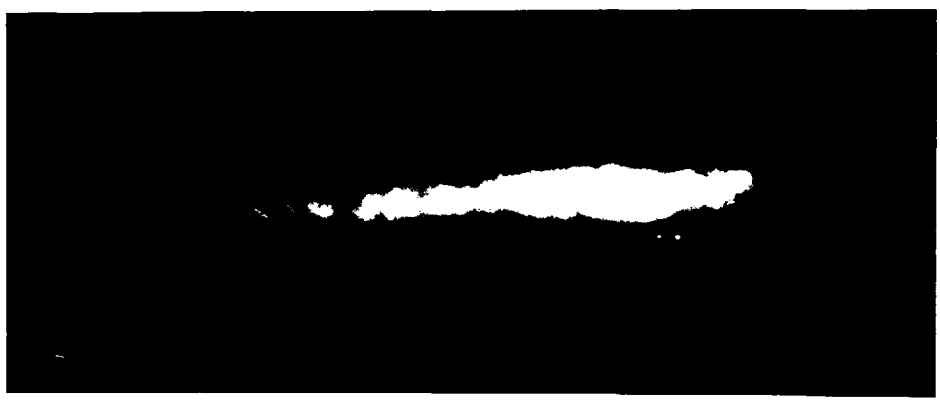


FIG. 55 B The trace image (40 μsec/cm.)



FIG. 55 C The trace image (200 μsec/cm.)

of the trace allowed through the gate with their corresponding decay tails can be seen in fig. 55c. The part of the image of the trace on the right-hand side of fig. 55c is due to that part of the electron image of the trace which makes only one transit in the delay-section of the tube, before being gated through the second "electron-gate". The part of the image of the trace on the left-hand side of fig. 55c corresponds to that part of the electron image of the trace which makes three transits of the delay-section of the tube before being gated through the second "electron-gate". The end of the left-hand part of the image of the trace can be seen from fig. 55c to occur ≃ 200 mμsec before the end right-hand part of the image of the trace. This interval is equal to the time taken for the electron stream to complete the two extra transits of the delay section, when the equipotential delay-section was held at 100 volts.

Thus this experiment clearly indicated that if a beam of electrons were returned to the photocathode region it would be partially reflected. More than one image of the trace was observed due to reflection; the number depending upon the sweep speed of the oscilloscope. The images became fainter with the successively increasing number of reflections made.

8.3 Experimental results gained from tubes numbered XI - XIII

It was considered possible that the spurious storage of electrons established in section 8.2.7, might be due to the presence

of the first "electron-gate". The first "electron-gate" was thought to distort the accelerating field in front of the photocathode, so that part of the returning electron stream was reflected at the discontinuity.

Tube number eleven was constructed, omitting the first "electron-gate" in order to test the hypothesis stated above. The experimental method used was the second one described in section 8.2.7. Besides the main image of the trace, due to the electron stream completing a single transit of the delay-section, further images were looked for due to reflection (such as the first reflected image shown in fig. 55c). Only the one main image was observed using tube number eleven. The tube went soft before any other methods of determining electron storage could be applied. There were two possible explanations of the observation made with tube eleven. The first explanation was that the removal of the gate had removed the partial reflection of the electron stream which returned to the photocathode region. The second explanation was that the pressure inside the tube had fallen to such a value that the mean free path was not large enough to allow the electron stream to complete more than one transit of the delay section and be observable at the tube output.

Tubes numbered twelve and thirteen were constructed to examine the electron storage effect further. The basic design of the tube, shown in fig. 38 was retained. Some of the metal electrodes in the tube were modified in the following manner. The internal diameter of

electrode 1, shown in fig. 38a, was enlarged to enable it to accept a larger photocathode plate of 40 mms external diameter. The internal diameter of the electrode 2, which held the tungsten mesh ring assembly (the first "electron-gate"), was also enlarged to 40 mms. The modified electrode and tungsten mesh ring assembly are shown in fig. 39b.(ii). The internal diameter of electrode 4, which held the cathode plate during activation, was also increased to 40 mms. The inconel structure shown in fig. 39i, was fitted into the equipotential delay section of the tube. This structure held four flashless getters. A series of electrodes of the type shown in fig. 39h were fitted 2 cm apart in the cascade-intensifier section of the tube. The twin cuts shown in the internal diameter of these electrodes allowed the passage of the multiplying sandwiches, after the tube was activated. The hinging action of electrode 10 was removed, being replaced by two slots which allowed the passage of the second multiplying sandwich. The modified electrode 10 is shown in fig. 39f.(ii).

The processing of the modified tube proceeded similarly to the earlier tubes described in section 8.1 except for the following differences. The tungsten mesh ring assembly was clipped against the inconel frame in the equipotential delay-section of the tube. After the tube was activated, sealed-off the pump and the photocathode plate and mica sandwiches moved to their operating positions, the tungsten mesh was unclipped and brought forward to its final position against electrode 2. If the tungsten mesh was not required in a particular

experiment it was removed from electrode 2 and clipped against the flat window in the processing compartment.

The enlarged area of the photocathode provided a useful increase in the total number of image elements which could be transmitted through the tube. The extra annuli in the cascade-intensifier section decreased the tube background. The four getters absorbed the gas liberated from the sealing-off process, and also any gas liberated inside the tube owing to outgassing. The getters would also prolong the life of a tube going soft.

8.3.1 The collection of photocurrent by the electrodes

The collection of photocurrent by the various electrodes, when there was no first "electron-gate" was determined in exactly the same manner as described for the earlier tubes in section 8.2.1. The experimental arrangement is illustrated in fig. 41 using galvanometers G_1, G_3, G_4 and G_5. The Galvanometer G_2 was shorted out, since there was no first "electron-gate".

The variation in the value of the collected currents with the potential applied to the second "electron-gate" is illustrated in fig. 56. These curves are very similar to those obtained in fig. 42. It can be seen that when the voltage applied to the second "electron-gate" was < 2 volts positive, the current supplied through the photocathode lead was only $\simeq 1/5$th that required when the second "electron-gate" voltage was > 4 volts positive. The former current was needed to supply the loss, to the wall of the equipotential delay-

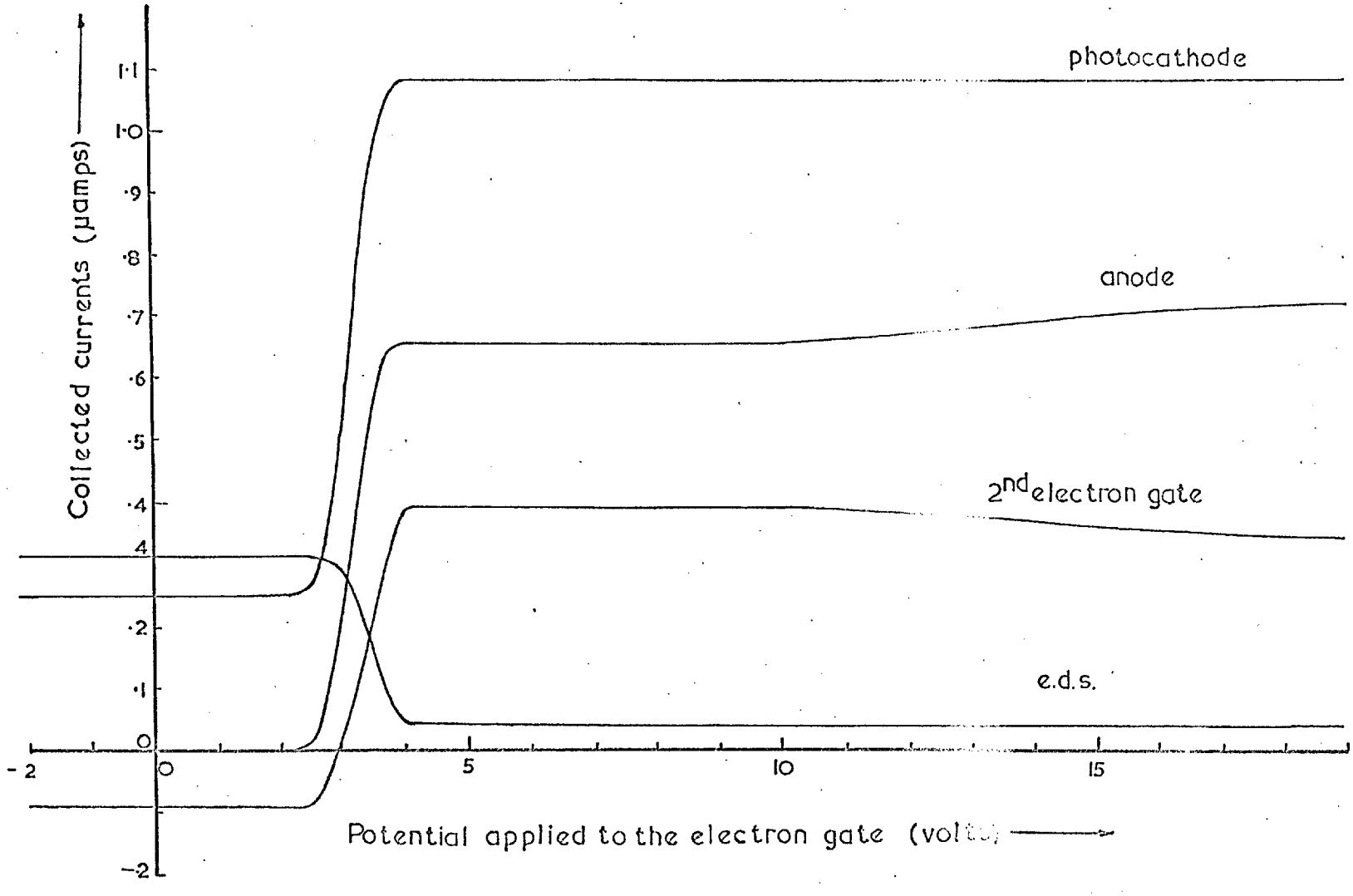


FIG.56 Electron collection in the delay tube

section, of current from the spuriously stored current flowing in the delay-section of the tube. The equipotential delay-section collects a current slightly in excess of that being lost by the spurious storage current; the excess being due to the generation of extra electrons during photoelectron-molecule collisions in the delay-section. This excess current equalled the difference between the current supplied to the photocathode and that collected by the equipotential delay-section.

The ratio of the values of 1_p and 1_o, which are defined in section 8.2.2 is .1302. When this value is substituted in the eqn

$$p = - \frac{\log_e(1-21_p/31_o)}{5.27.10^3} \text{ mms. Hg.}$$

a value of the pressure inside the tube of $p \triangleq 8.10^{-6}$ mms. Hg. is obtained.

It can be seen by comparing the curves in figs. 56 and 42 that the first "electron-gate" collected most of the current lost from the spurious storage current. The very presence of the first "electron-gate" caused approximately half of this loss. When the first "electron-gate" was removed, the current loss was collected by the equipotential delay-section.

A value of the fraction of the photocurrent stream reflected at the photocathode surface upon its return, could not be infered from the static measurements made above.

8.3.2 The further investigation of spurious electron storage in the delay-section of the tube

Two methods for the investigation of the spurious electron storage in the delay-section have been described in section 8.2.7. A third, more revealing method, will now be described. The experimental arrangement used for this method is illustrated in fig. 49. The equipment was operated in exactly the same manner that has been described for the third method of shutter speed measurement, described in section 8.2.6.

The calibrated delay provided by the gating circuit was adjusted to be accurate to $\pm$ 2% over a delay of 0-1,000 musec. The tungsten mesh, used as the first "electron-gate" was clipped into its position in front of the photocathode, and maintained at 20 volts positive. The equipotential delay-section was held at $\triangleq$ 200 volts positive. The oscilloscope was externally triggered by the gating circuit at $\triangleq$ 1Kc/s frequency. Electron pulses corresponding to the light pulses produced by the oscilloscope were produced in the tube. The gating circuit delay was increased from zero until the avalanche output pulse of $\triangleq$ 10 musec duration "sampled through", in the manner described in the third method of section 8.2.6, the electron pulse after its first single transit of the delay-section of the tube. As the delay was further increased the electron pulse had sufficient time to complete three single transits of the delay-section before being "sampled". The sampled pulse was then occuring when the electron pulse had been

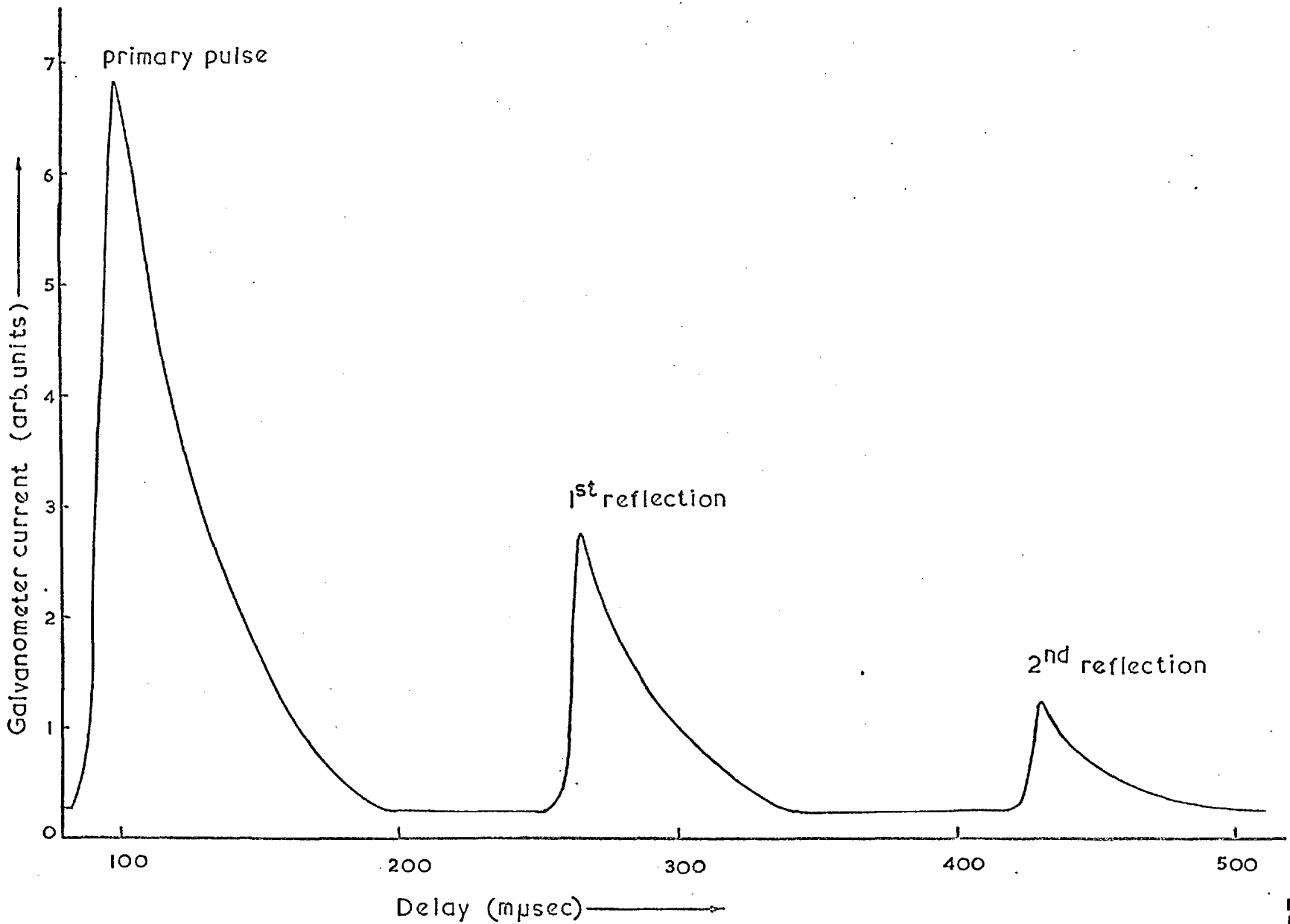


FIG. 57 The investigation of spurious storage

reflected only once from the photocathode, i.e. the first reflection. The delay of the circuit was further increased to enable the avalanche O/P pulse to "sample through" the 2nd, 3rd etc. reflected pulses. The output of this "sampling" action was converted from a light pulse to a current by the photomultiplier and recorded using a galvanometer. The delay provided by the gating circuit was increased in steps of 1 musec and the galvanometer current recorded. The galvanometer current plotted against the gating circuit delay, is shown in fig. 57. The ratio of successive maximum amplitudes can be seen to be $\triangleq$ 40%.

The ratio of the maximum amplitude of the first reflection to that of the primary pulse was measured as the voltage applied to the first "electron-gate" was varied, in steps of 5 volts, from 5 to 100 volts. There was however, no change in this ratio larger than the estimated experimental error of $\pm$5%. All possible variations of the applied potentials and magnetic flux were obtained and the value of the ratio indicated was measured. There was, however, again no appreciable change.

The first "electron-gate" was removed and the ratio again measured. The value, under these conditions, was within 5% of the value measured with the gate in place.

Three different tubes were investigated. The mean values of the ratios measured were 40%, 35% and 30% using tubes having primary photocathode sensitivities of 55 μA/Lm, 15 μA/Lm and 40 μA/Lm respectively.

The fact that the electron beam is partially reflected at the photocathode surface, may be explained as a combination of several factors..

(a) If an electron in a double transit of the delay-section, loses more axial energy than its emission energy from the photocathode, then it will be trapped in the "potential-well" of the delay-section and be unable to return to the photocathode. It is possible for an electron to lose axial energy, by having it converted to non-axial energy, at small inhomogeneities in the electrostatic and magnetic fields. A very small fraction of the electron beam also lose energy by collision with free-molecules.

(b) It is known, from the work of Bruining[163], that electrons can be elastically and inelastically reflected from surfaces in a vacuum. Bruining measured the coefficient of elastic reflection, δ_{refl} of electron beams having an incident energy of 50 eV and less. He found generally that δ_{refl} increased as the incident energy of the electron bream decreased. The values of δ_{refl} for BaO and Ag are 0·5 and 0·175 respectively at an incident energy of 4eV and 2eV respectively.

It does not seem improbable, therefore, that an electron stream returning to a photocathode with emission energy suffers a 30-40% reflection.

8.4 General conclusions from the performance of the tube

It has been demonstrated in this chapter that a tube comprising

an electron image delay, an electronic shutter and a cascade image intensifier could be successfully constructed employing the techniques described.

The primary function of this type of tube was to provide a "fast store" and "gate" for a luminescent chamber camera and a Cerenkov camera, described in sections 3.5.3 and 3.5.4 respectively. The tube was required to have an output geometrical resolution of ≥ 5 lp/mm and a blue light gain of $\geq 10^5$, in order that single photoelectrons could be photographically recorded in conjunction with the tube. The tubes made by the author had a measured blue light gains of between 10^4-10^5 at overall potentials of 45KV. A geometrical resolution of $\triangleq 5$ lp/mm was recorded photographically, when the tube was gated with a triangular shaped voltage pulse of 30 musec duration. A visually recorded measurement of the geometrical resolution, presented in the next chapter, of 10 lp/mm was obtained when the tube was gated with a square shaped voltage pulse of 10 musec duration. In both cases the applied magnetic flux density was .064 Webers/meters^2. An increase in geometrical resolution could be obtained by pulsing the magnetic coils with large currents, which would increase the magnetic field to 0.1-1 W/m^2. It is seen that the resolution and blue light gain of the tube were only just adequate to meet the requirements of the Nuclear physics experiments. The input and output diameters of the tube were 38 mms, which were adequate to meet the requirements. Only Sb-Cs photoemissive surfaces were used in the tubes constructed. The

tri-alkali surface, having a higher quantum efficiency, would be much more useful in detecting a small number of photons. Work is in progress at Imperial College on the improvement of the performance of the cascade image intensifier. The improved phosphor screens and their backings, developed by this group, would improve the geometrical resolution of the tube. These phosphor screens have increased efficiencies, which if used in conjunction with tri-alkali photocathode would increase the blue-light gain of the tube by a factor of $\simeq 20$, compared with the present tubes constructed by the author.

It was demonstrated that the tube provided a delay of $\simeq 100$ μsec and that the electronic gate could be operated at speeds of at least 10 μsec, which would be adequate for the Nuclear physics application. Electronic circuitry was developed which gated the tube fully on for the duration required, with an estimated jitter of $< 10^{-10}$ sec.

The main drawback of this tube was that the delay-section induced a spurious storage of electron information, because of the partial reflection of the returning electron stream at the photocathode. This meant that if a continuous stream of photon information were fed into the tube, the second "electron-gate" would gate through the wanted signal together with a spurious signal. The intensity of the spurious signal seemed to depend upon the photocathode surface. In the worst case measured the intensity of the spurious signal would approximately equal the wanted signal (in the tube having an Sb-Cs photosurface of 55 μA/Lm and a reflection coefficiency of $\simeq$ 40). In the best case

measured, the intensity of the wanted signal would be approximately double that of the spurious signal (in the tube having an Sb-Cs photosurface of 40 μA/Lm and a reflection coefficient •3). It was noted in section 3.6 that the use of a P.15 or P.24 phosphor as an information store, limited the acceptable flux rate of stored events to 10^5/sec, if the ratio of wanted signal to unwanted noise were to be greater than unity. The decay time to 1/e, of various types of plastic scintillator has been measured by Dreeskamp and Burton[161] and Falk and Katz[162] to lie between 2-5 mμsec. The latter experimenters found for all the plastic scintillators investigated, that if a slow-decay component existed, its peak intensity was only a few % of that of the fast component. Thus the decay time of the plastic scintillator limits the acceptable flux rate of particles through a scintillation chamber to $\simeq 10^8$ particles/sec. If the tube described in this chapter were used to enable the recording of a particle track in a scintillation chamber, a particle flux of 10^8 particles/sec would produce a continuous flux of photon information to be focused upon the tube. Under these conditions, as has been noted above, the spurious electron storage would be responsible for a ratio of wanted signal to unwanted noise at the tube output of just under unity. The tube using electron transit time information storage would produce the same signal to noise performance, at a particle flux of 10^8 particles/sec as a tube using phosphor screen information storage, operating at a flux rate of 10^5 particles/sec. Therefore, the use of

the tube described in this chapter would enable the satisfactory recording of a single track from a flux of particles having a rate of up to 10^3 times greater than that acceptable in conventional systems.

During the last three years most experimenters have turned away from the use of scintillation chambers to the use of spark chambers for the purpose of track visualisation of a Nuclear particle. The spark chamber may be used at particle flux rates of up to 5.10^6 particles/sec. The most important advantages that the spark chamber has compared with the scintillation chamber are:

a) It can be easily constructed.

b) It can be made much larger in size, which enables larger solid angles to be covered and greater angular accuracy to be achieved. The greater angular accuracy comes only from the greater size, since both systems have $\simeq$ 1 mm resolution.

c) The spark track can be recorded by direct photography, i.e. no expensive image-tube system need be employed.

d) Low density media may be employed, e.g. gaseous hydrogen, which makes the analysis of interactions easier.

The scintillation chamber may be used to advantage in a limited number of experiments where its following properties are important:

a) The sensitivity of the chamber to ionisation.

b) The ability to measure ranges well.

c) The ability to operate at higher flux rates than the spark chamber; if a plastic scintillator is used in conjunction with the

tube described in this chapter.

This tube can also be used to advantage in conjunction with the Cerenkov camera in those cases where the particle flux rate available is greater than that acceptable to conventional systems.

In general most image-intensifier tube systems have an input photocathode diameter of 1-2". In most Nuclear Physics experiments an input photocathode diameter of up to 10" is desirable, since geometrica resolution is lost in the optical demagnification required to focus the complete chamber onto existing image intensifiers. It is possible to obtain variable magnification in an image intensifier, using parallel electrical and magnetic fields. This method would permit the use of an input photocathode diameter of approximately four times that of the electron multiplying sandwiches which are used in present image intensifiers.

The tube may be used to select, in musec time-intervals, any part of the photon emission from a phenomenon, without the appearance of spuriously stored information, provided that the selection is completed within a time, from the start of the photon incidence upon the primary photocathode, equal to three times the transit time of an electron in the delay-section. It may be noted that,since no information is passed through the gate until the initial part of the electron stream has completed one transit of the delay-section, only the part of the photon emission occuring within a time equal twice the transit time of an electron in the delay may be investigated. It can be seen from fig. 11

that if a potential of 100 volts is applied to the equipotential delay-section, any part of the photon emission may be selected up to $\simeq$ 200 musec after the start of the phenomenon, with a time dispersion of $\simeq$ 3 musec. If a potential of 20 volts is applied to the equipotentia delay-section then 500 musec of photon information may be analysed with a time dispersion of $\simeq$ 15 musec. This "single shot" high speed shutter action of the tube would be very useful in the recording of a given part of a randomly occuring phenomenon; the transit time storage of the tube enabling electronic post selection using counter triggering.

Chapter 9 The preliminary investigation of a new type of framing camera

9.1 Introduction

The tube described in Chapter 8 was developed essentially for the purpose of recording a single frame of photon information. In many physical experiments there is a need for a device capable of recording separate frames at rates of $\geq 10^9$ frames/sec. This chapter describes a preliminary investigation of the possibility of operating the tube described in Chapter 8 at rates of $\geq 10^9$ frames/sec.

The closest approach to this specified performance has been achieved by Simonov and Kutukov[106] in Russia using a tube which incorporated a PIM 4 electron optical shutter and a cascade image intensifier, which had a light gain of 8,000. A framing rate of up to 10^8 frames/sec was obtained by these workers. The PIM 4 shutter, described in section 3.3 produced the first frame by opening to permit the electron stream to pass through, after which the c.r.t. deflection plates directed the stream to a given sector of the first phosphor screen of the cascade intensifier section. The shutter was then closed after which the potentials applied to the c.r.t. deflection plates were altered. When the shutter was reopened for the second frame, the electron beam was deflected to a sector of the phosphor screen adjacent to that of the first frame. Successive frames were taken using this proceedure. It must be noted that there is a "dead-time" between the frames during which information in the electron stream is

lost. This type of shutter requires the production of voltage pulses of several kilovolts amplitude for its operation and in the present state of high voltage pulse generating techniques rates of $> 10^8$ frames/sec have not been achieved.

The frame-rate of the PIM 4 shutter depends upon the rate at which the voltage pulses, applied to the shutter, can be produced. As will be seen later, the delay-tube can be operated as a framing-camera, whose frame-rate depends only upon the shape of the gating pulse. Since the shutter in the delay-tube is operated with a voltage of only $\pm$ 10 volts amplitude, frame-rates of $> 10^9$ frames/sec are possible using present techniques.

An illustration of the delay-tube operated in its "framing-mode" is shown in fig. 58. The framing action of the tube will now be described operating at a rate of 2.10^8 frames/sec. It can be seen from fig. 11 that, with a potential of 500 volts applied to the equipotential delay section (5), an electron stream would have a calculated transit time in the delay sections of 50 μsec with a calculated time dispersion of 0·6 μsec.

The delay-tube, as described in Chapter 8, is suitable for producing successive frames of a narrow line image or of an image of small dimensions compared with the primary photocathode area. In fig. 58, area A represents the image area of a phenomenon focused onto the edge of the primary photocathode (2) by the lens (1). A gating pulse (8) of 25 μsecs total duration is then applied to the first

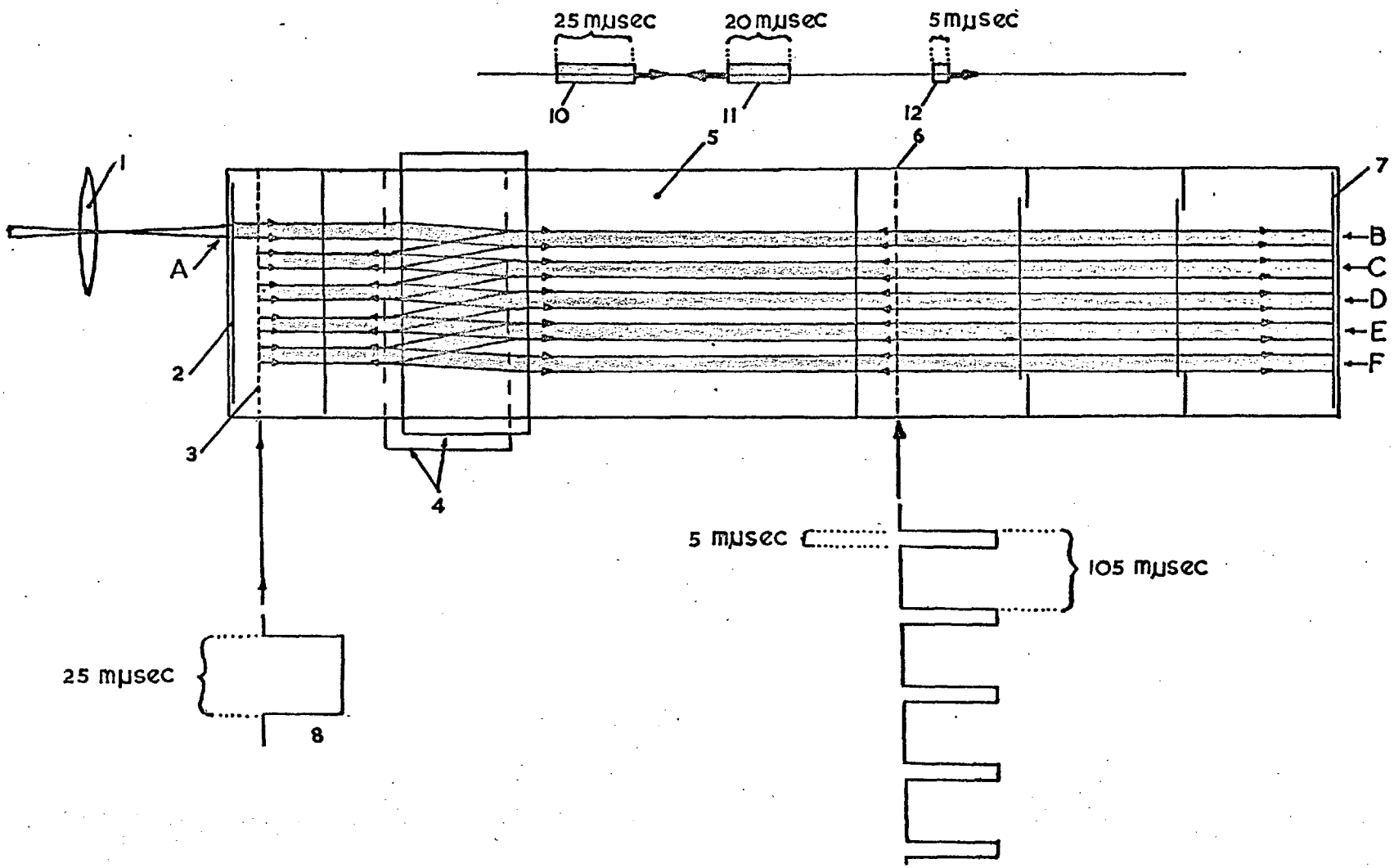


FIG.58 The operation of the delay tube as a framing-camera

"electron-gate" (3) which allows into the tube a stream of electrons (10) of 25 μsec duration, corresponding to that part of the object phenomenon which is required to be studied. This stream is then accelerated to enter the equipotential delay section with an energy of 500 eV. A pair of retangular deflection plates (4) are positioned outside the tube over a non-conducting region of the equipotential delay section. These plates, which are ≏4 cms long and are spaced ≏7 cms apart, produce a deflection of the electron stream of ≏5 mm in a direction mutually perpendicular to both the magnetic field and the constant electric field of ≏ 1KV between the deflection plates. If a line image were investigated, the plates would be positioned to provide a deflection across the tube perpendicular to the direction of the line. When the front edge of the electron stream arrives at the second "electron-gate", a gating pulse of 5 μsec duration allows the front segment of the stream, of 5 μsec duration, to pass through the gate. This pulse of electrons (12) of 5 μsec duration, passes through the cascade intensifier and appears on the output phosphor (7) in the area B. That part of the electron stream (11), of 20 μsec duration, which is not allowed through the second "electron-gate" is returned towards the primary photocathode end of the delay-section. When the electron stream of 20 μsec duration recrosses the deflection region, it suffers another deflection of the same magnitude and direction as the first. This stream is completely reflected from the first "electron-gate", which is now closed, and returns to the deflection

region to suffer another deflection. The stream returns to the second "electron-gate" where its front segment of 5 μsec duration, is allowed through the gate, to appear in the region C of the output phosphor. The remaining part of the electron stream undergoes similar transits of the delay section. Upon each return of the stream to the second "electron-gate" the front segment, having a 5 μsec duration, is allowed through. The electronic circuitry is required to produce a voltage pulse of 25 μsec duration applied to the first "electron-gate followed by a train of framing pulses, each of 5 μsec duration, to be applied to the second "electron-gate". In this case the delay between the front edge of the 25 μsec pulse and the front edge of the first framing pulse is required to be 50 μsec, and the delay between the front edges of successive framing pulses 105 μsec.

Thus it is possible for the tube, operating in the mode described above, to produce five successive separate frames with no "dead-time" between each frame. The framing speed is limited by the duration of the voltage pulse applied to the second "electron-gate" and by the time dispersion of the electron stream during its storage in the delay section. In the particular case described above the time dispersion of the electron stream does not limit the framing rate, since, as will be shown later, the total time dispersion of the electron stream after eleven transits in the delay section is only $\simeq$ •77 μsec.

The successful operation of the delay-tube in the framing-mode of operation, depends upon preserving the electron stream in an ordered

array over a large number of transits in the delay-section. A detailed consideration of the conditions necessary to preserve this ordered array is presented in the next section. This ordered array of electron information will be termed henceforth the electron-phalanx.

The tube can be used to produce a sequence of frames of a phenomenon which occurs randomly in time in one of two ways, depending upon which part of the phenomenon is required to be studied.

If the part of the phenomenon required to be studied occurs within a time, from the start of the phenomenon, equal to double the transit time of an electron in the delay section, then the tube may be operated in the following manner. The first "electron-gate" is initially held open and allows the electron image of the phenomenon to enter the delay-section of the tube. During the delay, provided by the transit-time storage of the delay-section, the detection system, which records the start of the phenomenon, has time to supply a trigger signal to the gating circuit. The gating circuit switches the first "electron-gate" off, and supplies a train of pulses to the second "electron-gate" to enable the framing action of the tube to take place in the manner described above.

If the part of the phenomenon required to be studied occurs after a time, from the start of the phenomenon, equal to double the transit time of an electron in the delay section, then the first method cannot be employed for the following reason. After the limiting time indicated the front of the electron-phalanx would have returned to the

photocathode, where it would be partially reflected and become intermingled with fresh electron information from the photocathode. Since the initial part of the phenomenon is not required for study, this time may now be used to enable the gating circuit to be triggered by the detection system. The first "electron-gate" is now initially held closed and only opened by the gating circuit when the light from that part of the phenomenon required for study is incident upon the photocathode. The second "electron-gate" is operated in the same manner as before.

Thus any section of a phenomenon may be studied, whatever the duration of the phenomenon. Since all the gating circuits are "locked" onto the initial signal from the detection system, the problems of synchronizing the framing camera with the phenomenon, which arise with conventional framing cameras are overcome. It may be noted that, sinc the electron information is stored in the delay section, the sequence of frames may be taken in any order of their occurence in time. The sequence of frames may be taken at a constant rate or a rate which varies continuously throughout the sequence.

9.2 The investigation of the change in the temporal distribution of the electron image with the number of transits made in the delay-section

Let an electron start from zero energy at the front of the delay section and be brought to zero energy at the end of the delay section, where the total distance traversed is $d_1+d_2+d_3$. The distance

d_2 is the length of the equipotential delay section, and d_1 is the distance from the front of the equipotential delay section to the point where the electrostatic potential first becomes zero (similarly with d_3). Thus d_1 and d_3 vary with the potentials applied to the "electron-gates", since these potentials are negative to reflect the electron-phalanx.

If a second electron, having an axial energy edV starts from the same point as the first electron it will still retain an energy edV upon completing the distance $d_1+d_2+d_3$. It was shown in section 4.2 that the difference in transit times Δt over the distance $d_1+d_2+d_3$ between the two electrons is given by

$$\Delta t = \sqrt{\frac{m}{2e}} \left\{ (2d_1+2d_3) \left(\frac{1}{\sqrt{V}} - \frac{1}{\sqrt{dV}+\sqrt{V+dV}}\right) + d_2 \left(\frac{1}{\sqrt{V}} - \frac{1}{\sqrt{V+dV}}\right) \right\} \quad .. \quad (1)$$

If a negative potential is applied to the second "electron-gate" the first electron returns towards the photocathode region after it has completed the distance $d_1+d_2+d_3$. The second electron, however, has to expend its extra energy edV and traverse an extra distance δd before it can start to return. Since the field gradient at the end of the delay section is V/d_3,

$$\frac{\delta d}{d_3} = \frac{dV}{V} \quad .. \quad .. \quad .. \quad (2)$$

Where V is the potential applied to the equipotential delay section. Now the extra time $\frac{1}{2}\Delta t$ required to traverse the extra distance is

given by

$$\tfrac{1}{2}\delta t = \frac{2\,\delta d}{v} \qquad .. \qquad .. \qquad (3)$$

Where $$v = \sqrt{\frac{2edV}{m}} \qquad .. \qquad .. \qquad (4)$$

Substituting eqns (4) and (2) in (3)

$$\tfrac{1}{2}\,\delta t = \frac{2d_3}{V}\sqrt{\frac{mdV}{2e}} \qquad .. \qquad (5)$$

Now this extra time difference occurs at both ends of the delay section. Therefore the mean extra time per transit of the second electron in the delay section is

$$\delta t_{mean} = \frac{2d_3+2d_1}{V}\sqrt{\frac{mdV}{2e}} \qquad .. \qquad (6)$$

Thus although the second electron completes the distance $d_1+d_2+d_3$ in a time ΔT before the first electron, it loses a time δt_{mean} before it can start the second transit of $d_1+d_2+d_3$. Let the net difference in transit times of the two electrons in the delay section be denoted by dt,

Where $$dt = \Delta t - \delta t_{mean} \qquad .. \qquad (7)$$

Fig. 59 shows the variation of dt, Δ t and δt_{mean} plotted against the potential applied to the equipotential delay section. The values of d_1, d_2 and d_3 in the calculation indicated above were taken as 5 cms, 50 cms and 3 cms respectively. It can be seen from fig. 59 that, under the conditions stated, δt_{mean} is approximately equal to

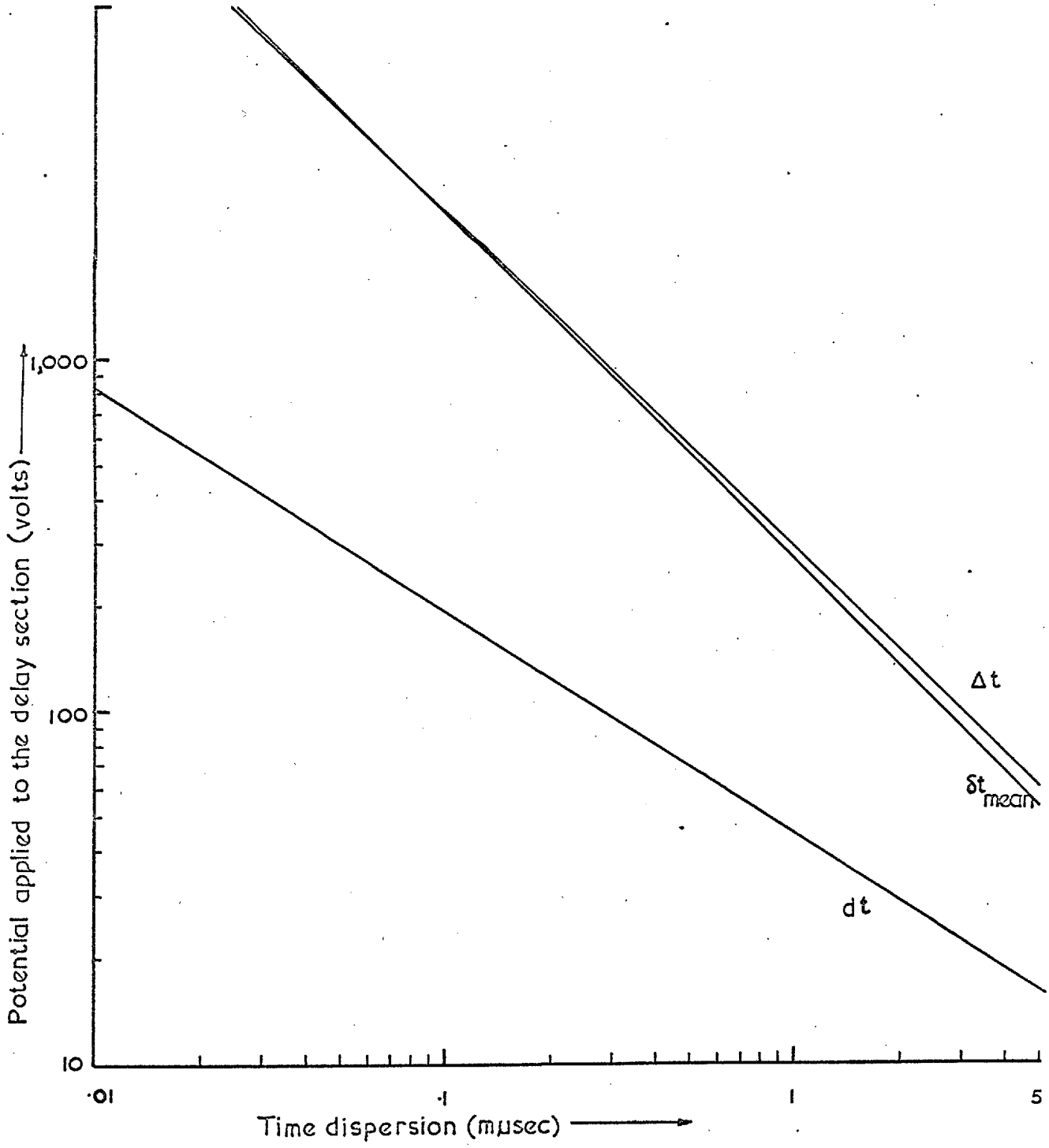


FIG.59 The variation of the time dispersions with the e.d.s. potential

Δt; i.e. dt is very small. Each frame is taken from the electron phalanx after it has completed an odd number of transits in the delay section. The time dispersion in a frame after 1, 3, 5, 7 transits is given by Δt, $\Delta t+2dt$, $\Delta t+4dt$, $\Delta t+6dt$., respectively. If a potential of 1,000 volts is applied to the delay-section, so that the electron phalanx returns to the second "electron-gate" every 70 μsec, successive frames would have a dispersion of 0·270, 0·284, 0·298, 0·312, 0·325 muse etc. In this case Δt = 0·27 μsec and dt = 0·007 μsec. It is seen that for a limited number of frames Δt makes the much greater contribution to the time dispersion.

It is possible to equate $\Delta t = \delta t_{mean}$, so that dt equals zero for a particular value of voltage, by adjusting the values of d_1, d_2 and d_3. The condition for $\Delta t = \delta t_{mean}$ is given by

$$\frac{d_2}{d_1+d_3} = 2\sqrt{1+dV/V}$$

from ~~the equating of the eqns~~ eqns 1 and 6. Since dV ≙ 1 volt and V ≙ 1,000 volts, dV ≪ V and

$$\frac{d_2}{d_1+d_3} \triangleq 2$$

Thus the time dispersions can be made to cancel out for all values of potential applied to the equipotential delay-section. In order to provide the same double transit time of 70 μsec as that of the previous geometrical design, d_1, d_2 and d_3 must have the values d_2 = 38 cms, d_1+d_3 = 19 cms. In this case Δt then has the value 0·759 μsec with

1,000 volts applied to the equipotential delay section. The value of dispersion is now a constant, for each frame taken, equal to the single transit dispersion of $\Delta t = 0{\cdot}759$ μsec, since the time dispersions over an even number of transits now cancel out. In the previous case the time dispersion was $\Delta t = 0{\cdot}270$ μsec for the first frame, increasin by 0·014 μsec for each successive frame. It can be seen that 36 frames would have to be taken before making dt equal to zero became advantageous.

If a limited number of frames are to be taken it is clearly more advantageous to reduce the value of Δt rather than to attempt to make dt zero. Since, as has been noted previously, the term containing $d_1 + d_3$ in eqn 1 makes the overwhelming contribution to Δt, Δt reduces almost linearly with a decrease in the value $d_1 + d_3$ It would be possible to reduce $d_1 + d_3$ to 1·5 cms, from its present value of 8 cms, i.e. Δt would be reduced to ± 50 psecs (V = 1,000 volts). It is clear that frame rates in the region 10^9 - 10^{10} frames/sec are physically possible.

The experimental arrangement, illustrated in fig. 49 was slightly modified in order to undertake the investigation of the temporal dispersion of an electron stream after prolonged storage in the delay section. The oscilloscope was replaced by a light source of constant intensity, which was focused onto the photocathode of the delay-tube. The output pulse of the first module (M2) of the gating circuit was applied to the first "electron-gate" which was biased to ± 8 volts

negative. The output impedance of the first module (M2) was mis-matched with its output cable, in order that the single output pulse appeared on the first "electron-gate" together with a reflected pulse. This double pulse was ≏ 15 volts in amplitude, with a separation of ≏ 12 mμsecs between the two peaks. The amplitude of the reverse bias on the first "electron-gate" was such that only the narrow top of each pulse allowed the electrons through the gate. It was estimated, by viewing the pulses on an oscilloscope, that the maximum width of the gating part of each pulse was ≏ 5 mμsec. The gating circuit delay was calibrated against the time base of the oscilloscope over a range 0 - 1,000 mμsec. A Texas 2N706A transistor was used as the output transistor of the second output module (M2). This output pulse, which had an amplitude of ≏ 16 volts, was applied to the second "electron-gate". A reverse bias of 10 volts negative was applied to the second "electron-gate", in order that the maximum width of the gating part of the output pulse was ≏ 4 mμsec.

The double voltage pulse, which was applied to the first "electron-gate", produced two short electron pulses in the delay section of the tube, which were"sampled"at the second "electron-gate" by the pulse of 4 mμsec duration. The amplified output of this "sampling" action appeared on the output phosphor of the delay-tube, where it was recorded as a current generated by the photomultiplier (P.M.). The current from the photomultiplier, due to the "sampling" action, is shown in fig. 60 plotted against the delay provided by the gating circuit. The potential

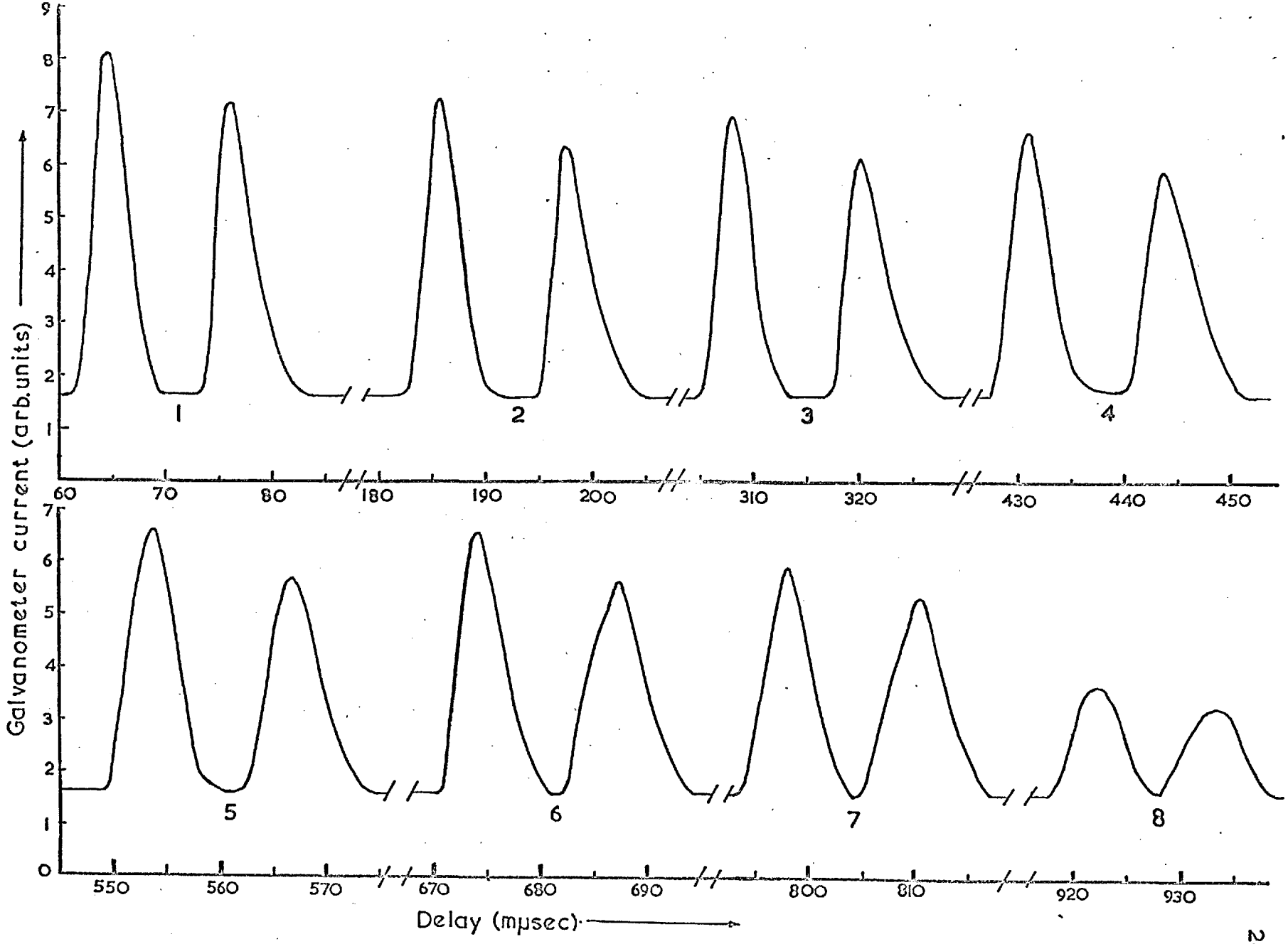


FIG. 60 The investigation of storage characteristics

applied to the equipotential delay section was 300 volts.

It can be seen from fig. 60 that the gating pulse on the second "electron-gate" "samples" through the two electron pulses after they have completed one, three, five, seven, nine, eleven, thirteen and fifteen transits in the delay section of the tube. It can also be seen that the pulses slightly broaden and decrease in amplitude as they complete an increasing number of transits in the delay section of the tube. The broadening over fourteen transits is approximately double that expected from the temporal dispersion due to the lev range in the emission energies of electrons from the photocathode. It can be seen from fig. 59 that, with a potential of 300 volts applied to the equipotential delay section, Δt has a value of $\triangleq$ 1 mμsec, which is common to all the "sampled" pulses. The accumulative effect of the net temporal dispersion dt over fourteen transits is $\triangleq$ .75 mμsec. Only this latter temporal dispersion contributes to the observable dispersion, which is $\triangleq$ 2 mμsec. The difference between the dispersion observed and that calculated may be attributed to a slight loss of axial energy which the majority of electrons suffer when making long-range elastic collisions with free molecules. It can be seen from fig. 15 that $\triangleq$ 25% of all the electrons originating from the photocathod will have had a collision when the electron stream has made fifteen transits in the delay section (the pressure in tube 13 was 8.10^{-6} mms. Hg. during this measurement). This rather poor vacuum accounts for the fact that the total number of electrons, indicated by the area under

the "sampled" pulse in fig. 60, fell to 80% of that of the first pulse after 14 extra transits. It must be noted that tube 13, with which these measurements was taken, later went soft. It is evident that the poor vacuum degrades the temporal storage characteristics of the delay section. It can be seen from fig. 11 that if a pressure of 1.10^{-7} mms.Hg. were maintained in the delay section, only ·5% of the initial photoelectron stream would suffer collisions during 21 transits in the delay section.

The sharp drop in the amplitude of the eighth "sampled" pulse was probable due to small inhomogeneities in the electric and magnetic fields producing successive deflections of the electron stream; so that after 17 transits the sampled pulse arrived partly off the small segment of the output phosphor viewed by the photomultiplier. The area of the output phosphor was restricted to a small segment in order to increase the signal to noise ratio of the output signal, since tube background was present over the whole output phosphor area.

9.3 The deterioration of the geometrical resolution of the electron image with prolonged temporal storage

It was important to investigate the deterioration of the geometrical resolution of the electron image as it was stored for an increasing number of transits in the delay section of the tube. The experimental arrangement used for this investigation was very similar to that shown in fig. 49. The test pattern described by Baum[156] was projected upon the primary photocathode of the delay-tube using the

Baum microprojector. The microprojector was operated with constant light intensity. The gating circuit was operated normally to apply a gating pulse of ≏ 10 mμsec duration to the first "electron-gate" followed, after a delay, by another pulse applied to the second "electron-gate". The short pulse applied to the first "electron-gate" allowed a short pulse of the electron image of the fan pattern into the delay section of the tube, where it was allowed through the second "electron-gate" after it had completed one, three, five...etc. transits in the delay section. The calibrated delay of the gating circuit was adjusted for optimum output resolution at each progressive coincidence of the calibrated delay with the arrival of the electron pulse at the copper mesh. The value of the visually measured image resolution, obtained at the output phosphor, plotted against the value of the calibrated delay at which each coincidence was made, is shown in fig.61. The gating pulses used were the square voltage pulses of 11 mμsec duration, described in section 6.4.2. A potential of ≏ 360 volts was applied to the equipotential delay section during the measurements.

Curve A in fig. 61 shows the maximum image resolution obtained with a potential of 10 volts positive applied to both the first and second "electron-gates"; i.e. the tube was ungated. The e.h.t. potentials on each stage of the cascade intensifier section of the delay tube were adjusted using a potentiometer control box, until the optimum resolution was obtained. The optimum resolution of 13·5 lp/mm was obtained at an overall potential of 30KV, which was maintained while

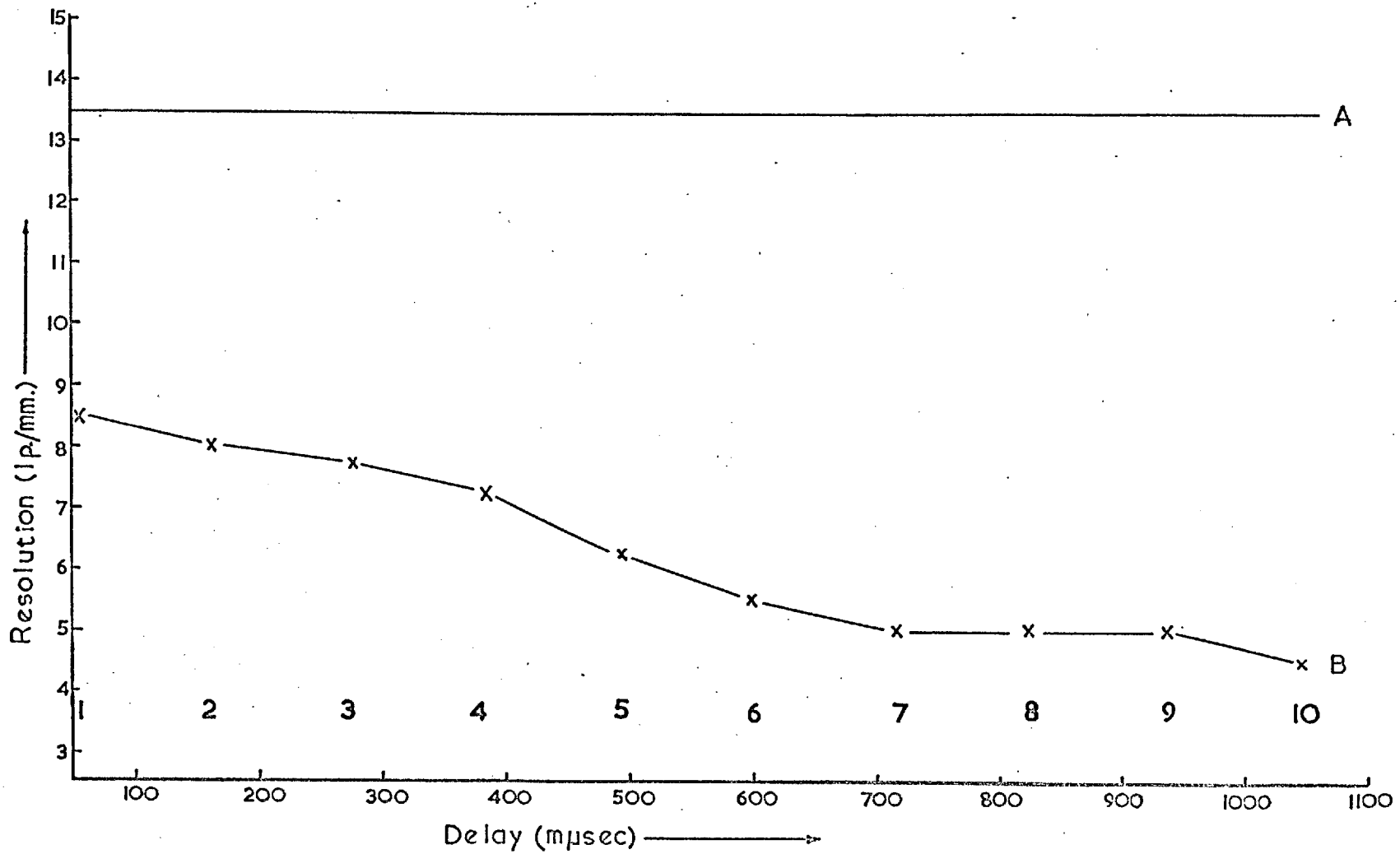


FIG. 61 The variation of image resolution with the number of transits it makes in the delay section

the tube was gated.

Curve B in fig. 61 shows the change of geometrical resolution over ten frames. It can be seen that the first frame has a resolution of 8•5 lp/mm, whereas the tenth frame has a resolution of 4•5 lp/mm.

9.4 The operation of the tube at high framing rates

If the delay-tube were operated as a framing camera in the mode described in section 9.1, a series of gating pulses of very short duration would be required. The circuitry required for the generation of such pulses has been described in section 6.4. It was established in section 8.2.7 that voltage gating pulses of 22 musec duration and 11 musec duration actually opened the second "electron-gate" for the periods of time corresponding to their duration. A slightly more refined technique was required to establish the actual shutter speed produced by the voltage pulse of 4•5 musec duration described in section 6.4.3. The experimental arrangement, illustrated in fig. 49, was modified in the following manner. A Gallium phosphide light-producing diode replaced the P.16 phosphor screen as the high speed light source. It was placed in close contact with the front window of the delay-tube, in order that as much of its light output as possible was transferred to the primary photocathode. The output pulse produced by the first output module (M.2) was used to switch on the light-diode, which broke-down and emitted light when reverse biased beyond $\pm$ 15 volts. This output pulse, which was produced by a Texas 2N706A transistor, had a maximum amplitude of 25 volts and a duration of 9 musec at an

amplitude of 15 volts. The sensitivity of calibrated delay, which was contained in modules M3 and M4, was increased by a factor of 6 by reducing the value of the timing condenser, shown in fig. 24b, from 120pF to 20pF. A 1·5KΩ resistor was placed between the timing condenser and the base of the following transistor to damp out any high frequency transients. The value of the delay, indicated on the digitized dial of the linear potentiometer, was then accurately calibrated against the 1 mμsec/cm scale of the N type sampling plug-in unit of the Tektronix 545A oscilloscope. The delayed output pulse, which was of 4·5 mμsec duration, generated in the second module 2 by the circuit described in section 6.4.3, was applied to the second "electron-gate". A steady bias of 1 volt positive was applied to the second "electron-gate" so that only that part of the output pulse above a 1 volt level allowed the electron stream through the gate, since it can be seen from fig. 56 that the second "electron-gate" just starts to allow through the electron stream at a potential of 2 volts positive. It can be seen from fig. 28 that the gating pulse has a duration of ≃4 mμsec at an amplitude of 1 volt.

The experiment was completed as described in the third method for measuring shutter speeds in section 8.2.7. Fig. 62 shows a graph of the current recorded on the Galvonometer plotted against the value of the calibrated delay. The potential applied to the equipotential delay section during this measurement was 360 volts.

It can be seen from fig. 62 that the rise time of the graph is

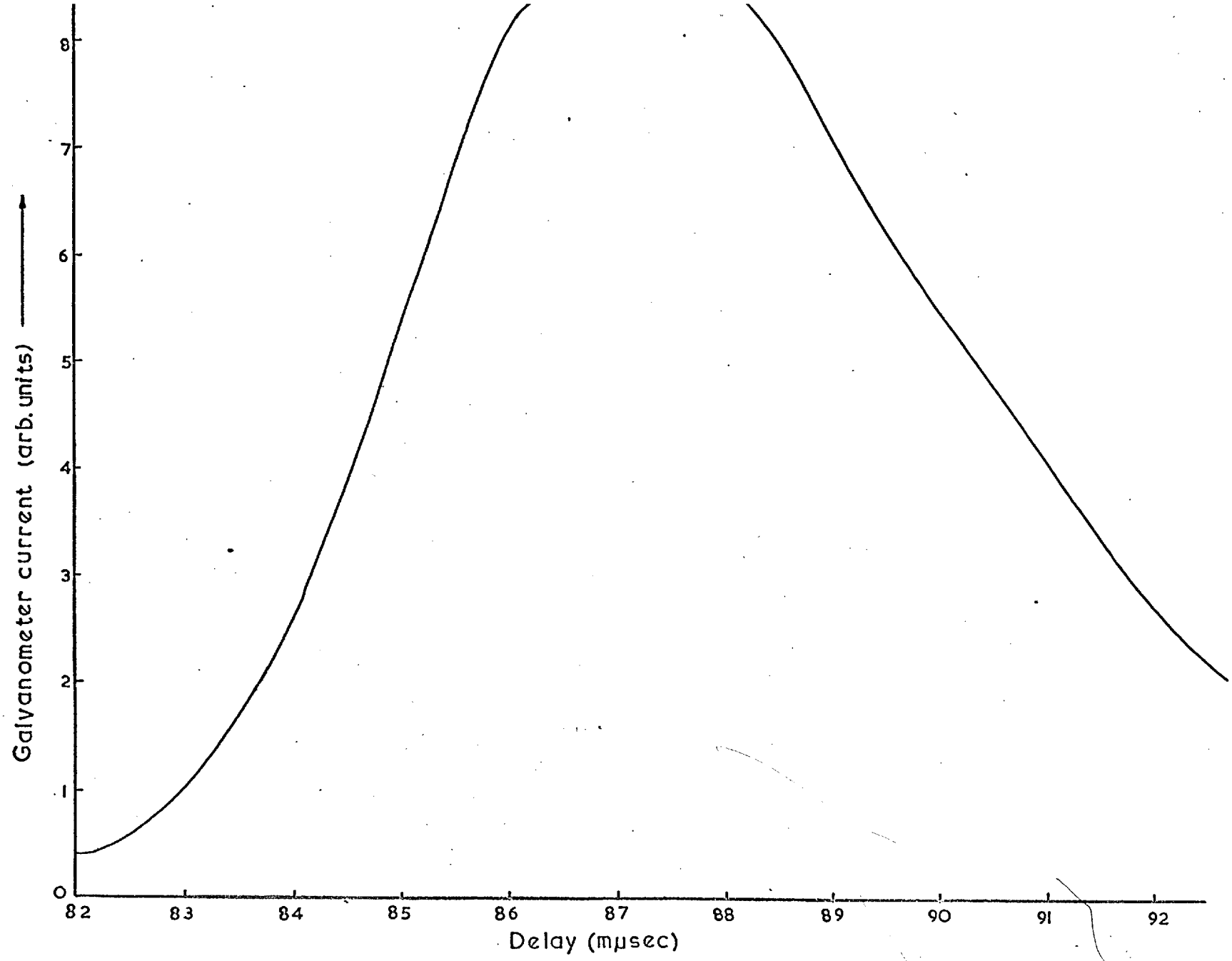


FIG.62 The measurement of shutter speed

4•4 μsec ± 0•2 μsec, which corresponds to the time during which the second "electron-gate" was gated open. This time equals almost exactly the duration of the voltage gating pulse. The total length of the recorded trace is ≙12•7 μsec, so that the actual duration of the light pulse from the diode is 8•3 μsec. It appears from the latter result that the duration of the light pulse from the Gallium phosphide diode corresponds almost exactly to the time during which the voltage pulse, which gated it on, was in excess of the 15 volts breakdown point of the diode.

The calculated transit time spread, Δt, (with 360 volts applied to the equipotential delay section) is given from fig. 59 as 0•8 μsec. It is seen from the experimentally determined shutter speed of 4•4 μsec, and the voltage pulse duration of 4 μsec, that the experimental value of Δt at 360 volts is ≙ 0•4 μsec ± 0•2 μsec.

Fig. 63 illustrates the experimental arrangement used in the verification of frame rates. The tube was operated by a gating circuit which comprised one M1 module, one M2 module and six M5 modules. These modules are fully described in section 6.3. A photograph of the circuit, housed in a Lektrokit chassis, is shown in fig. 22. The master oscillator contained in M1 was operated at a frequency of 2 Kc/S. The collector excursion of one of the transistors of the multivibrator was tapped, using a Tektronix probe, to provide an external trigger for the oscilloscope. As had been noted in section 8.2.7 the delay between the application of the external trigger to the oscilloscop

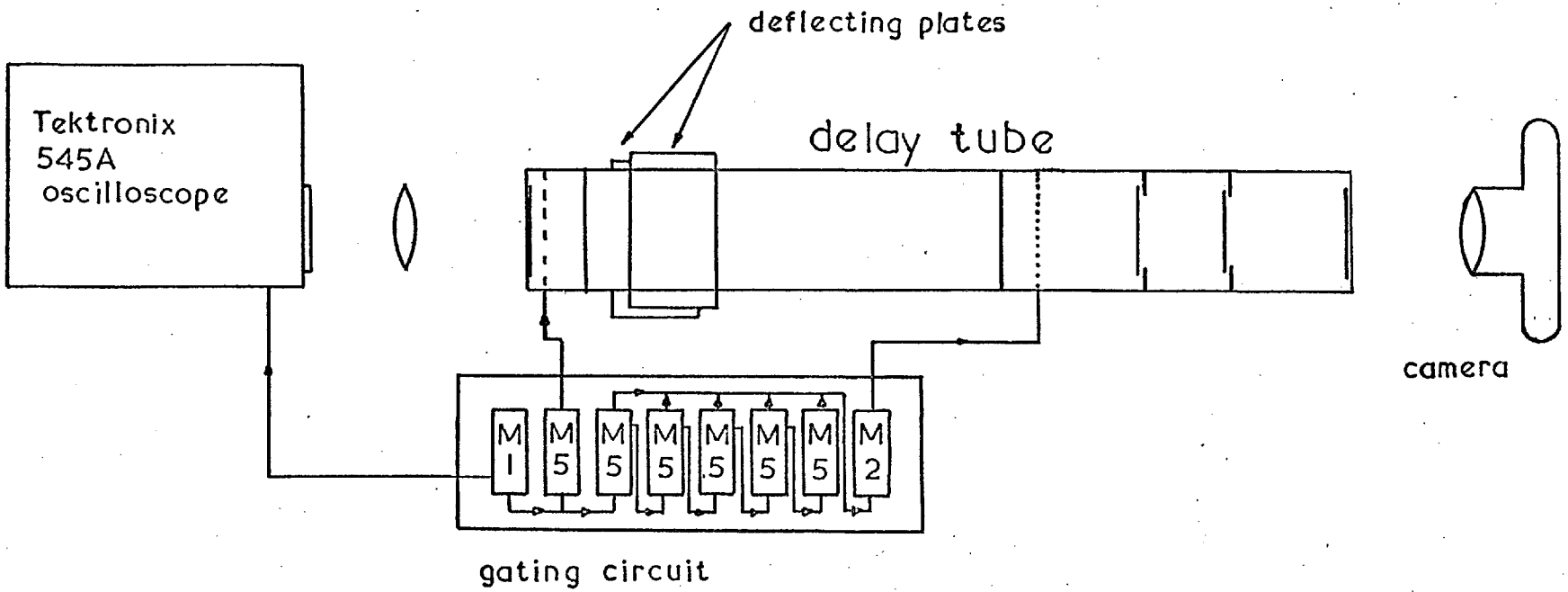


FIG. 63 The experimental arrangement used to determine the frame-rate

and the appearance of the trace in the centre of the oscilloscope's screen was 250 mμsec. Therefore the delay in the first M5 module, which was triggered from M1, was set to ≏ 220 mμsec in order that the output pulse of 60 mμsec duration opened the first "electron-gate" for the period during which the oscilloscope's trace was in the centre of the graticule. All the other M5 modules provided a variable delay between an input trigger pulse and two separate output pulses. The second M5 module was triggered from M1 and one of its two output pulses triggered the next M5 module. This successive triggering sequence applied to all the rest of the M5 modules. Those output pulses from the five M5 modules, not used as triggers for following M5 modules, were fed into a matching resistor network through 75Ω impedance sub-miniature cables. This network consists of five 56Ω resistances, each one terminating a 75Ω input cable to a common point. The output of the network is taken from this common point, through another 56Ω resistor, by a 75Ω impedance cable, and is the trigger line for the output module M2. Thus the output transistor in module M2 is triggered by a train of pulses which has an interpulse delay equal to double the transit time of an electron in the delay section of the tube. This almost perfect matching of the trigger lines to M2 prevents the multiple reflections of pulses in the lines which would cause the spurious firing of many transistors in the gating circuit. The loss in amplitude of the trigger pulses, caused by the matching, is not important since the resultant train of pulses has adequate amplitude for firing M2. The

gating pulses from M2 are fed onto the second "electron-gate" through a single matched 75Ω impedence cable.

The delay tube was operated with a potential of 270 volts applied to the equipotential delay section, in a field of .05 Webers/meters^2. The deflecting plates were operated with a potential of 600 volts between them. A 60 μsec portion of the trace of the oscilloscope was allowed into the delay section of the delay-tube where it was divided into a series of frames by operating the delay-tube in the "framing-modes" described in section 9.1. The deflection provided by the plates was perpendicular to the direction of the trace line. The various delay required in the gating circuit were adjusted to the correct operating values by monitoring the two output lines using a double beam oscilloscope. Fig. 64 shows some photographs of the output phosphor taken with the tube operating in a framing mode. The sweep speed of the oscilloscope in all the photographs was 20 μsec/cm division. Figs. 64a and 64b show the same five traces; 64a without the oscilloscope's graticule superimposed. It is seen from 64b that the heads of the five traces occured within a 60 μsec period, i.e. the tube frame rate was just under 10^8 frames/sec. The sharp head of each trace corresponds to the turn-off point of each framing pulse. The long tail of each trace, which obscurs the turn-on points of the gating pulse is due to the phosphor decay.

Figs. 64c and 64d show the same five traces, one with and one without the oscilloscope's graticule superimposed. It can be seen from

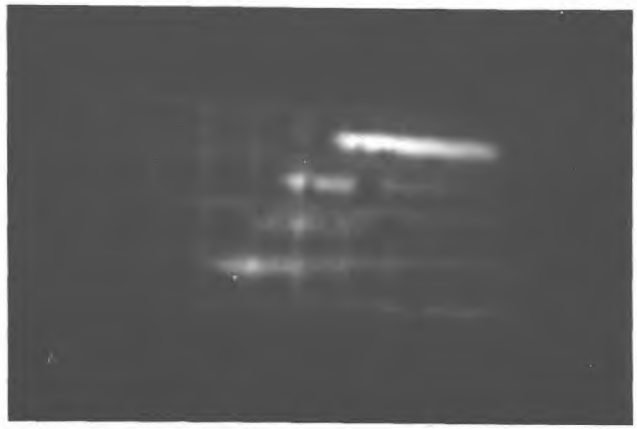


FIG. 64A



FIG. 64B



FIG. 64C

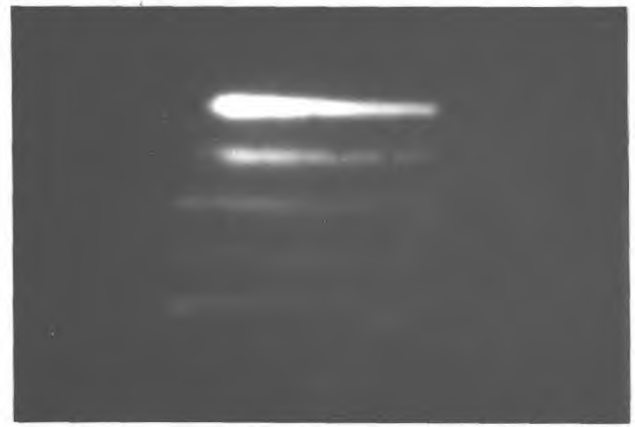


FIG. 64D

the latter figures that the five turn-off heads lie within a 20 mμsec period, i.e. the frame rate is 2.10^8 frames/sec. It must be noted that each gating pulse had a duration of 10 mμsec. Therefore, there was a considerable overlap of the total period during which the second "electron-gate" was open, compared with the duration of the electron-phalanx actually "framed".

This overlap was due to the fact that the gate was open for incident parts of the electron-phalanx, which had been allowed through the gate on previous transits in the delay-section.

A fan pattern was focused upon the primary photocathode, and the delay-tube operated at a rate of 2.10^8 frames/sec using the experimental arrangement shown in fig. 63. Fig. 65 shows two photographs taken of the output phosphor screen of the delay-tube, operated as a framing camera. Fig. 65a shows the first and the fourth frames of the five frame sequence; and 65b shows the full five frames taken in 25 mμsec. Each frame covers a 2 x 2 mms square area on the output phosphor. The geometrical resolution at the bottom of each fan pattern is 8 lp/mm.

9.5 The conclusions from the performance of the delay tube as a framing camera

It was shown that it is theoretically possible to operate the delay-tube at frame rates of 10^9 frames/sec. It was shown that over ten frames the intensity and geometrical resolution decrease to approximately half their initial values. It was suggested that the cause of this degradation was the rather poor vacuum in the tube. The

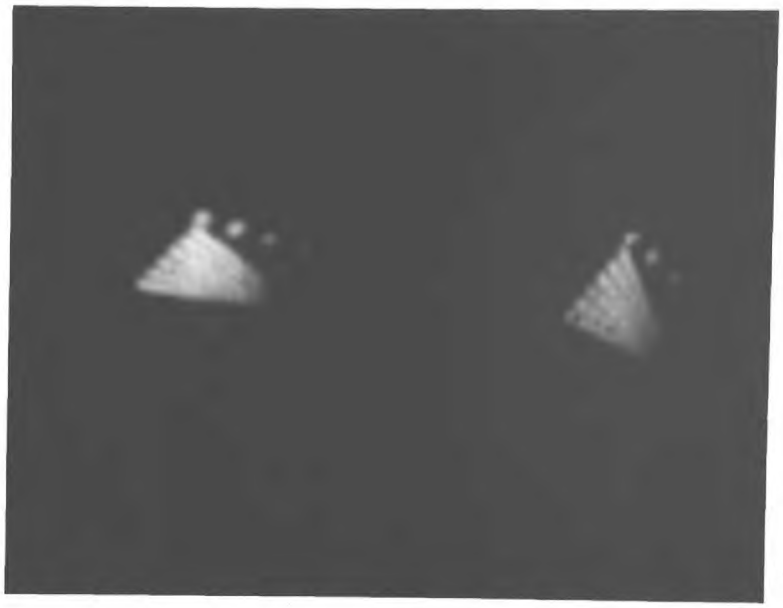


FIG. 65A

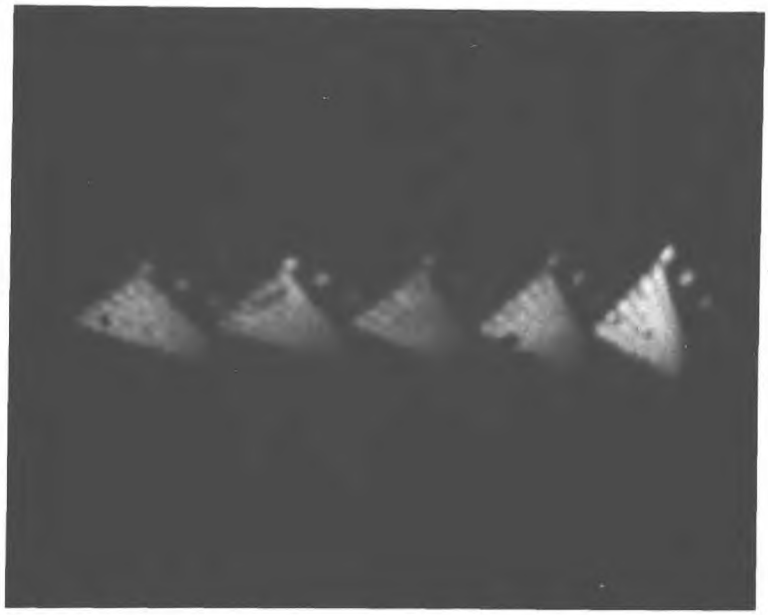


FIG. 65 B

absolute value of the resolution was between 5-10 lp/mm over the ten frames, which could probably have been increased by improving the homogeneity of the magnetic field and improving the electrostatic field of the tube by more carefully aligning the internal electrodes.

High framing rates using the electron transit time storage may be achieved in two ways, both of which depend upon the pulse shape produced by the gating circuit. The first method is to use a series of extremely short square framing pulses which gate consecutive parts of the electron phalanx through the second "electron-gate". There can be a small "dead time" between each frame, so that the trailing edges of the voltage puls producing a given frame have no influence upon the preceeding and succeeding frames. This influence, in the form of small perturbations of the electrostatic field, could reduce the geometrical resolution. It has been demonstrated, in section 6.4, that square gating pulses down to 4·5 μsec duration can be generated, using only one output transistor. It is considered quite possible to generate pulses of < 1 μsec duration using two transistors. The first transistor would produce the fast rise of the pulse; the second transistor producing the fast fall of the pulse. The second method for producing high frame-rate is to use a series of quite long framing pulses which possess an extremely short trailing edge. The frame-rate does not, in this case, depend upon the duration of the pulse. It is limited only by the sharpness of the trailing edge. The front of the electron-phalanx is "sliced-off" by the first gating pulse, and when it returns to the

second "electron-gate" the next portion of the electron-phalanx is "sliced-off", by the second gating pulse. This second gating pulse overlaps in time the part of the electron-phalanx previously "sliced-off" by the first, but makes a further small advance into a fresh part of the electron-phalanx. There is no "dead-time" between the frames in this case. Since the trailing edge of this type of gating pulse can be $\ll$ 1 mμsec, very high frame-rates are feasable. The overlapping of the trailing edges of the pulse into the period of the next frame may reduce the geometrical resolution. It can be seen from fig. 56 that when the second "electron-gate" is turned fully open, the equipotential delay section collects $\simeq$3% of the photocurrent. Since this current is unlikely to have been collected from the electron stream in a single transit of the delay section, it appears that the second "electron-gate" reflects a very small fraction of the electron-phalanx even when pulsed fully open. This implies that a small fraction of the electron-phalanx is left after it has been "sliced", which could appear in a later frame. This is seen to be extremely small, and could probably be greatly reduced by the use of a mesh of lower shadow ratio than that of the copper mesh employed for the second "electron-gate".

The various time delays in the gating circuitry, described in chapter six, produced firing "jitters" in the transistors of within 10^{-10} secs. This circuit "jitter" is adequate for the operation of the tube at 10^9 frames/sec. There was however, a noticeable drift in the delay times of the delay elements of the circuit, produced by a change

of temperature. This drift can be reduced to negligible proportions by the careful choice of semiconductor circuit elements and the use of circuits components having positive and negative temperature coefficients which cancel out.

There is a limited number of picture-points which can be transmitted through the tube. This number depends upon the geometrical resolution and the width of the information channel in the tube. When the delay-tube is operated as a framing camera the maximum number of picture-points per frame is equal to the total number of picture-points divided by the number of frames. The tube shown in fig. 66 is intended to utilize the maximum number of picture-points of the information channel of the tube in each frame. The whole area of the primary photocathode (1) is used to accept the input signal. The electron-phalanx is trapped in the equipotential delay section (3), using the two meshes (2 & 4) and is framed in exactly the same manner that has been described in section 9.2. The short pulses of electrons, corresponding to each frame, are allowed through the second "electron-gate" (4) and are amplified in the T.S.E. image intensifier (5) section of the tube (the extremely fast T.S.E. intensifier is necessary in comparison with the slow cascade imag intensifier, since the latter would retain a memory of the early frames which would appear in all the later frames). After the electron image has been amplified it is accelerated from the last multiplying dynode and brought out of the magnetic field (produced by the coils (9)) into the last section of the tube which is focused entirely electrostatically

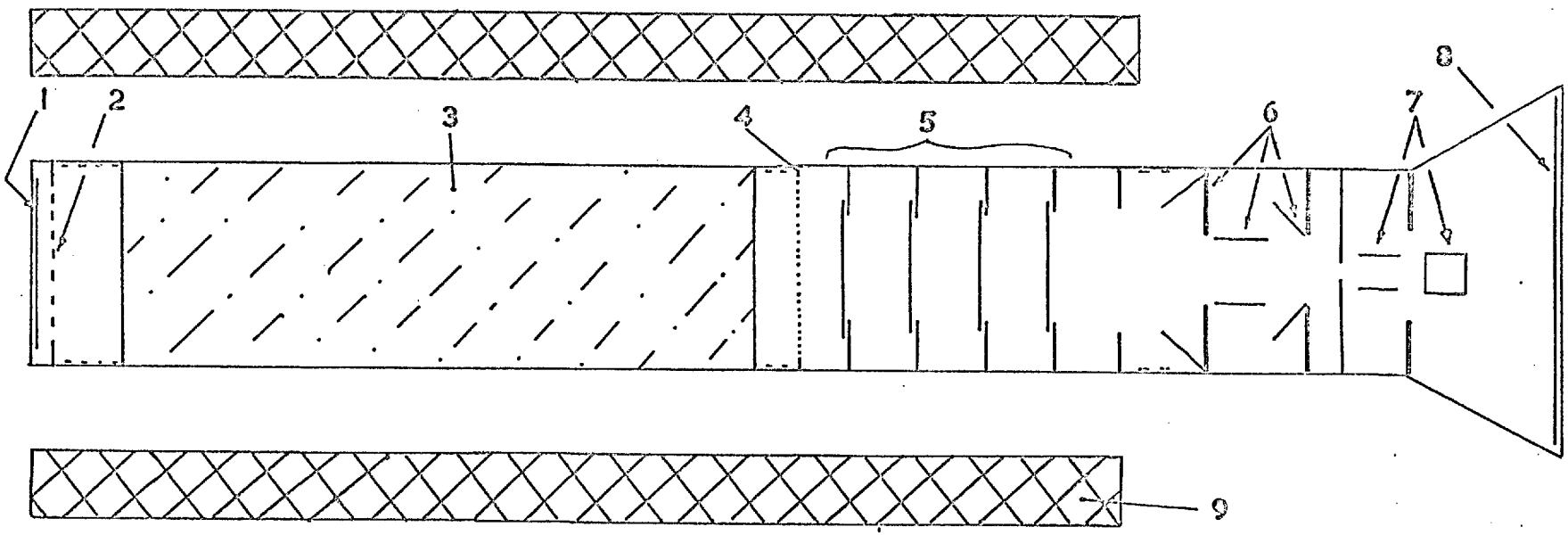


FIG. 66 The design for a framing-camera

It is hoped to be able to decelerate the electron image from the 15KV potential required to free it from the influence of the magnetic field, to an image cross-over point at 2KV, using the cone shaped electrodes (6). This cross-over point is situated at the centre of the two pairs of deflection plates (7). These deflection plates can be pulsed to direct each frame of the electron stream to a different part of the large output phosphor screen (8). It is hoped to so design the electrostatically focusing section, that the geometrical resolution obtained at the last dynode of the T.S.E. intensifier is maintained on the output phosphor screen. Since the amplitude of the voltage pulse to the deflection plates, required to produce sufficient deflection, depends upon the speed of the electron beam, the reduction in the speed of the electron beam by the cone shaped electrodes makes the use of only moderately large deflection voltages possible. This reduction in the voltage amplitude requirement reduces the complexity of the electronic circuitry required quite considerably.

All the frames appear on separate areas of the output phosphor, where they are easily recorded using a photographic camera at normal shutter speeds. Since the light from the output phosphor possesses a long tail decay component, any reciprocity failure in the photographic emulsion due to very short exposures, is considerably reduced. Work is in progress at Imperial College on this further development of the delay-tube.

Acknowledgements

The author is deeply indebted to Professor J.D. McGee for his interest and guidance in the work of this thesis.

The author would like to acknowledge, with much gratitude, the many stimulating discussions and the experimental assistance afforded him by Mr. A.D. Berg in the work covered in chapters 6, 8 and 9.

The author would like to thank Mr. G. Hirsch for designing and constructing the original electronic gating circuit, upon which all subsequent circuits were based.

The author would also like to thank the workshop staff, who supplied the metal electrodes, and the glassblowers, especially Mr. W. Goodway, for their assistance in the manufacture of the tube.

This research was supported from funds made available by the Paul Instrument Fund of the Royal Society.

References

(1) Mandel, L. Proc. Phys. Soc. (London), 72, 1037, 1958.

(2) Zweig, H.J. J.O.S.A. 51, 310, 1961.

(3) Jones, R.C. J.O.S.A. 50, 1166, 1960.

(4) Rose, A. J. Soc. Motion Picture Engrs. 47, 273, 1946.

(5) Rose, A. J.O.S.A. 38, 196, 1948.

(6) Rose, A. Advances in Electronics, 1, 131, 1948.

(7) Fellgett, P. Astronomical Optics, North Holland Publishing Co., p.225, 1956.

(8) Fellgett, P. Vistas in Astronomy, Pergamon Press, Vol. 1, p.479, 1955.

(9) Jones, R.C. Photo Sci. & Eng., 2, 191, 1958.

(10) Rose, A. Advances in Biol. & Med. Physics, 5, 211, 1957.

(11) Jones, R.C. J. Wash Acad. Sci., 47, 100, 1957.

(12) Jones, R.C. J.O.S.A. 49, 645, 1959.

(13) Fellgett, P. The present and the future of the telescope of moderate size, Univ. Pennsylvania Press, p.51, 1956.

(14) Fellgett, P. Monthly Notices, R.A.S. 118, 224, 1958.

(15) Jones, R.C. Photo Sci. & Eng., 2, 57, 1958.

(16) Sommer, A. Rev. Sci. Insts., 26, 725, 1955.

(17) Engstrom, R.W. Stoudenheimer, R.G., Palmer, H.L. and Bly, D.A. I.R.E. Trans. Nucl. Sci. N.S.5, 120, 1958.

(18) McGee, J.D. Astronomical Optics, North Holland Publishing Co., p.205, 1956.

(19) Jones, R.C. Advances in Electronics, 11, 87, 1959.

(20) Rose, A., Weiner, P.K. and Law, H.B. Proc. I.R.E. 34, 424, 1946.

(21) Morton, G.A. Trans. I.A.U., 9, 676, 1955.

(22) Morton, G.A. and Ruedy, J.E. Advances in Electronics, 12, 183, 1960.

(23) Reynolds, G.T. I.R.E. Trans. Nucl. Sci. N.S.7, 115, 1960.

(24) Mandel, L. J. Sci. Inst., 32, 405, 1955.

(25) McGee, J.D., Airey, R.W. and Wheeler, B.E. Advances in Electronics, 16, 61, 1962.

(26) Krassovsky, V.I. Trans. I.A.U. 9, 693, 1955.

(27) Zacharov, B. Ph.D. Thesis, University of London, 1960.

(28) Philips Gloeilampenfabrieken, Brit. Pat. No. 326,200 (5.11.28).

(29) Echart, F. Ann. Phys., 14, 98, 1954.

(30) Zavoiskii, E.K. Butslov, M.M. and Smolkin, G.E. Doklady Acad. Nauk. S.S.S.R. 100, 241, 1955.

(31) Morton, G.A. Trans. I.A.U. 9, 679, 1955.

(32) Stoudenheimer, R.G. Advances in Electronics 12, 41, 1960.

(33) Davis, G.P. Advances in Electronics, 16, 119, 1962.

(34) Gildemeister, O. and Giese, R. Advances in Electronics, 16, 113, 1962.

(35) Woodhead, A.W. Taylor, D.G. and Shagen, P. Advances in Electronics 16, 105, 1962.

(36) Catchpole, C.E. Private communication.

(37) Orvin, L.T. Brit. Pat. No. 445, 156 (1934).

(38) Wachtel, M.M., Doughty, D.D. and Anderson, A.E. Advances in Electronics 12, 59, 1960.

(39) Wachtel, M.M., Doughty, D.D. Goetze, G.W., Anderson, A.E. and Sternglass, E.J. Rev. Sci. Inst. 31, 576, 1960.

(40) Wilcock, W.L. Emberson, D.L. and Weekley, B. I.R.E. Trans. Nucl. Sci. N.S.7., 126, 1960.

(41) Emberson, D.L., Todkill, A. and Wilcock, W.L. Advances in Electronics 16, 127, 1962.

(42) Slark, N.A, and Woolgar, A.J. Advances in Electronics, 16, 141, 1962.

(43) Sephton, R. Private communication.

(44) McGee, J.D. Private communication.

(45) Goetze, G.W. Advances in Electronics 16, 145, 1962.

(46) McGee, J.D. Brit. Pat. No. 790, 416 (5.6.53.)

(47) Burns, J. and Neumann, M.J. Advances in Electronics 12, 87, 1960.

(48) McGee, J.D., Flinn, E.H. and Evans, H.D. Advances in Electronics 12, 156, 1960.

(49) Flinn, E.A. Advances in Electronics 16, 155, 1962.

(50) Lallemand, A. C.R. Acad. Sci. (Paris), 203, 243, 1936.

(51) Lallemand, A., Duchesne, M. and Wlerick, G. Advances in Electronics, 12, 5, 1960.

(52) Lallemand, A. Advances in Electronics 16, 1, 1962.

(53) Duchesne, M. Advances in Electronics 16, 27, 1962.

(54) Lallemand, A., Duchesne, M., Goldzahl, L., Duflo, J. and Baraigs, J. Comptes Rendus 248, 2191, 1959.

(55) Hiltner, W.A. The present and the future of the telescope of moderate size, Univ. of Pennsylvania Press, p.11, 1956.

(56) Hiltner, W.A. and Pesch, P. Advances in Electronics, 12, 17, 1960.

(57) Hiltner, W.A. and Niklas, W.F. Advances in Electronics, 16, 37, 1962.

(58) Hall, J.S., Ford, W.K. and Baum, W.A. Advances in Electronics, 12, 21, 1960.

(59) McGee, J.D. and Wheeler, B.E. Journ. Phot. Sci. 9, 106, 1961.

(60) McGee, J.D. and Wheeler, B.E. Advances in Electronics, 16, 47, 1962.

(61) Khogali, A. Private communication.

(62) Mandel, L. Brit. Journ. Appl. Phys., 10, 233, 1959.

(63) Calculated from data supplied by R.W. Airey.

(64) Sauter, F. Z. Naturforsche 4, 682, 1949.

(65) Baicker, J.A. Proc. I.R.E. Scintillation counter symposium, Washington 1959, p.14.

(66) Allen, J.S. Rev. Sci. Inst. 18, 739, 1947.

(67) Zeigler, M. Physica 3, 307, 1936.

(68) Lombard, F.J. and Martin, F. Rev. Sci. Inst. 32, 200, 1961.

(69) Flinn, E.A. Ph.D. Thesis, University of London, 1963, p.54.

(70) Wheeler, B.E. Ph.D. Thesis, University of London, 1962.

(71) Fleisher, V.G. Probory i. Technika Esperimenta 2, 115, 1962.

(72) Walters, J.R., Reynolds, G.T., Searl, D.B. and Zdanis, R.A. I.R.E. Trans. Nucl. Sci. N.S. 9, 239, 1962.

(73) Reynolds, G.T. and Walters, J.R. Nuclear Insts. & Methods, 20, 226, 1963

(74) Binnie, D.M., Jane, M.R., Newth, J.A., Potter, D.C. and Walters, J.R. Nuclear Insts. & Methods, 20, 221, 1963.

(75) Sephton, R.A. and Davison, M. Private communication.

(76) Todkill, A. Private communication.

(77) McGee, J.D. Electronics and their application to Industry, p.137, 1947.

(78) Krizek, V. and Vand, V. Electronic Eng., 18, 316, 1946.

(79) Morton, G.A. and Flory, L.E. Electronics, 19, 112, 1946.

(80) Courtney-Pratt, J.S. Research (London), 2, 287, 1949.

(81) Courtney-Pratt, J.S. Photo. Journ. B92, 137, 1952.

(82) Markstein, G.H. Phys. Rev. 74, 1230, 1948.

(83) Hogan, A.W. Proc. I.R.E. 39, 268, 1951.

(84) Saxe, R.F. and Prime, H.A. Proc. I.E. 96II, 662, 1949.

(85) Prime, H.A. and Turnock, R.C. Proc. I.E. 97II, 793, 1950.

(86) Devaux, P. Proc. 3rd. Inst. Cong. High Speed Phot., (1956), p.130.

(87) Jenkins, J.A. and Chippendale, R.A. J. Brit. I.R.E. 11, 505, 1951.

(88) Chippendale, R.A. Photo. J. B92, 149, 1952.

(89) Richards, M.S. Proc. I.E.E. 99, Pt.IIIA, 729, 1952.

(90) Gibson, F.C., Bowser, M.L. Rameley, C.W. and Scott, F.H. Rev. Sci. Inst., 25, 173, 1954.

(91) Saxe, R.F. and Chippendale, R.A. Brit. J. Appl. Phys. 6, 336, 1955.

(92) Saxe, R.F. Proc. 3rd Int. Cong. High Speed Photo. (1956), p.126.

(93) Grover, F.H. Journ. Sci. Inst. 38, 86, 1961.

(94) Curzon, F.L. Rev. Sci. Inst. 32, 1146, 1961.

(95) King, R.W. and Hett, J.H. J.S.M.P.T. 70, 270, 1961.

(96) Linden, B.R. and Snell, P.A. Proc. I.R.E. 45, 513, 1957.

(97) Stondenheimer, R.G. and Moir, J.C. R.C.A. Revue 18, 322, 1957.

(98) Butslov, M.M. Uspekhi Nauchnoi Fotografii 6, 76, 1959.

(99) Butslov, M.M., Zavoiskii, E.K., Plakhov, A.G., Smolkin, S.D. and Panchenko, S.D. Proc. 4th Int. Cong. High Speed Photo. p.230.

(100) Komelkov, V.S., Nesterikhin, Y.E., and Pergament, M.I. Proc. 5th Int. Cong. H.S.P. p.118.

(101) Nesterikhim, Y.E. and Komelkov, V.S. Proc. 4th Inst. Cong. H.S.P. p.243

(102) Zavoiskii, E.K. and Fanchenko, S.D. Doklady Acad. Nauk. 100, (4), 661, 1955.

(103) Zavoiskii, E.K. and Fanchenko, S.D. Doklady Acad. Nauk. 108 (2), 218, 1956.

(104) Mandel, L. J.S.M.P.E. 70, 716, 1961.

(105) Zavoiskii, E.K., Butslov, M.M. Plakhov, A.G. and Smolkin, G.E. Atomnaya Energiya 1 (4), 34, 1956.

(106) Simonov, V.A. and Kutukov 5th Int. Cong. on H.S.P.

(107) Huston, A.E. and Walters, F. Advances in Electronics, 16, 249, 1962.

(108) Chippendale, R.A. and Folkes, J.R. J.S.M.P.E. 70, 527, 1961.

(109) Emberson, D.L. I.R.E. Trans. N.S. 9 (3), 107, 1962.

(110) Saxe, R.F. Brit. J. Appl. Phys., 7, 336, 1956.

(111) Demidov, B.A., Skochkov, Yu.F. and Fanchenko, S.D. Zhurnal Eksp. i Teoreticheskoi Fiziki, 40, 385, 1961.

(112) Zavoiskii, E.K. and Smolkin, G.E. Atomnaya Energiya, 1 (4), 46, 1956.

(113) Babkin, M.V. Plakhov, A.G., Skachkov, Yu.F. and Shapkin, V.V. Atomnaya Energiya, 1 (4), 38, 1956.

(114) Malyshev, G.M., Razdobarin, G.T. and Sokolva, L.V. Doklady Acad. Nauk (S.S.S.R.), 145, 768, 1962.

(115) Akhmatov et. al. Zhurn. Eksp. i Teor. Fiz., 39, 536, 1960.

(116) Butslov, M.M., Plakhov, A.G. and Shapkin, Optika i Spektroskopiya, 12, 419, 1962.

(117) Perl, M.L. and Jones, L.W. Advances in Electronics, 12, 153, 1960.

(118) Perl, M.L. and Jones, L.W. Nucleonics, 18, 92, 1960.

(119) Reynolds, G.T. and Condon, P.E. Rev. Sci. Inst., 28, 1098, 1957.

(120) Potter, R.J. and Hopkins, R.E. I.R.E. Trans. Nucl. Sci., N.S.7., 150, 1960.

(121) Reynolds, G.T. Nucleonics, 16, 6, 1958.

(122) Condon, P.E. Advances in Electronics, 12, 123, 1958.

(123) Waters, J.R., Reynolds, G.T., Scarl, D.B. and Zdanis, R.A., I.R.E. Trans. Nucl. Sci. N.S.9, 239, 1962.

(124) Demidov, B.A. and Fanchenko, S.D., Zhurn. Eksp. i. Teor. Fizikii, 39, 64, 1960.

(125) Butslov, M.M., Medvedev, M.N. and Sheshundov, M.V. Nuclear Inst. & Methods, 20, 242, 1963.

(126) Reynolds, G.T., Giaccconi, R. and Scarl, D. Rev. Sci. Inst., 30, 497, 1959.

(127) Reynolds, G.T., Scarl, D.B., Swanson, R.A., Waters, J.R. and Zdanis, R.A. Advances in Electronics, 16, 487, 1962.

(128) Perl, M.L. and Jones, L.W. Phys. Rev. Letters, 2, 116, 1959.

(129) Perl, M.L. and Jones, L.W. Advances in Electronics, 12, 153, 1960.

(130) Perl, M.L. and Jones, L.W. Advances in Electronics, 16, 513, 1962.

(131) Jones, L.W., Lai, K., Newsome, R, and Perl, M.L., I.R.E. Trans. Nucl. Sci. N.S.7, 145, 1960.

(132) Hill, D.A., Caldwell, D.O. and Schluter, R.A., Advances in Electronics, 16, 475, 1962.

(133) Lande, K, Mann, A.K., Schachter, M.M., Skyrme, D.M. and Uto, H. Rev. Sci. Insts., 30, 496, 1959.

(134) Goetze, G. and Kanter, H. Nuclear Inst. & Methods, 10, 224, 1961.

(135) Anderson, A.E., Goetze, G. and Kanter, H. Proc. 5th Inst. Cong. on H.S.P. (1962), p.95.

(136) Gildermeister, O. and Geiss, R. Nuclear Inst. & Methods, 20, 233, 1963.

(137) Roberts, A. Nuclear Insts. & Methods, 9, 55, 1960.

(138) Binnie, D.M., Jane, M., Newth, J.A., Potter, D.C. and Walters, J., Advances in Electronics, 16, 501, 1962.

(139) Poultney, S.K. and Waters, J.R. I.R.E. Trans. Nucl. Sci., N.S.9, 243, 1962.

(140) Poultney, S.K., Reynolds, G.T. and Waters, J.R., Rev. Sci. Inst., 33, 57A, 1962.

(141) Butslov, M.M., Medvedev, M.N., Chuvilo, I.V. and Sheshundov, M.V., Nuclear Insts. & Methods, 20, 263, 1963.

(142) Binnie, D.M. et. al. Nuclear Insts. & Methods, 22, 81, 1963.

(143) Jones, L.W. and Perl, M.L., Nuclear Insts. & Methods, 10, 348, 1961.

(144) Waters, J.R., Reynolds, G.T., Scarl, D.B. and Zdanis, R.A., Nuclear Insts. & Methods, 17, 44, 1962.

(145) McGee, J.D. Proc. Symposium on Nuclear Instruments (Harwell, 1961), Heywood, p.1, 1962.

(146) Fischer, J. and Zorn, G.T., I.R.E. Trans. Nucl. Sci. N.S.9, 261, 1962.

(147) Mandel, L. Private communication.

(148) Miyake, K. Rev. Sci. Inst., 32, 929, 1961.

(149) Davis, E.J. J. Sci. Inst., 35, 308, 1958.

(150) Ulig, H.H. Trans. Electrochem. Soc., 78, 265, 1940.

(151) Shenkel, H. and Statz, H. Proc. National Electronics Cong. 10, 614, 195

(152) Ebers, J.J. and Miller, S.L., Bell System Tech. Journ. 34, 883, 1955.

(153) Fullwood, R. Rev. Sci. Inst., 31, 1186, 1960.

(154) Henebry, W.M. Rev. Sci. Inst., 32, 1198, 1961.

(155) Bowes, R.C. Proc. I.E., B106, Suppl.16, 793, 1959.

(156) Baum, W.A. Advances in Electronics, 16, 391, 1962.

(157) Barlow, F. Private communication.

(158) Khan, A.A. Ph.D. Thesis, University of London, 1961.

(159) Fano, U. Phys. Rev., 70, 44, 1946.

(160) Barkhausen, H. and Kurz, K. Phys. Zeit, 21, 1, 1920.

(161) Dreeskamp, H. and Burton, M. Phys. Rev. Letters, 2, 45, 1959.

(162) Falk, W.R. and Katz, L. Canadiam Journal of Physics, 40, 978, 1962.

(163) Bruining, H. Physica, 5, 913, 1938.